UNIVERSITE DE STRASBOURG
FACULTE DE MEDECINE DE STRASBOURG

ANNEE : 2019 N° : 56

THESE
PRESENTEE POUR LE DIPLOME DE
DOCTEUR EN MEDECINE

Diplôme d'État
Mention Oncologie option Radiothérapie

PAR

Clara LE FEVRE
Née le 11 mai 1988 à PLOEMEUR

Facteurs prédictifs de pseudoprogression versus vraie progression chez les patients atteints d'un glioblastome traités par chirurgie et chimioradiothérapie

Étude rétrospective portant sur 57 cas

Président et Directeur de Thèse : Professeur Georges NOËL

UNIVERSITÉ DE STRASBOURG

FACULTÉ DE MÉDECINE
(U.F.R. des Sciences Médicales)

Edition MARS 2018
Année universitaire 2017-2018

HOPITAUX UNIVERSITAIRES
DE STRASBOURG (HUS)
Directeur général :
M. GAUTIER Christophe

Les Hôpitaux Universitaires de STRASBOURG

- **Président de l'Université** M. DENEKEN Michel
- **Doyen de la Faculté** M. SIBILIA Jean

Assesseur du Doyen (13.01.10 et 08.02.11) M. GOICHOT Bernard
Doyens honoraires : (1976-1983) M. DORNER Marc
(1983-1989) M. MANTZ Jean-Marie
(1989-1994) M. VINCENDON Guy
(1994-2001) M. GERLINGER Pierre
(3.10.01-7.02.11) M. LUDES Bertrand

- **Chargé de mission auprès du Doyen** M. VICENTE Gilbert
- **Responsable Administratif** M. LE REST François

A1 - PROFESSEUR TITULAIRE DU COLLEGE DE FRANCE

MANDEL Jean-Louis — Chaire "Génétique humaine" (à compter du 01.11.2003)

A2 - MEMBRE SENIOR A L'INSTITUT UNIVERSITAIRE DE FRANCE (I.U.F.)

BAHRAM Séiamak — Immunologie biologique (01.10.2013 au 31.09.2018)
DOLLFUS Hélène — Génétique clinique (01.10.2014 au 31.09.2019)

A3 - PROFESSEUR(E)S DES UNIVERSITÉS - PRATICIENS HOSPITALIERS (PU-PH)

PO191

NOM et Prénoms	CS*	Services Hospitaliers ou Institut / Localisation	Sous-section du Conseil National des Universités	
ADAM Philippe P0001	NRPô NCS	• Pôle de l'Appareil locomoteur - Service de chirurgie orthopédique et de Traumatologie / HP	50.02	Chirurgie orthopédique et traumatologique
AKLADIOS Cherif P0191	NRPô NCS	• Pôle de Gynécologie-Obstétrique - Service de Gynécologie-Obstétriquel/ HP	54.03	Gynécologie-Obstétrique ; gynécologie médicale Option : **Gynécologie-Obstétrique**
ANDRES Emmanuel P0002	NRPô CS	• Pôle de Médecine Interne, Rhumatologie, Nutrition, Endocrinologie, Diabétologie (MIRNED) - Service de Médecine Interne, Diabète et Maladies métaboliques / HC	53.01	Option : médecine Interne
ANHEIM Mathieu P0003	NRPô NCS	• Pôle Tête et Cou-CETD - Service de Neurologie / Hôpital de Hautepierre	49.01	Neurologie
ARNAUD Laurent P0186	NRPô NCS	• Pôle MIRNED - Service de Rhumatologie / Hôpital de Hautepierre	50.01	Rhumatologie
BACHELLIER Philippe P0004	RPô CS	• Pôle des Pathologies digestives, hépatiques et de la transplantation - Serv. de chirurgie générale, hépatique et endocrinienne et Transplantation / HP	53.02	Chirurgie générale
BAHRAM Seiamak P0005	NRPô CS	• Pôle de Biologie - Laboratoire d'Immunologie biologique / Nouvel Hôpital Civil Institut d'Hématologie et d'Immunologie / Hôpital Civil / Faculté	47.03	Immunologie (option biologique)
BALDAUF Jean-Jacques P0006	NRPô NCS	• Pôle de Gynécologie-Obstétrique - Service de Gynécologie-Obstétrique / Hôpital de Hautepierre	54.03	Gynécologie-Obstétrique ; gynécologie médicale Option **: Gynécologie-Obstétrique**
BAUMERT Thomas P0007	NRPô CU	• Pôle Hépato-digestif de l'Hôpital Civil - Unité d'Hépatologie - Service d'Hépato-Gastro-Entérologie / NHC	52.01	Gastro-entérologie ; **hépatologie** Option : hépatologie
Mme BEAU-FALLER Michèle M0007 / PO170	NRPô NCS	• Pôle de Biologie - Laboratoire de Biochimie et de Biologie moléculaire / HP	44.03	Biologie cellulaire (option biologique)
BEAUJEUX Rémy P0008	NRPô Resp	• Pôle d'Imagerie - CME / Activités transversales • Unité de Neuroradiologie interventionnelle / Hôpital de Hautepierre	43.02	Radiologie et imagerie médicale (option clinique)
BECMEUR François P0009	RPô NCS	• Pôle médico-chirurgical de Pédiatrie - Service de Chirurgie Pédiatrique / Hôpital Hautepierre	54.02	Chirurgie infantile
BERNA Fabrice P0192	NRPô NCS	• Pôle de Psychiatrie, Santé mentale et Addictologie - Service de Psychiatrie I / Hôpital Civil	49.03	Psychiatrie d'adultes ; Addictologie Option : **Psychiatrie d'Adultes**
BERTSCHY Gilles P0013	NRPô CS	• Pôle de Psychiatrie et de santé mentale - Service de Psychiatrie II / Hôpital Civil	49.03	Psychiatrie d'adultes
BIERRY Guillaume P0178	NRPô NCS	• Pôle d'Imagerie - Service d'Imagerie II - Neuroradiologie-imagerie ostéoarticulaire-Pédiatrie / Hôpital Hautepierre	43.02	Radiologie et Imagerie médicale (option clinique)
BILBAULT Pascal P0014	NRPô CS	• Pôle d'Urgences / Réanimations médicales / CAP - Service des Urgences médico-chirurgicales Adultes / Hôpital de Hautepierre	48.02	Réanimation ; **Médecine d'urgence** Option : médecine d'urgence
BODIN Frédéric P0187	NRPô NCS	• Pôle de Chirurgie Maxillo-faciale, morphologie et Dermatologie - Service de Chirurgie maxillo-faciale et réparatrice / Hôpital Civil	50.04	**Chirurgie Plastique, Reconstructrice et Esthétique ;** Brûlologie
Mme BOEHM-BURGER Nelly P0016	NCS	• Institut d'Histologie / Faculté de Médecine	42.02	Histologie, Embryologie et Cytogénétique (option biologique)
BONNOMET François P0017	NRPô CS	• Pôle de l'Appareil locomoteur - Service de Chirurgie orthopédique et de Traumatologie / HP	50.02	Chirurgie orthopédique et traumatologique
BOURCIER Tristan P0018	NRPô NCS	• Pôle de Spécialités médicales-Ophtalmologie / SMO - Service d'Opthalmologie / Nouvel Hôpital Civil	55.02	Ophtalmologie
BOURGIN Patrice P0020	NRPô NCS	• Pôle Tête et Cou - CETD - Service de Neurologie / Hôpital Civil	49.01	Neurologie
Mme BRIGAND Cécile P0022	NRPô NCS	• Pôle des Pathologies digestives, hépatiques et de la transplantation - Service de Chirurgie générale et Digestive / HP	53.02	Chirurgie générale

NHC = Nouvel Hôpital Civil HC = Hôpital Civil HP = Hôpital de Hautepierre PTM = Plateau technique de microbiologie

NOM et Prénoms	CS*	Services Hospitaliers ou Institut / Localisation	Sous-section du Conseil National des Universités
BRUANT-RODIER Catherine P0023	NRPô CS	• Pôle de l'Appareil locomoteur - Service de Chirurgie Maxillo-faciale et réparatrice / Hôpital Civil	50.04 Option : chirurgie plastique, reconstructrice et esthétique
Mme CAILLARD-OHLMANN Sophie P0171	NRPô NCS	• Pôle de Spécialités médicales-Ophtalmologie / SMO - Service de Néphrologie-Transplantation / NHC	52.03 Néphrologie
CANDOLFI Ermanno P0025	RPô CS	• Pôle de Biologie - Laboratoire de Parasitologie et de Mycologie médicale / PTM HUS • Institut de Parasitologie / Faculté de Médecine	45.02 Parasitologie et mycologie (option biologique)
CASTELAIN Vincent P0027	NRPô NCS	• Pôle Urgences - Réanimations médicales / Centre antipoison - Service de Réanimation médicale / Hôpital Hautepierre	48.02 Réanimation
CHAKFE Nabil P0029	NRPô CS	• Pôle d'activité médico-chirurgicale Cardio-vasculaire - Service de Chirurgie Vasculaire et de transplantation rénale / NHC	51.04 **Chirurgie vasculaire** ; médecine vasculaire / Option : chirurgie vasculaire
CHARLES Yann-Philippe M0013 / P0172	NRPô NCS	• Pôle de l'Appareil locomoteur - Service de Chirurgie du rachis / Chirurgie B / HC	50.02 Chirurgie orthopédique et traumatologique
Mme CHARLOUX Anne P0028	NRPô NCS	• Pôle de Pathologie thoracique - Service de Physiologie et d'Explorations fonctionnelles / NHC	44.02 Physiologie (option biologique)
Mme CHARPIOT Anne P0030	NRPô NCS	• Pôle Tête et Cou - CETD - Serv. d'Oto-rhino-laryngologie et de Chirurgie cervico-faciale / HP	55.01 Oto-rhino-laryngologie
CHAUVIN Michel P0040	NRPô CS	• Pôle d'activité médico-chirurgicale Cardio-vasculaire - Service de Cardiologie / Nouvel Hôpital Civil	51.02 Cardiologie
CHELLY Jameleddine P0173	NRPô CS	• Pôle de Biologie - Laboratoire de Diagnostic génétique / NHC	47.04 Génétique (option biologique)
Mme CHENARD-NEU Marie-Pierre P0041	NRPô CS	• Pôle de Biologie - Service de Pathologie / Hôpital de Hautepierre	42.03 Anatomie et cytologie pathologiques (option biologique)
CLAVERT Philippe P0044	NRPô NCS	• Pôle de l'Appareil locomoteur - Service d'Orthopédie / CCOM d'Illkirch	42.01 Anatomie (option clinique, orthopédie traumatologique)
COLLANGE Olivier PO193	NRPô NCS	• Pôle d'Anesthésie / Réanimations chirurgicales / SAMU-SMUR - Service d'Anesthésiologie-Réanimation Chirurgicale / NHC	48.01 **Anesthésiologie-Réanimation** ; Médecine d'urgence (option Anesthésiologie-Réanimation - Type clinique)
CRIBIER Bernard P0045	NRPô CS	• Pôle d'Urologie, Morphologie et Dermatologie - Service de Dermatologie / Hôpital Civil	50.03 Dermato-Vénéréologie
DANION Jean-Marie P0046	NRPô CS	• Pôle de Psychiatrie et de santé mentale - Service de Psychiatrie 1 / Hôpital Civil	49.03 Psychiatrie d'adultes
Mme DANION-GRILLIAT Anne P0047 (1) (8)	S/nb Cons	• Pôle de Psychiatrie et de santé mentale - Service Psychothérapique pour Enfants et Adolescents / HC et Hôpital de l'Elsau	49.04 Pédopsychiatrie
de BLAY de GAIX Frédéric P0048	RPô NCS	• Pôle de Pathologie thoracique - Service de Pneumologie / Nouvel Hôpital Civil	51.01 Pneumologie
DEBRY Christian P0049	NRPô CS	• Pôle Tête et Cou - CETD - Serv. d'Oto-rhino-laryngologie et de Chirurgie cervico-faciale / HP	55.01 Oto-rhino-laryngologie
de SEZE Jérôme P0057	NRPô NCS	• Pôle Tête et Cou - CETD - Service de Neurologie / Hôpital de Hautepierre	49.01 Neurologie
DIEMUNSCH Pierre P0051	RPô CS	• Pôle d'Anesthésie / Réanimations chirurgicales / SAMU-SMUR - Service d'Anesthésie-Réanimation Chirurgicale / Hôpital de Hautepierre	48.01 Anesthésiologie-réanimation (option clinique)
Mme DOLLFUS-WALTMANN Hélène P0054	NRPô CS	• Pôle de Biologie - Service de Génétique Médicale / Hôpital de Hautepierre	47.04 Génétique (type clinique)
DUCLOS Bernard P0055	NRPô CS	• Pôle des Pathologies digestives, hépatiques et de la transplantation - Service d'Hépato-Gastro-Entérologie et d'Assistance Nutritive / HP	52.01 Option : Gastro-entérologie
DUFOUR Patrick (5) (7) P0056	S/nb Cons	• Centre Régional de Lutte contre le cancer Paul Strauss (convention)	47.02 Option : Cancérologie clinique
EHLINGER Matfhieu P0188	NRPô NCS	• Pôle de l'Appareil Locomoteur - Service de Chirurgie Orthopédique et de Traumatologie/Hôpital de Hautepierre	50.02 Chirurgie Orthopédique et Traumatologique
Mme ENTZ-WERLE Natacha P0059	NRPô NCS	• Pôle médico-chirurgical de Pédiatrie - Service de Pédiatrie III / Hôpital de Hautepierre	54.01 Pédiatrie
Mme FACCA Sybille P0179	NRPô NCS	• Pôle de l'Appareil locomoteur - Service de la Main et des Nerfs périphériques / CCOM Illkirch	50.02 Chirurgie orthopédique et traumatologique
Mme FAFI-KREMER Samira P0060	NRPô CS	• Pôle de Biologie - Laboratoire (Institut) de Virologie / PTM HUS et Faculté	45.01 Bactériologie-**Virologie** ; Hygiène Hospitalière Option Bactériologie-**Virologie** biologique
FALCOZ Pierre-Emmanuel P0052	NRPô NCS	• Pôle de Pathologie thoracique - Service de Chirurgie Thoracique / Nouvel Hôpital Civil	51.03 Chirurgie thoracique et cardio-vasculaire
GANGI Afshin P0062	RPô CS	• Pôle d'Imagerie - Service d'Imagerie A interventionnelle / Nouvel Hôpital Civil	43.02 Radiologie et imagerie médicale (option clinique)
GAUCHER David P0063	NRPô NCS	• Pôle des Spécialités Médicales - Ophtalmologie / SMO - Service d'Ophtalmologie / Nouvel Hôpital Civil	55.02 Ophtalmologie
GENY Bernard P0064	NRPô CS	• Pôle de Pathologie thoracique - Service de Physiologie et d'Explorations fonctionnelles / NHC	44.02 Physiologie (option biologique)
GICQUEL Philippe P0065	NRPô CS	• Pôle médico-chirurgical de Pédiatrie - Service de Chirurgie Pédiatrique / Hôpital Hautepierre	54.02 Chirurgie infantile

NOM et Prénoms	CS*	Services Hospitaliers ou Institut / Localisation	Sous-section du Conseil National des Universités
GOICHOT Bernard P0066	RPô CS	• Pôle de Médecine Interne, Rhumatologie, Nutrition, Endocrinologie, Diabétologie (MIRNED) - Service de Médecine interne et de nutrition / HP	54.04 Endocrinologie, diabète et maladies métaboliques
Mme GONZALEZ Maria P0067	NRPô CS	• Pôle de Santé publique et santé au travail - Service de Pathologie Professionnelle et Médecine du Travail / HC	46.02 Médecine et santé au travail Travail
GOTTENBERG Jacques-Eric P0068	NRPô CS	• Pôle de Médecine Interne, Rhumatologie, Nutrition, Endocrinologie, Diabétologie (MIRNED) - Service de Rhumatologie / Hôpital Hautepierre	50.01 Rhumatologie
GRUCKER Daniel (1) P0069	S/nb	• Pôle de Biologie - Labo. d'Explorations fonctionnelles par les isotopes in vitro / NHC • Institut de Physique biologique / Faculté de Médecine	43.01 Biophysique et médecine nucléaire
HANNEDOUCHE Thierry P0071	NRPô CS	• Pôle de Spécialités médicales - Ophtalmologie / SMO - Service de Néphrologie - Dialyse / Nouvel Hôpital Civil	52.03 Néphrologie
HANSMANN Yves P0072	NRPô CS	• Pôle de Spécialités médicales - Ophtalmologie / SMO - Service des Maladies infectieuses et tropicales / Nouvel Hôpital Civil	45.03 Option : Maladies infectieuses
HERBRECHT Raoul P0074	RPô NCS	• Pôle d'Oncolo-Hématologie - Service d'hématologie et d'Oncologie / Hôp. Hautepierre	47.01 **Hématologie** ; Transfusion
HIRSCH Edouard P0075	NRPô NCS	• Pôle Tête et Cou - CETD - Service de Neurologie / Hôpital de Hautepierre	49.01 Neurologie
HOCHBERGER Jürgen P0076 (Disponibilité 30.04.18)	NRPô CU	• Pôle Hépato-digestif de l'Hôpital Civil - Unité de Gastro-Entérologie - Service d'Hépato-Gastro-Entérologie / Nouvel Hôpital Civil	52.01 Option : Gastro-entérologie
IMPERIALE Alessio P0194	NRPô NCS	• Pôle d'Imagerie - Service de Biophysique et de Médecine nucléaire/Hôpital de Hautepierre	43.01 Biophysique et médecine nucléaire
ISNER-HOROBETI Marie-Eve P0189		• Pôle de l'Appareil Locomoteur - Institut Universitaire de Réadaptation / Clémenceau	49.05 **Médecine Physique et Réadaptation**
JAULHAC Benoît P0078	NRPô CS	• Pôle de Biologie - Institut (Laboratoire) de Bactériologie / PTM HUS et Faculté de Méd.	45.01 Option : **Bactériologie**-virologie (biologique)
Mme JEANDIDIER Nathalie P0079	NRPô CS	• Pôle de Médecine Interne, Rhumatologie, Nutrition, Endocrinologie, Diabétologie (MIRNED) - Service d'Endocrinologie, diabète et nutrition / HC	54.04 Endocrinologie, diabète et maladies métaboliques
KAHN Jean-Luc P0080	 NRPô CS NCS	• Institut d'Anatomie Normale / Faculté de Médecine • Pôle de chirurgie plastique reconstructrice et esthétique, chirurgie maxillo-faciale, morphologie et dermatologie - Serv. de Morphologie appliquée à la chirurgie et à l'imagerie / FAC - Service de Chirurgie Maxillo-faciale et réparatrice / HC	42.01 Anatomie (option clinique, chirurgie maxillo-faciale et stomatologie)
KALTENBACH Georges P0081	RPô CS	• Pôle de Gériatrie - Service de Médecine Interne - Gériatrie / Hôpital de la Robertsau	53.01 Option : gériatrie et biologie du vieillissement
KEMPF Jean-François P0083	RPô CS	• Pôle de l'Appareil locomoteur - Centre de Chirurgie Orthopédique et de la Main-CCOM / Illkirch	50.02 Chirurgie orthopédique et traumatologique
Mme KESSLER Laurence P0084	NRPô NCS	• Pôle de Médecine Interne, Rhumatologie, Nutrition, Endocrinologie, Diabétologie (MIRNED) - Service d'Endocrinologie, Diabète, Nutrition et Addictologie / Méd. B / HC	54.04 Endocrinologie, diabète et maladies métaboliques
KESSLER Romain P0085	NRPô NCS	• Pôle de Pathologie thoracique - Service de Pneumologie / Nouvel Hôpital CIvil	51.01 Pneumologie
KINDO Michel P0195	NRPô NCS	• Pôle d'activité médico-chirurgicale Cardio-vasculaire - Service de Chirurgie Cardio-vasculaire / Nouvel Hôpital Civil	51.03 Chirurgie thoracique et cardio-vasculaire
KOPFERSCHMITT Jacques P0086	NRPô NCS	• Pôle Urgences - Réanimations médicales / Centre antipoison - Service d'Urgences médico-chirurgicales adultes/Nouvel Hôpital Civil	48.04 Thérapeutique (option clinique)
Mme KORGANOW Anne-Sophie P0087	NRPô CS	• Pôle de Spécialités médicales - Ophtalmologie / SMO - Service de Médecine Interne et d'Immunologie Clinique / NHC	47.03 Immunologie (option clinique)
KREMER Stéphane M0038 / P0174	NRPô CS	• Pôle d'Imagerie - Service Imagerie 2 - Neuroradio Ostéoarticulaire - Pédiatrie / HP	43.02 Radiologie et imagerie médicale (option clinique)
KRETZ Jean Georges (1) (8) P0088	S/nb Cons	• Pôle d'activité médico-chirurgicale Cardio-vasculaire - Service de Chirurgie Vasculaire et de transplantation rénale / NHC	51.04 **Chirurgie vasculaire** ; médecine vasculaire (option chirurgie vasculaire)
KUHN Pierre P0175	NRPô NCS	• Pôle médico-chirurgical de Pédiatrie - Service de Néonatologie et Réanimation néonatale (Pédiatrie II) / Hôpital de Hautepierre	54.01 Pédiatrie
KURTZ Jean-Emmanuel P0089	NRPô CS	• Pôle d'Onco-Hématologie - Service d'hématologie et d'Oncologie / Hôpital Hautepierre	47.02 Option : Cancérologie (clinique)
LANG Hervé P0090	NRPô NCS	• Pôle de Chirurgie plastique reconstructrice et esthétique, Chirurgie maxillo-faciale, Morphologie et Dermatologie - Service de Chirurgie Urologique / Nouvel Hôpital Civil	52.04 Urologie
LANGER Bruno P0091	RPô NCS	• Pôle de Gynécologie-Obstétrique - Service de Gynécologie-Obstétrique / Hôpital de Hautepierre	54.03 **Gynécologie-Obstétrique** ; gynécologie médicale : option gynécologie-Obstétrique
LAUGEL Vincent P0092	NRPô CS	• Pôle médico-chirurgical de Pédiatrie - Service de Pédiatrie 1 / Hôpital Hautepierre	54.01 Pédiatrie
LE MINOR Jean-Marie P0190	NRPô NCS	• Pôle d'Imagerie - Institut d'Anatomie Normale / Faculté de Médecine - Service de Neuroradiologie, d'imagerie Ostéoarticulaire et interventionnelle/ Hôpital de Hautepierre	42.01 **Anatomie**
LIPSKER Dan P0093	NRPô NCS	• Pôle de Chirurgie plastique reconstructrice et esthétique, Chirurgie maxillo-faciale, Morphologie et Dermatologie - Service de Dermatologie / Hôpital Civil	50.03 Dermato-vénéréologie

NOM et Prénoms	CS*	Services Hospitaliers ou Institut / Localisation	Sous-section du Conseil National des Universités
LIVERNEAUX Philippe P0094	NRPô CS	• Pôle de l'Appareil locomoteur - Service de Chirurgie de la main - CCOM / Illkirch	50.02 Chirurgie orthopédique et traumatologique
MARESCAUX Christian (5) P0097	NRPô NCS	• Pôle Tête et Cou - CETD -Service de Neurologie / Hôpital de Hautepierre	49.01 Neurologie
MARK Manuel P0098	NRPô NCS	• Pôle de Biologie - Laboratoire de Cytogénétique, Cytologie et Histologie quantitative / Hôpital de Hautepierre	54.05 Biologie et médecine du développement et de la reproduction (option biologique)
MARTIN Thierry P0099	NRPô NCS	• Pôle de Spécialités médicales - Ophtalmologie / SMO - Service de Médecine Interne et d'Immunologie Clinique / NHC	47.03 Immunologie (option clinique)
MASSARD Gilbert P0100	NRPô NCS	• Pôle de Pathologie thoracique - Service de Chirurgie Thoracique / Nouvel Hôpital Civil	51.03 Chirurgie thoracique et cardio-vasculaire
Mme MATHELIN Carole P0101	NRPô NCS	• Pôle de Gynécologie-Obstétrique - Unité de Sénologie - Hôpital Civil	**Gynécologie-Obstétrique** ; Gynécologie 54.03 Médicale
MAUVIEUX Laurent P0102	NRPô CS	• Pôle d'Onco-Hématologie - Laboratoire d'Hématologie Biologique - Hôpital de Hautepierre • Institut d'Hématologie / Faculté de Médecine	47.01 **Hématologie** ; Transfusion Option Hématologie Biologique
MAZZUCOTELLI Jean-Philippe P0103	RPô CS	• Pôle d'activité médico-chirurgicale Cardio-vasculaire - Service de Chirurgie Cardio-vasculaire / Nouvel Hôpital Civil	51.03 Chirurgie thoracique et cardio-vasculaire
MERTES Paul-Michel P0104	NRPô CS	• Pôle d'Anesthésiologie / Réanimations chirurgicales / SAMU-SMUR - Service d'Anesthésiologie-Réanimation chirurgicale / Nouvel Hôpital Civil	48.01 Option : Anesthésiologie-Réanimation (type mixte)
MEYER Nicolas P0105	NRPô NCS	• Pôle de Santé publique et Santé au travail - Laboratoire de Biostatistiques / Hôpital Civil • Biostatistiques et Informatique / Faculté de médecine / Hôpital Civil	46.04 Biostatistiques, Informatique Médicale et Technologies de Communication (option biologique)
MEZIANI Ferhat P0106	NRPô NCS	• Pôle Urgences - Réanimations médicales / Centre antipoison - Service de Réanimation Médicale / Nouvel Hôpital Civil	48.02 Réanimation
MONASSIER Laurent P0107	NRPô CS	• Pôle de Pharmacie-pharmacologie • Unité de Pharmacologie clinique / Nouvel Hôpital Civil	48.03 Option : Pharmacologie fondamentale
MOREL Olivier P0108	NRPô NCS	• Pôle d'activité médico-chirurgicale Cardio-vasculaire - Service de Cardiologie / Nouvel Hôpital Civil	51.02 Cardiologie
MOULIN Bruno P0109	NRPô CS	• Pôle de Spécialités médicales - Ophtalmologie / SMO - Service de Néphrologie - Transplantation / Nouvel Hôpital Civil	52.03 Néphrologie
MUTTER Didier P0111	RPô CS	• Pôle Hépato-digestif de l'Hôpital Civil - Service de Chirurgie Digestive / NHC	52.02 Chirurgie digestive
NAMER Izzie Jacques P0112	NRPô CS	• Pôle d'Imagerie - Service de Biophysique et de Médecine nucléaire / Hautepierre / NHC	43.01 Biophysique et médecine nucléaire
NISAND Israël P0113	NRPô CS	• Pôle de Gynécologie-Obstétrique - Service de Gynécologie Obstétrique / Hôpital de Hautepierre	54.03 **Gynécologie-Obstétrique** ; gynécologie médicale : option gynécologie-Obstétrique
NOEL Georges P0114	 NCS	• Centre Régional de Lutte Contre le Cancer Paul Strauss (par convention) - Département de radiothérapie	Cancérologie ; **Radiothérapie** 47.02 Option Radiothérapie biologique
OHLMANN Patrick P0115	NRPô NCS	• Pôle d'activité médico-chirurgicale Cardio-vasculaire - Service de Cardiologie / Nouvel Hôpital Civil	51.02 Cardiologie
Mme PAILLARD Catherine P0180	NRPô CS	• Pôle médico-chirurgicale de Pédiatrie - Service de Pédiatrie III / Hôpital de Hautepierre	54.01 Pédiatrie
Mme PERRETTA Silvana P0117	NRPô NCS	• Pôle Hépato-digestif de l'Hôpital Civil - Service d'Urgence, de Chirurgie Générale et Endocrinienne / NHC	52.02 Chirurgie digestive
PESSAUX Patrick P0118	NRPô NCS	• Pôle des Pathologies digestives, hépatiques et de la transplantation - Service d'Urgence, de Chirurgie Générale et Endocrinienne / NHC	53.02 Chirurgie Générale
PETIT Thierry P0119	 CDp	• Centre Régional de Lutte Contre le Cancer - Paul Strauss (par convention) - Département de médecine oncologique	47.02 **Cancérologie** ; Radiothérapie Option : Cancérologie Clinique
POTTECHER Julien P0181	NRPô NCS	• Pôle d'Anesthésie / Réanimations chirurgicales / SAMU-SMUR - Service d'Anesthésie et de Réanimation Chirurgicale / Hôpital de Hautepierre	48.01 **Anesthésiologie-réanimation** ; Médecine d'urgence (option clinique)
PRADIGNAC Alain P0123	NRPô NCS	• Pôle de Médecine Interne, Rhumatologie, Nutrition, Endocrinologie, Diabétologie (MIRNED) - Service de Médecine interne et nutrition / HP	44.04 Nutrition
PROUST François P0182	NRPô CS	• Pôle Tête et Cou - Service de Neurochirurgie / Hôpital de Hautepierre	49.02 Neurochirurgie
Mme QUOIX Elisabeth P0124	NRPô CS	• Pôle de Pathologie thoracique - Service de Pneumologie / Nouvel Hôpital Civil	51.01 Pneumologie
Pr RAUL Jean-Sébastien P0125	NRPô CS	• Pôle de Biologie - Service de Médecine Légale, Consultation d'Urgences médico-judiciaires et Laboratoire de Toxicologie / Faculté et NHC • Institut de Médecine Légale / Faculté de Médecine	46.03 Médecine Légale et droit de la santé
REIMUND Jean-Marie P0126	NRPô NCS	• Pôle des Pathologies digestives, hépatiques et de la transplantation - Service d'Hépato-Gastro-Entérologie et d'Assistance Nutritive / HP	52.01 Option : Gastro-entérologie
Pr RICCI Roméo P0127	NRPô NCS	• Pôle de Biologie - Laboratoire de Biochimie et de Biologie moléculaire / HP	44.01 Biochimie et biologie moléculaire
ROHR Serge P0128	NRPô CS	• Pôle des Pathologies digestives, hépatiques et de la transplantation - Service de Chirurgie générale et Digestive / HP	53.02 Chirurgie générale

NOM et Prénoms	CS*	Services Hospitaliers ou Institut / Localisation	Sous-section du Conseil National des Universités	
Mme ROSSIGNOL -BERNARD	NRPô	• Pôle médico-chirurgical de Pédiatrie		
Sylvie	CS	- Service de Pédiatrie I / Hôpital de Hautepierre	54.01	Pédiatrie
PO196				
ROUL Gérald	NRPô	• Pôle d'activité médico-chirurgicale Cardio-vasculaire		
P0129	NCS	- Service de Cardiologie / Nouvel Hôpital Civil	51.02	Cardiologie
Mme ROY Catherine	NRPô	• Pôle d'Imagerie		
P0140	CS	- Serv. d'Imagerie B - Imagerie viscérale et cardio-vasculaire / NHC	43.02	Radiologie et imagerie médicale (opt clinique)
SAUDER Philippe	NRPô	• Pôle Urgences - Réanimations médicales / Centre antipoison		
P0142	CS	- Service de Réanimation médicale / Nouvel Hôpital Civil	48.02	Réanimation
SAUER Arnaud	NRPô	• Pôle de Spécialités médicales - Ophtalmologie / SMO		
P0183	NCS	- Service d'Ophtalmologie / Nouvel Hôpital Civil	55.02	Ophtalmologie
SAULEAU Erik-André	NRPô	• Pôle de Santé publique et Santé au travail	46.04	Biostatiqtiques, Informatique médicale et Technologies de Communication (option biologique)
P0184	NCS	- Laboratoire de Biostatistiques / Hôpital Civil		
		• Biostatistiques et Informatique / Faculté de médecine / HC		
SAUSSINE Christian	RPô	• Pôle d'Urologie, Morphologie et Dermatologie		
P0143	CS	- Service de Chirurgie Urologique / Nouvel Hôpital Civil	52.04	Urologie
SCHNEIDER Francis	RPô	• Pôle Urgences - Réanimations médicales / Centre antipoison		
P0144	CS	- Service de Réanimation médicale / Hôpital de Hautepierre	48.02	Réanimation
Mme SCHRÖDER Carmen	NRPô	• Pôle de Psychiatrie et de santé mentale		
P0185	CS	- Service de Psychothérapie pour Enfants et Adolescents / Hôpital Civil	49.04	**Pédopsychiatrie** ; Addictologie
SCHULTZ Philippe	NRPô	• Pôle Tête et Cou - CETD		
P0145	NCS	- Serv. d'Oto-rhino-laryngologie et de Chirurgie cervico-faciale / HP	55.01	Oto-rhino-laryngologie
SERFATY Lawrence	NRPô	• Pôle des Pathologies digestives, hépatiques et de la transplantation		Gastro-entérologie ; Hépatologie ; Addictologie
P0197	NCS	- Service d'Hépato-Gastro-Entérologie et d'Assistance Nutritive / HP	52.01	
				Option : **Hépatologie**
SIBILIA Jean	NRPô	• Pôle de Médecine Interne, Rhumatologie, Nutrition, Endocrinologie, Diabétologie (MIRNED)	50.01	Rhumatologie
P0146	CS	- Service de Rhumatologie / Hôpital Hautepierre		
Mme SPEEG-SCHATZ Claude	RPô	• Pôle de Spécialités médicales - Ophtalmologie / SMO		
P0147	CS	- Service d'Ophtalmologie / Nouvel Hôpital Civil	55.02	Ophtalmologie
Mme STEIB Annick	RPô	• Pôle d'Anesthésie / Réanimations chirurgicales / SAMU-SMUR		
P0148	NCS	- Service d'Anesthésiologie-Réanimation Chirurgicale / NHC	48.01	Anesthésiologie-réanimation (option clinique)
STEIB Jean-Paul	NRPô	• Pôle de l'Appareil locomoteur		
P0149	CS	- Service de Chirurgie du rachis / Hôpital Civil	50.02	Chirurgie orthopédique et traumatologique
STEPHAN Dominique	NRPô	• Pôle d'activité médico-chirurgicale Cardio-vasculaire		
P0150	CS	- Service des Maladies vasculaires - HTA - Pharmacologie clinique / Nouvel Hôpital Civil	51.04	Option : Médecine vasculaire
THAVEAU Fabien	NRPô	• Pôle d'activité médico-chirurgicale Cardio-vasculaire		
P0152	NCS	- Service de Chirurgie vasculaire et de transplantation rénale / NHC	51.04	Option : Chirurgie vasculaire
Mme TRANCHANT Christine	NRPô	• Pôle Tête et Cou - CETD		
P0153	CS	- Service de Neurologie / Hôpital de Hautepierre	49.01	Neurologie
VEILLON Francis	NRPô	• Pôle d'Imagerie		
P0155	CS	- Service d'Imagerie 1 - Imagerie viscérale, ORL et mammaire / Hôpital Hautepierre	43.02	Radiologie et imagerie médicale (option clinique)
VELTEN Michel	NRPô	• Pôle de Santé publique et Santé au travail		
P0156	NCS	- Département de Santé Publique / Secteur 3 - Epidémiologie et Economie de la Santé / Hôpital Civil	46.01	Epidémiologie, économie de la santé et prévention (option biologique)
		• Laboratoire d'Epidémiologie et de santé publique / HC / Fac de Médecine		
	CS	• Centre de Lutte contre le Cancer Paul Strauss - Serv. Epidémiologie et de biostatistiques		
VETTER Denis	NRPô	• Pôle de Médecine Interne, Rhumatologie, Nutrition, Endocrinologie, Diabétologie (MIRNED)		
P0157	NCS	- Service de Médecine Interne, Diabète et Maladies métaboliques/HC	52.01	Option : Gastro-entérologie
VIDAILHET Pierre	NRPô	• Pôle de Psychiatrie et de santé mentale		
P0158	NCS	- Service de Psychiatrie I / Hôpital Civil	49.03	Psychiatrie d'adultes
VIVILLE Stéphane	NRPô	• Pôle de Biologie	54.05	Biologie et médecine du développement
P0159	NCS	- Laboratoire de Parasitologie et de Pathologies tropicales / Fac. de Médecine		et de la reproduction (option biologique)
VOGEL Thomas	NRPô	• Pôle de Gériatrie	51.01	Option : Gériatrie et biologie du vieillissement
P0160	CS	- Service de soins de suite et réadaptations gériatriques / Hôpital de la Robertsau		
WATTIEZ Arnaud	NRPô	• Pôle de Gynécologie-Obstétrique		**Gynécologie-Obstétrique** ; Gynécologie
P0161	NCS	- Service de Gynécologie-Obstétrique / Hôpital de Hautepierre	54.03	médicale / Opt Gynécologie -Obstétrique
(Dispo 31.07.2019)				
WEBER Jean-Christophe Pierre	NRPô	• Pôle de Spécialités médicales - Ophtalmologie / SMO		
P0162	CS	- Service de Médecine Interne / Nouvel Hôpital Civil	53.01	Option : Médecine Interne
WOLF Philippe	NRPô	• Pôle des Pathologies digestives, hépatiques et de la transplantation	53.02	Chirurgie générale
P0164	NCS	- Service de Chirurgie Générale et de Transplantations multiorganes / HP		
		- Coordonnateur des activités de prélèvements et transplantations des HU		
Mme WOLFRAM-GABEL (5)	S/nb	• Pôle de Chirurgie plastique reconstructrice et esthétique, Chirurgie maxillo-faciale, Morphologie et Dermatologie	42.01	Anatomie (option biologique)
Renée		- Service de Morphologie appliquée à la chirurgie et à l'imagerie / Faculté		
P0165		• Institut d'Anatomie Normale / Hôpital Civil		

NOM et Prénoms	CS*	Services Hospitaliers ou Institut / Localisation	Sous-section du Conseil National des Universités

HC : Hôpital Civil - HP : Hôpital de Hautepierre - NHC : Nouvel Hôpital Civil
* : CS (Chef de service) ou NCS (Non Chef de service hospitalier) Cspi : Chef de service par intérim CSp : Chef de service provisoire (un an)
CU : Chef d'unité fonctionnelle
Pô : Pôle RPô (Responsable de Pôle) ou NRPô (Non Responsable de Pôle)
Cons. : Consultanat hospitalier (poursuite des fonctions hospitalières sans chefferie de service) Dir : Directeur
(1) En surnombre universitaire jusqu'au 31.08.2018
(3) (7) Consultant hospitalier (pour un an) éventuellement renouvelable --> 31.08.2017
(5) En surnombre universitaire jusqu'au 31.08.2019 (8) Consultant hospitalier (pour une 2ème année) --> 31.08.2017
(6) En surnombre universitaire jusqu'au 31.08.2017 (9) Consultant hospitalier (pour une 3ème année) --> 31.08.2017

A4 - PROFESSEUR ASSOCIE DES UNIVERSITES

HABERSETZER François	CS	Pôle Hépato-digestif 4190 Service de Gastro-Entérologie - NHC	52.01 Gastro-Entérologie

MO112 B1 - MAITRES DE CONFERENCES DES UNIVERSITES - PRATICIENS HOSPITALIERS (MCU-PH)

NOM et Prénoms	CS*	Services Hospitaliers ou Institut / Localisation	Sous-section du Conseil National des Universités
AGIN Arnaud M0001		• Pôle d'Imagerie - Service de Biophysique et de Médecine nucléaire/Hôpital de Hautepierre	43.01 Biophysique et Médecine nucléaire
Mme ANTAL Maria Cristina M0003		• Pôle de Biologie - Service de Pathologie / Hautepierre • Faculté de Médecine / Institut d'Histologie	42.02 Histologie, Embryologie et Cytogénétique (option biologique)
Mme ANTONI Delphine M0109		• Centre de lutte contre le cancer Paul Strauss	47.02 Cancérologie ; **Radiothérapie**
ARGEMI Xavier M0112		• Pôle de Spécialités médicales - Ophtalmologie / SMO - Service des Maladies infectieuses et tropicales / Nouvel Hôpital Civil	45.03 Maladies infectieuses ; Maladies tropicales Option : **Maladies infectieuses**
Mme BARNIG Cindy M0110		• Pôle de Pathologie thoracique - Service de Physiologie et d'Explorations Fonctionnelles / NHC	44.02 **Physiologie**
Mme BARTH Heidi M0005 (Dispo → 31.12.2018)		• Pôle de Biologie - Laboratoire de Virologie / Hôpital Civil	45.01 Bactériologie - Virologie (Option biologique)
Mme BIANCALANA Valérie M0008		• Pôle de Biologie - Laboratoire de Diagnostic Génétique / Nouvel Hôpital Civil	47.04 Génétique (option biologique)
BLONDET Cyrille M0091		• Pôle d'Imagerie - Service de Biophysique et de Médecine nucléaire/Hôpital de Hautepierre	43.01 Biophysique et médecine nucléaire
BONNEMAINS Laurent M0099		• Pôle d'activité médico-chirurgicale Cardio-vasculaire - Service de Chirurgie cardio-vasculaire / Nouvel Hôpital Civil	54.01 Pédiatrie
BOUSIGES Olivier M0092		• Pôle de Biologie - Laboratoire de Biochimie et de Biologie moléculaire / HP	44.01 Biochimie et biologie moléculaire
CARAPITO Raphaël M0113		• Pôle de Biologie - Laboratoire d'Immunologie biologique / Nouvel Hôpital Civil	47.03 Immunologie
CERALINE Jocelyn M0012		• Pôle d'Oncologie et d'Hématologie - Service d'Oncologie et d'Hématologie / HP	47.02 **Cancérologie** ; Radiothérapie (option biologique)
CHOQUET Philippe M0014		• Pôle d'Imagerie - Service de Biophysique et de Médecine nucléaire / HP	43.01 Biophysique et médecine nucléaire
COLLONGUES Nicolas M0016		• Pôle Tête et Cou-CETD - Centre d'Investigation Clinique / NHC et HP	49.01 Neurologie
DALI-YOUCEF Ahmed Nassim M0017		• Pôle de Biologie - Laboratoire de Biochimie et Biologie moléculaire / NHC	44.01 Biochimie et biologie moléculaire
Mme de MARTINO Sylvie M0018		• Pôle de Biologie - Laboratoire de Bactériologie / PTM HUS et Faculté de Médecine	**Bactériologie**-virologie 45.01 Option bactériologie-virologie biologique
Mme DEPIENNE Christel M0100 (Dispo->15.08.18)	CS	• Pôle de Biologie - Laboratoire de Cytogénétique / HP	47.04 Génétique
DEVYS Didier M0019		• Pôle de Biologie - Laboratoire de Diagnostic génétique / Nouvel Hôpital Civil	47.04 Génétique (option biologique)
DOLLÉ Pascal M0021		• Pôle de Biologie -Laboratoire de Biochimie et biologie moléculaire / NHC	44.01 Biochimie et biologie moléculaire
Mme ENACHE Irina M0024		• Pôle de Pathologie thoracique - Service de Physiologie et d'Explorations fonctionnelles / NHC	44.02 Physiologie
FILISETTI Denis M0025		• Pôle de Biologie - Labo. de Parasitologie et de Mycologie médicale / PTM HUS et Faculté	45.02 Parasitologie et mycologie (option biologique)
FOUCHER Jack M0027		• Institut de Physiologie / Faculté de Médecine • Pôle de Psychiatrie et de santé mentale - Service de Psychiatrie I / Hôpital Civil	44.02 Physiologie (option clinique)
GUERIN Eric M0032		• Pôle de Biologie - Laboratoire de Biochimie et de Biologie moléculaire / HP	44.03 Biologie cellulaire (option biologique)
Mme HELMS Julie M0114		• Pôle d'Urgences / Réanimations médicales / CAP - Service de Réanimation médicale / Nouvel Hôpital Civil	48.02 Réanimation ; Médecine d'urgence Option : **Réanimation**
HUBELE Fabrice M0033		• Pôle d'Imagerie - Service de Biophysique et de Médecine nucléaire / HP et NHC	43.01 Biophysique et médecine nucléaire
Mme JACAMON-FARRUGIA Audrey M0034		• Pôle de Biologie - Service de Médecine Légale, Consultation d'Urgences médico-judiciaires et Laboratoire de Toxicologie / Faculté et HC • Institut de Médecine Légale / Faculté de Médecine	46.03 Médecine Légale et droit de la santé
JEGU Jérémie M0101		• Pôle de Santé publique et Santé au travail - Service de Santé Publique / Hôpital Civil	46.01 Epidémiologie, Economie de la santé et Prévention (option biologique)
JEHL François M0035		• Pôle de Biologie - Institut (Laboratoire) de Bactériologie / PTM HUS et Faculté	45.01 Option : **Bactériologie** -virologie (biologique)
KASTNER Philippe M0089		• Pôle de Biologie - Laboratoire de diagnostic génétique / Nouvel Hôpital Civil	47.04 Génétique (option biologique)
Mme KEMMEL Véronique M0036		• Pôle de Biologie - Laboratoire de Biochimie et de Biologie moléculaire / HP	44.01 Biochimie et biologie moléculaire
Mme LAMOUR Valérie M0040		• Pôle de Biologie - Laboratoire de Biochimie et de Biologie moléculaire / HP	44.01 Biochimie et biologie moléculaire

NOM et Prénoms	CS*	Services Hospitaliers ou Institut / Localisation	Sous-section du Conseil National des Universités
Mme LANNES Béatrice M0041		• Institut d'Histologie / Faculté de Médecine • Pôle de Biologie - Service de Pathologie / Hôpital de Hautepierre	42.02 Histologie, Embryologie et Cytogénétique (option biologique)
LAVAUX Thomas M0042		• Pôle de Biologie - Laboratoire de Biochimie et de Biologie moléculaire / HP	44.03 Biologie cellulaire
LAVIGNE Thierry M0043	CS	• Pôle de Santé Publique et Santé au travail - Service d'Hygiène hospitalière et de médecine préventive / PTM et HUS - Equipe opérationnelle d'Hygiène	46.01 Epidémiologie, économie de la santé et prévention (option biologique)
Mme LEJAY Anne M0102		• Pôle de Pathologie thoracique - Service de Physiologie et d'Explorations fonctionnelles / NHC	44.02 Physiologie (Biologique)
LENORMAND Cédric M0103		• Pôle de Chirurgie maxillo-faciale, Morphologie et Dermatologie - Service de Dermatologie / Hôpital Civil	50.03 Dermato-Vénéréologie
LEPILLER Quentin M0104 (Dispo → 31.08.2018)		• Pôle de Biologie - Laboratoire de Virologie / PTM HUS et Faculté de Médecine	45.01 **Bactériologie-Virologie** ; Hygiène hospitalière (Biologique)
Mme LETSCHER-BRU Valérie M0045		• Pôle de Biologie - Laboratoire de Parasitologie et de Mycologie médicale / PTM HUS • Institut de Parasitologie / Faculté de Médecine	45.02 Parasitologie et mycologie (option biologique)
LHERMITTE Benoît M0115		• Pôle de Biologie - Service de Pathologie / Hôpital de Hautepierre	42.03 Anatomie et cytologie pathologiques
Mme LONSDORFER-WOLF Evelyne M0090		• Institut de Physiologie Appliquée - Faculté de Médecine • Pôle de Pathologie thoracique - Service de Physiologie et d'Explorations fonctionnelles / NHC	44.02 Physiologie
LUTZ Jean-Christophe M0046		• Pôle de Chirurgie plastique reconstructrice et esthétique, Chirurgie maxillo-faciale, Morphologie et Dermatologie - Serv. de Chirurgie Maxillo-faciale, plastique reconstructrice et esthétique/HC	55.03 Chirurgie maxillo-faciale et stomatologie
MEYER Alain M0093		• Institut de Physiologie / Faculté de Médecine • Pôle de Pathologie thoracique - Service de Physiologie et d'Explorations fonctionnelles / NHC	44.02 Physiologie (option biologique)
MIGUET Laurent M0047		• Pôle de Biologie - Laboratoire d'Hématologie biologique / Hôpital de Hautepierre et NHC	44.03 Biologie cellulaire (type mixte : biologique)
Mme MOUTOU Céline ép. GUNTHNER M0049	CS	• Pôle de Biologie - Laboratoire de Diagnostic préimplantatoire / CMCO Schiltigheim	54.05 Biologie et médecine du développement et de la reproduction (option biologique)
MULLER Jean M0050		• Pôle de Biologie - Laboratoire de Diagnostic génétique / Nouvel Hôpital Civil	47.04 Génétique (option biologique)
NOLL Eric M0111		• Pôle d'Anesthésie Réanimation Chirurgicale SAMU-SMUR - Service Anesthésiologie et de Réanimation Chirurgicale - Hôpital Hautepierre	48.01 **Anesthésiologie-Réanimation** ; Médecine d'urgence
Mme NOURRY Nathalie M0011		• Pôle de Santé publique et Santé au travail - Service de Pathologie professionnelle et de Médecine du travail - HC	46.02 Médecine et Santé au Travail (option clinique)
PELACCIA Thierry M0051		• Pôle d'Anesthésie / Réanimation chirurgicales / SAMU-SMUR - Service SAMU/SMUR	48.02 Réanimation et anesthésiologie Option : Médecine d'urgences
PENCREAC'H Erwan M0052		• Pôle de Biologie - Laboratoire de Biochimie et biologie moléculaire / Nouvel Hôpital Civil	44.01 Biochimie et biologie moléculaire
PFAFF Alexander M0053		• Pôle de Biologie - Laboratoire de Parasitologie et de Mycologie médicale / PTM HUS	45.02 Parasitologie et mycologie
Mme PITON Amélie M0094		• Pôle de Biologie - Laboratoire de Diagnostic génétique / NHC	47.04 Génétique (option biologique)
PREVOST Gilles M0057		• Pôle de Biologie - Institut (Laboratoire) de Bactériologie / PTM HUS et Faculté	45.01 Option : **Bactériologie**-virologie (biologique)
Mme RADOSAVLJEVIC Mirjana M0058		• Pôle de Biologie - Laboratoire d'Immunologie biologique / Nouvel Hôpital Civil	47.03 Immunologie (option biologique)
Mme REIX Nathalie M0095		• Pôle de Biologie - Labo. d'Explorations fonctionnelles par les isotopes / NHC • Institut de Physique biologique / Faculté de Médecine	43.01 Biophysique et médecine nucléaire
RIEGEL Philippe M0059		• Pôle de Biologie - Institut (Laboratoire) de Bactériologie / PTM HUS et Faculté	45.01 Option : **Bactériologie**-virologie (biologique)
ROGUE Patrick (cf. A2) M0060		• Pôle de Biologie - Laboratoire de Biochimie et biologie moléculaire / NHC	44.01 Biochimie et biologie moléculaire (option biologique)
ROMAIN Benoît M0061		• Pôle des Pathologies digestives, hépatiques et de la transplantation - Service de Chirurgie générale et Digestive / HP	53.02 Chirurgie générale
Mme RUPPERT Elisabeth M0106		• Pôle Tête et Cou - Service de Neurologie - Unité de Pathologie du Sommeil / Hôpital Civil	49.01 Neurologie
Mme SABOU Alina M0096		• Pôle de Biologie - Laboratoire de Parasitologie et de Mycologie médicale / PTM HUS • Institut de Parasitologie / Faculté de Médecine	45.02 Parasitologie et mycologie (option biologique)
Mme SAMAMA Brigitte M0062		• Institut d'Histologie / Faculté de Médecine	42.02 Histologie, Embryologie et Cytogénétique (option biologique)
Mme SCHNEIDER Anne M0107		• Pôle médico-chirurgical de Pédiatrie - Service de Chirurgie pédiatrique / Hôpital de Hautepierre	54.02 Chirurgie Infantile
SCHRAMM Frédéric M0068		• Pôle de Biologie - Institut (Laboratoire) de Bactériologie / PTM HUS et Faculté	45.01 Option : **Bactériologie** -virologie (biologique)

NOM et Prénoms	CS*	Services Hospitaliers ou Institut / Localisation	Sous-section du Conseil National des Universités	
Mme SORDET Christelle M0069		• Pôle de Médecine Interne, Rhumatologie, Nutrition, Endocrinologie, Diabétologie (MIRNED) - Service de Rhumatologie / Hôpital de Hautepierre	50.01	Rhumatologie
TALHA Samy M0070		• Pôle de Pathologie thoracique - Service de Physiologie et explorations fonctionnelles / NHC	44.02	Physiologie (option clinique)
Mme TALON Isabelle M0039		• Pôle médico-chirurgical de Pédiatrie - Service de Chirurgie Infantile / Hôpital Hautepierre	54.02	Chirurgie infantile
TELETIN Marius M0071		• Pôle de Biologie - Service de Biologie de la Reproduction / CMCO Schiltigheim	54.05	Biologie et médecine du développement et de la reproduction (option biologique)
Mme URING-LAMBERT Béatrice M0073		• Institut d'Immunologie / HC • Pôle de Biologie - Laboratoire d'Immunologie biologique / Nouvel Hôpital Civil	47.03	Immunologie (option biologique)
VALLAT Laurent M0074		• Pôle de Biologie - Laboratoire d'Hématologie Biologique - Hôpital de Hautepierre	47.01	**Hématologie** ; Transfusion Option Hématologie Biologique
Mme VILLARD Odile M0076		• Pôle de Biologie - Labo. de Parasitologie et de Mycologie médicale / PTM HUS et Fac	45.02	Parasitologie et mycologie (option biologique)
Mme WOLF Michèle M0010		• Chargé de mission - Administration générale - Direction de la Qualité / Hôpital Civil	48.03	Option : Pharmacologie fondamentale
Mme ZALOSZYC Ariane ép. MARCANTONI M0116		• Pôle Médico-Chirurgical de Pédiatrie - Service de Pédiatrie I / Hôpital de Hautepierre	54.01	Pédiatrie
ZOLL Joffrey M0077		• Pôle de Pathologie thoracique - Service de Physiologie et d'Explorations fonctionnelles / HC	44.02	Physiologie (option clinique)

B2 - PROFESSEURS DES UNIVERSITES (monoappartenant)

Pr BONAH Christian	P0166	Département d'Histoire de la Médecine / Faculté de Médecine	72.	Epistémologie - Histoire des sciences et des techniques
Mme la Pre RASMUSSEN Anne	P0186	Département d'Histoire de la Médecine / Faculté de Médecine	72.	Epistémologie - Histoire des Sciences et des techniques

B3 - MAITRES DE CONFERENCES DES UNIVERSITES (monoappartenant)

Mr KESSEL Nils		Département d'Histoire de la Médecine / Faculté de Médecine	72.	Epistémologie - Histoire des Sciences et des techniques
Mr LANDRE Lionel		ICUBE-UMR 7357 - Equipe IMIS / Faculté de Médecine	69.	Neurosciences
Mme THOMAS Marion		Département d'Histoire de la Médecine / Faculté de Médecine	72.	Epistémologie - Histoire des Sciences et des techniques
Mme SCARFONE Marianna	M0082	Département d'Histoire de la Médecine / Faculté de Médecine	72.	Epistémologie - Histoire des Sciences et des techniques

B4 - MAITRE DE CONFERENCE DES UNIVERSITES DE MEDECINE GENERALE

Mme CHAMBE Juliette	M0108	Département de Médecine générale / Faculté de Médecine	53.03	Médecine générale (01.09.15)

C - ENSEIGNANTS ASSOCIES DE MEDECINE GENERALE

C1 - PROFESSEURS ASSOCIES DES UNIVERSITES DE M. G. (mi-temps)

Pr Ass. GRIES Jean-Luc	M0084	Médecine générale (01.09.2017)
Pr Ass. KOPP Michel	P0167	Médecine générale (depuis le 01.09.2001, renouvelé jusqu'au 31.08.2016)
Pr Ass. LEVEQUE Michel	P0168	Médecine générale (depuis le 01.09.2000 ; renouvelé jusqu'au 31.08.2018)

C2 - MAITRE DE CONFERENCES DES UNIVERSITES DE MEDECINE GENERALE - TITULAIRE

Dre CHAMBE Juliette	M0108	53.03 Médecine générale (01.09.2015)

C3 - MAITRES DE CONFERENCES ASSOCIES DES UNIVERSITES DE M. G. (mi-temps)

Dre BERTHOU anne	M0109	Médecine générale (01.09.2015 au 31.08.2018)
Dr BREITWILLER-DUMAS Claire		Médecine générale (01.09.2016 au 31.08.2019)
Dr GUILLOU Philippe	M0089	Médecine générale (01.11.2013 au 31.08.2016)
Dr HILD Philippe	M0090	Médecine générale (01.11.2013 au 31.08.2016)
Dr ROUGERIE Fabien	M0097	Médecine générale (01.09.2014 au 31.08.2017)

D - ENSEIGNANTS DE LANGUES ETRANGERES

D1 - PROFESSEUR AGREGE, PRAG et PRCE DE LANGUES

Mme ACKER-KESSLER Pia	M0085	Professeure certifiée d'Anglais (depuis 01.09.03)
Mme CANDAS Peggy	M0086	Professeure agrégée d'Anglais (depuis le 01.09.99)
Mme SIEBENBOUR Marie-Noëlle	M0087	Professeure certifiée d'Allemand (depuis 01.09.11)
Mme JUNGER Nicole	M0088	Professeure certifiée d'Anglais (depuis 01.09.09)
Mme MARTEN Susanne	M0098	Professeure certifiée d'Allemand (depuis 01.09.14)

E - PRATICIENS HOSPITALIERS - CHEFS DE SERVICE NON UNIVERSITAIRES

Dr ASTRUC Dominique	NRPô	• Pôle médico-chirurgical de Pédiatrie
	CS	- Serv. de Néonatalogie et de Réanimation néonatale (Pédiatrie 2) / Hôpital de Hautepierre
Dr ASTRUC Dominique (par intérim)	NRPô	• Pôle médico-chirurgical de Pédiatrie
	CS	- Service de Réanimation pédiatrique spécialisée et de surveillance continue / Hôpital de Hautepierre
Dr CALVEL Laurent	NRPô	• Pôle Spécialités médicales - Ophtalmologie / SMO
	CS	- Service de Soins Palliatifs / NHC et Hôpital de Hautepierre
Dr DELPLANCQ Hervé	NRPô	- SAMU-SMUR
	CS	
Dr GARBIN Olivier	CS	- Service de Gynécologie-Obstétrique / CMCO Schiltigheim
Dre GAUGLER Elise	NRPô	• Pôle Spécialités médicales - Ophtalmologie / SMO
	CS	- UCSA - Centre d'addictologie / Nouvel Hôpital Civil
Dre GERARD Bénédicte	NRPô	• Pôle de Biologie
	CS	- Département de génétique / Nouvel Hôpital Civil
Mme GOURIEUX Bénédicte	RPô	• Pôle de Pharmacie-pharmacologie
	CS	- Service de Pharmacie-Stérilisation / Nouvel Hôpital Civil
Dr KARCHER Patrick	NRPô	• Pôle de Gériatrie
	CS	- Service de Soins de suite de Longue Durée et d'hébergement gériatrique / EHPAD / Hôpital de la Robertsau
Pr LESSINGER Jean-Marc	NRPô	• Pôle de Biologie
	CS	- Laboratoire de Biologie et biologie moléculaire / Nouvel Hôpital Civil + Hautepierre
Mme Dre LICHTBLAU Isabelle	NRpô	• Pôle de Biologie
	Resp	- Laboratoire de biologie de la reproduction / CMCO de Schiltigheim
Mme Dre MARTIN-HUNYADI	NRPô	• Pôle de Gériatrie
Catherine	CS	- Secteur Evaluation / Hôpital de la Robertsau
Dr NISAND Gabriel	RPô	• Pôle de Santé Publique et Santé au travail
	CS	- Service de Santé Publique - DIM / Hôpital Civil
Dr REY David	NRPô	• Pôle Spécialités médicales - Ophtalmologie / SMO
	CS	- «Le trait d'union» - Centre de soins de l'infection par le VIH / Nouvel Hôpital Civil
Dr TCHOMAKOV Dimitar	NRPô	• Pôle Médico-chirurgical de Pédiatrie
	CS	- Service des Urgences Médico-Chirurgicales pédiatriques - HP
Mme Dre TEBACHER-ALT Martine	NRPô	• Pôle d'Activité médico-chirurgicale Cardio-vasculaire
	NCS	- Service de Maladies vasculaires et Hypertension
	Resp	- Centre de pharmacovigilance / Nouvel Hôpital Civil
Mme Dre TOURNOUD Christine	NRPô	• Pôle Urgences - Réanimations médicales / Centre antipoison
	CS	- Centre Antipoison-Toxicovigilance / Nouvel Hôpital Civil

F1 - PROFESSEURS ÉMÉRITES

- ***de droit et à vie*** *(membre de l'Institut)*
  CHAMBON Pierre (Biochimie et biologie moléculaire)
- *pour trois ans (1er septembre 2015 au 31 août 2018)* BERTHEL Marc (Gériatrie)
  BURSZTEJN Claude (Pédo-psychiatrie)
  HASSELMANN Michel (Réanimation médicale)
  POTTECHER Thierry (Anesthésie-Réanimation)
- *pour trois ans (1er septembre 2016 au 31 août 2019)* BOUSQUET Pascal
  PINGET Michel
- *pour trois ans (1er septembre 2017 au 31 août 2020)*
  BELLOCQ Jean-Pierre (Anatomie Cytologie pathologique)
  CHRISTMANN Daniel (Maladies Infectieuses et tropicales) MULLER André (Thérapeutique)

F2 - PROFESSEUR des UNIVERSITES ASSOCIE (mi-temps)

M. SOLER Luc	CNU-31	IRCAD (01.09.2009 - 30.09.2012 / renouvelé 01.10.2012-30.09.2015-30.09.2018)

F3 - PROFESSEURS CONVENTIONNÉS* DE L'UNIVERSITE

Dr BRAUN Jean-Jacques	ORL (2012-2013 / 2013-2014 / 2014-2015 / 2015-2016)
Dr CALVEL Laurent	Soins palliatifs (2016-2017 / 2017-2018)
Pr CHARRON Dominique	Université Paris Diderot (2016-2017)
Mme GUI Yali	(Shaanxi/Chine) (2016-2017)
Mme Dre GRAS-VINCENDON Agnès	Pédopsychiatrie (2013-2014 / 2014-2015 / 2015-2016)
Dr JENNY Jean-Yves	Chirurgie orthopédique (2014-2015 / 2015-2016 / 2016-2017)
Mme KIEFFER Brigitte	IGBMC (2014-2015 / 2015-2016 / 2016-2017)
Dr KINTZ Pascal	Médecine Légale (2016-2017 / 2017-2018)
Dr LAND Walter G.	Immunologie (2013-2014 à 2015-2016 / 2016-2017)
Dr LANG Jean-Philippe	Psychiatrie (2015-2016 / 2016-2017)
Dr LECOCQ Jehan	IURC - Clémenceau (2016-2017 / 2017-2018)
Dr REIS Jacques	Neurologie (2017-2018)
Pr REN Guo Sheng	(Chongqing / Chine) / Oncologie (2014-2015 à 2016-2017)
Dr RICCO Jean-Baptiste	CHU Poitiers (2017-2018)
Dr SALVAT Eric	Centre d'Evaluation et de Traitement de la Douleur (2016-2017 / 2017-2018)

(* 4 années au maximum)

G1 - PROFESSEURS HONORAIRES

ADLOFF Michel (Chirurgie digestive) / 01.09.94
BABIN Serge (Orthopédie et Traumatologie) / 01.09.01
BAREISS Pierre (Cardiologie) / 01.09.12
BATZENSCHLAGER André (Anatomie Pathologique) / 01.10.95
BAUMANN René (Hépato-gastro-entérologie) / 01.09.10
BERGERAT Jean-Pierre (Cancérologie) / 01.01.16
BIENTZ Michel (Hygiène) / 01.09.2004
BLICKLE Jean-Frédéric (Médecine Interne) / 15.10.2017
BLOCH Pierre (Radiologie) / 01.10.95
BOURJAT Pierre (Radiologie) / 01.09.03 BRECHENMACHER Claude (Cardiologie) / 01.07.99 BRETTES Jean-Philippe (Gynécologie-Obstétrique) / 01.09.10 BROGARD Jean-Marie (Médecine interne) / 01.09.02 BUCHHEIT Fernand (Neurochirurgie) / 01.10.99 BURGHARD Guy (Pneumologie) / 01.10.86
CANTINEAU Alain (Medecine et Santé au travail) / 01.09.15 CAZENAVE Jean-Pierre (Hématologie) / 01.09.15
CHAMPY Maxime (Stomatologie) / 01.10.95 CINQUALBRE Jacques (Chirurgie générale) / 01.10.12 CLAVERT Jean-Michel (Chirurgie infantile) / 31.10.16 COLLARD Maurice (Neurologie) / 01.09.00
CONRAUX Claude (Oto-Rhino-Laryngologie) / 01.09.98
CONSTANTINESCO André (Biophysique et médecine nucléaire) /01.09.11 DIETEMANN Jean-Louis (Radiologie) / 01.09.17 DOFFOEL Michel (Gastroentérologie) / 01.09.17
DORNER Marc (Médecine Interne) / 01.10.87
DUPEYRON Jean-Pierre (Anesthésiologie-Réa.Chir.) / 01.09.13
EISENMANN Bernard (Chirurgie cardio-vasculaire) / 01.04.10
FABRE Michel (Cytologie et histologie) / 01.09.02 FISCHBACH Michel (Pédiatrie / 01.10.2016) FLAMENT Jacques (Ophtalmologie) / 01.09.2009
GAY Gérard (Hépato-gastro-entérologie) / 01.09.13
GERLINGER Pierre (Biol. de la Reproduction) / 01.09.04
GRENIER Jacques (Chirurgie digestive) / 01.09.97
GROSSHANS Edouard (Dermatologie) / 01.09.03 GUT Jean-Pierre (Virologie) / 01.09.14
HAUPTMANN Georges (Hématologie biologique) / 01.09.06
HEID Ernest (Dermatologie) / 01.09.04
IMBS Jean-Louis (Pharmacologie) / 01.09.2009
IMLER Marc (Médecine interne) / 01.09.98
JACQMIN Didier (Urologie) / 09.08.17
JAECK Daniel (Chirurgie générale) / 01.09.11
JAEGER Jean-Henri (Chirurgie orthopédique) /01.09.2011
JESEL Michel (Médecine physique et réadaptation) / 01.09.04
KEHR Pierre (Chirurgie orthopédique) / 01.09.06
KEMPF François (Radiologie) / 12.10.87
KEMPF Ivan (Chirurgie orthopédique) / 01.09.97
KEMPF Jules (Biologie cellulaire) / 01.10.95
KIRN André (Virologie) / 01.09.99
KREMER Michel (Parasitologie) / 01.05.98
KRIEGER Jean (Neurologie) / 01.01.07
KUNTZ Jean-Louis (Rhumatologie) / 01.09.08
KUNTZMANN Francis (Gériatrie) / 01.09.07
KURTZ Daniel (Neurologie) / 01.09.98
LANG Gabriel (Orthopédie et traumatologie) / 01.10.98 LANG Jean-Marie (Hématologie clinique) /01.09.2011 LEVY Jean-Marc (Pédiatrie) / 01.10.95
LONSDORFER Jean (Physiologie) / 01.09.10 LUTZ Patrick (Pédiatrie) / 01.09.16
MAILLOT Claude (Anatomie normale) / 01.09.03 MAITRE Michel (Biochimie et biol. moléculaire) / 01.09.13
MANDEL Jean-Louis (Génétique) / 01.09.16
MANGIN Patrice (Médecine Légale) / 01.12.14 MANTZ Jean-Marie (Réanimation médicale) / 01.10.94
MARESCAUX Jacques (Chirurgie digestive) / 01.09.16
MARK Jean-Joseph (Biochimie et biologie cellulaire) / 01.09.99
MESSER Jean (Pédiatrie) / 01.09.07
MEYER Christian (Chirurgie générale) / 01.09.13
MEYER Pierre (Biostatistiques, informatique méd.) / 01.09.10
MINCK Raymond (Bactériologie) / 01.10.93
MONTEIL Henri (Bactériologie) / 01.09.2011 MOSSARD Jean-Marie (Cardiologie) / 01.09.2009 OUDET Pierre (Biologie cellulaire) / 01.09.13 PASQUALI Jean-Louis (Immunologie clinique) / 01.09.15 PATRIS Michel (Psychiatrie) / 01.09.15
Mme PAULI Gabrielle (Pneumologie) / 01.09.2011
REYS Philippe (Chirurgie générale) / 01.09.98 RITTER Jean (Gynécologie-Obstétrique) / 01.09.02 ROEGEL Emile (Pneumologie) / 01.04.90 RUMPLER Yves (Biol. développement) / 01.09.10 SANDNER Guy (Physiologie) / 01.09.14 SAUVAGE Paul (Chirurgie infantile) / 01.09.04 SCHAFF Georges (Physiologie) / 01.10.95 SCHLAEDER Guy (Gynécologie-Obstétrique) / 01.09.01 SCHLIENGER Jean-Louis (Médecine Interne) / 01.08.11 SCHRAUB Simon (Radiothérapie) / 01.09.12
SCHWARTZ Jean (Pharmacologie) / 01.10.87 SICK Henri (Anatomie Normale) / 01.09.06

STIERLE Jean-Luc (ORL) / 01.09.10
STOLL Claude (Génétique) / 01.09.2009
STOLL-KELLER Françoise (Virologie) / 01.09.15
STORCK Daniel (Médecine interne) / 01.09.03
TEMPE Jean-Daniel (Réanimation médicale) / 01.09.06
TONGIO Jean (Radiologie) / 01.09.02
TREISSER Alain (Gynécologie-Obstétrique / 24.03.08
VAUTRAVERS Philippe (Médecine physique et réadaptation) / 01.09.16 VETTER Jean-Marie (Anatomie pathologique) / 01.09.13
VINCENDON Guy (Biochimie) / 01.09.08
WALTER Paul (Anatomie Pathologique) / 01.09.09
WEITZENBLUM Emmanuel (Pneumologie) /01.09.11
WIHLM Jean-Marie (Chirurgie thoracique) / 01.09.13
WILK Astrid (Chirurgie maxillo-faciale) / 01.09.15
WILLARD Daniel (Pédiatrie) / 01.09.96
WITZ JEAN-Paul (Chirurgie thoracique) / 01.10.90

Légende des adresses :

FAC : Faculté de Médecine : 4, rue Kirschleger - F - 67085 Strasbourg Cedex - Tél. : 03.68.85.35.20 - Fax : 03.68.85.35.18 ou 03.68.85.34.67
HOPITAUX UNIVERSITAIRES DE STRASBOURG (HUS) :
- NHC : ***Nouvel Hôpital Civil :*** 1, place de l'Hôpital - BP 426 - F - 67091 Strasbourg Cedex - Tél. : 03 69 55 07 08
- HC : ***Hôpital Civil :*** 1, Place de l'Hôpital - B.P. 426 - F - 67091 Strasbourg Cedex - Tél. : 03.88.11.67.68
- HP : ***Hôpital de Hautepierre :*** Avenue Molière - B.P. 49 - F - 67098 Strasbourg Cedex - Tél. : 03.88.12.80.00
- ***Hôpital de La Robertsau :*** 83, rue Himmerich - F - 67015 Strasbourg Cedex - Tél. : 03.88.11.55.11
- ***Hôpital de l'Elsau :*** 15, rue Cranach - 67200 Strasbourg - Tél. : 03.88.11.67.68

CMCO - Centre Médico-Chirurgical et Obstétrical : 19, rue Louis Pasteur - BP 120 - Schiltigheim - F - 67303 Strasbourg Cedex - Tél. : 03.88.62.83.00
C.C.O.M. - Centre de Chirurgie Orthopédique et de la Main : 10, avenue Baumann - B.P. 96 - F - 67403 Illkirch Graffenstaden Cedex - Tél. : 03.88.55.20.00
E.F.S. : Etablissement Français du Sang - Alsace : 10, rue Spielmann - BP N°36 - 67065 Strasbourg Cedex - Tél. : 03.88.21.25.25
Centre Régional de Lutte contre le cancer "Paul Strauss" - 3, rue de la Porte de l'Hôpital - F-67085 Strasbourg Cedex - Tél. : 03.88.25.24.24
IURC - Institut Universitaire de Réadaptation Clemenceau - CHU de Strasbourg et UGECAM (Union pour la Gestion des Etablissements des Caisses d'Assurance Maladie) - 45 boulevard Clemenceau - 67082 Strasbourg Cedex

---

RESPONSABLE DE LA BIBLIOTHÈQUE DE MÉDECINE ET ODONTOLOGIE ET DU DÉPARTEMENT SCIENCES, TECHNIQUES ET SANTÉ DU SERVICE COMMUN DE DOCUMENTATION DE L'UNIVERSITÉ DE STRASBOURG

Monsieur Olivier DIVE, Conservateur

LA FACULTÉ A ARRETÉ QUE LES OPINIONS ÉMISES DANS LES DISSERTATIONS QUI LUI SONT PRÉSENTÉES DOIVENT ETRE CONSIDERÉES COMME PROPRES A LEURS AUTEURS ET QU'ELLE N'ENTEND NI LES APPROUVER, NI LES IMPROUVER

SERMENT D'HIPPOCRATE

En présence des maîtres de cette école, de mes chers condisciples, je promets et je jure au nom de l'Etre suprême d'être fidèle aux lois de l'honneur et de la probité dans l'exercice de la médecine. Je donnerai mes soins gratuits à l'indigent et n'exigerai jamais un salaire au-dessus de mon travail.

Admise à l'intérieur des maisons, mes yeux ne verront pas ce qui s'y passe.

Ma langue taira les secrets qui me seront confiés et mon état ne servira pas à corrompre les mœurs ni à favoriser les crimes.

Respectueuse et reconnaissante envers mes maîtres je rendrai à leurs enfants l'instruction que j'ai reçue de leurs pères.

Que les hommes m'accordent leur estime si je suis restée fidèle à mes promesses. Que je sois couverte d'opprobre et méprisée de mes confrères si j'y manque.

REMERCIEMENTS

Au Professeur Georges NOEL,
Je vous remercie pour votre soutien, votre patience et votre très grande disponibilité tout au long de ce travail. Merci de m'avoir accompagnée pendant mes sept années d'internat et d'avoir partagé avec moi votre savoir, toujours source de motivation et d'inspiration.

Au Professeur Jean-Marc CONSTANS,
Je vous remercie pour l'accueil que vous m'avez réservé lors de mes séjours à Amiens, pour votre grande disponibilité, vos bons conseils et votre aide précieuse dans l'élaboration et l'aboutissement de ma thèse. Ce fut un plaisir de vous rencontrer et de travailler avec vous.

Au Professeur François PROUST,
Je vous remercie de m'avoir fait l'honneur d'accepter de prendre part au jury de ma thèse. Je vous remercie également pour la relecture attentive de mon travail et vos encouragements.

Au Docteur Delphine ANTONI,
Je te remercie pour ta présence à mes côtés tout au long de ces années d'internat, pour ton soutien, ta bienveillance et ton enseignement. Je te remercie également pour ton aide, tes corrections et commentaires sur mon travail de thèse.

Au Docteur Hélène CEBULA,
Je vous remercie de m'avoir fait l'honneur d'accepter de faire partie de mon jury de thèse et d'avoir jugé mon travail. Merci pour vos précieux conseils, vos corrections et vos réponses rapides à chacune de mes questions.

Au Docteur Benoit LHERMITTE,
Je vous remercie pour votre participation et pour votre aide au recueil de données et à l'écriture des articles. Merci de vous être rendu disponible à plusieurs reprises pour me rencontrer et répondre à mes questions.

Au Professeur Xavier PIVOT,
Je vous remercie de m'accueillir au sein de votre équipe en tant que CCU-AH et de me faire participer à l'aventure ICANS.

Au Docteur Alicia THIERY,
Merci pour ton soutien et ta très grande disponibilité tout au long de ce travail. Merci d'avoir toujours répondu présente à mes appels de détresse statistique et de m'avoir rassurée avec ton franc parlé et ta bonne humeur.

Au Docteur Éric GUERIN,
Merci pour votre aide précieuse dans l'élaboration initiale du projet, le recueil de données et la réalisation des analyses complémentaires.

Un très grand merci au Docteur Audrey Keller, au Dr Roland Schott, au Dr Guido Ahle, au Docteur Benjamin Leroy-Freschini, au Docteur Caroline Bund et au Docteur Pierre Wagner.

Un grand merci à l'ensemble des médecins du service de radiothérapie du Centre Paul Strauss.

Merci à l'ensemble du service de radiothérapie pour m'avoir accompagnée tous au long de mes différents projets.

Merci à Marie T. et Laure D. pour ce semestre d'onco inoubliable.

Merci à Hélène et Anaïs pour m'avoir si bien accueillie au sein du laboratoire de recherche.

Merci à Christophe, Marion et Agnieszka, qui m'ont fait vivre une année de M2 incroyable.

A mes co-internes : Youssef, Waisse, Benjamin, Yvan, Agathe, Véronique, Thomas, Philippe, Justine, Laure S. et Martin. Merci pour ces très belles années.

A mes co-internes qui m'ont supportée cette année : Joffrey (le vieil ORL), Isabelle (la Zaza de l'espace), Guillaume (le BG), Adrien (l'ébouriffé du balai), Christian (le plus beau et le meilleur de tous), Cécile (l'aventurière en gilet de sauvetage), Maxime (l'Homme du Sud) et Camille (la Miss Léo). Merci pour votre soutien tout au long de cette dernière ligne droite.

A ma Chloé-Line, merci d'avoir partagé ces derniers moments d'internat, merci pour ton soutien, merci d'avoir été là pour moi.

A mes trois amies Sophie, Inès et Audrey, je vous adore !

A Pti Bouc, Chacha, K*, Popo, Moumoutte et Julie.

A mon Gouzille et ma Touf.

A Jelena, ma plus belle rencontre.

A ma famille.

A Caroline, ma grande sœur de cœur.

A Jean-Baptiste, mon grand Amour.

A Ambre, ma beauté suprême de l'infini, mon petit rayon de soleil qui illumine mes jours (comme mes nuits…).

TABLE DES MATIERES

MEASUREMENTS OF VOLUMETRIC TUMOR SIZE IN GLIOBLASTOMA: 3D DIAMETERS VOLUME MEASUREMENTS VERSUS DELINEATED VOLUME MEASUREMENTS, STUDY ON 114 MRI

PREDICTIVE FACTORS OF PSEUDOPROGRESSION VERSUS TRUE PROGRESSION IN PATIENTS TREATED WITH SURGERY AND CHEMORADIOTHERAPY FOR GLIOBLASTOMA: A RETROSPECTIVE STUDY OF 57 PATIENTS

LISTE DES ABREVIATIONS

ADC: Apparent Diffusion Coefficient

AMT: Methyl-L-Tryptophan

APTW: Amide Proton Transfer-Weighted

ASL: Arterial Spin Labeling

ATRX: Alpha-Thalassemia/mental Retardation syndrome X-linked

BG: Background

BPTI: International Brain Tumor Imaging

CBF: Cerebral Blood Flow

CBV: Cerebral Blood Volume

CE: Contrast Enhancement

CEL: contrast enhanced lesion

CI: Confidence Interval

Cho: Choline

Cr: Creatinine

CR: Complete Response

CRT: Chemoradiotherapy

CT: Computed Tomography

CTC: Circulating Tumor Cells

CTV: Clinical Target Volume

CV: Calculated Volume

DCE: Dynamic Contrast Enhanced

DMSA: Dimercaptosuccinic Acid

DSC: Dynamic Susceptibility Contrast

DTI: Diffusion Tensor Imaging

DWI: Diffusion Weight Imaging

EES: Extravascular extracellular space

EGFR: Epidermal Growth Factor Receptor

EV: Extracellular Vesicles

FA: Fractional Anisotropy

FBPA: Fluoro-Borono-Phenylalanine

FDOPA: Fluoro-L-Dopa

FDG: Fluoro-Deoxy-Glucose

FET: Fluoroethyl-L-Tyrosine

FLT: Fluorothymidine

FMISO: Fluoromisonidazole

FTB: Fractional Tumor Burden

GBM: Glioblastoma

GHA: Glucoheptonate

GTV: Gross Target Volume

HGG: High Grade Glioma

IDH: Isocitrate Deshydrogenase

IMRT: Intensity Modulated Radiation Therapy

IMT: Iodine-Methyl Tyrosine

$\mathbf{K_{ep}}$: Transfer constant from the extracellular-extravascular space into the plasma

KPS: Karnofsky Performance Status

$\mathbf{K^{trans}}$: Volume Transfer Constant

Lact: Lactate

Lip: Lipid

MET: Methyl-L-Methionine

MGMT: Methylguanine-Methyltransferase

MMSE: Mini Mental Status

MRI: Magnetic Resonance Imaging

MRS: Magnetic Resonance Spectroscopy

MV: Measured Volume

NA: Not available

NAA: N-acetylaspartate

NANO: Neurologic Assessment in Neuro-oncology

NCCN: National Comprehensive Cancer Network

NEC: Necrosis Area

NR: Not reached

OS: Overall Survival

PD: Progressive Disease

PET: Positron Emission Tomography

PFS: Progression Free Survival

PH: Peak Height

PPS: Post-Progression Survival

PR: Partial Response

PRM: Parametric Response Map

PRO: Patient Reported Outcome

PsP: Pseusoprogression

PsR: Pseudoresponse

PSR: Percentage of Signal intensity Recovery

PTV: Planning Target Volume

RANO: Response Assessment in Neuro-Oncology

RN: Radionecrosis

RPA: Recursive Partitioning Analysis

RT: Radiotherapy

SD: Stable Disease

SP: Suspicious of Progression

SPECT: Single Photon Emission Computed Tomography

SUV: Standardized Uptake Value

SWI: Susceptibility-weighted imaging

TAC: Time Activity Curve

TBR: Tumor to Brain Ratio

TF: Tetrofosmin

TMZ: Temozolomide

TNR: Tumor-to-Normal brain Ratio

TP: True Progression

TP 53: Tumor Protein 53

TTP: Time to Progression

VAS: Visual Analog Scale

$\mathbf{V_e}$: Volume of extravascular-extracellular space

$\mathbf{V_p}$: Vascular plasma volume

VVMC: Volume-weighted Voxel-based Multiparametric Clustering

WHO: World Health Classification

INTRODUCTION GENERALE

Le glioblastome est la tumeur cérébrale primitive de l'adulte la plus fréquente et représente environ 60% de l'ensemble des gliomes. Même si le pronostic du glioblatome reste sombre et incertain, la chimioradiothérapie concomitante selon le protocole de l'EORTC/NCIC, devenue le standard thérapeutique, a permis d'améliorer la médiane de survie des patients jusqu'à 18 mois. Après une chimioradiothérapie, entre 3% et 50% des patients présenteraient une pseudoprogression, apparaissant le plus souvent dans les six mois suivant le traitement. Il n'existe pas de définition universelle de la pseudoprogression. Elle est le plus souvent considérée comme l'apparition ou l'augmentation transitoire de la prise de contraste sur l'IRM en séquence T1 avec injection de gadolinium, mimant une vraie progression. Le diagnostic de pseudoprogression versus vraie progression est un réel dilemme en routine clinique et nécessite une décision thérapeutique adaptée. En effet, en cas de pseudoprogression, le traitement par temozolomide adjuvant doit être poursuivi ou le suivi du patient maintenu. A l'inverse, en cas de vraie progression, une nouvelle chirurgie, une chimiothérapie de seconde ligne ou une réirradiation doivent être discutées. Un diagnostic excessif de vraie progression peut mener à l'arrêt d'un traitement efficace ou à une chirurgie inutile. Au contraire, un diagnostic excessif de pseudoprogression conduit à poursuivre un traitement inefficace. Le diagnostic de certitude de pseudoprogression est histologique. Cependant, c'est par l'IRM conventionnelle, qui demeure l'examen de référence pour le suivi des patients, que le diagnostic est fréquemment posé. Il a pourtant été prouvé que la concordance radio-histologique pour le diagnostic de pseudoprogression ne dépassait pas 50%. Pour guider le diagnostic et la décision thérapeutique, certains critères existent, notamment les critères de RANO ou les critères de RANO modifiés. De plus, les imageries multimodales associant IRM conventionnelle, IRM de diffusion, IRM de perfusion, spectroscopie ou encore PET-scanner peuvent être d'une grande aide, apportant

des données anatomiques, cellulaires, biologiques et métaboliques. Il en est de même pour les données histopathologiques et génomiques. Il a d'ailleurs été démontré une plus grande incidence de pseudoprogression en cas de méthylation du promoteur de MGMT. L'accessibilité et la réalisation de ces différents examens complémentaires restent, à ce jour, insuffisantes. Les données actuelles de la littérature ne permettent pas de définir des facteurs prédictifs spécifiques de pseudoprogression du fait d'une grande hétérogénéité de méthodologie et de résultats. Le clinicien est donc toujours confronté, dans sa pratique quotidienne, à la difficulté de distinguer vraie progression et pseudoprogression.

Le but du travail était d'identifier des facteurs prédictifs de pseudoprogression afin d'améliorer son diagnostic et de guider le clinicien dans la décision thérapeutique. Pour ce faire, une revue exhaustive de la littérature a été entreprise et présentée en deux parties : la première concernait les marqueurs cliniques et histologiques de pseudoprogression, et la seconde, présentait les différentes techniques d'imagerie et les potentiels biomarqueurs de pseudoprogression. Par la suite, une étude portant sur 57 patients atteints d'un glioblastome, traités selon le protocole EORTC/NCIC, a été menée, permettant d'identifier certains facteurs prédictifs potentiels de pseudoprogression. D'autre part, une étude parallèle a comparé deux méthodes d'estimation du volume des différents compartiments tumoraux du glioblastome, permettant ainsi de conclure à la possible utilisation d'une méthode basée sur le calcul (volume d'une ellipse) pour estimer le volume tumoral, plus rapide et pratique que le contourage manuel. Au final, ce travail a permis l'élaboration d'un score de probabilité de pseudoprogression, faisant aide au diagnostic de pseudoprogression versus vraie progression afin de faciliter la décision thérapeutique du clinicien dans sa pratique courante.

Pseudoprogression versus true progression in patients treated with surgery and chemoradiotherapy for glioblastoma: multi-approach literature review

Part 1 – Clinical, pathological features and markers, impact on survival

Résumé

Avec les nouveaux protocoles thérapeutiques, l'incidence des images IRM suspectes de progression a augmenté chez les patients traités pour un glioblastome. On parle alors de pseudoprogression. La pseudoprogression doit être différenciée de la vraie progression. En effet, en cas de pseudoprogression, il est admis de maintenir la surveillance ou de poursuivre le traitement par temozolomide, le patient étant considéré comme stable. A l'inverse, en cas de vraie progression, un nouveau traitement doit être discuté. Actuellement, le diagnostic de certitude de pseudoprogression nécessite une confirmation histologique. Cependant, elle est loin d'être systématique, le diagnostic étant le plus souvent radiologique. Des critères d'aide au diagnostic existent mais restent limités. Le but de cette revue de la littérature était de présenter les marqueurs cliniques et histologiques de pseudoprogression.

Mots clés

Facteurs prédictifs, Glioblastome, MGMT, Progression, Pseudoprogression, Survie globale

Pseudoprogression versus true progression in patients treated with surgery and chemoradiotherapy for glioblastoma: multi-approach literature review

Part 1 – Clinical, pathological features and markers, impact on survival

Clara Le Fèvre[1], MSc, Benoit Lhermitte[2], Guido Ahle[3], MD, Isabelle Chambrelant[1], MSc, Hélène Cebula[4], MD MSc, Delphine Antoni[1], MD MSc, Audrey Keller[1], MD, Roland Schott[5], MD, MSc, Alicia Thiery[6], MD MSc, Georges Noël[1,*], MD PhD.

[1] Department of radiotherapy, Comprehensive Cancer Center Paul Strauss, UNICANCER, 3 rue de la porte de l'Hôpital, 67065 Strasbourg Cedex, France.

[2] Département of Pathology, Hautepierre University Hospital, 1, avenue Molière, 67200 Strasbourg, France

[3] Departement of Neurology, Hôpitaux Civils de Colmar, 39 Avenue de la Liberté, 68024 Colmar, France

[4] Departement of Neurosurgery, Hautepierre University Hospital, 1, avenue Molière, 67200 Strasbourg, France

[5] Departement of medical oncology, comprehensive cancer center Paul Strauss, UNICANCER, 3 rue de la porte de l'Hôpital, 67065 Strasbourg Cedex, France.

[6] Department of public health, comprehensive cancer center Paul Strauss, UNICANCER, 3 rue de la porte de l'Hôpital, 67065 Strasbourg Cedex, France.

*: Corresponding author: Pr Georges NOEL, same address, gnoel@strasbourg.unicancer.fr

Abstract

With the new therapeutic protocols, more patients treated for a glioblastoma have experienced a suspicious image of progression (termes pseudoprogression) during follow-up. Pseudoprogression should be differentiated from true progression because management is completely different. In the case of pseudoprogression, the follow-up continues and the patient is considered as stable. In the case of true progression, a treatment adjustment is necessary. Presently, pseudoprogression diagnosis certainly needs a pathological confirmation. Some important efforts in radiological, histopathological, and genomic fields have been made to differentiate pseudoprogression from true progression, and assessment of response criteria exists but remains limited. The aim of this paper is to highlight the clinical and pathological markers to differentiate pseudoprogression from true progression through a literature review.

Key words

Glioblastoma, MGMT, Overall survival, Predictive factors, Progression, Pseudoprogression,

Introduction

Glioblastoma multiforme (GBM), the most common malignant brain primary tumor in adults, represents about 60% of all gliomas (1–3). The incidence of GBM is 3/100,000 in Europe and North America (12,000 patients per year) (4–6). Standard treatment consists of maximal debulking surgical resection followed by concomitant chemoradiotherapy (CRT) with daily temozolomide (TMZ) and adjuvant TMZ (STUPP protocol) (7,8). One-third of patients with GBM survive 1 year, with a median survival of 15 to 18 months, and the survival rate is less than 5% at 5 years (1,2,8,9). Despite this protocol, most patients experience tumor recurrence or progression during the follow-up (1,8,10,11), with a median time of recurrence of 8 to 9 months (12).

Conventional gadolinium-enhanced magnetic resonance imaging (MRI) is the cornerstone examination for monitoring treatment response but fails to distinguish true progression (TP) from pseudoprogression (PsP). However, the concordance for PsP between radiological interpretation and subsequent histological features can be as low as 32% of cases (13). Some efforts have been made to elaborate standardized criteria, resulting in Response Assessment in Neuro-Oncology (RANO) criteria (14), which has updated the Macdonald criteria (15).

PsP can be defined as subacute radiographic changes (enlarged or new contrast enhancement within the radiation field) mimicking tumor progression that resolves spontaneously without modifying therapy (16–18). The identification of PsP is challenging, and repeated follow-up imaging is necessary (19,20). The diagnosis of PsP indicates treatment efficacity, and continuing adjuvant TMZ or follow-up should be encouraged. Conclusion of TP means that current treatment must be modified, (e.g., antiangiogenic therapy, radiotherapy, surgery, or combined treatments) (21). This differentiation is required to avoid unnecessary reoperations and the premature discontinuation of TMZ, which can be sources of distress in patients (22–24).

In addition to imaging, histopathology and genomic information can help in the diagnosis of PsP. A higher incidence of PsP has already been shown in patients with O^6- methylguanine-DNA methyltransferase (MGMT) promoter methylation as well as an increase of overall survival (OS) (25). Features of macroscopic images can be combined with genomic features to improve characterization of the GBM and facilitate the diagnosis of PsP or TP (26).

In clinical trials, the criteria to define PsP are often different as are the time points of the evaluation (24). This results in the inclusion of patients with PsP in TP groups because of a false diagnosis of TP as well as falsely improved progression-free-survival (PFS). The eligibility for salvage treatment could be hindered in the case of misinterpretation (27,28).

The aim of this review was to identify clinical and pathological markers for differentiating PsP and TP and their impact on the survival rate of GBM patients treated by the STUPP protocol.

Methods

A literature search was conducted using Medline/PubMed, ScienceDirect and the Cochrane Wiley database. Search terms included ("glioblastoma" OR "gliomas" OR "high grade gliomas") AND ("pseudoprogression" OR "pseudo-progression"). Articles concerning PsP in adult patients with glioma, high grade glioma (HHG) and GBM who were treated with the STUPP protocol were examined. References provided from relevant articles were also examined to identify additional studies for inclusion. Any irrelevant entries and non-English articles were excluded. Twenty-four articles about response assessment criteria, 17 about the definition of PsP, 56 about PsP incidence, 19 about PsP occurrence delay, 19 about PsP predictive factors, 30 about PsP survival impact, and 48 about PsP histopathological characteristics were included in this review.

Response evaluation tools

Uniform rigorous criteria of response assessment and an image standardized protocol in neuro-oncology were necessary (16,29,30). In 1990, Macdonald *et al.* proposed the first criteria for response assessment in HGGs based on the Levin criteria (31). Radiologic criteria were initially based on computed tomography. These criteria were then extrapolated on MRI, taking into account the two-dimensional measurements (sum of the product of the perpendicular diameters) of the enhancing tumor area. They were associated with clinical criteria (neurologic symptoms) and the use of corticosteroids (Table 1) (15). Some limitations of the Macdonald criteria have been raised (27,32,33). The measurement of enhancing lesions was observer dependent mainly for irregularly shaped tumors, cystic tumors, or in the case of surgical cavities (34). The use of cross-sectional area measurement was poorly reproducible and was considered unusable in the case of multiple lesions. Furthermore, no criteria were available for nonenhancing lesions, multifocal lesions, or in the case of gross total resection (14). Sorensen *et al.* proposed fluid-attenuated inversion recovery (FLAIR) images in addition to T1 gadolinium images. They also suggested that a stable dose of corticosteroids be considered for an unchanged dose for at least 3 days before imaging. Moreover, they recommended a T1 contrast-enhanced MRI volumetric approach instead of the two-dimensional lesion measurement to decrease the inter-observer variability (32). However, some studies have compared diameter and volumetric measurements with discordant results (35–39). The Macdonald criteria were based on enhancing lesion measurement, but this was not clearly described and was never clearly associated with tumor growth or tumor activity. This observation was especially true when antiangiogenic treatment, radiation therapy, and corticosteroids were used or in postsurgery conditions (27).

In 2009, motivated by the use of antiangiogenic therapies, the RANO working group, composed initially of five volunteer collaborators, proposed criteria for treatment response in HGG in order to make the design of trials uniform. The RANO criteria included radiological

and clinical criteria and took into account the use of corticosteroids (14). Those criteria included a definition of patients who could participate in a trial and introduced the definition of PsP. Radiological response was evaluated in comparison with the lesion measurement on baseline MRI (pretreatment postsurgical MRI or MRI in which the smallest size of the lesions was observed during the follow-up). Complete response, partial response, stable disease, and progressive disease criteria are defined in Table 1. RANO defined measurable lesions as a bidimensional contrast-enhancing lesion with shape demarcation, and at least two perpendicular diameters of ≥ 10 mm that were visible on two or more slices. Cystic and surgical cavities were excluded from lesion measurement. Nonmeasurable lesions were defined as unidimensional measurable lesions without a shape demarcation and diameters of ≤ 10 mm. In the case of multiple contrast-enhancing lesions, lesion size was the sum of the product of the perpendicular diameters from two and five lesions. Because of the high incidence of PsP during the first 12 weeks after CRT, RANO criteria proposed to exclude patients from clinical trials who had progression during this period. However, progression could be considered during this period if there was a new enhancement outside the 80% isodose line or histopathological exam confirming tumor progression. RANO criteria defined PsP as a transient 25% increase in the sum of the product of the perpendicular diameters of measurable contrast-enhancing lesions associated or not with an increase in T2/ FLAIR within 12 weeks after CRT that decreased or disappeared 4 weeks after MRI.

Even if RANO criteria were developed to standardize the HGG treatment response assessment, some shortcomings remain:

- RANO criteria included FLAIR assessment to improve the accuracy of the diagnosis of progression in the case of antiangiogenic treatment but did not defined an objective measurement guidelines for FLAIR imaging as it did for T1-weighted imaging (34,40).

- A precise definition of neurological deterioration did not exist, and neurological evaluation was left to the clinician's judgement. However, the authors proposed guidelines for Karnofsky Performance Status (KPS) and World Health Organization (WHO) performance status scores degradation (Table 2), but these scores were not sensitive or specific for treatment response (41).
- The threshold of corticosteroid dose to specify an increase, stabilization, or decrease in consumption was not identified, nor was there a level of change or a time period analysis.
- RANO criteria excluded patients with progression signs other than histopathological proof of progression or increased enhancement outside of the radiation field within the first 12 weeks after CRT to avoid including patients with PsP. However PsP can occur during the first 6 months after CRT completion and even after this period (17).
- RANO criteria did not propose a volumetric approach to measure the contrast-enhancing tumor size or require the use of bidirectional measurements as in the Macdonald criteria (15).
- Postsurgical MRI was chosen as the baseline for the response assessment evaluation, but this could present some issues due to such imaging artifacts as postsurgical bleeding, vascular permeability modifications, or images modification due to a high steroids dose postsurgery, and changes can appear between the postoperative MRI and the MRI used for radiotherapy delineation, often performed some weeks after the postoperative MRI.

In 2017, Ellingson *et al.* proposed modified RANO criteria to evaluate the radiological response when a treatment affecting the contrast enhancement was administered (Table 1) (42). Indeed, radiotherapy or cytotoxic chemotherapy increase contrast enhancement (i.e., PsP), whereas anti-angiogenic drugs decrease contrast enhancement, inducing a pseudo-

response (43–49). In response to these findings, the authors developed an international brain tumor imaging protocol (BTIP) with sequence and parameter recommendations to standardize the imaging protocol (50). Moreover, in addition to two-dimensional measurement, a volumetric approach was defined (51). The postradiation MRI was proposed as baseline imaging instead of postsurgical MRI as in RANO criteria. In the case of suspicion of PsP or pseudo-response, the authors recommended a new imaging control within 4 to 8 weeks after the MRI, as it suggests potential progression. Consequently, the authors introduced the terms "preliminary complete response (CR)" and "durable CR", "preliminary PR" and "durable PR" and "preliminary progression disease (PD)" and "confirmed PD". They deleted the T2/FLAIR evaluation from the criteria and considered only measurable enhancing lesions for better interobserver concordance. The T2/FLAIR tumor progression evaluation was too complex, subjective, and controversial to be integrated as a radiographic endpoint. The neurological clinical status could be classified as "stable, better, or worse", but the clinical evaluation remained subjective. The status of steroids use could be classified as "no" when the patients did not received corticosteroids or when the corticosteroids dose consumption was physiologic, "increased" if the dexamethasone (or equivalent) treatment dose increased at least 2 mg, "decreased" if the dexamethasone treatment dose decreased at least 2 mg, or "stable" in the other cases.

To respond to critics of the RANO criteria, several more specific scales were designed (52). The Immunotherapy Response Assessment for Neuro-Oncology (iRANO) suggested that within the first 6 months after the start of immunotherapy, if MRI showed progression without clinical deterioration, immunotherapy could be continued until the next MRI 3 months later (53). The Neurologic Assessment in Neuro-oncology (NANO) was a more objective and quantifiable neurological symptoms score evaluating supratentorial, infratentorial, and brainstem functions (54). NANO was an objective, relevant, fast, and

simple scale developed with the aim to reflect tumor activity via clinical parameters to identify progression. Wen *et al.* exposed also the RANO-HGG (high grade glioma), the RANO-BM (brain metastasis) (55), the RANO-LM (leptomeningeal metastasis) (56), RANO-LGG (low grade glioma) (57), RANO seizures, RAPNO (pediatric), SPINO (spine tumors), RANO-meningioma, RANO PET (Positron Emission Tomography), RANO surgery, RANO steroids, RANO PRO (patient-reported outcome), and RANO histologic assessment (41), maintaining the confusion in the evaluation tools.

The importance of criteria to define PsP and TP cannot be ignored. Those criteria are essential for patient management and the evaluation of the disease prognosis. Linhares *et al.* underlined the importance of criteria to differentiate PsP and TP. They analyzed data from 70 patients with GBM treated with surgery and CRT and compared RANO and Macdonald criteria. Thirty-two patients were identified as having TP according to the Macdonald criteria and 13 patients according to the RANO criteria. Ten patients were identified as having PsP according to the Macdonald criteria and two patients according to the RANO criteria. According to the Macdonald versus RANO criteria, the median OS for the TP group was 12 months versus 9 month and was 24 months versus 13 months for the PsP group. The difference in OS between the PsP and TP groups was significant only for the patients classified with the Macdonald response ($p=0.01$). The median PFS rates were 6 months for the Macdonald versus RANO criteria in the TP group and 16 months versus 7 months in the PsP group, respectively (58). Similarly, for Kucharczyk *et al.*, the incidence of PsP was 15% and 19% using the RANO and MacDonald criteria, respectively (59). Van Mieghem *et al.* conducted a retrospective study of 136 patients with GBM who underwent CRT or radiotherapy (RT) alone after surgery. They used two different definitions of PsP: 1) the stringent criteria, which defined PsP as a ≥ 25% increase in size or new contrast-enhancing lesion that spontaneously regressed to baseline, and 2) the liberal criteria, which defined PsP as a ≥ 25% increase in tumor volume followed

by stable size for at least 6 months. The authors identified 14% versus 23% of PsPs using the stringent and liberal criteria, respectively, with a median OS of 27.7 months versus 32.4 months, respectively (60).

Recently, the use of automated neural networks on MRI for response assessment and time to progression (TTP) in brain tumors was developed and compared with the RANO criteria with great expectation of improving clinical decision making (61).

Definition of PsP

Many definitions of PsP have been published in the literature. PsP was reported for the first time in 1979 by Hoffman *et al.* (62). Then, in 2004, De Wit *et al.* described "progressive MRI lesions shortly after radiotherapy with spontaneous improvement or stabilization without additional treatment" (63). In 2007, Chamberlain *et al.* reported that the use of TMZ in CRT could influenced the PsP incidence (64). Eventually, in 2008, Taal *et al.* characterized the term *PsP* as a "progressive MRI lesion immediately after the end of concurrent CRT with TMZ, with spontaneous improvement without further treatment other than adjuvant TMZ" (65). Usually, PsP is a subacute secondary effect of treatment that is clinically asymptomatic and mimics progression (19,66,67). PsP reflects the response to treatment rather than treatment failure (68). The definition of PsP can include a component of clinical impairment, but its appreciation remains variable and blurry. Radiological images are often contrasted with minimal neurological deterioration (69). Several works showed that clinical deterioration in PsP was less severe than in TP (25,65,70). This variability of definition could explain the published large incidences rates, ranging from 2% to more than 54% (10,11,16,17,25,51,53,54,58,60–67,70–110) (Table 3), with a rate of 36% reported a recent meta-analysis (111).

In Imaging, PsP is defined as an increase in the size of preexisting contrast enhancement or a new contrast enhancement in the nontumoral enhancing area but within the radiation field,

with stabilization or resolution without further new treatment, after additional cycles of adjuvant TMZ or follow-up (17,34,71,99,112). These features are associated with tissue damage, remodeling, and inflammatory response to treatment (16). PsP could occur in parenchymal or leptomeningeal brain, and progression images must be correlated with the radiation dose map (113).

The time of appearance is relatively large and cannot be used to differentiate PsP and TP. It ranges from the first 3 months after CRT (23,66,70,73,80,84,114) to more than 6 months after CRT (17,67,115). It was also documented after 1 year (116,117). Gahramanov *et al.* analyzed 68 patients with GBM and showed that 35% of them experienced PsP with a median time of 6 weeks (75% within 12 weeks and 25% beyond 12 weeks) (81). Moreover, Radbruck *et al.* showed no difference in the incidence of PsP at 1, 4, and 7 months (17). In addition, Agarwal *et al.* concluded that there was no difference in appearance time between PsP and TP (94). To increase the difficulties of differentiation, Abbasi *et al.*, in a meta-analysis, concluded that the mean interval of TP was 10.5 months (range, 1.7–37.6 months) compared with 13.0 months (range, 1.2–40.0 months) for PsP (111). However, Jang *et al.*, using machine-learning algorithm, showed that the interval between treatment and suspicious progression images was shorter in the PsP group than in the TP group (82 days versus 123.5 days; p=0.02) (105).

The incidence of PsP tends to increase with new therapeutics. Many authors showed that PsP was more frequent after CRT than after RT alone (25,65,66,86), probably because of the radiosensitizing effect of TMZ (118). Moreover, new modalities of imaging, improvement in imaging techniques, early imaging follow-up, and re-irradiation increase the incidence of PsP.

Predictive factors of PsP

Patients characteristics

Patients developing PsP could be younger than those with TP (65) but this factor was avoided in an analysis with machine learning (105) or by some logistic regression model

(11,53,75,76,103). Female patients could develop PsP more often than male patients (105) but this observation was largely discussed by other authors (11,76,103). Less deteriorated neurological status was described in patients with PsP (65,70) but this has not been found by others (103). In the study by Brandes *et al.*, clinical deterioration was less frequent in the PsP group (34%) than in the TP group (56%), without a significant difference (p=0.14) (25). However, WHO performance status was not predictive of PsP (65) nor KPS (53,75,103). Several scores were studied and found not to be related to PsP, such as the Mini-Mental Status Examination (103) and Recursive Partitioning Analysis (RPA) (53).

Treatment features

Gerstner *et al.* demonstrated on univariate analysis, that the extent of surgery (biopsy versus subtotal resection versus gross total resection) was significantly associated with PsP (p=0.04)(86), but this factor remains disputable (11,53,65,75,98,103,119). The interval between surgery and radiotherapy was not retrieved as a predictive factor (11). The time elapsed before the second surgery for progression was not a significant factor of PsP versus TP (120). RT alone provided fewer cases of PsP than CRT, from 10% to 30% (25,65,68,70,86,119). The addition of bevacizumab seemed to decrease the incidence of PsP in the AVAglio phase 3 trial, with comparable patients characteristics in both arms (10,23). RT dose was questionable (66), as Yang and Aghi concluded that a high dose of RT significantly increased the rate of PsP (119), but others authors concluded in its lack of impact (53,75). Radiotherapy schedules have not been demonstrated as predictive factors (11). The volume of the radiation field was not identified as significantly different between the PsP and TP groups (53,65). Schedules of adjuvant TMZ were also suspected but not proved as predictive factors of PsP (98).

Additional treatment

Some authors showed that patients with PsP required fewer corticosteroids than patients with TP (70) and that this treatment at the start of CRT could be related to PsP incidence (103), whereas other authors did not find this association with corticosteroids (81). Anticonvulsant drugs were studied by authors without a correlation determined (103).

Tumor characteristics

Initial tumor volume or size was not associated with the risk of PsP (53,103), but some authors demonstrated that volume rather surface or diameter could be predictive of PsP (96). Tumor location was not correlated with PsP (53,103). Some authors showed that unmethylated MGMT promoter was an independent risk factor for TP (p=0.005) (70) or was correlated with risk of PsP (25,103), but others recused this conclusion (98,105). Isocitrate dehydrogenase (IDH) mutations were also shown to be independent risk factors of PsP (76), although not in all the publications (103). The overexpression of tumor protein 53 (TP 53) could influence the development of PsP (11). However, epidermal growth factor receptor (EGFR) amplification (76) and phosphatase and tensin homolog (PTEN) mutation (76) were not retrieved as prognostic.

Influence of PsP on survival

Results of the literature are presented in Table 4.

Some authors showed that patients with PsP had a better prognosis and better treatment response and consequently a better OS or median OS compared with those with TP (13,16,25,70,73,79–81,83,85–87,89,90,95,96,98,102–104,109,121,122). Rare were the studies that did not observe an improvement in OS for patients with PsP compared with those without (90,107,122). Nasseri *et al.* demonstrated that the median, 1-year and 2-year OS were better for patients with a PsP that developed after 3 months of the CRT completion compared with patients with PsP appearing in the first 3 months after CRT, but without significant difference (p=0.15) (65). In the Topkan *et al.* study, the survival analysis revealed that patients with PsP

had superior 1-year OS and PFS (100% versus 70.6%; p=0.03 and 83.3% versus 42.2%, p=0.02 respectively) and 2-year OS and PFS (56.8% versus 25.8%, p=0.007 and 30% versus 9.6%, p=0.002, respectively) (104). Moreover, Radbruch *et al.* showed that the median OS in patients with stable PsP/PsP shrinking <50% versus those with a total disappearance of PsP/PsP decrease >50% was 35.4 months versus 23.6 months, respectively, without significant difference (p=0.7) (17). Independently to OS, PFS and objective response rate were endpoints that were studied according to PsP and TP (42,103). PFS was usually showed to be superior for patients with PsP than with TP (81,85–87,90,104). With regard to the median time to progression (TTP), Brandes *et al.* showed that patients with PsP had a better TTP than patients with TP (20.7 versus 5.7 months, $p < 0.001$) and the median time interval between recording PsP and subsequent TP was 16.2 months (25). Kang *et al.* reported that the median TTP was 7 and 3.1 for patients with PsP and TP, respectively ($p < 0.01$) (11). Despite a better median OS in patients with PsP, Balana *et al.* failed to show a better median postprogression survival in the PsP group (5.4 versus 7.2 months; p=0.43) (79).

For Gunjur *et al.*, better OS can be considered as an indication that PsP is a sign of tumoral response rather than a complication of the treatment (81). Brandes *et al.* showed that OS was significantly influenced by the detection of PsP (p=0.045) (25), Soike *et al.* concluded that PsP was an improved factor of PFS (p=0.046) (87), and Kang *et al.* showed that PsP was a factor of prolonged median survival time (11). The methylation of the MGMT promoter has been identified as improving survival (25,85) but this was debated (98). Thomas *et al.* observed that advantages of better OS were deleted when OS was adjusted for several patient characteristics (age, KPS, MGMT methylation) (123). Gzell *et al.* demonstrated that survival was reduced when surgical cavity volume and contrast enhancement volume increased ≥5% at 3 and 5 months after CRT (p=0.006) (124).

Histological and Pathological findings

Histopathologic examination was the reference method in the differential diagnosis of progression, PsP, and radionecrosis (RN). However, interpreting surgical samples was complex because a large proportion of patients could be categorized as “mixed”. These findings failed to resolve the ambiguity of the process and did not inform on progression versus initial tumor (13). PsP was a continuum between the subacute radiation reaction and treatment-related necrosis (125). Some authors supported the idea that RN was the continuum of PsP, but this was debated (65,66,126). Both pathophysiological mechanisms, vascular injury and cellular effects, were still incompletely understood and characterized (126). Inflammation and vascular endothelial damages led to blood-brain barrier disruption, increased permeability, and vasogenic oedema, resulting in MRI contrast enhancement (14,126). Cell necrosis and local tissue reaction increased cytokines and proinflammatory mediators that also increased vascular permeability. Endothelial cells apoptosis resulted from the effects of free radicals effects and cell membrane damage that induced ceramides and apoptotic mechanisms (112). Cellular hypoxia activated hypoxia-regulated molecules from the tumor and cells and increased permeability and tumor enhancement (127). The vascular endothelium, blood-brain barrier, and oligodendroglial injuries provoked an exaggerated response to effective therapy, which led to inflammation, vascular dilatation and increased permeability (24,128). PsP showed typical pathological findings after radiation, such as perivascular edema, bland necrosis, fibrosis, gliosis, endothelial thickening, hyalinization, platelet fibrin thrombi and occlusion (13,24,53). Cell analysis showed paucicellularity, scattered rare or no atypical cells with a lack of mitotic figures except in inflammatory cells, a reduced number of endothelial cell nuclei, low density of pleiomorphic tumor cell, low mitotic index, hyalinization of vessel walls, fibrinoid necrosis, fibrillary and gemistocytic astrocytes, pleiomorphic astrocytes, and mild perivascular lymphocyte and monocyte infiltrations (126). There was a preponderance of reactive cells including astrocytes, microglia

and macrophages (129). Focal areas of demyelination were secondary to oligodendroglial cell loss (130,131). In contrast, recurrent tumors were characterized by the presence of tumor cells, increased cellularity, and vascular proliferation (131,132).

MGMT

MGMT is an enzyme that repairs the DNA damage caused by alkylating agents such as TMZ. Injuries to DNA leads to apoptotic cell death. Methylation of the promoter of MGMT reduces the intracellular level of MGMT and inhibits the repair mechanism of DNA (85). The MGMT methylation status is associated with PsP. Patients with MGMT methylation showed more PsP, and about two-thirds of MGMT-methylated tumors exhibit PsP (25,60,63,76,87,103,114,123,133,134). Patients with methylated MGMT promoter had a 3.5-fold increased risk having PsP than TP in the case of MRI suggesting progression (103). Only few studies did not show any correlation between MGMT and PsP (91). The sensitivity and specificity of MGMT promoter methylation status for detecting PsP were 66% and 89%, respectively (55). GBM of patients with PsP exhibited more frequently a methylated MGMT promoter and conversely, patients with tumor exhibiting methylated MGMT promoter more frequently developed PsP (77,87). The higher sensitivity of GBM with MGMT methylation to an alkylating agent such as TMZ could explained the high rate of PsP in these patients (112).

IDH

Mutant IDH was infrequent in patients with GBM as opposed to patients with lower-grade gliomas that showed a higher frequency of mutant IDH (135,136). IDH wild-type GBM represented close to 90% of GBM cases, corresponding to primary or de novo GBM and mostly affecting patients older than 55 years (137). IDH-mutant GBM corresponded to secondary GBM and mostly affected younger patients. Some authors concluded that IDH status was not associated with PsP (87). However, others authors suggested that IDH could be

a molecular biomarker for PsP (76,103,138), with a sensitivity of 67% and a specificity of 100% (91).

TP 53

TP 53 is a tumor suppressor gene, important in the cellular response to DNA damages, with a frequency in primary GBM of about 30% and in secondary GBM of about 70% (139). The role of TP 53 in PsP is debated. Overexpressed TP 53 was more frequent in PsP tumors than in TP tumors (11), but in contrast, the authors concluded that the expression level of TP 53 was not predictive of PsP (99).

Ki67

Ki67 is a marker of cellular proliferation, which was identified as a marker of OS (140). It could be a prognostic marker to distinguish PsP from TP, with a higher rate for tumors of patients who developed PsP (99). Nevertheless this observation was disputable because other observed reversed results (141), and some articles did not reveal any clear differences in Ki67 between PsP and TP (13,142).

Other findings

ATRX (alpha-thalassemia/mental retardation syndrome X-linked), EGFR, PTEN, 1p19q deletion, interferon regulatory factor 9 (IRF9), and x-ray cross-complementary gene 1 (XRCC1) were also studied with conflicted or isolated results, making definitive conclusions impossible (76,106,143–145).

Blood-based biomarkers

Classically, brain tumors are characterized by histopathology analysis and molecular analysis via tissue samples. Because of the heterogeneity of gliomas, a biopsy or a sample analysis of the tumor could not reflect all tumor characteristics. That is why liquid biopsy from blood or cerebral spinal fluid, which is a quick, inexpensive and non-invasive method, could be more representative of the entire tumor and its heterogeneity (146,147). Limitations of liquid biopsy

were the lack of consensus and standardization of biological fluid type, nucleic acids type, and the analytical technique to use (146). In case of doubt between PsP and TP, and to avoid surgery, blood-based methods could help to orientate the diagnosis by a genomic analysis. The isolation of circulating tumor cells (148) could be useful during follow-up (147–151) as a complement to radiographic features (152). Circulating micro-RNA analysis could be interesting for identifying TP versus PsP because miRNA accurately identifies cancer tissue (147) as circulating tumor stem cells (153,154), circulating cell-free nucleic acids (146) or circulating tumor cell clusters (155). Extracellular vesicles (EV) contained many of the same transcripts as primary tumor cells and had proved a high sensitivity and specificity to identify, for example, BRAF, KRAS, or EGFR mutations. EV analysis could be promising in the differentiation between PsP and TP (156). The authors demonstrated a higher EV plasma levels in GBM patients that could guide GBM diagnosis and monitoring response assessment to treatment with a decrease after surgery and an increase in the case of progression (157). However, the utility of differentiating PsP from TP needs to be proven, but the potential to identify tumor cell proliferation and invasion, angiogenesis, and biomarkers and to evaluate the response to treatment exists. The implementation in clinical practice could improve the personalized medicine in terms of diagnosis, treatment, and follow-up.

Differentiation with RN

Contrary to PsP, which has a radiological definition, RN has a histological definition (117). RN corresponds to a severe local tissue reaction to RT and has an incidence ranging from 5% to 40% (89,121). It occurs months to years after irradiation, usually 6 to 24 months after CRT. Although PsP and RN have distinct clinical and pathological mechanisms, they shared histologic similarities that translate into similar imaging characteristics (88). However, contrary to PsP, RN is not associated with a better prognosis and progresses without treatment

(89,121). Frequent treatments consist of corticosteroids (158), bevacizumab (159–161) or surgery (162).

RN differs from PsP in many ways. Clinically, RN is usually asymptomatic but can also cause irreversible neurological deficits and anatomical injuries. In MRI, RN corresponds to a contrast enhancement ring with a central hypoT1 responsible for edema and a mass effect. On T1 MRI, RN shows images with features described as “Swiss cheese” or “soap bubble” (163). RN is a late injury corresponding to white matter necrosis. PsP and RN do not have the same histopathological and biological mechanisms. RN is secondary to chronic inflammation, wall thickening, hyalinization of vessels, and with occasional reactive telangiectasia responsible for micro-vessel collapse around the tumor (72,163). Radiations target vascular endothelial cells and oligodendrocytes that lead to the clonogenic death, then vascular lesions as blood-brain barrier breaks down, then ischemia, vasogenic edema, and hypoxia. Those phenomena stimulate vascular endothelial growth factor (VEGF) and increase vascular permeability, which leads to necrosis and demyelination. Moreover, radiations stimulate glioma cells and activates VEGF, which decreases apoptosis in tumor cells (68). Hemorrhages and calcifications can be present (66). White matter necrosis occurs through multiple mechanisms and three mediators: endothelial cell apoptosis, VEGF, and glioblastoma cell necrosis. Radiation-induced DNA and membrane damages lead to the creation of free radicals and activate ceramides, causing endothelial cell apoptosis. This process provokes blood-brain barrier disruption, demyelination, and tissue necrosis. Hypoxia up-regulates VEGF expression, resulting in edema (119). Risk factors for RN are high total dose and fractional dose of radiation, hyperfractionation, stereotactic radiosurgery, reirradiation, concomitant chemotherapy and radiotherapy, and volume of radiation (119).

Conclusion

Currently, in clinical routine, the only way to make the distinction between PsP and TP is surgery with a pathological confirmation, but follow-up MRI is less invasive and thus mostly used. The diagnosis of certainty of PsP poses considerable diagnostic challenges to clinicians and radiologists. False interpretation of treatment-related changes in TP induces the premature discontinuation of efficient treatment and unnecessary surgery. Clinical, pathological, and genomic features could help in the differentiation between PsP and TP, but they remain insufficient. Noninvasive imaging methods could be the key to solving this dilemma, but further studies are needed to determine the optimal solution of PsP identification.

Bibliography

1. Ostrom QT, Gittleman H, Stetson L, Virk SM, Barnholtz-Sloan JS. Epidemiology of gliomas. Cancer Treat Res. 2015;163:1–14.
2. Ostrom QT, Gittleman H, Farah P, Ondracek A, Chen Y, Wolinsky Y, et al. CBTRUS statistical report: Primary brain and central nervous system tumors diagnosed in the United States in 2006-2010. Neuro-Oncol. 2013 Nov;15 Suppl 2:ii1-56.
3. Ahmed R, Oborski MJ, Hwang M, Lieberman FS, Mountz JM. Malignant gliomas: current perspectives in diagnosis, treatment, and early response assessment using advanced quantitative imaging methods. Cancer Manag Res. 2014;6:149–70.
4. Dolecek TA, Propp JM, Stroup NE, Kruchko C. CBTRUS Statistical Report: Primary Brain and Central Nervous System Tumors Diagnosed in the United States in 2005–2009. Neuro-Oncol. 2012 Nov 1;14(suppl_5):v1–49.
5. Albert NL, Weller M, Suchorska B, Galldiks N, Soffietti R, Kim MM, et al. Response Assessment in Neuro-Oncology working group and European Association for Neuro-Oncology recommendations for the clinical use of PET imaging in gliomas. Neuro-Oncol. 2016;18(9):1199–208.
6. Bleeker FE, Molenaar RJ, Leenstra S. Recent advances in the molecular understanding of glioblastoma. J Neurooncol. 2012 May;108(1):11–27.
7. Stupp R, Hegi ME, Mason WP, van den Bent MJ, Taphoorn MJB, Janzer RC, et al. Effects of radiotherapy with concomitant and adjuvant temozolomide versus radiotherapy alone on survival in glioblastoma in a randomised phase III study: 5-year analysis of the EORTC-NCIC trial. Lancet Oncol. 2009 May;10(5):459–66.
8. Stupp R, Mason WP, van den Bent MJ, Weller M, Fisher B, Taphoorn MJB, et al. Radiotherapy plus concomitant and adjuvant temozolomide for glioblastoma. N Engl J Med. 2005 Mar 10;352(10):987–96.
9. Seystahl K, Wick W, Weller M. Therapeutic options in recurrent glioblastoma--An update. Crit Rev Oncol Hematol. 2016 Mar;99:389–408.
10. Chinot OL, Wick W, Mason W, Henriksson R, Saran F, Nishikawa R, et al. Bevacizumab plus Radiotherapy–Temozolomide for Newly Diagnosed Glioblastoma. N Engl J Med. 2014 Feb 20;370(8):709–22.
11. Kang H-C, Kim C-Y, Han JH, Choe GY, Kim JH, Kim JH, et al. Pseudoprogression in patients with malignant gliomas treated with concurrent temozolomide and radiotherapy: potential role of p53. J Neurooncol. 2011 Mar;102(1):157–62.
12. McNeill K, Aldape K, Fine HA. Adult High-Grade (Diffuse) Glioma. In: Karajannis MA, Zagzag D, editors. Molecular Pathology of Nervous System Tumors: Biological Stratification and Targeted Therapies [Internet]. New York, NY: Springer New York; 2015 [cited 2018 Sep 3]. p. 77–93. (Molecular Pathology Library). Available from: https://doi.org/10.1007/978-1-4939-1830-0_6
13. Melguizo-Gavilanes I, Bruner JM, Guha-Thakurta N, Hess KR, Puduvalli VK. Characterization of pseudoprogression in patients with glioblastoma: is histology the gold standard? J Neurooncol. 2015 May;123(1):141–50.
14. Wen PY, Macdonald DR, Reardon DA, Cloughesy TF, Sorensen AG, Galanis E, et al. Updated response assessment criteria for high-grade gliomas: response assessment in neuro-oncology working group. J Clin Oncol Off J Am Soc Clin Oncol. 2010 Apr 10;28(11):1963–72.
15. Macdonald DR, Cascino TL, Schold SC, Cairncross JG. Response criteria for phase II studies of supratentorial malignant glioma. J Clin Oncol Off J Am Soc Clin Oncol. 1990 Jul;8(7):1277–80.
16. Ellingson BM, Wen PY, van den Bent MJ, Cloughesy TF. Pros and cons of current

brain tumor imaging. Neuro-Oncol. 2014 Oct;16 Suppl 7:vii2-11.
17. Radbruch A, Fladt J, Kickingereder P, Wiestler B, Nowosielski M, Bäumer P, et al. Pseudoprogression in patients with glioblastoma: clinical relevance despite low incidence. Neuro-Oncol. 2015 Jan;17(1):151–9.
18. Dietrich J, Winter SF, Klein JP. Neuroimaging of Brain Tumors: Pseudoprogression, Pseudoresponse, and Delayed Effects of Chemotherapy and Radiation. Semin Neurol. 2017;37(5):589–96.
19. Hygino da Cruz LC, Rodriguez I, Domingues RC, Gasparetto EL, Sorensen AG. Pseudoprogression and pseudoresponse: imaging challenges in the assessment of posttreatment glioma. AJNR Am J Neuroradiol. 2011 Dec;32(11):1978–85.
20. Zhang J, Yu H, Qian X, Liu K, Tan H, Yang T, et al. Pseudo progression identification of glioblastoma with dictionary learning. Comput Biol Med. 2016 01;73:94–101.
21. Strauss SB, Meng A, Ebani EJ, Chiang GC. Imaging Glioblastoma Posttreatment: Progression, Pseudoprogression, Pseudoresponse, Radiation Necrosis. Radiol Clin North Am [Internet]. 2019 Aug 16 [cited 2019 Aug 27]; Available from: http://www.sciencedirect.com/science/article/pii/S0033838919300934
22. Peca C, Pacelli R, Elefante A, Del MBDC, Vergara P, Mariniello G, et al. Early clinical and neuroradiological worsening after radiotherapy and concomitant temozolomide in patients with glioblastoma: tumour progression or radionecrosis? Clin Neurol Neurosurg. 2009 May;111(4):331–4.
23. Wick W, Chinot OL, Bendszus M, Mason W, Henriksson R, Saran F, et al. Evaluation of pseudoprogression rates and tumor progression patterns in a phase III trial of bevacizumab plus radiotherapy/temozolomide for newly diagnosed glioblastoma. Neuro-Oncol. 2016;18(10):1434–41.
24. Yoo R-E, Choi SH. Recent Application of Advanced MR Imaging to Predict Pseudoprogression in High-grade Glioma Patients. Magn Reson Med Sci MRMS Off J Jpn Soc Magn Reson Med. 2016;15(2):165–77.
25. Brandes AA, Franceschi E, Tosoni A, Blatt V, Pession A, Tallini G, et al. MGMT promoter methylation status can predict the incidence and outcome of pseudoprogression after concomitant radiochemotherapy in newly diagnosed glioblastoma patients. J Clin Oncol Off J Am Soc Clin Oncol. 2008 May 1;26(13):2192–7.
26. Gutman DA, Cooper LAD, Hwang SN, Holder CA, Gao J, Aurora TD, et al. MR imaging predictors of molecular profile and survival: multi-institutional study of the TCGA glioblastoma data set. Radiology. 2013 May;267(2):560–9.
27. van den Bent MJ, Vogelbaum MA, Wen PY, Macdonald DR, Chang SM. End point assessment in gliomas: novel treatments limit usefulness of classical Macdonald's Criteria. J Clin Oncol Off J Am Soc Clin Oncol. 2009 Jun 20;27(18):2905–8.
28. Delgado-López PD, Riñones-Mena E, Corrales-García EM. Treatment-related changes in glioblastoma: a review on the controversies in response assessment criteria and the concepts of true progression, pseudoprogression, pseudoresponse and radionecrosis. Clin Transl Oncol Off Publ Fed Span Oncol Soc Natl Cancer Inst Mex. 2018 Aug;20(8):939–53.
29. Reardon DA, Ballman KV, Buckner JC, Chang SM, Ellingson BM. Impact of imaging measurements on response assessment in glioblastoma clinical trials. Neuro-Oncol. 2014 Oct;16(Suppl 7):vii24–35.
30. Ellingson BM, Bendszus M, Sorensen AG, Pope WB. Emerging techniques and technologies in brain tumor imaging. Neuro-Oncol. 2014 Oct;16 Suppl 7:vii12-23.
31. Levin VA, Crafts DC, Norman DM, Hoffer PB, Spire JP, Wilson CB. Criteria for evaluating patients undergoing chemotherapy for malignant brain tumors. J Neurosurg. 1977 Sep;47(3):329–35.
32. Sorensen AG, Batchelor TT, Wen PY, Zhang W-T, Jain RK. Response criteria for

glioma. Nat Clin Pract Oncol. 2008 Nov;5(11):634–44.
33. Henson JW, Ulmer S, Harris GJ. Brain tumor imaging in clinical trials. AJNR Am J Neuroradiol. 2008 Mar;29(3):419–24.
34. Yang D. Standardized MRI assessment of high-grade glioma response: a review of the essential elements and pitfalls of the RANO criteria. Neuro-Oncol Pract. 2016 Mar 1;3(1):59–67.
35. Galanis E, Buckner JC, Maurer MJ, Sykora R, Castillo R, Ballman KV, et al. Validation of neuroradiologic response assessment in gliomas: measurement by RECIST, two-dimensional, computer-assisted tumor area, and computer-assisted tumor volume methods. Neuro-Oncol. 2006 Apr;8(2):156–65.
36. Shah GD, Kesari S, Xu R, Batchelor TT, O'Neill AM, Hochberg FH, et al. Comparison of linear and volumetric criteria in assessing tumor response in adult high-grade gliomas. Neuro-Oncol. 2006 Jan;8(1):38–46.
37. Sorensen AG, Patel S, Harmath C, Bridges S, Synnott J, Sievers A, et al. Comparison of diameter and perimeter methods for tumor volume calculation. J Clin Oncol Off J Am Soc Clin Oncol. 2001 Jan 15;19(2):551–7.
38. Warren KE, Patronas N, Aikin AA, Albert PS, Balis FM. Comparison of one-, two-, and three-dimensional measurements of childhood brain tumors. J Natl Cancer Inst. 2001 Sep 19;93(18):1401–5.
39. Ellingson BM, Nguyen HN, Lai A, Nechifor RE, Zaw O, Pope WB, et al. Contrast-enhancing tumor growth dynamics of preoperative, treatment-naive human glioblastoma. Cancer. 2016;122(11):1718–27.
40. Pope WB, Hessel C. Response assessment in neuro-oncology criteria: implementation challenges in multicenter neuro-oncology trials. AJNR Am J Neuroradiol. 2011 May;32(5):794–7.
41. Wen PY, Chang SM, Van den Bent MJ, Vogelbaum MA, Macdonald DR, Lee EQ. Response Assessment in Neuro-Oncology Clinical Trials. J Clin Oncol Off J Am Soc Clin Oncol. 2017 Jul 20;35(21):2439–49.
42. Ellingson BM, Wen PY, Cloughesy TF. Modified Criteria for Radiographic Response Assessment in Glioblastoma Clinical Trials. Neurother J Am Soc Exp Neurother. 2017;14(2):307–20.
43. Pope WB, Lai A, Nghiemphu P, Mischel P, Cloughesy TF. MRI in patients with high-grade gliomas treated with bevacizumab and chemotherapy. Neurology. 2006 Apr 25;66(8):1258–60.
44. Chamberlain MC. MRI in patients with high-grade gliomas treated with bevacizumab and chemotherapy. Neurology. 2006 Dec 12;67(11):2089; author reply 2089.
45. Kang TY, Jin T, Elinzano H, Peereboom D. Irinotecan and bevacizumab in progressive primary brain tumors, an evaluation of efficacy and safety. J Neurooncol. 2008 Aug;89(1):113–8.
46. Batchelor TT, Sorensen AG, di Tomaso E, Zhang W-T, Duda DG, Cohen KS, et al. AZD2171, a pan-VEGF receptor tyrosine kinase inhibitor, normalizes tumor vasculature and alleviates edema in glioblastoma patients. Cancer Cell. 2007 Jan;11(1):83–95.
47. Friedman HS, Prados MD, Wen PY, Mikkelsen T, Schiff D, Abrey LE, et al. Bevacizumab alone and in combination with irinotecan in recurrent glioblastoma. J Clin Oncol Off J Am Soc Clin Oncol. 2009 Oct 1;27(28):4733–40.
48. Vredenburgh JJ, Desjardins A, Herndon JE, Dowell JM, Reardon DA, Quinn JA, et al. Phase II trial of bevacizumab and irinotecan in recurrent malignant glioma. Clin Cancer Res Off J Am Assoc Cancer Res. 2007 Feb 15;13(4):1253–9.
49. Vredenburgh JJ, Desjardins A, Herndon JE, Marcello J, Reardon DA, Quinn JA, et al. Bevacizumab plus irinotecan in recurrent glioblastoma multiforme. J Clin Oncol Off J Am

Soc Clin Oncol. 2007 Oct 20;25(30):4722–9.
50. Ellingson BM, Bendszus M, Boxerman J, Barboriak D, Erickson BJ, Smits M, et al. Consensus recommendations for a standardized Brain Tumor Imaging Protocol in clinical trials. Neuro-Oncol. 2015 Sep;17(9):1188–98.
51. Chappell R, Miranpuri SS, Mehta MP. Dimension in defining tumor response. J Clin Oncol Off J Am Soc Clin Oncol. 1998 Mar;16(3):1234.
52. Quant EC, Wen PY. Response assessment in neuro-oncology. Curr Oncol Rep. 2011 Feb;13(1):50–6.
53. Tsien C, Galbán CJ, Chenevert TL, Johnson TD, Hamstra DA, Sundgren PC, et al. Parametric response map as an imaging biomarker to distinguish progression from pseudoprogression in high-grade glioma. J Clin Oncol Off J Am Soc Clin Oncol. 2010 May 1;28(13):2293–9.
54. Nayak L, DeAngelis LM, Brandes AA, Peereboom DM, Galanis E, Lin NU, et al. The Neurologic Assessment in Neuro-Oncology (NANO) scale: a tool to assess neurologic function for integration into the Response Assessment in Neuro-Oncology (RANO) criteria. Neuro-Oncol. 2017 01;19(5):625–35.
55. Lin NU, Lee EQ, Aoyama H, Barani IJ, Barboriak DP, Baumert BG, et al. Response assessment criteria for brain metastases: proposal from the RANO group. Lancet Oncol. 2015 Jun;16(6):e270-278.
56. Chamberlain M, Junck L, Brandsma D, Soffietti R, Rudà R, Raizer J, et al. Leptomeningeal metastases: a RANO proposal for response criteria. Neuro-Oncol. 2017 01;19(4):484–92.
57. van den Bent MJ, Wefel JS, Schiff D, Taphoorn MJB, Jaeckle K, Junck L, et al. Response assessment in neuro-oncology (a report of the RANO group): assessment of outcome in trials of diffuse low-grade gliomas. Lancet Oncol. 2011 Jun;12(6):583–93.
58. Linhares P, Carvalho B, Figueiredo R, Reis RM, Vaz R. Early Pseudoprogression following Chemoradiotherapy in Glioblastoma Patients: The Value of RANO Evaluation [Internet]. Journal of Oncology. 2013 [cited 2019 May 4]. Available from: https://www.hindawi.com/journals/jo/2013/690585/abs/
59. Kucharczyk MJ, Parpia S, Whitton A, Greenspoon JN. Evaluation of pseudoprogression in patients with glioblastoma. Neuro-Oncol Pract. 2017 Jun;4(2):120–34.
60. Van Mieghem E, Wozniak A, Geussens Y, Menten J, De Vleeschouwer S, Van Calenbergh F, et al. Defining pseudoprogression in glioblastoma multiforme. Eur J Neurol. 2013 Oct;20(10):1335–41.
61. Kickingereder P, Isensee F, Tursunova I, Petersen J, Neuberger U, Bonekamp D, et al. Automated quantitative tumour response assessment of MRI in neuro-oncology with artificial neural networks: a multicentre, retrospective study. Lancet Oncol. 2019 May;20(5):728–40.
62. Hoffman WF, Levin VA, Wilson CB. Evaluation of malignant glioma patients during the postirradiation period. J Neurosurg. 1979 May;50(5):624–8.
63. de Wit MCY, de Bruin HG, Eijkenboom W, Sillevis Smitt P a. E, van den Bent MJ. Immediate post-radiotherapy changes in malignant glioma can mimic tumor progression. Neurology. 2004 Aug 10;63(3):535–7.
64. Chamberlain MC, Glantz MJ, Chalmers L, Van Horn A, Sloan AE. Early necrosis following concurrent Temodar and radiotherapy in patients with glioblastoma. J Neurooncol. 2007 Mar;82(1):81–3.
65. Taal W, Brandsma D, de Bruin HG, Bromberg JE, Swaak-Kragten AT, Smitt PAES, et al. Incidence of early pseudo-progression in a cohort of malignant glioma patients treated with chemoirradiation with temozolomide. Cancer. 2008 Jul 15;113(2):405–10.
66. Brandsma D, Stalpers L, Taal W, Sminia P, van den Bent MJ. Clinical features, mechanisms, and management of pseudoprogression in malignant gliomas. Lancet Oncol.

2008 May;9(5):453–61.
67. Jefferies S, Burton K, Jones P, Burnet N. Interpretation of Early Imaging after Concurrent Radiotherapy and Temozolomide for Glioblastoma. Clin Oncol. 2007 Apr 1;19(3):S33.
68. Jahangiri A, Aghi MK. Pseudoprogression and treatment effect. Neurosurg Clin N Am. 2012 Apr;23(2):277–87, viii–ix.
69. Reardon DA, Weller M. Pseudoprogression: fact or wishful thinking in neuro-oncology? Lancet Oncol. 2018 Dec 1;19(12):1561–3.
70. Rowe LS, Butman JA, Mackey M, Shih JH, Cooley-Zgela T, Ning H, et al. Differentiating pseudoprogression from true progression: analysis of radiographic, biologic, and clinical clues in GBM. J Neurooncol. 2018 May 16;
71. Brahm CG, den Hollander MW, Enting RH, de Groot JC, Solouki AM, den Dunnen WFA, et al. Serial FLT PET imaging to discriminate between true progression and pseudoprogression in patients with newly diagnosed glioblastoma: a long-term follow-up study. Eur J Nucl Med Mol Imaging. 2018 Jul 21;
72. Kumar AJ, Leeds NE, Fuller GN, Van Tassel P, Maor MH, Sawaya RE, et al. Malignant gliomas: MR imaging spectrum of radiation therapy- and chemotherapy-induced necrosis of the brain after treatment. Radiology. 2000 Nov;217(2):377–84.
73. Nasseri M, Gahramanov S, Netto JP, Fu R, Muldoon LL, Varallyay C, et al. Evaluation of pseudoprogression in patients with glioblastoma multiforme using dynamic magnetic resonance imaging with ferumoxytol calls RANO criteria into question. Neuro-Oncol. 2014 Aug;16(8):1146–54.
74. Mangla R, Singh G, Ziegelitz D, Milano MT, Korones DN, Zhong J, et al. Changes in relative cerebral blood volume 1 month after radiation-temozolomide therapy can help predict overall survival in patients with glioblastoma. Radiology. 2010 Aug;256(2):575–84.
75. Lee WJ, Choi SH, Park C-K, Yi KS, Kim TM, Lee S-H, et al. Diffusion-weighted MR imaging for the differentiation of true progression from pseudoprogression following concomitant radiotherapy with temozolomide in patients with newly diagnosed high-grade gliomas. Acad Radiol. 2012 Nov;19(11):1353–61.
76. Li H, Li J, Cheng G, Zhang J, Li X. IDH mutation and MGMT promoter methylation are associated with the pseudoprogression and improved prognosis of glioblastoma multiforme patients who have undergone concurrent and adjuvant temozolomide-based chemoradiotherapy. Clin Neurol Neurosurg. 2016 Dec;151:31–6.
77. Kong D-S, Kim ST, Kim E-H, Lim DH, Kim WS, Suh Y-L, et al. Diagnostic dilemma of pseudoprogression in the treatment of newly diagnosed glioblastomas: the role of assessing relative cerebral blood flow volume and oxygen-6-methylguanine-DNA methyltransferase promoter methylation status. AJNR Am J Neuroradiol. 2011 Feb;32(2):382–7.
78. Baek HJ, Kim HS, Kim N, Choi YJ, Kim YJ. Percent change of perfusion skewness and kurtosis: a potential imaging biomarker for early treatment response in patients with newly diagnosed glioblastomas. Radiology. 2012 Sep;264(3):834–43.
79. Chan DTM, Ng RYT, Siu DYW, Tang P, Kam MKM, Ma BBY, et al. Pseudoprogression of malignant glioma in Chinese patients receiving concomitant chemoradiotherapy. Hong Kong Med J Xianggang Yi Xue Za Zhi. 2012 Jun;18(3):221–5.
80. Chang JH, Kim C-Y, Choi BS, Kim YJ, Kim JS, Kim IA. Pseudoprogression and pseudoresponse in the management of high-grade glioma : optimal decision timing according to the response assessment of the neuro-oncology working group. J Korean Neurosurg Soc. 2014 Jan;55(1):5–11.
81. Gahramanov S, Muldoon LL, Varallyay CG, Li X, Kraemer DF, Fu R, et al. Pseudoprogression of glioblastoma after chemo- and radiation therapy: diagnosis by using dynamic susceptibility-weighted contrast-enhanced perfusion MR imaging with ferumoxytol

versus gadoteridol and correlation with survival. Radiology. 2013 Mar;266(3):842–52.
82. Clarke JL, Iwamoto FM, Sul J, Panageas K, Lassman AB, DeAngelis LM, et al. Randomized phase II trial of chemoradiotherapy followed by either dose-dense or metronomic temozolomide for newly diagnosed glioblastoma. J Clin Oncol Off J Am Soc Clin Oncol. 2009 Aug 10;27(23):3861–7.
83. Roldán GB, Scott JN, McIntyre JB, Dharmawardene M, de Robles PA, Magliocco AM, et al. Population-based study of pseudoprogression after chemoradiotherapy in GBM. Can J Neurol Sci J Can Sci Neurol. 2009 Sep;36(5):617–22.
84. Chaskis C, Neyns B, Michotte A, De Ridder M, Everaert H. Pseudoprogression after radiotherapy with concurrent temozolomide for high-grade glioma: clinical observations and working recommendations. Surg Neurol. 2009 Oct;72(4):423–8.
85. Fabi A, Russillo M, Metro G, Vidiri A, Giovanni SD, Cognetti F. Pseudoprogression and MGMT Status in Glioblastoma Patients: Implications in Clinical Practice. Anticancer Res. 2009 Jul 1;29(7):2607–10.
86. Gerstner ER, McNamara MB, Norden AD, Lafrankie D, Wen PY. Effect of adding temozolomide to radiation therapy on the incidence of pseudo-progression. J Neurooncol. 2009 Aug;94(1):97–101.
87. Soike MH, McTyre ER, Shah N, Puchalski RB, Holmes JA, Paulsson AK, et al. Glioblastoma radiomics: can genomic and molecular characteristics correlate with imaging response patterns? Neuroradiology. 2018 Oct;60(10):1043–51.
88. Prager AJ, Martinez N, Beal K, Omuro A, Zhang Z, Young RJ. Diffusion and perfusion MRI to differentiate treatment-related changes including pseudoprogression from recurrent tumors in high-grade gliomas with histopathologic evidence. AJNR Am J Neuroradiol. 2015 May;36(5):877–85.
89. Sanghera P, Perry J, Sahgal A, Symons S, Aviv R, Morrison M, et al. Pseudoprogression following chemoradiotherapy for glioblastoma multiforme. Can J Neurol Sci J Can Sci Neurol. 2010 Jan;37(1):36–42.
90. Yaman E, Buyukberber S, Benekli M, Oner Y, Coskun U, Akmansu M, et al. Radiation induced early necrosis in patients with malignant gliomas receiving temozolomide. Clin Neurol Neurosurg. 2010 Oct;112(8):662–7.
91. Motegi H, Kamoshima Y, Terasaka S, Kobayashi H, Yamaguchi S, Tanino M, et al. IDH1 mutation as a potential novel biomarker for distinguishing pseudoprogression from true progression in patients with glioblastoma treated with temozolomide and radiotherapy. Brain Tumor Pathol. 2013 Apr;30(2):67–72.
92. Song YS, Choi SH, Park C-K, Yi KS, Lee WJ, Yun TJ, et al. True progression versus pseudoprogression in the treatment of glioblastomas: a comparison study of normalized cerebral blood volume and apparent diffusion coefficient by histogram analysis. Korean J Radiol. 2013 Aug;14(4):662–72.
93. Choi YJ, Kim HS, Jahng G-H, Kim SJ, Suh DC. Pseudoprogression in patients with glioblastoma: added value of arterial spin labeling to dynamic susceptibility contrast perfusion MR imaging. Acta Radiol Stockh Swed 1987. 2013 May;54(4):448–54.
94. Agarwal A, Kumar S, Narang J, Schultz L, Mikkelsen T, Wang S, et al. Morphologic MRI features, diffusion tensor imaging and radiation dosimetric analysis to differentiate pseudo-progression from early tumor progression. J Neurooncol. 2013 May;112(3):413–20.
95. Gunjur A, Lau E, Taouk Y, Ryan G. Early post-treatment pseudo-progression amongst glioblastoma multiforme patients treated with radiotherapy and temozolomide: a retrospective analysis. J Med Imaging Radiat Oncol. 2011 Dec;55(6):603–10.
96. Gladwish A, Koh E-S, Hoisak J, Lockwood G, Millar B-A, Mason W, et al. Evaluation of early imaging response criteria in glioblastoma multiforme. Radiat Oncol Lond Engl. 2011 Sep 23;6:121.

97. Park C-K, Kim J, Yim SY, Lee AR, Han JH, Kim C-Y, et al. Usefulness of MS-MLPA for detection of MGMT promoter methylation in the evaluation of pseudoprogression in glioblastoma patients. Neuro-Oncol. 2011 Feb;13(2):195–202.
98. Young RJ, Gupta A, Shah AD, Graber JJ, Zhang Z, Shi W, et al. Potential utility of conventional MRI signs in diagnosing pseudoprogression in glioblastoma. Neurology. 2011 May 31;76(22):1918–24.
99. Pouleau H-B, Sadeghi N, Balériaux D, Mélot C, De Witte O, Lefranc F. High levels of cellular proliferation predict pseudoprogression in glioblastoma patients. Int J Oncol. 2012 Apr;40(4):923–8.
100. Young RJ, Gupta A, Shah AD, Graber JJ, Chan TA, Zhang Z, et al. MRI perfusion in determining pseudoprogression in patients with glioblastoma. Clin Imaging. 2013 Feb;37(1):41–9.
101. Neal ML, Trister AD, Ahn S, Baldock A, Bridge CA, Guyman L, et al. Response classification based on a minimal model of glioblastoma growth is prognostic for clinical outcomes and distinguishes progression from pseudoprogression. Cancer Res. 2013 May 15;73(10):2976–86.
102. Danish H, Schreibmann E, Holder C, Vincentelli C, Hao C, Curran W, et al. Postradiation Diffusion MRIs May Distinguish True Progression from Pseudoprogression in GBM Patients. Int J Radiat Oncol • Biol • Phys. 2013 Oct 1;87(2):S19.
103. Balaña C, Capellades J, Pineda E, Estival A, Puig J, Domenech S, et al. Pseudoprogression as an adverse event of glioblastoma therapy. Cancer Med. 2017 Dec;6(12):2858–66.
104. Topkan E, Topuk S, Oymak E, Parlak C, Pehlivan B. Pseudoprogression in patients with glioblastoma multiforme after concurrent radiotherapy and temozolomide. Am J Clin Oncol. 2012 Jun;35(3):284–9.
105. Jang B-S, Jeon SH, Kim IH, Kim IA. Prediction of Pseudoprogression versus Progression using Machine Learning Algorithm in Glioblastoma. Sci Rep. 2018 Aug 21;8(1):12516.
106. Yang K, Jung SW, Shin H, Lim DH, Lee J-I, Kong D-S, et al. Cancer genetic markers according to radiotherapeutic response in patients with primary glioblastoma - Radiogenomic approach for precision medicine. Radiother Oncol J Eur Soc Ther Radiol Oncol. 2019 Feb;131:66–74.
107. Mohammadi H, Shiue K, Juratli TA, Verma V, Engellandt K, Daubner D, et al. Multi-institutional Series Evaluating the Rate of Pseudoprogression in Isocitrate Dehydrogenase 1 Mutated Glioblastomas. Int J Radiat Oncol • Biol • Phys. 2017 Oct 1;99(2):E94–5.
108. Lewis R, Bhandari A, McKintosh E, Plowman P, Lansley J, Evanson J, et al. Differentiating tumour progression from pseudoprogression in patients with glioblastoma using multiparametric MRI imaging: Data from Barts Health NHS trust London. Eur J Surg Oncol. 2016 Nov 1;42(11):S248–9.
109. Nasseri M, Gahramanov S, Neuwelt EA. Does Pseudoprogression Occur Beyond 3 Months Following Standard Chemoradiation Therapy in Glioblastoma Patients? Int J Radiat Oncol • Biol • Phys. 2012 Nov 1;84(3):S759–60.
110. Kebir S, Fimmers R, Galldiks N, Schäfer N, Mack F, Schaub C, et al. Late Pseudoprogression in Glioblastoma: Diagnostic Value of Dynamic O-(2-[18F]fluoroethyl)-L-Tyrosine PET. Clin Cancer Res Off J Am Assoc Cancer Res. 2016 01;22(9):2190–6.
111. Abbasi AW, Westerlaan HE, Holtman GA, Aden KM, van Laar PJ, van der Hoorn A. Incidence of Tumour Progression and Pseudoprogression in High-Grade Gliomas: a Systematic Review and Meta-Analysis. Clin Neuroradiol. 2018 Sep;28(3):401–11.
112. Sanghera P, Rampling R, Haylock B, Jefferies S, McBain C, Rees JH, et al. The concepts, diagnosis and management of early imaging changes after therapy for

glioblastomas. Clin Oncol R Coll Radiol G B. 2012 Apr;24(3):216–27.
113. Kinger N, Hoch MJ, Shu H-KG, Weinberg BD. Glioblastoma with brainstem leptomeningeal pseudoprogression following radiation therapy. Radiol Case Rep. 2019 May;14(5):613–7.
114. Zikou A, Sioka C, Alexiou GA, Fotopoulos A, Voulgaris S, Argyropoulou MI. Radiation Necrosis, Pseudoprogression, Pseudoresponse, and Tumor Recurrence: Imaging Challenges for the Evaluation of Treated Gliomas. Contrast Media Mol Imaging. 2018;2018:6828396.
115. Tran DKT, Jensen RL. Treatment-related brain tumor imaging changes: So-called "pseudoprogression" vs. tumor progression: Review and future research opportunities. Surg Neurol Int. 2013;4(Suppl 3):S129-135.
116. Larsen VA, Simonsen HJ, Law I, Larsson HBW, Hansen AE. Evaluation of dynamic contrast-enhanced T1-weighted perfusion MRI in the differentiation of tumor recurrence from radiation necrosis. Neuroradiology. 2013 Feb;55(3):361–9.
117. Voss M, Franz K, Steinbach JP, Fokas E, Forster M-T, Filipski K, et al. Contrast enhancing spots as a new pattern of late onset pseudoprogression in glioma patients. J Neurooncol. 2019 Mar;142(1):161–9.
118. Chakravarti A, Erkkinen MG, Nestler U, Stupp R, Mehta M, Aldape K, et al. Temozolomide-Mediated Radiation Enhancement in Glioblastoma: A Report on Underlying Mechanisms. Clin Cancer Res. 2006 Aug 1;12(15):4738–46.
119. Yang I, Aghi MK. New advances that enable identification of glioblastoma recurrence. Nat Rev Clin Oncol. 2009 Nov;6(11):648–57.
120. Yovino SG, Ye X, Grossman S. Results of Early Reoperation for Suspected Pseudoprogression in Patients with Glioblastoma Multiforme. Int J Radiat Oncol • Biol • Phys. 2011 Oct 1;81(2):S276.
121. Ellingson BM, Chung C, Pope WB, Boxerman JL, Kaufmann TJ. Pseudoprogression, radionecrosis, inflammation or true tumor progression? challenges associated with glioblastoma response assessment in an evolving therapeutic landscape. J Neurooncol. 2017 Sep;134(3):495–504.
122. Galldiks N, Law I, Pope WB, Arbizu J, Langen K-J. The use of amino acid PET and conventional MRI for monitoring of brain tumor therapy. NeuroImage Clin. 2017;13:386–94.
123. Thomas AA, Arevalo-Perez J, Kaley T, Lyo J, Peck KK, Shi W, et al. Dynamic contrast enhanced T1 MRI perfusion differentiates pseudoprogression from recurrent glioblastoma. J Neurooncol. 2015 Oct;125(1):183–90.
124. Gzell CE, Wheeler HR, McCloud P, Kastelan M, Back M. Small increases in enhancement on MRI may predict survival post radiotherapy in patients with glioblastoma. J Neurooncol. 2016;128(1):67–74.
125. Hein PA, Eskey CJ, Dunn JF, Hug EB. Diffusion-weighted imaging in the follow-up of treated high-grade gliomas: tumor recurrence versus radiation injury. AJNR Am J Neuroradiol. 2004 Feb;25(2):201–9.
126. Oberheim Bush NA, Cha S, Chang SM, Clarke JL. Chapter 55 - Pseudoprogression in Neuro-Oncology: Overview, Pathophysiology, and Interpretation. In: Newton HB, editor. Handbook of Neuro-Oncology Neuroimaging (Second Edition) [Internet]. San Diego: Academic Press; 2016 [cited 2019 Jun 13]. p. 681–95. Available from: http://www.sciencedirect.com/science/article/pii/B9780128009451000550
127. Jensen RL. Brain tumor hypoxia: tumorigenesis, angiogenesis, imaging, pseudoprogression, and as a therapeutic target. J Neurooncol. 2009 May;92(3):317–35.
128. Fatterpekar GM, Galheigo D, Narayana A, Johnson G, Knopp E. Treatment-related change versus tumor recurrence in high-grade gliomas: a diagnostic conundrum--use of dynamic susceptibility contrast-enhanced (DSC) perfusion MRI. AJR Am J Roentgenol. 2012

Jan;198(1):19–26.
129. Hu LS, Eschbacher JM, Heiserman JE, Dueck AC, Shapiro WR, Liu S, et al. Reevaluating the imaging definition of tumor progression: perfusion MRI quantifies recurrent glioblastoma tumor fraction, pseudoprogression, and radiation necrosis to predict survival. Neuro-Oncol. 2012 Jul;14(7):919–30.
130. Calvo W. Experimental radiation damage of the central nervous system. Recent Results Cancer Res Fortschritte Krebsforsch Progres Dans Rech Sur Cancer. 1993;130:175–88.
131. Hopewell JW, Calvo W, Jaenke R, Reinhold HS, Robbins ME, Whitehouse EM. Microvasculature and radiation damage. Recent Results Cancer Res Fortschritte Krebsforsch Progres Dans Rech Sur Cancer. 1993;130:1–16.
132. Wesseling P, Ruiter DJ, Burger PC. Angiogenesis in brain tumors; pathobiological and clinical aspects. J Neurooncol. 1997 May;32(3):253–65.
133. Galldiks N, Dunkl V, Stoffels G, Hutterer M, Rapp M, Sabel M, et al. Diagnosis of pseudoprogression in patients with glioblastoma using O-(2-[18F]fluoroethyl)-L-tyrosine PET. Eur J Nucl Med Mol Imaging. 2015 Apr;42(5):685–95.
134. Yoon RG, Kim HS, Paik W, Shim WH, Kim SJ, Kim JH. Different diagnostic values of imaging parameters to predict pseudoprogression in glioblastoma subgroups stratified by MGMT promoter methylation. Eur Radiol. 2017 Jan;27(1):255–66.
135. Nobusawa S, Watanabe T, Kleihues P, Ohgaki H. IDH1 mutations as molecular signature and predictive factor of secondary glioblastomas. Clin Cancer Res Off J Am Assoc Cancer Res. 2009 Oct 1;15(19):6002–7.
136. Wang Q, Zhang J, Li F, Xu X, Xu B. Diagnostic performance of clinical properties and conventional magnetic resonance imaging for determining the IDH1 mutation status in glioblastoma: a retrospective study. PeerJ. 2019;7:e7154.
137. Siegal T. Clinical impact of molecular biomarkers in gliomas. J Clin Neurosci Off J Neurosurg Soc Australas. 2015 Mar;22(3):437–44.
138. Kebir S, Rauschenbach L, Gielen GH, Schäfer N, Tzaridis T, Scheffler B, et al. Recurrent pseudoprogression in isocitrate dehydrogenase 1 mutant glioblastoma. J Clin Neurosci Off J Neurosurg Soc Australas. 2018 Jul;53:255–8.
139. Rodriguez FJ, Vizcaino MA, Lin M-T. Recent Advances on the Molecular Pathology of Glial Neoplasms in Children and Adults. J Mol Diagn JMD. 2016;18(5):620–34.
140. Henker C, Kriesen T, Schneider B, Glass Ä, Scherer M, Langner S, et al. Correlation of Ki-67 Index with Volumetric Segmentation and its Value as a Prognostic Marker in Glioblastoma. World Neurosurg. 2019 May 1;125:e1093–103.
141. Mehrkens JH, Pöpperl G, Rachinger W, Herms J, Seelos K, Tatsch K, et al. The positive predictive value of O-(2-[18F]fluoroethyl)-L-tyrosine (FET) PET in the diagnosis of a glioma recurrence after multimodal treatment. J Neurooncol. 2008 May;88(1):27–35.
142. Kim J-H, Bae Kim Y, Han JH, Cho K-G, Kim S-H, Sheen SS, et al. Pathologic diagnosis of recurrent glioblastoma: morphologic, immunohistochemical, and molecular analysis of 20 paired cases. Am J Surg Pathol. 2012 Apr;36(4):620–8.
143. Qian X, Tan H, Zhang J, Liu K, Yang T, Wang M, et al. Identification of biomarkers for pseudo and true progression of GBM based on radiogenomics study. Oncotarget. 2016 Aug 23;7(34):55377–94.
144. McNulty SN, Cottrell CE, Vigh-Conrad KA, Carter JH, Heusel JW, Ansstas G, et al. Beyond sequence variation: assessment of copy number variation in adult glioblastoma through targeted tumor somatic profiling. Hum Pathol. 2019 Apr;86:170–81.
145. Monga V, Jones K, Chang S. CLINICAL RELEVANCE OF MOLECULAR MARKERS IN GLIOMAS. Rev Médica Clínica Las Condes. 2017 May 1;28(3):343–51.
146. Klekner Á, Szivos L, Virga J, Árkosy P, Bognár L, Birkó Z, et al. Significance of

liquid biopsy in glioblastoma - A review. J Biotechnol. 2019 Jun 10;298:82–7.
147. Zachariah MA, Oliveira-Costa JP, Carter BS, Stott SL, Nahed BV. Blood-based biomarkers for the diagnosis and monitoring of gliomas. Neuro-Oncol. 2018 Aug 2;20(9):1155–61.
148. Sullivan JP, Nahed BV, Madden MW, Oliveira SM, Springer S, Bhere D, et al. Brain tumor cells in circulation are enriched for mesenchymal gene expression. Cancer Discov. 2014 Nov;4(11):1299–309.
149. Haber DA, Velculescu VE. Blood-based analyses of cancer: circulating tumor cells and circulating tumor DNA. Cancer Discov. 2014 Jun;4(6):650–61.
150. Macarthur KM, Kao GD, Chandrasekaran S, Alonso-Basanta M, Chapman C, Lustig RA, et al. Detection of brain tumor cells in the peripheral blood by a telomerase promoter-based assay. Cancer Res. 2014 Apr 15;74(8):2152–9.
151. Müller C, Holtschmidt J, Auer M, Heitzer E, Lamszus K, Schulte A, et al. Hematogenous dissemination of glioblastoma multiforme. Sci Transl Med. 2014 Jul 30;6(247):247ra101.
152. Gao F, Cui Y, Jiang H, Sui D, Wang Y, Jiang Z, et al. Circulating tumor cell is a common property of brain glioma and promotes the monitoring system. Oncotarget. 2016 Nov 1;7(44):71330–40.
153. van Schaijik B, Wickremesekera AC, Mantamadiotis T, Kaye AH, Tan ST, Stylli SS, et al. Circulating tumor stem cells and glioblastoma: A review. J Clin Neurosci Off J Neurosurg Soc Australas. 2019 Mar;61:5–9.
154. Liu T, Xu H, Huang M, Ma W, Saxena D, Lustig RA, et al. Circulating Glioma Cells Exhibit Stem Cell-like Properties. Cancer Res. 2018 Dec 1;78(23):6632–42.
155. Krol I, Castro-Giner F, Maurer M, Gkountela S, Szczerba BM, Scherrer R, et al. Detection of circulating tumour cell clusters in human glioblastoma. Br J Cancer. 2018 Aug;119(4):487–91.
156. Koch CJ, Lustig RA, Yang X-Y, Jenkins WT, Wolf RL, Martinez-Lage M, et al. Microvesicles as a Biomarker for Tumor Progression versus Treatment Effect in Radiation/Temozolomide-Treated Glioblastoma Patients. Transl Oncol. 2014 Dec;7(6):752–8.
157. Osti D, Del Bene M, Rappa G, Santos M, Matafora V, Richichi C, et al. Clinical Significance of Extracellular Vesicles in Plasma from Glioblastoma Patients. Clin Cancer Res Off J Am Assoc Cancer Res. 2019 Jan 1;25(1):266–76.
158. Shaw PJ, Bates D. Conservative treatment of delayed cerebral radiation necrosis. J Neurol Neurosurg Psychiatry. 1984 Dec;47(12):1338–41.
159. Levin VA, Bidaut L, Hou P, Kumar AJ, Wefel JS, Bekele BN, et al. Randomized double-blind placebo-controlled trial of bevacizumab therapy for radiation necrosis of the central nervous system. Int J Radiat Oncol Biol Phys. 2011 Apr 1;79(5):1487–95.
160. Delishaj D, Ursino S, Pasqualetti F, Cristaudo A, Cosottini M, Fabrini MG, et al. Bevacizumab for the Treatment of Radiation-Induced Cerebral Necrosis: A Systematic Review of the Literature. J Clin Med Res. 2017 Apr;9(4):273–80.
161. Furuse M, Nonoguchi N, Kuroiwa T, Miyamoto S, Arakawa Y, Shinoda J, et al. A prospective, multicentre, single-arm clinical trial of bevacizumab for patients with surgically untreatable, symptomatic brain radiation necrosis†. Neuro-Oncol Pract. 2016 Dec;3(4):272–80.
162. Siu A, Wind JJ, Iorgulescu JB, Chan TA, Yamada Y, Sherman JH. Radiation necrosis following treatment of high grade glioma--a review of the literature and current understanding. Acta Neurochir (Wien). 2012 Feb;154(2):191–201; discussion 201.
163. Miyatake S-I, Nonoguchi N, Furuse M, Yoritsune E, Miyata T, Kawabata S, et al. Pathophysiology, diagnosis, and treatment of radiation necrosis in the brain. Neurol Med Chir (Tokyo). 2015;55(1):50–9.

164. Chu HH, Choi SH, Ryoo I, Kim SC, Yeom JA, Shin H, et al. Differentiation of true progression from pseudoprogression in glioblastoma treated with radiation therapy and concomitant temozolomide: comparison study of standard and high-b-value diffusion-weighted imaging. Radiology. 2013 Dec;269(3):831–40.

Table 1: Response assessment classifications

	Macdonald criteria 1990 (15)	RANO criteria 2010 (14)		Modified RANO criteria 2017 (42)
Complete Response (CR)	All Complete disappearance of enhancing lesions least 4 weeks No new lesion No corticosteroids Clinically stable or improved	All Complete disappearance of *measurable and non-measurable enhancing lesions* at least 4 weeks No new lesion *Stable or improved T2/FLAIR lesions* No corticosteroids Clinically stable or improved		All Complete disappearance of measurable and non measurable enhancing lesions at least 4 weeks **No criteria on T2/FLAIR lesions** No corticosteroids Clinically stable or improved
Partial response (PR)	All Measurable enhancing lesions: ≥50% decrease in the sum of the product of perpendicular diameters at least 4 weeks Corticosteroids dose stable or decreased Clinically stable or improved	All Measurable enhancing lesions: ≥50% decrease in the sum of the product of perpendicular diameters at least 4 weeks *No progression of nonmeasurable lesions* *No new lesion* *Stable or improved T2/FLAIR lesions* Corticosteroids dose stable or decreased Clinically stable or improved		All Measurable enhancing lesions: ≥50% decrease in the sum of the product of perpendicular diameters or **≥65% decrease in total volume at least 4 weeks** **No criteria on T2/FLAIR lesions** Corticosteroids dose stable or decreased Clinically stable or improved
Stable disease (SD)	No CR nor PR nor PD	All No CR nor PR nor PD *Stable T2/FLAIR lesions* *Corticosteroids dose stable or decreased*		No CR nor PR nor PD
	Any	*<12 weeks after CRT*	*≥12 weeks after CRT*	Any

Progressive disease (PD)	Measurable enhancing lesions: ≥25% increase in the sum of the product of perpendicular diameters New lesion Corticosteroids dose stable or increased Clinical deterioration	*New enhancement outside the radiation field (80% isodose line)* *Histopathological proof of progression*	Any Measurable enhancing lesions: ≥25% increase in the sum of the product of perpendicular diameters *Increase in T2/FLAIR lesions* New lesion *Progression of non-measurable lesions that became measurable* Clinical deterioration	In two sequential MRI separated by ≥ 4 weeks Enhancing lesions: ≥25% increase in the sum of the product of perpendicular diameters or **≥40% increase in the total volume** Clinical deterioration

In *italic*, changes between Macdonald and RANO criteria. In **bold** changes between RANO and modified RANO criteria.

Table 2: RANO criteria for KPS and WHO status deterioration

KPS	
Baseline	**Deterioration**
100% - 90%	**70% or less**
80% - 60%	**Decrease 20% or more**
< or = 50%	**decrease**
WHO status	
Baseline	**Deterioration**
0 or 1	**2 or more**
2	**3**

KPS: Karnofsky Performance Status, **WHO**: World Health Classification

Table 3: Incidence of pseudoprogression (PsP) in the literature

Authors	Year	Country	Design	N	Incidence of increase of contrast enhancing lesions or new lesions in all study's patients	Incidence of PsP in all study's patients	Interval between end of treatment and PsP
Kumar *et al.* (72)	2000	USA	Retrospective	148	67%	13%	6 months
de Wit *et al.* (63)	2004	The Netherlands	Retrospective	32	28%	9%	3 months
Jefferies *et al.* (67)	2007	UK	Prospective	15	53%	20%	6 months
Chamberlain *et al.* (64)	2007	USA	Retrospective	51	51%	14%	6 months
Taal *et al.* (65)	2008	The Netherlands	Retrospective	85	42%	21%	4 weeks
Brandes *et al.* (25)	2008	Italy	Prospective	103	49%	31%	1 month
Clarke *et al.* (82)	2009	USA	Prospective	85	41%	12%	2-4 weeks
Roldan *et al.* (83)	2009	Canada	Retrospective	43	58%	23%	4-6 weeks
Chaskis *et al.* (84)	2009	Belgium	Retrospective	54	NA	6%	6 months
Fabi *et al.* (85)	2009	Italy	Retrospective	12	33%	17%	2 months
Gerstner *et al.* (86)	2009	USA	Retrospective	45	53%	29%	2-4 weeks
Sanghera *et al.* (89)	2010	Canada	Retrospective	104	26%	7%	2 months
Yaman *et al.* (90)	2010	Turkey	Retrospective	67	25%	6%	6 months

Mangla *et al.* (74)	2010	USA Sweden	Retrospective	36	53%	19%	1 month
Tsien *et al.* (53)	2010	USA	Prospective	27	52%	22%	1-3months
Kang *et al.* (11)	2011	Korea	Retrospective	35	51%	23%	1 months
Kong *et al.* (77)	2011	Korea	Prospective	90	66%	29%	2 months
Young *et al.* (98)	2011	USA	Retrospective	321	29%	9%	2-4 weeks
Gunjur *et al.* (95)	2011	Australia	Retrospective	68	60%	21%	3 months
Gladwich *et al.* (96)	2011	Canada	Prospective	25	52%	20%	1 month
Park *et al.* (97)	2011	Korea	Retrospective	48	52%	23%	4 weeks
Pouleau *et al.* (99)	2012	Belgium	Retrospective	63	52%	11%	8 weeks
Topkan *et al.* (104)	2012	Turkey	Retrospective	63	44%	19%	≤6 months
Baek *et al.* (78)	2012	Korea	Retrospective	135	59%	27%	4 weeks
Chan *et al.* (79)	2012	China	Retrospective	28	46%	18%	3 months
Motegi *et al.* (91)	2012	Japan	Retrospective	32	34%	6%	6 months
Nasseri *et al.* (109)	2012	USA	Retrospective	61	NA	28% 21% 49%	≤3 months >3 months total

Lee *et al.* (75)	2012	Korea	Retrospective	22	NA	54%	12 weeks
Young *et al.* (100)	2013	USA	Retrospective	95	51%	4%	2-4 weeks
Neal *et al.* (101)	2013	USA	Retrospective	58	62%	21%	180 days
Linhares *et al.* (58)	2013	Portugal Brazil	Retrospective	70	60%	14%	1 month
Song *et al.* (92)	2013	Korea	Retrospective	20	NA	50%	2 months
Choi *et al.* (93)	2013	Korea	Retrospective	117	53%	24%	4 weeks
Agarwal *et al.* (94)	2013	USA	Retrospective	163	28%	6%	12 weeks
Van Mieghem *et al.* (60)	2013	Belgium	Retrospective	136	60%	7%	4 weeks
Danish *et al.* (102)	2013	USA	Retrospective	131	65%	24%	6 months
Chu *et al.* (78)	2013	Korea	Retrospective	20	NA	50%	2 months
Gahramanov *et al.* (81)	2013	USA	Prospective	19	NA	35%	6 weeks
Nasseri *et al.* (73)	2014	USA	Retrospective	56	52%	34% 14% 48%	≤3 months >3 months total

Ellingson *et al.* (16)	2014	USA	Retrospective	301 329 161	46% 47% 30%	23% 19% 6%	1 month 2 months 6 months
Chang *et al.* (80)	2014	Korea	Retrospective	55	38%	9%	4 weeks
Chinot *et al.* (10)	2014	International	Prospective	463	NA	9%	4 weeks
Prager *et al.* (88)	2015	USA	Retrospective	68	NA	15%	<6 months
Radbruch *et al.* (17)	2015	Germany	Retrospective	79	NA	11%	10 weeks
Gzell *et al.* (124)	2016	Australia	Retrospective	49	NA	2%-8%	6 months
Lewis *et al.* (108)	2016	UK	Retrospective	26	73%	15%	6 months
Kebir *et al.* (110)	2016	Germany	Retrospective	26	NA	27%	6 months
Li *et al.* (76)	2016	China	Retrospective	145	52%	26%	3 months
Mohammadi *et al.* (107)	2017	USA	Retrospective	30	NA	30%	4 weeks
Balana *et al.* (103)	2017	Spain	Retrospective	256	49%	22%	2 months
Jang *et al.* (105)	2018	Korea	Retrospective	79	NA	38%	NA
Rowe *et al.* (70)	2018	USA	Retrospective	67	52%	22%	12 weeks
Brahm *et al.* (71)	2018	The Netherland	Prospective	24	58%	29%	10 weeks

Soike *et al.* (87)	2018	USA	Retrospective	74	NA	19%	NA
Yang *et al.* (106)	2019	Korea	Retrospective	49	55%	26%	3 months

NA: No Available ; **UK** : United Kingdom ; **USA**: United State of America

Table 4: Median overall survival (OS) and median progression free-survival (PFS) of patients with pseudoprogression (PsP) or true progression (TP) in the literature

		Median OS (months)			Median PFS (months)		
Authors	**population**	**PsP**	**TP**	**p value**	**PsP**	**TP**	**p value**
Brandes *et al*., 2008 (25)	GBM	38	10.2	<0.001			
Gerstner *et al.*, 2009 (86)	GBM	24.4	22	NA	15.9	7	NA
Roldan *et al.*, 2009 (83)	GBM	14.5	9.1	0.025			
Sanghera *et al.*, 2010 (89)	GBM	27.8	8	0.0286			
Yaman *et al.*, 2010 (90)	HHG	NA	NA	NS	7	5	0.004
Young *et al.*, 2011 (98)	GBM	10.6	14.7	0.003			
Kong *et al.*, 2011 (77)	GBM	21.7	13.5	NA			
Gunjur *et al.*, 2011 (95)	GBM	27.4	10.4	0.003			
Gladwich *et al.*, 2011 (96)	GBM	19.0	7.2	<0.001			
Topkan *et al.*, 2012 (104)	GBM	NA	14.8	0.009	17.5	10.0	0.014
Nasseri *et al.*, 2012 (109)	GBM	18-20	8	NA			
Chan *et al.*, 2012 (79)	GBM	22	11	NS			
Danish *et al.*, 2013 (102)	GBM	18.5	14.1	0.006			
Gahramanov *et al.*, 2013	GBM	34.4	13.4	<0.0001	31.4	8.4	<0.0001
Nasseri *et al.*, 2014 (73)	GBM	35.2	14.3	<0.0001			
Melguizo-Gavilanes *et al.*, 2015 (13)	GBM	14.4	17.1	0.82	4.8	7.5	0.69
Radbruch *et al.*, 2015 (17)	GBM	29.6	15.8	0.012			
Galldiks *et al.*, 2015 (133)	Gliomas	16	8	0.006			
Li *et al.*, 2016 (76)	GBM	39	12	<0.001			
Balana *et al.*, 2017 (103)	GBM	18.9	12.3	0.0001	10.5	5.3	0.01
Soike *et al.*, 2018 (87)	GBM	23.8	15.7	0.36	15	7.7	0.08
Rowe *et al.*, 2018 (70)	GBM	23.6	13.2	0.032			

NA: not available, **NS:** not significant

Pseudoprogression versus true progression in patients treated with surgery and chemoradiotherapy for glioblastoma: multi-approache literature review

Part 2 – Radiological features

Résumé

Les patients atteints de glioblastome et traités par chimioradiothérapie peuvent présenter une pseudoprogression au cours du suivi. Il est nécessaire de la distinguer de la vraie progression pour pouvoir adapter le traitement et la surveillance. Le diagnostic de pseudoprogression est histologique mais il reste le plus souvent radiologique par le biais de l'IRM conventionnelle qui manque de fiabilité. L'émergence de nouvelles techniques d'imagerie par IRM de diffusion et de perfusion, spectroscopie, et TEP a grandement amélioré la précision diagnostique. Cette revue de la littérature présente les différentes techniques d'imagerie et les potentiels marqueurs de pseudoprogression pouvant guider le diagnostic et différencier pseudoprogression et vraie progression.

Mots clés

Glioblastome, IRM de diffusion, IRM de perfusion, Pseudoprogression, Progression, Spectroscopie, TEP

Pseudoprogression versus true progression in patients treated with surgery and chemoradiotherapy for glioblastoma: multi-approache literature review

Part 2 – Radiological features

Clara Le Fèvre[1], MSc, Caroline Bund[2], MD, MSc, Isabelle Chambrelant[1], MSc, Delphine Antoni[1], MD MSc, Benjamin Leroy-Freschini[3], MD, Hélène Cebula[4], MD, MSc, Roland Schott[5], MD, MSc, Pierre Wagner[6], MD, Jean-Marc Constans[7], MD PhD, Georges Noël[1*], MD PhD.

[1] Department of radiotherapy, comprehensive cancer center Paul Strauss, UNICANCER, 3 rue de la porte de l'Hôpital, 67065 Strasbourg Cedex, France.

[2]Department of Nuclear Medicine, comprehensive University Hospital Hautepierre, 1 avenue Molière, 67098 Strasbourg Cedex, France.

[3]Department of Nuclear Medicine, comprehensive cancer center Paul Strauss, UNICANCER, 3 rue de la porte de l'Hôpital, 67065 Strasbourg Cedex, France

[4]Department of Neurosurgery, Hautepierre University Hospital, 1, avenue Molière, 67200 Strasbourg, France

[5] Departement of medical oncology, comprehensive cancer center Paul Strauss, UNICANCER, 3 rue de la porte de l'Hôpital, 67065 Strasbourg Cedex, France.

[6] Department of Radiology, comprehensive cancer center Paul Strauss, UNICANCER, 3 rue de la porte de l'Hôpital, 67065 Strasbourg Cedex, France.

[7] Department of Radiology, Amiens-Picardie University Hospital, 1 rond-point du Professeur Christian Cabrol, 80054 Amiens Cedex 1, France.

*: Corresponding author: Pr Georges NOEL, same address, gnoel@strasbourg.unicancer.fr

Abstract

After chemoradiotherapy for glioblastoma, pseudoprogression can occur and must be distinguished from true progression to correctly manage glioblastoma treatment and follow-up. Conventional treatment response assessment is evaluated via conventional MRI (contrast-enhanced T1-weighted and T2/FLAIR), which is unreliable. The emergence of advanced MRI techniques, MR spectroscopy, and PET tracers improved the pseudoprogression diagnostic accuracy. This review presents the different imaging techniques and potential imaging biomarkers to differentiate pseudoprogression from true progression through a literature review.

Key words

Diffusion MRI, Glioblastoma, MRS, Perfusion MRI, PET tracers, Pseudoprogression, Progression

Introduction

Since the introduction of chemoradiotherapy (CRT) and adjuvant temozolomide (TMZ) following surgery, more patients with glioblastoma (GBM) have experienced pseudoprogression (PsP) (1–3) compared to those receiving radiotherapy (RT) alone (4). PsP is usually a subacute effect that occurs in the first six months after CRT (5–15). Its mimics progression that evokes response to treatment rather than treatment failure (6,12,16,17). Its incidence remains variable; literature reports rate from 2% to more than 50%, with a rate of 36% in a recent meta-analysis (18). During magnetic resonance imaging (MRI) follow-up of patients treated with surgery, CRT and adjuvant TMZ for GBM, suspected images of progression can occur at the site of previously treated GBM or at distance. Progression is suspected when conventional MRI shows new or enlarged contrast enhancing imaging compared to presurgery, postsurgery, or pre-RT MRI (5). To differenciate between PsP and true progression (TP), MRI is often repeated 4 to 8 weeks after the MRI showing progression, in the absence of pathological proof (19). However, the images *per se* are not specific of PsP or TP. Some groups had proposed criteria to guide response assessment to treatment but those criteria have limits (20–24). The Macdonald criteria were the first to measure radiological response through the two-dimensional measurement of contrast enhancement (22). In 2010, the RANO criteria took into account the T2/FLAIR signal changes in addition to contrast 2D enhancement measurement (21). Modified criteria were published for immune therapies and others clinical situations (20,24). No single imaging features or combination of features have been validated to date to differentiate PsP and TP (25). New therapeutics that impact MRI further complicate PsP diagnosis. Moreover, contrast-enhanced image signal MRI is dependent on the contrast dose, injection timing, magnetic field strength, and choice of image sequences (19). Conventional MRI is limited in response assessment and disease progression monitoring. Some authors proposed advanced imaging, now routinely available, to find non-

invasive imaging markers and improve PsP diagnosis to improve patient outcome (26,27). In addition to supplying structural and anatomical information, advanced MRI provide cellular, biological, and metabolic information (28). A meta-analysis including 941 patients with GBM showed that advanced MRI techniques had higher diagnostic accuracy than conventional MRI for the distinction of PsP and TP with sensitivity and specificity of 71-92% and 85-95% vs 68% and 77%, respectively. Magnetic resonance spectroscopy (MRS) had the best accuracy with sensitivity and specificity of 91% and 95%, respectively, followed by perfusion MRI with dynamic contrast-enhanced MRI (DCE) (29). The authors developed a model-based metric of therapy response based on T1 contrast-enhanced MRI and used linear, 4D-spherical, and 4D-anatomic models to distinguish PsP from TP with a sensitivity of 79%, a specificity of 59%, a positive predictive value (PPV) of 50%, and a negative predictive value (NPV) of 93% (30). The combination of advanced modalities in multiparametric imaging improve accuracy but require training, clinical trial data, and standardization.

The aim of this analytic review was to discuss the metrics of diffusion MRI, perfusion MRI, MRS, and positron emission tomography (PET) techniques to distinguish PsP from TP.

Methods

A literature search was conducted using the Medline/PubMed, ScienceDirect, and Cochrane Wiley databases. The search terms used included (“glioblastoma” OR “gliomas” OR “high grade gliomas”) AND (“pseudoprogression” OR “pseudo-progression”). Articles concerning PsP in adult patients treated for glioma, high grade glioma and glioblastoma treated with the Stupp protocol were examined. References provided from relevant articles were also examined to identify additional studies for inclusion. Any irrelevant entries and non-English articles were excluded. A total of 23 articles about conventional MRI, 43 about diffusion MRI, 58 about perfusion MRI, 25 about MRS, 59 about PET scan, and 14 about SPECT were included in this review.

Conventional MRI

Conventional gadolinium contrast-enhanced MRI is the gold standard for the measurement of response to treatment but is not efficient to distinguish TP from PsP (16). Conventionally, PsP conventional MR images show a vasogenic edema due to increased vascular permeability and increased contrast enhancement (6,31). Santra *et al*. concluded that the overall sensitivity, specificity, PPV, NPV and accuracy of conventional MRI to detect TP was 83%, 25%, 77%, 33%, and 67%, respectively (32). For the following of GBM patients treated with CRT, the National Comprehensive Cancer Network (NCCN) suggests 1) a preoperative MRI, 2) an intraoperative MRI for optimal tumor resection (when available), 3) a 48-72h postoperative MRI 4) a 4-week post-CRT MRI, and 5) repeat MRI every 2–4 months according to the disease status and clinical course (33). To assist clinicians in PsP diagnosis and uniform practices, the International Standardized Brain Tumor Imaging Protocol (BTIP) established the minimum image acquisition requirements for 1.5T and 3T MR scans: sagittal/axial T1, axial FLAIR and axial DWI prior to contrast administration, and axial T2 and sagittal/axial T1 after contrast administration (23).

T1-weighted contrast-enhanced images

Some studies reported that the size of enhancing lesion was higher in the TP than in the PsP (34,35). Several TP radiological markers were identified as the involvement of the corpus callosum with multiple enhancing foci crossing the midline and multiple enhancing lesions or with subependymal spread and multiple enhancing lesions (36), subependymal enhancement (37,38), the spreading wave front of enhancement (38), the enhancing lesion crossed the midline (34), and solid enhancement with distinct margins and focally enhancing nodules (39). In 3D MRI, a more spherical and symmetric shape of contrast enhancement and fuller with reduced perforations in the outer shell of the enhanced region was conducted for TP diagnosis (40). However, some studies showed that the increase in T1 contrast enhancement

was not statistically significant between PsP and TP (7) and the change in the size of the enhancing lesion between baseline MRI and progression MRI was not a determinant criterion between PsP and TP (34). No difference was found in the location of the recurrent volume between PsP and TP (34). Moreover, no correlation between MRI changes and radiation dose distribution was demonstrated between PsP and TP (34). The authors showed that the sharp demarcation was poorly defined in PsP compared to TP (34). Others authors demonstrated that new enhancement, marginal enhancement around, nodular enhancement, callosal enhancement, spreading wave front of enhancement, cystic or necrotic changes, increased peritumoral intensity, subsequent decreased enhancement, and diffusion restrictions were not found as predictive factors of PsP (37). Textural features analysis of conventional MRI could help differentiate PsP and TP (41).

The T1-weighted enhancement MR images interpretation can be prudent because they may be influenced by radiological technique, corticosteroids use (42), antiangiogenic agents (43) or MGMT promoter methylation (1). Moreover, differential non-tumoral diagnoses of enhancing lesions can be used, such as inflammation, seizure, postsurgical changes, and ischemia.

T2/FLAIR

An increase in FLAIR signal intensity oriented toward TP (34,44) was discussed (7). Some authors showed an increase in the FLAIR volume favoring TP (45) as the increase in the bidimensional size measurement (34). Moreover, the FLAIR volume in the 45 Gy (75%) isodose favored PsP (45).

The T2/FLAIR signal must be interpreted with caution because it can be influenced by treatment effects, corticosteroids, demyelination, infection, or seizure (21).

Due to the similarities between PsP and TP on conventional MRI and the difficulties faced by clinicians and neuroradiologists, advanced imaging techniques were necessary, such as MRS, diffusion-weighted MRI (DWI), MR perfusion imaging, diffusion-tensor imaging and PET-

based strategies (46,47). Multiples sequences were developed allowing several metric measurements and are described in Table 1.

Diffusion-weighted MRI (DWI) and Diffusion tensor imaging (DTI)

Advanced MRI techniques can provide additional information when conventional MRI is ambiguous to improve the distinction between PsP and TP (26,48). Different diffusion modalities were developed. DWI measures the degree of water diffusion within tissue, detecting the displacement of water molecules. DTI is a complete and intricate version of DWI that is based on the direction of water diffusion (17,49). Different metrics are available, such as apparent diffusion coefficient (ADC) and fractional anisotropy (FA). The association of DWI with conventional MRI could help the clinical differentiation of tumor tissue, edema, and healthy tissue, creating tissue profile and tumor map to evaluate the extent and heterogeneous composition of the tumor. It could guide biopsy or improve re-contouring after irradiation to match the anteriorly irradiated volume (50). Radiation injuries images usually showed heterogeneity on DWI images and often included spotty and marked hypo-intensity (51). Analyzing signal intensity patterns on DWI, Lee *et al*. showed that patients with TP had a higher incidence of homogeneous or multifocal high signal intensity than those with PsP who had rim high or no high intensity signal (p=0.027). The PsP volume was higher than the TP volume (p=0.009) (52). Xu *et al*. concluded that DTI offered a sensitivity, specificity, PPV, and NPV of 85%, 87%, 89%, and 81% respectively. The lesion classification accuracy was 86% (53).

Apparent Diffusion Coefficient (ADC)

ADC values quantify the mobility of water molecules at the cellular level, with the potential to differentiate between necrosis, edema and recurrent tumor. Areas with high cellularity have decreased ADC values because the diffusivity of water molecules is expected to be decreased due to the relative reductions in extracellular space, as compared with treatment-related

changes with low cellularity. It helps to distinguish if enhancing lesion resulted from TP or not with the hypothesis that recurrent tumor had low ADC values (17,51,54,55). An increase in tumor ADC values following therapy compared to pre-treatment ADC was predictive of favorable response (56). ADC values within a single tumor are often heterogeneous, likely reflecting a mixture of viable and necrotic tumor tissue (57). Necrosis, gliosis, ischemia, hemorrhage, inflammation, infection, and fibrous scar tissue can impact the ADC values, and peritumoral edema is characterized by high ADC values (31,58,59). Van Dijken *et al.* in a meta-analysis of 35 studies and 1174 patients retrieved an ADC pooled sensitivity and specificity of 71% and 87%, respectively, to differentiate PsP and TP (29). ADC could be interesting for the differentiation of PsP and TP. Some authors reported that ADC values and ADC ratios were higher in PsP patients than in TP patients (51,53,54,60–67) but others did not demonstrate a difference (34,55,68) (Table 2). Al Sayyari *et al*. used susceptibility-weighted imaging (SWI), which was susceptible to visualize heterogeneous tissue patterns, providing information on microvascularity, necrosis, blood-brain barrier, and evaluation of ADC values in the context of abnormal blood-brain barrier. The authors compared contrast-enhanced T1-weighted imaging (CE-T1) and contrast-enhanced susceptibility-weighted imaging (CE-SWI) of 17 patients with a new contrast enhancement after CRT and created ADC maps. They reported that the CE-SWI volume was reduced compared to CE-T1 ($p=0.002$) with no difference in the median ADC value. An increase in CE-SWI volume was associated with a reduction in ADC oriented toward TP. Patients with TP had significantly reduced ADC values vs patients with PsP who had significantly elevated ADC values within the CE-SWI enhancement volume (69). The fifth percentile of ADC maps could be helpful for distinguishing PsP and TP. Song *et al*. proposed a threshold value of fifth percentile of 0.892×10^{-3} mm^2/s to differentiate PsP and TP with a sensitivity of 90% and a specificity of 90% (70). Chu *et al*. analyzed histograms of ADC maps. The fifth percentile was significantly

lower in TP than in PsP regardless of standard or high b value ($p=0.049$ and $p<0.001$, respectively). The authors concluded that the fifth percentile of the cumulative ADC histogram was a promising parameter with an accuracy of 89% for high b values (b3000) and 67% for standard b values (b1000) (71).

Fractional Anisotropy (FA)

FA measures the fraction of anisotropic diffusion and is useful for the detection of peritumoral swelling, radiation necrosis, and infiltrating tumor cells (17). The FA value varies between 0 and 1 and reflects the anisotropic degree of diffusion (72,73). The FA value was higher in TP than in PsP in some studies (53,65,74), but some authors reported no difference (34,55). Alexiou *et al*. proposed a FA ratio cut-off value of >0.47 for TP with 57% sensitivity and 100% specificity (65). In Xu *et al*. study, a TP was suggested when either an ADC ratio <1.65 or/and a FA ratio >0.36 at the contrast-enhancing lesion (53). Wang *et al*. showed a FA threshold value of >0.13 to diagnose TP had a sensitivity of 71% and a specificity of 75% (74).

Sensitivity of diffusion MRI was probably sufficient to differentiate PsP and TP but specificity remained low (31). Larger studies with more sophisticated and especially precise analytical techniques are required to determine uniform diffusion parameters.

Perfusion imaging findings

Perfusion MRI provides cerebral and tumor vascular perfusion and permeability information. It can be interesting for tumor grading, molecular characterization, treatment response assessment, or tumor differential diagnosis (75). Several perfusion MRI techniques can be used to determine tumor progression: dynamic susceptibility-weighted contrast-enhanced MRI (DSC), dynamic contrast-enhanced MRI (DCE) and arterial spin labeling (ASL) (57,76). In a recent European survey, perfusion MRI seemed to be used most frequently to differentiate TP and radiation effects (77). Variable findings in studies resulted from the

variability of perfusion MRI acquisition protocols and analytic techniques and small sample size (78). Kelm *et al*. compared several DSC software packages and found significant variations in the relative cerebral blood volume (rCBV) according to the package used (79). Consequently, to improve the consistency of perfusion MRI, efforts are necessary to standardize the acquisition and analysis (31,57). Optimal thresholds must be determined and validated prospectively to confirm that the accuracy is sufficient for clinical use.

Dynamic susceptibility contrast MRI (DSC)

DSC is the most used perfusion modality. DSC is a T2/T2*-weighted technique using gadolinium contrast agent and measuring rCBV, offering a marker of angiogenesis and microvasculature (80). It is the most validated parameter that informs on tumor grade, vascularity, or focal transformation. An inherent limitation of DSC is underestimation of the blood volume in areas of significant blood-brain barrier breakdown (81). DSC is widely available and has a short acquisition time, a lower resolution, fewer artifacts, and needs leakage correction (57,78). DSC can evaluate different metrics: rCBV, cerebral blood flow (CBF), relative peak height (rPH), and percentage of signal intensity recovery (PSR). TP is usually characterized by increased blood volume and blood flow secondary to neocapillary formation and dilation of preexisting vasculature leading to an increase in rCBV compared to PsP that is always typified by a decrease in rCBV (82,83). A meta-analysis reported DSC had a sensitivity of 89% and a specificity of 80% to diagnose PsP. With a mean rCBV ranging from 0.9 and 2.15 and a maximum rCBV ranging from 1.49 and 3.1, the sensitivity and specificity to detect TP were 88%/88%, and 93%/76%, respectively (80). Van Dijken *et al*. in a meta-analysis reported a DSC pooled sensitivity and specificity of 87% and 86%, respectively, to diagnose TP (29).

In some studies, rCBV was significantly higher in TP than in PsP (15,62–65,68,74,84–95) but few studies demonstrated no difference (7,70,96–98) (Table 3). Mangla *et al*. showed that, at

one month after CRT, patients with PsP and with TP had a mean decrease in rCBV of 41% and 12%, respectively (99). Kong *et al*. prospectively studied DSC of 59 GBM patients with new or enlarged enhancing lesions after CRT. A significance difference was observed in rCBV between PsP (0.87) and TP (3.25) for patients with unmethylated O^6-methylguanine-DNA methyltransferase (MGMT) promoter (p=0.009), while no significant difference was found between rCBV in PsP and in TP for patients with MGMT promoter methylation (1.56 vs 2.34, p=0.258) (100). Analyzing changes in kurtosis and skewness derived from normalized CBV between the first and second post-CRT follow-up of 79 patients with GBM as an imaging biomarker predictor for early treatment response to CRT, Baek *et al*. demonstrated that histogram parameters (maximum, mode, range, percent change of skewness and kurtosis, and histographic patterns) showed statistical differences between PsP and TP. In multivariate analysis, maximum and histographic patterns were independent predictors of TP. Histogram analysis of rCBV can help to differentiate PsP from TP with sensitivity of 85.7% and a specificity of 89.2% (101). rPH and PSR were found significantly higher and lower, respectively, in TP patients compared to PsP (84,93). However some authors disputed the difference retrieved with PSR (64).

Dynamic contrast enhanced MRI (DCE)

DCE is a T1-based technique allowing measurement of vascular permeability in tumors using gadolinium-based contrast agents. DCE has a higher resolution but a long-time acquisition. DCE can also model rCBV. Metrics that can be evaluated by DCE are transfer coefficient between the intra- and extravascular spaces called the volume transfer constant (K^{trans}), volume of extravascular-extracellular space (V_e) corresponding to the extravascular extracellular space per unit volume of tissue, transfer constant from the extracellular-extravascular space into the plasma (K_{ep}), or the blood plasma volume per unit volume of tissue calles the vascular plasma volume (Vp). DCE was identified as biomarker of PsP (102).

K^{trans} was significantly higher in TP patients (85,103–105), as V_e (104) and V_p (105) but some studies did not show differences in V_e (85,98,103) , V_p (104) or K_{ep} (98,103) (Table 3). However, the evaluation time seemed longer since Shin *et al*. demonstrated that, three months after CRT, rCBV and rK^{trans} were significantly higher in a TP group than in a PsP group (p=0.007 and p=0.026, respectively), but not within three months (p=0.511 and p= 0.399, respectively) (98).

A meta-analysis by Van Dijken *et al*. reported a DCE pooled sensitivity and specificity of 92% and 85%, respectively, to diagnose TP (29).

Arterial spin labeling (ASL)

ASL is a less frequently used non-invasive perfusion MRI technique allowing the quantification of tissue perfusion with no need for contrast administration evaluating the CBF (57,106,107). It uses magnetically labeled blood as an endogenous tracer instead of exogenous gadolinium-based contrast agents. ASL is particularly useful for patients with renal failure or with difficult intravenous access. Moreover, CBF is not affected by leakage effects (19). ASL can help the distinction between PsP and TP (108). ASL was an independent predictor of TP (OR=4.73; p= 0.0017) with a sensitivity of 79%, a specificity of 64% and improved diagnostic accuracy (from 76% to 89%) when interpreted qualitatively in conjunction with DSC (106). A meta-analysis retrieved an ASL pooled sensitivity and specificity varying from 52% to 79% and from 64% to 82%, respectively (29). ASL had a higher sensitivity than DSC (94% vs 71%) for diagnosing TP (109). The rCBF was significantly higher in patients with TP than in those with PsP (85,95) or not (15,85) according to the authors (Table 3).

Combination of parameters

Multiparametric imaging was useful in the diagnosis of TP vs PsP (110). Cha *et al*. examined a multiparametric approach combining DWI and perfusion MRI with rCBV and ADC values

in 35 patients with GBM. Diagnoses based on the multiparametric approach were more accurate than those based on the uniparametric approach, with 82% sensitivity and 100% specificit,y and rCBV was the best predictor of TP ($p<0.001$)(82). Kim *et al*. performed measurements using two readers. They demonstrated that the addition of conventional MRI and DWI with either DSC ($p<0.001$ and $p=0.002$ for each reader, respectively) or DCE ($p<0.001$ for foth readers) improved prediction of TP. With the combination of conventional MRI, DWI and DSC, the sensitivity and specificity varied from 82% to 84% and from 95% to 96%, respectively. With the combination of conventional MRI, DWI, and DCE, the sensitivity and specificity varied from 91% to 92% and from 84% to 87%, respectively (38). Combining DSC and DWI, Prager *et al*. showed that the sensitivity and specificity of predicting TP were 93% and 83%, respectively (64). In a retrospective study, Park *et al*. analyzed a volume-weighted voxel-based multiparametric clustering (VVMC) method to distinguish PsP and TP in 162 patients (108 in a training set and 54 in ta est set) vs single parametric methods (ADC and CBV). In the entire population, VVMC was significantly improved in differentiating TP and PsP compared with any single parameter, with a sensitivity, specificity, and accuracy varying from 87% to 91%, for the three parameters (111). Seeger *et al*. demonstrated that the combination of DCE and DCS perfusion techniques led to an increase in the sensitivity and accuracy. ASL could improve the accuracy but not the diagnostic performance of the preexisting combination of DCE and DSC. However, the best multiparametric approach was perfusion MRI and MRS, with an accuracy of 90%, a sensitivity of 83%, and a specificity of 100% (85). Yoon *et al*. studied DWI, DSC, and DCE parameters in 75 GBM patients presenting enlarged contrast-enhanced lesions one month after CRT, and 55% had MGMT promoter methylation. In patients with MGMT promoter methylation, the probability of PsP was 96% when CBV90 value was <4.02 and 90% when ADC10 was >0.94. The results suggested that MR imaging parameters were stronger

predictors of PsP when MGMT promoter was methylated than when it was unmethylated and DSC had the highest accuracy for PsP (112).

Others modalities

After CRT, patients treated for GBM are prone to blood-brain barrier disruption, so rCBV can be underestimated when gadolinium-based contrast agents are used. Ferumoxytol is a very small supramagnetic iron oxide nanoparticle (30 nm) that can be a relevant substitute because of its potential to act as a blood pool agent shortly afterward (11,113). In 2011, a pilot study showed a difference between ferumoxytol rCBV and gadoteridol rCBV values ($p=0.002$) in a TP group but not in a PsP group ($p=0.9$) (91). In 2013, the same authors reportes significantly improved survival in patients with rCBV values ≤1.75 ($p=0.001$) using ferumoxytol as a prognostic biomarker in differentiating TP from PsP and predicting survival in GBM patients who did not required contrast agent leakage correction (114). Other authors proposed ferumoxytol as a gadolinium contrast mismatch ratio for PsP biomarker (115).

Ma *et al*. reports the use of 3T using amide proton transfer-weighted (APTW) imaging features for the differentiation between PsP and TP. $APTW_{mean}$ and $APTW_{max}$ signal intensity were higher in a TP group than in a PsP group (2.75% vs 1.56%; $p< 0.001$ and 3.29% vs 1.95%; $p<0.001$). The respective $APTW_{mean}$ and $APTW_{max}$ thresholds for predicting TP were 2.42% (sensitivity of 85% and specificity of 100%) and 2.54% (sensitivity of 95% and specificity of 92%) (116).

Tsien *et al*. proposed using parametric response mapping (PRM). PRM is a voxel-based imaging method applied to perfusion maps to quantify early hemodynamic alterations after treatment. It can measure the difference between serial rCBV maps for each voxel. P PRM_{rCBV} was significantly different between PsP and TP ($p<0.001$) and could be considered potential biomarker to distinguish TP from PsP (97).

Perfusion MRI-fractional tumor burden (pMRI-FTB) was correlated most strongly with histologic tumor fraction compared to other metrics and could be a promising TP biomarker (89).

Radiomic features combined with clinical and genomic features could improve the diagnostic differenciation between PsP and TP (117–119).

Magnetic Resonance Spectroscopy (MRS)

MRS detects different metabolites in brain tissue: choline (Cho), *N*-acetylaspartate (NAA), creatinine (Cr), lipid (Lip), and lactate (Lac). Classically, tumors demonstrate an increase in Cho levels (due to increase in cell membrane turnover) and a decrease in NAA levels compared to normal white matter. Necrosis has elevated lipid and lactate peaks and decrease NAA levels (67,120). However, both PsP and TP may demonstrate neuronal loss or dysfunction (low NAA), abnormal cellular membrane (high Cho), or anaerobic metabolism (high Lac and Lip) (16). Different technical parameters exist such as single or multivoxel techniques. Multivoxel techniques seem to be more informative compared to single voxel techniques because high grade gliomas (HGG) are often mixed lesions (19,63). They can account for spatial heterogeneity in tissues and appear to improve diagnostic accuracy for tumor detection. Moreover, a longitudinal evaluation with MRS could improve specificity (57). A meta-analysis of 455 patients showed that MRS alone had a moderate impact on the diagnosis of TP and a Cho/Cr ratio threshold ranging from 1.05 to 2.60 had a sensitivity and a specificity of 83%, respectively, and Cho/NAA ratio threshold ranging from 0.88 to 1.90 had a sensitivity and a specificity of 88% and 86%, respectively. Consequently, the authors recommended the combination of MRS with advanced imaging technologies (121).

MRS can be effective in distinguishing PsP and TP (16,120,122). In Zeng *et al.* study, MRS correctly classified 85% of patients in both TP and PsP groups (61). Table 4 summarized the literature data concerning metabolite ratios of MRS (55,61–63,66–68,85,86,123–127). Elias *et*

al. demonstrated the ability of non-normalized Cho/NAA and NAA/Cr ratios to identify TP with sensitivity, specificity, PPV, and NPV of 86%, 90%, 93%, and 82% and 84%, 93%, 70%, and 82%, respectively. The normalized Cho/NAA ratio offered a sensitivity, specificity, PPV, and NPV of 73%, 40%, 65%, and 50%, respectively (128).

Other authors studied the effect of the combination of different imaging modalities to improve PsP identification. Fink *et al*. compared the capacity of multivoxel MRS, single voxel MRS, DSC, and DWI to diagnose TP. The authors suggested that single voxel MRS was inadequate and multivoxel MRS should be used to differentiate TP and radiation injuries. The authors proposed a multivoxel Cho/Cr peak area ≥1.54 for sensitivity, specificity, PPV, NPV, and accuracy of 96%, 83%, 96%, 83%, and 93%, respectively, and a multivoxel Cho/NAA peak height ≥1.05 for sensitivity, specificity, PPV, NPV, and accuracy of 91%, 83%, 95%, 71%, and 90%, respectively (63). The conjunction of the metabolite ratios of MRS and ADC of DWI showed that 96% of patients were classified into the correct group. The sensitivity, specificity, and diagnostic accuracy of 3D-MRS were 94%, 100% and 96%, respectively (61). Di Costanzo *et al*. studied the combination of MRS, conventional MRI, DWI, and perfusion MRI. The discrimination accuracy was 79% when considering only Cho/Cr, 86% when considering Cho/Cr and ADC, 90% when considering Cho/Cr and rCBV, and 97% when considering Cho/Cr, ADC, and rCBV (129). Matsusue *et al*. demonstrated a threshold of 1.30 for ADC ratio, 2.10 for the rCBV ratio, 1.29 for Cho/Cr ratio, and 1.06 for Cho/NAA ratio for an accuracy of 87%, 87%, and 85%, respectively. The accuracy of distinguishing TP from PsP reached 93% by combining DWI, DSC, and MRS (130). A comparison of conventional MRI to MRS, perfusion MRI and FDG-PET showed the PPV was 50%, 92%, 75%, and 100% respectively. The NPV for MRS, perfusion MRI, and FDG-PET was 100%, 61%, and 100% respectively, demonstrating the superiority of MRS and perfusion MRI vs FDG-PET for

diagnosing TP (131). Verma *et al.* proposed 3D echo-planar spectroscopy to differentiate PsP and TP (132).

Because of user variability to determine the regions of interest and lower spatial resolution, MRS-induced uncertainty, and lack of reproducibility. The definition and validation of the thresholds to diagnose PsP and TP are necessary in clinical practice and clinical trials. The limitations of MRS could be the voxel sizes with the risk of partial volume effects, time acquisition, signal contamination, and various metabolite ratios used in studies (29,55,61,85,86,129).

Positron-Emission-Tomography (PET)

PET uses biologically active molecules with short-lived positron-emitting isotopes. It can provide information on tumor metabolism and orientates clinical decisions, especially in cases of non-informative or ambiguous MRI findings. The most common and available is fluoro-deoxy-glucose (FDG)-PET, which has often standardized image acquisition but was limited for distinguishing PsP and TP. Novel tracers with lower background brain activity were studied to evaluate TP (133). Some authors found that amino acid tracers such as methyl-L-methionine (MET), fluoroethyl-L-tyrosine (FET) or fluoro-L-dopa (FDOPA) had higher diagnostic accuracy than conventional and advanced MRI in the differentiation of TP and PsP (134). The European Association of Nuclear Medicine (EANM), the Society of Nuclear Medicine and Molecular Imaging (SNMMI), the European Association of Neurooncology (EANO), and the Working Group for Response Assessment in Neurooncology with PET (PET-RANO) published guidelines for FDG, MET, FET and FDOPA-PET (135). The PET images could be fusioned with contrast-enhanced T1 and T2/FLAIR MRI images for the interpretation. The different PET tracers are summarized in Table 5.

Standardization of the methodology and analytical approaches is needed to improved comparability and harmonize practices (136).

2-Deoxy-2-[fluorine-18]fluoro- D-glucose positron emission tomography (^{18}F-FDG PET)

Although FDG-PET has already been validated to distinguish PsP and TP (15,32), it has some limitations in the assessment of TP (14,57,137,138). First, normal brain had a high utilization of glucose and the determination of FDG uptake in lesions near gray matter is difficult (133). The detection of small lesions is limited with a poor resolution although it has significantly improved since 2011 (139). The dual time acquisition improved the FDG-PET performance with image acquisition at one hour and 4-5 hours (140,141). Then, intrinsic evolution of the tumor could affect FDG uptake and limit sensitivity (142) and necrotic lesions could have increased glucose metabolism due to inflammation (143). Similar to GBM progression, which demonstrated increased glucose metabolism, radiation injury can also demonstrate increased FDG uptake (144). Methods to define a cut-off standardized uptake value (SUV) were unreliable because the relative glucose uptake and FDG-PET varied widely for tumors and was different for normal brain (144). Ricci *et al*. concluded that FDG-PET was not a useful tool for the diagnosis of PsP or TP and a comparison with contralateral white matter provided a sensitivity, specificity, PPV, and NPV for diagnosis of TP of 86%, 22%, 73% and 50%, respectively, and a comparison with contralateral gray matter of 73%, 56%, 80%, and 46%, respectively (145). However, Santra *et al*. demonstrated an overall sensitivity, specificity, PPV, NPV, and accuracy of diagnosing TP in a GBM subgroup of 50%, 100%, 100%, 40%, and 63%, respectively, and concluded that FDG-PET was a highly specific modality for detecting TP (32). In Larsen *et al*., DCE and FDG-PET obtained an 81% concordance in the classification of new contrast-enhanced lesion (15). When FDG-PET was combined with perfusion MRI, DWI, and MRS, the diagnostic accuracy improved (62).

Others novels tracers such as FDOPA, MET, and FET can be more useful.

^{18}F-fluoro-L-dopa positron emission tomography (^{18}F-FDOPA PET)

FDOPA is another ^{18}F labeled amino acid analogue. It was used primarily to measure dopamine synthesis and evaluate patients with Parkinsonian syndromes. It was used for brain tumor evaluation and showed an increased uptake in gliomas, which resulted from an increased transport via the L amino acid transport system for large neutral amino acids, namely the subtypes LAT1 and LAT2 (146). FDOPA-PET was useful for the diagnosis of GBM and evaluating the possible progression with the complementary role of MRI, detecting recurrence earlier than MRI (147–149). Chen *et al*. compared FDOPA-PET and FDG-PET and concluded that the sensitivity of FDOPA-PET was higher than FDG-PET for detecting tumors with the same specificity, with a sensitivity, specificity, accuracy, PPV, and NPV of FDOPA-PET and FDG-PET of 96%, 43%, 83%, 85%, and 75%, and 61%, 43%, 57%, 78%, and 25%, respectively. The authors proposed a threshold of tumor uptake to striatum uptake (T/S) and tumor uptake to normal hemispheric tissue uptake (T/N) of >1.0 and >1.3 for a sensitivity and a specificity of 96%/100% and 96%/86%, respectively (147). Hermann *et al.* showed that SUV_{max}, SUV_{mean}, T/N_{max}, T/N_{mean}, T/S_{max}, and T/S_{mean} were significantly higher in GBM patients with TP vs no progression and the T/S_{max} ≥1.0 threshold had a sensitivity of 84%, a specificity of 62%, and an accuracy of 78% (150). In another study, the sensitivity, specificity, and accuracy of FDG-PET and FDOPA-PET were 48%, 100%, and 61%, and 100%, 86%, and 96%, respectively, with FDOPA-PET more sensitive and specific at detecting recurrence (151). FDOPA-PET and MRI fusion provided anatomical localization precision of abnormal FDOPA-PET activity and the concordance between both enhancing and non-enhancing lesion on MRI and increased FDOPA-PET uptake was around 90%. FDOPA-PET could identify tumors not visible on MRI and was able to distinguish recurrent non-enhancing tumors from other causes of T2 signal changes on MRI (148). A meta-analysis reported that FDOPA-PET was more effective than FET-PET (p=0.015) (152), another amino tracer that was used and studied.

O-(2-[^{18}F]fluoroethyl)-L-tyrosine positron emission tomography (^{18}F-FET PET)

FET-PET was developed in the late 1990s as an ^{18}F labeled tracer (153). FET is an analog of tyrosine not metabolized into proteins. Its uptake is mediated by the L-type AA transport system in tumor cells. Unlike MET or FDOPA, FET has very high stability. In addition to FET-PET static images, the acquisition of dynamic images with a time-activity curve (TAC) containing additional biological information is useful for glioma grading and the differentiation of PsP and TP (146,154).

Several metrics of FET-PET were identified as imaging biomarkers of TP or PsP. In a retrospective study, the mean and maximum tumor-to-brain ratios (TBR_{mean} and TBR_{max}) obtained using FET-PET were higher in a TP group (2.3 and 2.8) than in a PsP group (1.8 and 1.9) ($p<0.001$) and the mean time to peak (TTP) was shorter in the TP group than in the PsP group ($p=0.05$). The optimal TBR_{max} and TBR_{mean} cut-off values for identifying PsP were 2.3 and 2.0, respectively, with a sensitivity of 100% and 82%, a specificity of 91% and 82%, and an accuracy of 96% and 82%, respectively (155). In another study, the same authors evaluated static and dynamic FET-PET. The TBR_{max}, TBR_{mean}, and TTP thresholds for identifying TP were 2.3, 2.0, and <45 min with sensitivity of 68%, 74%, and 82%; specificity of 100%, 91%, and 73%, and accuracy of 71%, 75%, and 81%, respectively. The combined analysis of TBR_{max}, TBR_{mean} cut-off, and kinetic patterns had a sensitivity of 93%, a specificity of 73%, and an accuracy of 91% but the combined TBR_{mean} cut-off and TTP cut-off had the best results with a sensitivity of 93%, a specificity of 100%, and an accuracy of 93% (156). Pauleit *et al*. demonstrated that the TBR ratio was an independent significant coefficient for the distinction of tumor ($p=0.004$) and reported that the TBR_{mean} was 2.6 in TP vs 1.2 in peritumoral tissue ($p<0.001$). The sensitivity and specificity were 92% and 81%, respectively, with a TBR ratio threshold of 1.6 (157). Kebir *et al.* analyzed 26 GBM patients and reported that TBR_{max} and TBR_{mean} were significantly higher in TP patients than in PsP patients (2.4 vs

1.5, p=0.003 and 2.1 vs 1.5, p=0.012, respectively) and TTP was lower in a TP group (25 min vs 40 min, p<0.001). A TBR_{max} threshold of 1.9 showed a sensitivity, specificity, and accuracy of 84%, 86%, and 85%, respectively (158). Mihovilovic *et al.* proposed a TBR_{max} threshold of 3.52 with an accuracy of 86% for late PsP (159). The EANM/SNMMI/EANO/RANO groups recommended the use of FET-PET with a TBR_{max} threshold of 2.3 to differentiate early PsP and TP and a TBR_{max} and TBR_{mean} threshold of 1.9, respectively, to differentiate late PsP and TP (135).

SUV_{max} was superior in cases of TP, and an SUV_{max} threshold of 2.2 had the best differentiation between TP and treatment-related changes. The SUV_{max}/background (BG) ratio threshold had a discriminatory power of 100%. There was also a correlation between the SUV_{max} value and the tumor grade with high values for high grades (160). With an SUV_{max}/BG ratio of >2.0, the PPV of FET-PET was 84% for identifying TP (161). In a pilot study based on textural FET-PET features, Kebir *et al*. suggested that textural FET-PET features were more predictive of PsP (p=0.041) than the maximum tumor-to-normal brain ratio (TNR_{max}) at an optimal cut-off of 2.1 (p=0.07) with a sensitivity, specificity, PPV, and NPV of 90%, 75%, 90%, and 75% and 70%, 100%, 100%, and 57%, respectively (162).

Compared to conventional MRI, FET-PET was significantly more accurate (p<0.01) (163). The adjunction of FET-PET to MRI significantly improved the identification of TP with a sensitivity and specificity of 93% and 94%, respectively (157). The combination of FET-PET and ADC increased the accuracy from 69% to 89% for the differentiation of TP and PsP (164).

Compared to MET-PET, FET-PET provided a comparable ability to differentiate treatment-related changes and TP and to delineate the gross target volume (GTV) of tumors with a sensitivity of 91% and specificity of 100% for both tracers (165).

^{11}C-methyl-L-methionine positron emission tomography (^{11}C-MET PET)

MET is an essential amino acid labeled with carbon 11. It is transported across the blood-brain barrier by the L-type amino acid transport system and accumulated by tumor cells. ^{11}C has a short physical half-life of 20 min that requires the use of an on-site cyclotron unit for MET-PET unlike the half-life of ^{18}F of 110 minutes used in other tracers (165). For that, the application of ^{11}C MET-PET is limited to a small number of research centers (146). More studies of this tracer are needed before routine clinical use can be justified (133).

Many studies have demonstrated the use of MET-PET for the management of gliomas. MET-PET's sensitivity, specificity, and accuracy for detecting TP were 100%, 60%, and 82%, respectively (166). The intensity of MET uptake is associated with the grade of gliomas so a high uptake is associated with a poor survival time as a prognostic factor (57,167). The mean T/N ratio was significantly higher in TP: 4.0 vs 1.8 (168), 4.3 vs 1.8 (169), 2.18 vs 1.49 ($p<0.01$) (126), 2.69 vs 1.01 ($p=0.06$) (170), 1.89 vs 1.44 ($p=0.0079$) (171), and 2.38 vs 1.04 (86). The maximum L/N was 2.62 vs 2.11 ($p=0.052$), respectively (171). A T/N ratio threshold of 2 had a sensitivity of 86%, specificity of 100% (126), T/N ratio cut-off of >1.9, sensitivity of 95%, and specificity of 89%, respectively (170). The SUV_{max} of 2.89 vs 1.49 (86) and 3.19 vs 2.66 ($p=0.036$) (171) and SUV_{mean} of 2.65 vs 1.28 (86) and 2.31 vs 1.82 ($p=0.017$) (171) were both higher in TP patients and the SUV_{lesion}/BG ratio was also higher in a TP group (2.79 and 1.53) ($p<0.05$) (172). With an SUV/BG threshold of 2.35, the sensitivity and specificity were 90% and 100%, respectively (172). A maximal lesion uptake to maximal contralateral cerebral white matter uptake ratio (L/R_{max}) ratio of 2.64 had a sensitivity and specificity of 75% and 100%, respectively (92). Terakawa *et al*. determined that L/N_{mean} was the most informative index and an L/N_{mean} cut-off of 1.58 had a sensitivity and specificity of 75% and 75%, respectively (171).

Some authors did not demonstrate the use of MET-PET for the differentiation between TP and treatment-related changes. Analyzing MET uptake in lesions and in four specific regions

(around the lesion, in the contralateral frontal lobe, in the contralateral area, and in the contralateral cerebellar cortex), MET-PET failed to differentiate treatment-related changes from TP with no significant differences in quantitative or qualitative assessments (173). No significant differences were reported between treatment-related changes and TP patients in the T/N_{mean} ratio of 1.31 vs 1.87 (166), L/R_{max} ratio of 2.07 vs 3.33; p=0.257 (92), and SUV_{mean} of 1.81 vs 2.44 (166).

Compared to FDG-PET, MET-PET was superior to FDG-PET for the detection of tumor recurrence with a sensitivity, specificity, and accuracy of 96%, 87%, and 94% and 46%, 100%, and 58%, respectively (174). The FDG-PET and MET-PET combination provided the highest accuracy (p=0.003) with an accuracy, sensitivity, and specificity of 83%, 95%, and 60%, respectively (175). With a T/N cut-off of >0.75, FDG had a sensitivity and specificity of 81% and 89%, respectively, for identifying recurrence whereas at a T/N cut-off of >1.9, MET had a sensitivity and specificity of 95% and 89%, respectively for identifying recurrence (170).

Compared to advanced MRI, MET-PET was more sensitive for diagnosing TP with a sensitivity, specificity, and accuracy of 95%, 80%, and 90%, respectively, whereas advanced MRI was more specific with a sensitivity, specificity, and accuracy of 84%, 90%, and 86%, respectively (86). Dandois *et al*. reported that perfusion MRI and MET PET both assisted diagnosing TP in HGG. Of 33 combined MRI and PET studies, 31 matched perfectly and rCBV had equal performance with MET-PET (176). Another study reported that perfusion MRI with rCBV was superior to MET-PET or FDG-PET for the differentiation between treatment-related changes and TP (92). Deuschl *et al*. proposed a combined use of MRI and PET with hybrid MET-PET/MRI to differentiate treatment-related changes from TP. The sensitivity, specificity, accuracy, and PPV were 86%, 71%, 82%, and 89% for MRI alone, 97%, 74%, 88%, and 86% for MET-PET, and 97%, 93%, 96%, and 97% for MET-PET/MRI.

There was a significant difference between MET-PET/MRI and MRI (p=0.008), but no differences between MET-PET and MRI alone (p=0.021) or MET-PET/MRI and MET-PET alone (p=1.000) (177).

3'-deoxy-3'[(18)F]-fluorothymidine positron emission tomography (^{18}F-FLT PET)

Similar to other ^{18}F radiolabeled amino acids, thymidine nucleoside analogue FLT with its longer half-life could be useful for differentiating TP and PsP. It is a substrate of thymidine kinase-1 (cytosolic enzyme in the salvage pathway), which reflects cell proliferation as a proliferation marker (146). FLT is trapped in cells by thymidine phosphorylation kinase-1 but not incorporated in DNA. In the normal brain, there is no proliferative activity and the blood-brain barrier is intact so FLT is not taken up, which is different in tumors.

According to different studies, FLT can assist with glioma detection and grading characterization because its uptake in normal brain is low, the image contrast is significant, and FLT uptake correlates with the Ki67 index (178–181). It represents a non-invasive method to potentially predict disease progression and response to therapy in gliomas (182,183). In Choi *et al*., FLT uptake was correlated with the Ki67 index (p=0.007) and its change was associated with response to therapy (181). However, FLT uptake depended on blood-brain barrier disruption, which impacted its efficiency in clinical examination (184). Muzi *et al*. proposed a kinetic analysis of FLT, quantifying FLT uptake and analyzing blood-brain barrier disruption and retention in tumor tissue due to metabolic trapping of FLT nucleotides to separate transport effects from tissue retention. They produced a parametric image map of blood-to-tissue transport (Kl) and metabolic flux (KFLT). When the blood-brain barrier broke down, transport dominated FLT uptake, but when the blood brain-barrier was intact, transport was limited and FLT-PET was inefficient. The authors concluded that FLT was not the best tracer for necrosis or non-enhancing lesions (185). In another study, Kl, KFLT, and phosphorylation (K3) were significantly different between TP and treatment-

related changes ($p<0.0001$, $p=0.0009$, and $p=0.0012$, respectively) with the t-test, but with the Wilcoxon test, only KFLT and K3 demonstrated significant difference. The authors suggested that FLT-PET was promising for the diagnosis of TP with rigorous dynamic parameters (186). Some authors demonstrated that FLT-PET had no use for the discrimination of PsP vs TP. In den Hollander *et al*., no difference in SUV_{max} was found between patients with TP or PsP (187). In a more recent prospective study, SUV_{max} and the T/N ratio did not differ significantly between PsP and TP groups (1.41 vs 1.28, $p=0.699$, and 4.03 vs 3.59, $p=0.699$, respectively) (188). Compared to FDG-PET, FLT-PET was not more reliable than FDG-PET for the distinction between TP and treatment-related changes with a sensitivity and specificity varying from 73% to 91% and 75% vs from 91% to 100% and 75%, respectively (189).

Others PET tracers

Other PET tracers were evaluated in the literature. ^{11}C-choline (190), ^{11}C-methyl-L-tryptophan (MLT) (191), ^{18}F-fluoromisonidazole (FMISO) (146,192), ^{18}F-fluoromethylcholine (FCho) (193), and 4-borono-2-18F-fluoro-phenylalanine (^{18}F-FBPA) (194,195) could be useful for the differentiation between PsP and TP but studies are currently too rare to promote their use.

Single photon-emission computed tomography (SPECT)

In a meta-analysis of 893 patients with gliomas, SPECT was able to differentiate PsP and TP with a sensitivity of 89% and a specificity of 87% (196). Some SPECT tracers were studied in the literature.

In a retrospective study, thallium 201 (^{201}Tl)-SPECT had better sensitivity, specificity, PPV, and NPV than conventional MRI (84%, 100%, 100%, and 57% vs 65%, 75%, 92%, and 33%, respectively) and a higher TP diagnostic accuracy (86% vs 67%) (197). Caresia *et al.* found that the sensibility, specificity, and accuracy of ^{201}Tl-SPECT were 100%, respectively (198). Vos *et al*. estimated that the sensitivity and specificity of ^{201}Tl-SPECT ranged from 43% to

100% and from 25% to 100%, respectively. However, the poor methodological quality and small sample sizes of the included studies impeded conclusions (199). Compared to FDG-PET, ^{201}Tl-SPECT had a higher sensitivity but a lower specificity and was better at excluding TP (200).

Sestamibi technetium 99m (^{99m}Tc-MIBI) SPECT had a sensitivity, specificity, and accuracy of 89%, 83%, and 87%, respectively, for diagnosing TP (201). Compared with MRS, ^{99m}Tc-MIBI-SPECT had a sensitivity, specificity, accuracy, PPV, and NPV of 90%, 100%, 93%, 100%, and 83%, respectively, and the combination of ^{99m}Tc-MIBI-SPECT and MRS had a sensitivity, specificity, accuracy, PPV, and NPV of 95%, 100%, 97%, 100%, and 91%, respectively (202).

Plotkin *et al*. investigated 123-iodine-a-methyl tyrosine (^{123}I-IMT) SPECT and single voxel MRS and reported that although ^{123}I-IMT SPECT had a trend of better performance than single voxel MRS, no significant differences were observed in the accuracy, sensitivity, and specificity between both modalities ($p>0.05$) for diagnosing TP (127).

Amin *et al*. compared technetium-99m dimercaptosuccinic acid (^{99m}Tc(V)DMSA)-SPECT and MRS in 24 patients with HGG treated with surgery and RCT and concluded that ^{99m}Tc(V)DMSA-SPECT was more effective than MRS for diagnosing TP with a sensitivity, specificity, accuracy, PPV, and NPV of 89%, 100%, 92%, 75%, and 100%, respectively (203).

In 2007, Alexiou *et al*. studied ^{99m}Tc-tetrofosmin (^{99m}Tc-TF) SPECT and proposed a lesion uptake to normal brain tissue uptake ratio (L/N) threshold value of 4.76 for diagnosing TP (204). In 2014, the same authors compared DTI, DSC, and ^{99m}Tc-TF-SPECT in a prospective study of 30 HGG patients and reported an L/N threshold value of 4 with 100% sensitivity and 100% specificity (65).

A comparison of ^{99m}Tc-methionine-SPECT, FDG-PET, and conventional MRI demonstrated that the specificity of ^{99m}Tc-MET-SPECT was significantly higher than the specificity of conventional MRI ($p<0.0001$) but not the specificity of FDG-PET ($p=0.36$). No significant difference was observed between them for sensitivity and accuracy (205).

^{99m}Tc-glucoheptonate (GHA) SPECT is a low-cost radiopharmaceutical agent that can be strongly recommended for detecting residual tumors after surgery/radiotherapy and progression (206).

^{99m}TcMDM (bis-methionine-DTPA) SPECT had a comparable sensitivity and specificity to DSC (92% and 79% for MDM SPECT and 92% and 71% for DSC MRI) (207).

True progression vs pseudoprogression

According to the literature review results, Figure 1 proposes a decisional diagram to orientate clinical decisions and assist with the distinction between PsP and TP. The order of radiological imaging features proposed resulted in the specificity and PPV of the different radiological examinations in the literature to certify PsP not to identify it.

Conclusion

PsP doubt is a common situation in clinical routines and clinicians need uniform and standardized criteria to guarantee this diagnosis. The use of advanced radiological imaging and imaging biomarkers are promising in this context and provide pathophysiological information. This report demonstrated the superiority of advanced MRI techniques and PET for the diagnosis of PsP but efforts to create uniform practices and protocols are necessary. It is essential that imaging is available, accessible, reproducible, and cost-effective. Reviewing the literature, no rigorous methodology seemed to guide researchers to provide comparable results because of a large number of parameter cut-off values, different imaging protocols, small sample sizes, different population characteristics, and a lack of study reproducibility. The extent of isotopes for TEP and SPECT and sequences for MRI multiplied by the large

numbers of metrics is significant. Algorithms proposed by artificial intelligence and radiomics were used to analyze the results and improved the usefulness of the data.

Bibliography

1. Brandes AA, Franceschi E, Tosoni A, Blatt V, Pession A, Tallini G, et al. MGMT promoter methylation status can predict the incidence and outcome of pseudoprogression after concomitant radiochemotherapy in newly diagnosed glioblastoma patients. J Clin Oncol Off J Am Soc Clin Oncol. 2008 May 1;26(13):2192–7.
2. Chamberlain MC, Glantz MJ, Chalmers L, Van Horn A, Sloan AE. Early necrosis following concurrent Temodar and radiotherapy in patients with glioblastoma. J Neurooncol. 2007 Mar;82(1):81–3.
3. Taal W, Brandsma D, de Bruin HG, Bromberg JE, Swaak-Kragten AT, Smitt PAES, et al. Incidence of early pseudo-progression in a cohort of malignant glioma patients treated with chemoirradiation with temozolomide. Cancer. 2008 Jul 15;113(2):405–10.
4. Stupp R, Mason WP, van den Bent MJ, Weller M, Fisher B, Taphoorn MJB, et al. Radiotherapy plus concomitant and adjuvant temozolomide for glioblastoma. N Engl J Med. 2005 Mar 10;352(10):987–96.
5. Wick W, Chinot OL, Bendszus M, Mason W, Henriksson R, Saran F, et al. Evaluation of pseudoprogression rates and tumor progression patterns in a phase III trial of bevacizumab plus radiotherapy/temozolomide for newly diagnosed glioblastoma. Neuro-Oncol. 2016;18(10):1434–41.
6. Brandsma D, Stalpers L, Taal W, Sminia P, van den Bent MJ. Clinical features, mechanisms, and management of pseudoprogression in malignant gliomas. Lancet Oncol. 2008 May;9(5):453–61.
7. Rowe LS, Butman JA, Mackey M, Shih JH, Cooley-Zgela T, Ning H, et al. Differentiating pseudoprogression from true progression: analysis of radiographic, biologic, and clinical clues in GBM. J Neurooncol. 2018 May 16;
8. Chaskis C, Neyns B, Michotte A, De Ridder M, Everaert H. Pseudoprogression after radiotherapy with concurrent temozolomide for high-grade glioma: clinical observations and working recommendations. Surg Neurol. 2009 Oct;72(4):423–8.
9. Chang JH, Kim C-Y, Choi BS, Kim YJ, Kim JS, Kim IA. Pseudoprogression and pseudoresponse in the management of high-grade glioma : optimal decision timing according to the response assessment of the neuro-oncology working group. J Korean Neurosurg Soc. 2014 Jan;55(1):5–11.
10. Zikou A, Sioka C, Alexiou GA, Fotopoulos A, Voulgaris S, Argyropoulou MI. Radiation Necrosis, Pseudoprogression, Pseudoresponse, and Tumor Recurrence: Imaging Challenges for the Evaluation of Treated Gliomas. Contrast Media Mol Imaging. 2018;2018:6828396.
11. Nasseri M, Gahramanov S, Netto JP, Fu R, Muldoon LL, Varallyay C, et al. Evaluation of pseudoprogression in patients with glioblastoma multiforme using dynamic magnetic resonance imaging with ferumoxytol calls RANO criteria into question. Neuro-Oncol. 2014 Aug;16(8):1146–54.
12. Jefferies S, Burton K, Jones P, Burnet N. Interpretation of Early Imaging after Concurrent Radiotherapy and Temozolomide for Glioblastoma. Clin Oncol. 2007 Apr 1;19(3):S33.
13. Radbruch A, Fladt J, Kickingereder P, Wiestler B, Nowosielski M, Bäumer P, et al. Pseudoprogression in patients with glioblastoma: clinical relevance despite low incidence. Neuro-Oncol. 2015 Jan;17(1):151–9.
14. Tran DKT, Jensen RL. Treatment-related brain tumor imaging changes: So-called “pseudoprogression” vs. tumor progression: Review and future research opportunities. Surg Neurol Int. 2013;4(Suppl 3):S129-135.
15. Larsen VA, Simonsen HJ, Law I, Larsson HBW, Hansen AE. Evaluation of dynamic

contrast-enhanced T1-weighted perfusion MRI in the differentiation of tumor recurrence from radiation necrosis. Neuroradiology. 2013 Feb;55(3):361–9.
16. Hygino da Cruz LC, Rodriguez I, Domingues RC, Gasparetto EL, Sorensen AG. Pseudoprogression and pseudoresponse: imaging challenges in the assessment of posttreatment glioma. AJNR Am J Neuroradiol. 2011 Dec;32(11):1978–85.
17. Jahangiri A, Aghi MK. Pseudoprogression and treatment effect. Neurosurg Clin N Am. 2012 Apr;23(2):277–87, viii–ix.
18. Abbasi AW, Westerlaan HE, Holtman GA, Aden KM, van Laar PJ, van der Hoorn A. Incidence of Tumour Progression and Pseudoprogression in High-Grade Gliomas: a Systematic Review and Meta-Analysis. Clin Neuroradiol. 2018 Sep;28(3):401–11.
19. Thust SC, van den Bent MJ, Smits M. Pseudoprogression of brain tumors. J Magn Reson Imaging JMRI. 2018 May 7;
20. Wen PY, Chang SM, Van den Bent MJ, Vogelbaum MA, Macdonald DR, Lee EQ. Response Assessment in Neuro-Oncology Clinical Trials. J Clin Oncol Off J Am Soc Clin Oncol. 2017 Jul 20;35(21):2439–49.
21. Wen PY, Macdonald DR, Reardon DA, Cloughesy TF, Sorensen AG, Galanis E, et al. Updated response assessment criteria for high-grade gliomas: response assessment in neuro-oncology working group. J Clin Oncol Off J Am Soc Clin Oncol. 2010 Apr 10;28(11):1963–72.
22. Macdonald DR, Cascino TL, Schold SC, Cairncross JG. Response criteria for phase II studies of supratentorial malignant glioma. J Clin Oncol Off J Am Soc Clin Oncol. 1990 Jul;8(7):1277–80.
23. Ellingson BM, Bendszus M, Boxerman J, Barboriak D, Erickson BJ, Smits M, et al. Consensus recommendations for a standardized Brain Tumor Imaging Protocol in clinical trials. Neuro-Oncol. 2015 Sep;17(9):1188–98.
24. Ellingson BM, Wen PY, Cloughesy TF. Modified Criteria for Radiographic Response Assessment in Glioblastoma Clinical Trials. Neurother J Am Soc Exp Neurother. 2017;14(2):307–20.
25. Lieberman F. Glioblastoma update: molecular biology, diagnosis, treatment, response assessment, and translational clinical trials. F1000Research [Internet]. 2017 Oct 26 [cited 2018 Sep 3];6. Available from: https://www.ncbi.nlm.nih.gov/pmc/articles/PMC5658706/
26. Masch WR, Wang PI, Chenevert TL, Junck L, Tsien C, Heth JA, et al. Comparison of Diffusion Tensor Imaging and Magnetic Resonance Perfusion Imaging in Differentiating Recurrent Brain Neoplasm From Radiation Necrosis. Acad Radiol. 2016 May;23(5):569–76.
27. Shukla G, Alexander GS, Bakas S, Nikam R, Talekar K, Palmer JD, et al. Advanced magnetic resonance imaging in glioblastoma: a review. Chin Clin Oncol. 2017 Aug;6(4):40.
28. Hyare H, Thust S, Rees J. Advanced MRI Techniques in the Monitoring of Treatment of Gliomas. Curr Treat Options Neurol. 2017 Mar;19(3):11.
29. van Dijken BRJ, van Laar PJ, Holtman GA, van der Hoorn A. Diagnostic accuracy of magnetic resonance imaging techniques for treatment response evaluation in patients with high-grade glioma, a systematic review and meta-analysis. Eur Radiol. 2017 Oct;27(10):4129–44.
30. Neal ML, Trister AD, Ahn S, Baldock A, Bridge CA, Guyman L, et al. Response classification based on a minimal model of glioblastoma growth is prognostic for clinical outcomes and distinguishes progression from pseudoprogression. Cancer Res. 2013 May 15;73(10):2976–86.
31. Ellingson BM, Chung C, Pope WB, Boxerman JL, Kaufmann TJ. Pseudoprogression, radionecrosis, inflammation or true tumor progression? challenges associated with glioblastoma response assessment in an evolving therapeutic landscape. J Neurooncol. 2017 Sep;134(3):495–504.

32. Santra A, Kumar R, Sharma P, Bal C, Kumar A, Julka PK, et al. F-18 FDG PET-CT in patients with recurrent glioma: comparison with contrast enhanced MRI. Eur J Radiol. 2012 Mar;81(3):508–13.
33. https://www.nccn.org/professionals/physi- cian_gls/f_guidelines.asp#cns.
34. Agarwal A, Kumar S, Narang J, Schultz L, Mikkelsen T, Wang S, et al. Morphologic MRI features, diffusion tensor imaging and radiation dosimetric analysis to differentiate pseudo-progression from early tumor progression. J Neurooncol. 2013 May;112(3):413–20.
35. Gladwish A, Koh E-S, Hoisak J, Lockwood G, Millar B-A, Mason W, et al. Evaluation of early imaging response criteria in glioblastoma multiforme. Radiat Oncol Lond Engl. 2011 Sep 23;6:121.
36. Mullins ME, Barest GD, Schaefer PW, Hochberg FH, Gonzalez RG, Lev MH. Radiation necrosis versus glioma recurrence: conventional MR imaging clues to diagnosis. AJNR Am J Neuroradiol. 2005 Sep;26(8):1967–72.
37. Young RJ, Gupta A, Shah AD, Graber JJ, Zhang Z, Shi W, et al. Potential utility of conventional MRI signs in diagnosing pseudoprogression in glioblastoma. Neurology. 2011 May 31;76(22):1918–24.
38. Kim HS, Goh MJ, Kim N, Choi CG, Kim SJ, Kim JH. Which combination of MR imaging modalities is best for predicting recurrent glioblastoma? Study of diagnostic accuracy and reproducibility. Radiology. 2014 Dec;273(3):831–43.
39. Reddy K, Westerly D, Chen C. MRI patterns of T1 enhancing radiation necrosis versus tumour recurrence in high-grade gliomas. J Med Imaging Radiat Oncol. 2013 Jun;57(3):349–55.
40. Hansen MR, Pan E, Wilson A, McCreary M, Wang Y, Stanley T, et al. Post-gadolinium 3-dimensional spatial, surface, and structural characteristics of glioblastomas differentiate pseudoprogression from true tumor progression. J Neurooncol. 2018 Jun 7;
41. Chen X, Wei X, Zhang Z, Yang R, Zhu Y, Jiang X. Differentiation of true-progression from pseudoprogression in glioblastoma treated with radiation therapy and concomitant temozolomide by GLCM texture analysis of conventional MRI. Clin Imaging. 2015 Oct;39(5):775–80.
42. Zaki HS, Jenkinson MD, Du Plessis DG, Smith T, Rainov NG. Vanishing contrast enhancement in malignant glioma after corticosteroid treatment. Acta Neurochir (Wien). 2004 Aug;146(8):841–5.
43. de Groot JF, Fuller G, Kumar AJ, Piao Y, Eterovic K, Ji Y, et al. Tumor invasion after treatment of glioblastoma with bevacizumab: radiographic and pathologic correlation in humans and mice. Neuro-Oncol. 2010 Mar;12(3):233–42.
44. Ito-Yamashita T, Nakasu Y, Mitsuya K, Mizokami Y, Namba H. Detection of tumor progression by signal intensity increase on fluid-attenuated inversion recovery magnetic resonance images in the resection cavity of high-grade gliomas. Neurol Med Chir (Tokyo). 2013;53(7):496–500.
45. Abel R, Jones J, Mandelin P, Cen S, Pagnini P. Distinguishing Pseudoprogression From True Progression by FLAIR Volumetric Characteristics Compared to 45 Gy Isodose Volumes in Treated Glioblastoma Patients. Int J Radiat Oncol • Biol • Phys. 2012 Nov 1;84(3):S275.
46. Abdulla S, Saada J, Johnson G, Jefferies S, Ajithkumar T. Tumour progression or pseudoprogression? A review of post-treatment radiological appearances of glioblastoma. Clin Radiol. 2015 Nov;70(11):1299–312.
47. Oberheim Bush NA, Cha S, Chang SM, Clarke JL. Chapter 55 - Pseudoprogression in Neuro-Oncology: Overview, Pathophysiology, and Interpretation. In: Newton HB, editor. Handbook of Neuro-Oncology Neuroimaging (Second Edition) [Internet]. San Diego: Academic Press; 2016 [cited 2019 Jun 13]. p. 681–95. Available from:

http://www.sciencedirect.com/science/article/pii/B9780128009451000550
48. Gerstner ER, McNamara MB, Norden AD, Lafrankie D, Wen PY. Effect of adding temozolomide to radiation therapy on the incidence of pseudo-progression. J Neurooncol. 2009 Aug;94(1):97–101.
49. Zhang J, Yu H, Qian X, Liu K, Tan H, Yang T, et al. Pseudo progression identification of glioblastoma with dictionary learning. Comput Biol Med. 2016 01;73:94–101.
50. Verma R, Zacharaki EI, Ou Y, Cai H, Chawla S, Lee S-K, et al. Multiparametric tissue characterization of brain neoplasms and their recurrence using pattern classification of MR images. Acad Radiol. 2008 Aug;15(8):966–77.
51. Asao C, Korogi Y, Kitajima M, Hirai T, Baba Y, Makino K, et al. Diffusion-weighted imaging of radiation-induced brain injury for differentiation from tumor recurrence. AJNR Am J Neuroradiol. 2005 Jul;26(6):1455–60.
52. Lee WJ, Choi SH, Park C-K, Yi KS, Kim TM, Lee S-H, et al. Diffusion-weighted MR imaging for the differentiation of true progression from pseudoprogression following concomitant radiotherapy with temozolomide in patients with newly diagnosed high-grade gliomas. Acad Radiol. 2012 Nov;19(11):1353–61.
53. Xu J-L, Li Y-L, Lian J-M, Dou S, Yan F-S, Wu H, et al. Distinction between postoperative recurrent glioma and radiation injury using MR diffusion tensor imaging. Neuroradiology. 2010 Dec;52(12):1193–9.
54. Hein PA, Eskey CJ, Dunn JF, Hug EB. Diffusion-weighted imaging in the follow-up of treated high-grade gliomas: tumor recurrence versus radiation injury. AJNR Am J Neuroradiol. 2004 Feb;25(2):201–9.
55. Sundgren PC, Fan X, Weybright P, Welsh RC, Carlos RC, Petrou M, et al. Differentiation of recurrent brain tumor versus radiation injury using diffusion tensor imaging in patients with new contrast-enhancing lesions. Magn Reson Imaging. 2006 Nov;24(9):1131–42.
56. Chenevert TL, Stegman LD, Taylor JM, Robertson PL, Greenberg HS, Rehemtulla A, et al. Diffusion magnetic resonance imaging: an early surrogate marker of therapeutic efficacy in brain tumors. J Natl Cancer Inst. 2000 Dec 20;92(24):2029–36.
57. Huang RY, Neagu MR, Reardon DA, Wen PY. Pitfalls in the neuroimaging of glioblastoma in the era of antiangiogenic and immuno/targeted therapy - detecting illusive disease, defining response. Front Neurol. 2015;6:33.
58. Yamasaki F, Kurisu K, Satoh K, Arita K, Sugiyama K, Ohtaki M, et al. Apparent diffusion coefficient of human brain tumors at MR imaging. Radiology. 2005 Jun;235(3):985–91.
59. Sugahara T, Korogi Y, Kochi M, Ikushima I, Shigematu Y, Hirai T, et al. Usefulness of diffusion-weighted MRI with echo-planar technique in the evaluation of cellularity in gliomas. J Magn Reson Imaging JMRI. 1999 Jan;9(1):53–60.
60. Reimer C, Deike K, Graf M, Reimer P, Wiestler B, Floca RO, et al. Differentiation of pseudoprogression and real progression in glioblastoma using ADC parametric response maps. PLoS ONE [Internet]. 2017 Apr 6 [cited 2019 Apr 28];12(4). Available from: https://www.ncbi.nlm.nih.gov/pmc/articles/PMC5383222/
61. Zeng Q-S, Li C-F, Liu H, Zhen J-H, Feng D-C. Distinction between recurrent glioma and radiation injury using magnetic resonance spectroscopy in combination with diffusion-weighted imaging. Int J Radiat Oncol Biol Phys. 2007 May 1;68(1):151–8.
62. Jena A, Taneja S, Jha A, Damesha NK, Negi P, Jadhav GK, et al. Multiparametric Evaluation in Differentiating Glioma Recurrence from Treatment-Induced Necrosis Using Simultaneous 18F-FDG-PET/MRI: A Single-Institution Retrospective Study. AJNR Am J Neuroradiol. 2017 May;38(5):899–907.
63. Fink JR, Carr RB, Matsusue E, Iyer RS, Rockhill JK, Haynor DR, et al. Comparison

of 3 Tesla proton MR spectroscopy, MR perfusion and MR diffusion for distinguishing glioma recurrence from posttreatment effects. J Magn Reson Imaging JMRI. 2012 Jan;35(1):56–63.
64. Prager AJ, Martinez N, Beal K, Omuro A, Zhang Z, Young RJ. Diffusion and perfusion MRI to differentiate treatment-related changes including pseudoprogression from recurrent tumors in high-grade gliomas with histopathologic evidence. AJNR Am J Neuroradiol. 2015 May;36(5):877–85.
65. Alexiou GA, Zikou A, Tsiouris S, Goussia A, Kosta P, Papadopoulos A, et al. Comparison of diffusion tensor, dynamic susceptibility contrast MRI and (99m)Tc-Tetrofosmin brain SPECT for the detection of recurrent high-grade glioma. Magn Reson Imaging. 2014 Sep;32(7):854–9.
66. Bulik M, Kazda T, Slampa P, Jancalek R. The Diagnostic Ability of Follow-Up Imaging Biomarkers after Treatment of Glioblastoma in the Temozolomide Era: Implications from Proton MR Spectroscopy and Apparent Diffusion Coefficient Mapping [Internet]. BioMed Research International. 2015 [cited 2019 Apr 28]. Available from: https://www.hindawi.com/journals/bmri/2015/641023/
67. Kazda T, Bulik M, Pospisil P, Lakomy R, Smrcka M, Slampa P, et al. Advanced MRI increases the diagnostic accuracy of recurrent glioblastoma: Single institution thresholds and validation of MR spectroscopy and diffusion weighted MR imaging. NeuroImage Clin. 2016;11:316–21.
68. Bobek-Billewicz B, Stasik-Pres G, Majchrzak H, Zarudzki L. Differentiation between brain tumor recurrence and radiation injury using perfusion, diffusion-weighted imaging and MR spectroscopy. Folia Neuropathol. 2010;48(2):81–92.
69. Al Sayyari A, Buckley R, McHenery C, Pannek K, Coulthard A, Rose S. Distinguishing recurrent primary brain tumor from radiation injury: a preliminary study using a susceptibility-weighted MR imaging-guided apparent diffusion coefficient analysis strategy. AJNR Am J Neuroradiol. 2010 Jun;31(6):1049–54.
70. Song YS, Choi SH, Park C-K, Yi KS, Lee WJ, Yun TJ, et al. True progression versus pseudoprogression in the treatment of glioblastomas: a comparison study of normalized cerebral blood volume and apparent diffusion coefficient by histogram analysis. Korean J Radiol. 2013 Aug;14(4):662–72.
71. Chu HH, Choi SH, Ryoo I, Kim SC, Yeom JA, Shin H, et al. Differentiation of true progression from pseudoprogression in glioblastoma treated with radiation therapy and concomitant temozolomide: comparison study of standard and high-b-value diffusion-weighted imaging. Radiology. 2013 Dec;269(3):831–40.
72. O'Donnell LJ, Westin C-F. An introduction to diffusion tensor image analysis. Neurosurg Clin N Am. 2011 Apr;22(2):185–96, viii.
73. Yousaf T, Dervenoulas G, Politis M. Chapter Two - Advances in MRI Methodology. In: Politis M, editor. International Review of Neurobiology [Internet]. Academic Press; 2018 [cited 2019 Jun 9]. p. 31–76. (Imaging in Movement Disorders: Imaging Methodology and Applications in Parkinson's Disease; vol. 141). Available from: http://www.sciencedirect.com/science/article/pii/S0074774218300758
74. Wang S, Martinez-Lage M, Sakai Y, Chawla S, Kim SG, Alonso-Basanta M, et al. Differentiating Tumor Progression from Pseudoprogression in Patients with Glioblastomas Using Diffusion Tensor Imaging and Dynamic Susceptibility Contrast MRI. AJNR Am J Neuroradiol. 2016 Jan;37(1):28–36.
75. Zhang J, Liu H, Tong H, Wang S, Yang Y, Liu G, et al. Clinical Applications of Contrast-Enhanced Perfusion MRI Techniques in Gliomas: Recent Advances and Current Challenges. Contrast Media Mol Imaging. 2017;2017:7064120.
76. Cao Y, Shen Z, Chenevert TL, Ewing JR. Estimate of vascular permeability and

cerebral blood volume using Gd-DTPA contrast enhancement and dynamic T2*-weighted MRI. J Magn Reson Imaging JMRI. 2006 Aug;24(2):288–96.
77. Thust SC, Heiland S, Falini A, Jäger HR, Waldman AD, Sundgren PC, et al. Glioma imaging in Europe: A survey of 220 centres and recommendations for best clinical practice. Eur Radiol. 2018 Aug;28(8):3306–17.
78. Steidl E, Müller M, Müller A, Herrlinger U, Hattingen E. Longitudinal, leakage corrected and uncorrected rCBV during the first-line treatment of glioblastoma: a prospective study. J Neurooncol. 2019 Sep;144(2):409–17.
79. Kelm ZS, Korfiatis PD, Lingineni RK, Daniels JR, Buckner JC, Lachance DH, et al. Variability and accuracy of different software packages for dynamic susceptibility contrast magnetic resonance imaging for distinguishing glioblastoma progression from pseudoprogression. J Med Imaging Bellingham Wash. 2015 Apr;2(2):026001.
80. Patel P, Baradaran H, Delgado D, Askin G, Christos P, John Tsiouris A, et al. MR perfusion-weighted imaging in the evaluation of high-grade gliomas after treatment: a systematic review and meta-analysis. Neuro-Oncol. 2017;19(1):118–27.
81. Fatterpekar GM, Galheigo D, Narayana A, Johnson G, Knopp E. Treatment-related change versus tumor recurrence in high-grade gliomas: a diagnostic conundrum--use of dynamic susceptibility contrast-enhanced (DSC) perfusion MRI. AJR Am J Roentgenol. 2012 Jan;198(1):19–26.
82. Cha J, Kim ST, Kim H-J, Kim B-J, Kim YK, Lee JY, et al. Differentiation of tumor progression from pseudoprogression in patients with posttreatment glioblastoma using multiparametric histogram analysis. AJNR Am J Neuroradiol. 2014 Jul;35(7):1309–17.
83. Cha S, Knopp EA, Johnson G, Wetzel SG, Litt AW, Zagzag D. Intracranial mass lesions: dynamic contrast-enhanced susceptibility-weighted echo-planar perfusion MR imaging. Radiology. 2002 Apr;223(1):11–29.
84. Barajas RF, Chang JS, Segal MR, Parsa AT, McDermott MW, Berger MS, et al. Differentiation of recurrent glioblastoma multiforme from radiation necrosis after external beam radiation therapy with dynamic susceptibility-weighted contrast-enhanced perfusion MR imaging. Radiology. 2009 Nov;253(2):486–96.
85. Seeger A, Braun C, Skardelly M, Paulsen F, Schittenhelm J, Ernemann U, et al. Comparison of three different MR perfusion techniques and MR spectroscopy for multiparametric assessment in distinguishing recurrent high-grade gliomas from stable disease. Acad Radiol. 2013 Dec;20(12):1557–65.
86. D'Souza MM, Sharma R, Jaimini A, Panwar P, Saw S, Kaur P, et al. 11C-MET PET/CT and advanced MRI in the evaluation of tumor recurrence in high-grade gliomas. Clin Nucl Med. 2014 Sep;39(9):791–8.
87. Heidemans-Hazelaar C, Verbeek AY, Oosterkamp HM, Van der Kallen B, Vecht CJ. Use of perfusion MR imaging for differentiation between tumor progression and pseudo-progression in recurrent glioblastoma multiforme. J Clin Oncol. 2010 May 20;28(15_suppl):2026–2026.
88. Hu LS, Baxter LC, Smith KA, Feuerstein BG, Karis JP, Eschbacher JM, et al. Relative cerebral blood volume values to differentiate high-grade glioma recurrence from posttreatment radiation effect: direct correlation between image-guided tissue histopathology and localized dynamic susceptibility-weighted contrast-enhanced perfusion MR imaging measurements. AJNR Am J Neuroradiol. 2009 Mar;30(3):552–8.
89. Hu LS, Eschbacher JM, Heiserman JE, Dueck AC, Shapiro WR, Liu S, et al. Reevaluating the imaging definition of tumor progression: perfusion MRI quantifies recurrent glioblastoma tumor fraction, pseudoprogression, and radiation necrosis to predict survival. Neuro-Oncol. 2012 Jul;14(7):919–30.
90. Gasparetto EL, Pawlak MA, Patel SH, Huse J, Woo JH, Krejza J, et al. Posttreatment

recurrence of malignant brain neoplasm: accuracy of relative cerebral blood volume fraction in discriminating low from high malignant histologic volume fraction. Radiology. 2009 Mar;250(3):887–96.
91. Gahramanov S, Raslan AM, Muldoon LL, Hamilton BE, Rooney WD, Varallyay CG, et al. Potential for differentiation of pseudoprogression from true tumor progression with dynamic susceptibility-weighted contrast-enhanced magnetic resonance imaging using ferumoxytol vs. gadoteridol: a pilot study. Int J Radiat Oncol Biol Phys. 2011 Feb 1;79(2):514–23.
92. Kim YH, Oh SW, Lim YJ, Park C-K, Lee S-H, Kang KW, et al. Differentiating radiation necrosis from tumor recurrence in high-grade gliomas: assessing the efficacy of 18F-FDG PET, 11C-methionine PET and perfusion MRI. Clin Neurol Neurosurg. 2010 Nov;112(9):758–65.
93. Young RJ, Gupta A, Shah AD, Graber JJ, Chan TA, Zhang Z, et al. MRI perfusion in determining pseudoprogression in patients with glioblastoma. Clin Imaging. 2013 Feb;37(1):41–9.
94. Hu X, Wong KK, Young GS, Guo L, Wong ST. Support vector machine multiparametric MRI identification of pseudoprogression from tumor recurrence in patients with resected glioblastoma. J Magn Reson Imaging JMRI. 2011 Feb;33(2):296–305.
95. Jain R, Scarpace L, Ellika S, Schultz LR, Rock JP, Rosenblum ML, et al. First-pass perfusion computed tomography: initial experience in differentiating recurrent brain tumors from radiation effects and radiation necrosis. Neurosurgery. 2007 Oct;61(4):778–86; discussion 786-787.
96. Boxerman JL, Ellingson BM, Jeyapalan S, Elinzano H, Harris RJ, Rogg JM, et al. Longitudinal DSC-MRI for Distinguishing Tumor Recurrence From Pseudoprogression in Patients With a High-grade Glioma. Am J Clin Oncol. 2017 Jun;40(3):228–34.
97. Tsien C, Galbán CJ, Chenevert TL, Johnson TD, Hamstra DA, Sundgren PC, et al. Parametric response map as an imaging biomarker to distinguish progression from pseudoprogression in high-grade glioma. J Clin Oncol Off J Am Soc Clin Oncol. 2010 May 1;28(13):2293–9.
98. Shin KE, Ahn KJ, Choi HS, Jung SL, Kim BS, Jeon SS, et al. DCE and DSC MR perfusion imaging in the differentiation of recurrent tumour from treatment-related changes in patients with glioma. Clin Radiol. 2014 Jun;69(6):e264-272.
99. Mangla R, Singh G, Ziegelitz D, Milano MT, Korones DN, Zhong J, et al. Changes in relative cerebral blood volume 1 month after radiation-temozolomide therapy can help predict overall survival in patients with glioblastoma. Radiology. 2010 Aug;256(2):575–84.
100. Kong D-S, Kim ST, Kim E-H, Lim DH, Kim WS, Suh Y-L, et al. Diagnostic dilemma of pseudoprogression in the treatment of newly diagnosed glioblastomas: the role of assessing relative cerebral blood flow volume and oxygen-6-methylguanine-DNA methyltransferase promoter methylation status. AJNR Am J Neuroradiol. 2011 Feb;32(2):382–7.
101. Baek HJ, Kim HS, Kim N, Choi YJ, Kim YJ. Percent Change of Perfusion Skewness and Kurtosis: A Potential Imaging Biomarker for Early Treatment Response in Patients with Newly Diagnosed Glioblastomas. Radiology. 2012 Sep 1;264(3):834–43.
102. Suh CH, Kim HS, Choi YJ, Kim N, Kim SJ. Prediction of pseudoprogression in patients with glioblastomas using the initial and final area under the curves ratio derived from dynamic contrast-enhanced T1-weighted perfusion MR imaging. AJNR Am J Neuroradiol. 2013 Dec;34(12):2278–86.
103. Bisdas S, Naegele T, Ritz R, Dimostheni A, Pfannenberg C, Reimold M, et al. Distinguishing recurrent high-grade gliomas from radiation injury: a pilot study using dynamic contrast-enhanced MR imaging. Acad Radiol. 2011 May;18(5):575–83.
104. Yun TJ, Park C-K, Kim TM, Lee S-H, Kim J-H, Sohn C-H, et al. Glioblastoma treated

with concurrent radiation therapy and temozolomide chemotherapy: differentiation of true progression from pseudoprogression with quantitative dynamic contrast-enhanced MR imaging. Radiology. 2015 Mar;274(3):830–40.
105. Thomas AA, Arevalo-Perez J, Kaley T, Lyo J, Peck KK, Shi W, et al. Dynamic contrast enhanced T1 MRI perfusion differentiates pseudoprogression from recurrent glioblastoma. J Neurooncol. 2015 Oct;125(1):183–90.
106. Choi YJ, Kim HS, Jahng G-H, Kim SJ, Suh DC. Pseudoprogression in patients with glioblastoma: added value of arterial spin labeling to dynamic susceptibility contrast perfusion MR imaging. Acta Radiol Stockh Swed 1987. 2013 May;54(4):448–54.
107. Yoo R-E, Choi SH. Recent Application of Advanced MR Imaging to Predict Pseudoprogression in High-grade Glioma Patients. Magn Reson Med Sci MRMS Off J Jpn Soc Magn Reson Med. 2016;15(2):165–77.
108. Jovanovic M, Radenkovic S, Stosic-Opincal T, Lavrnic S, Gavrilovic S, Lazovic-Popovic B, et al. Differentiation between progression and pseudoprogresion by arterial spin labeling MRI in patients with glioblastoma multiforme. J BUON Off J Balk Union Oncol. 2017 Aug;22(4):1061–7.
109. Ozsunar Y, Mullins ME, Kwong K, Hochberg FH, Ament C, Schaefer PW, et al. Glioma recurrence versus radiation necrosis? A pilot comparison of arterial spin-labeled, dynamic susceptibility contrast enhanced MRI, and FDG-PET imaging. Acad Radiol. 2010 Mar;17(3):282–90.
110. Lewis R, Bhandari A, McKintosh E, Plowman P, Lansley J, Evanson J, et al. Differentiating tumour progression from pseudoprogression in patients with glioblastoma using multiparametric MRI imaging: Data from Barts Health NHS trust London. Eur J Surg Oncol. 2016 Nov 1;42(11):S248–9.
111. Park JE, Kim HS, Goh MJ, Kim SJ, Kim JH. Pseudoprogression in Patients with Glioblastoma: Assessment by Using Volume-weighted Voxel-based Multiparametric Clustering of MR Imaging Data in an Independent Test Set. Radiology. 2015 Jun;275(3):792–802.
112. Yoon RG, Kim HS, Paik W, Shim WH, Kim SJ, Kim JH. Different diagnostic values of imaging parameters to predict pseudoprogression in glioblastoma subgroups stratified by MGMT promoter methylation. Eur Radiol. 2017 Jan;27(1):255–66.
113. Varallyay CG, Muldoon LL, Gahramanov S, Wu YJ, Goodman JA, Li X, et al. Dynamic MRI using iron oxide nanoparticles to assess early vascular effects of antiangiogenic versus corticosteroid treatment in a glioma model. J Cereb Blood Flow Metab Off J Int Soc Cereb Blood Flow Metab. 2009 Apr;29(4):853–60.
114. Gahramanov S, Muldoon LL, Varallyay CG, Li X, Kraemer DF, Fu R, et al. Pseudoprogression of glioblastoma after chemo- and radiation therapy: diagnosis by using dynamic susceptibility-weighted contrast-enhanced perfusion MR imaging with ferumoxytol versus gadoteridol and correlation with survival. Radiology. 2013 Mar;266(3):842–52.
115. Barajas RF, Hamilton BE, Schwartz D, McConnell HL, Pettersson DR, Horvath A, et al. Combined iron oxide nanoparticle ferumoxytol and gadolinium contrast enhanced MRI define glioblastoma pseudoprogression. Neuro-Oncol. 2019 Mar 18;21(4):517–26.
116. Ma B, Blakeley JO, Hong X, Zhang H, Jiang S, Blair L, et al. Applying amide proton transfer-weighted MRI to distinguish pseudoprogression from true progression in malignant gliomas. J Magn Reson Imaging JMRI. 2016;44(2):456–62.
117. Elshafeey N, Kotrotsou A, Hassan A, Elshafei N, Hassan I, Ahmed S, et al. Multicenter study demonstrates radiomic features derived from magnetic resonance perfusion images identify pseudoprogression in glioblastoma. Nat Commun. 2019 Jul 18;10(1):3170.
118. Ismail M, Hill V, Statsevych V, Huang R, Prasanna P, Correa R, et al. Shape Features of the Lesion Habitat to Differentiate Brain Tumor Progression from Pseudoprogression on

Routine Multiparametric MRI: A Multisite Study. AJNR Am J Neuroradiol. 2018 Dec;39(12):2187–93.
119. Galldiks N, Kocher M, Langen K-J. Pseudoprogression after glioma therapy: an update. Expert Rev Neurother. 2017 Nov;17(11):1109–15.
120. Kamada K, Houkin K, Abe H, Sawamura Y, Kashiwaba T. Differentiation of cerebral radiation necrosis from tumor recurrence by proton magnetic resonance spectroscopy. Neurol Med Chir (Tokyo). 1997 Mar;37(3):250–6.
121. Zhang H, Ma L, Wang Q, Zheng X, Wu C, Xu B-N. Role of magnetic resonance spectroscopy for the differentiation of recurrent glioma from radiation necrosis: a systematic review and meta-analysis. Eur J Radiol. 2014 Dec;83(12):2181–9.
122. Rabinov JD, Lee PL, Barker FG, Louis DN, Harsh GR, Cosgrove GR, et al. In vivo 3-T MR spectroscopy in the distinction of recurrent glioma versus radiation effects: initial experience. Radiology. 2002 Dec;225(3):871–9.
123. Anbarloui MR, Ghodsi SM, Khoshnevisan A, Khadivi M, Abdollahzadeh S, Aoude A, et al. Accuracy of magnetic resonance spectroscopy in distinction between radiation necrosis and recurrence of brain tumors. Iran J Neurol. 2015 Jan 5;14(1):29–34.
124. Smith EA, Carlos RC, Junck LR, Tsien CI, Elias A, Sundgren PC. Developing a clinical decision model: MR spectroscopy to differentiate between recurrent tumor and radiation change in patients with new contrast-enhancing lesions. AJR Am J Roentgenol. 2009 Feb;192(2):W45-52.
125. Weybright P, Sundgren PC, Maly P, Hassan DG, Nan B, Rohrer S, et al. Differentiation between brain tumor recurrence and radiation injury using MR spectroscopy. AJR Am J Roentgenol. 2005 Dec;185(6):1471–6.
126. Nakajima T, Kumabe T, Kanamori M, Saito R, Tashiro M, Watanabe M, et al. Differential diagnosis between radiation necrosis and glioma progression using sequential proton magnetic resonance spectroscopy and methionine positron emission tomography. Neurol Med Chir (Tokyo). 2009 Sep;49(9):394–401.
127. Plotkin M, Eisenacher J, Bruhn H, Wurm R, Michel R, Stockhammer F, et al. 123I-IMT SPECT and 1H MR-spectroscopy at 3.0 T in the differential diagnosis of recurrent or residual gliomas: a comparative study. J Neurooncol. 2004 Oct;70(1):49–58.
128. Elias AE, Carlos RC, Smith EA, Frechtling D, George B, Maly P, et al. MR spectroscopy using normalized and non-normalized metabolite ratios for differentiating recurrent brain tumor from radiation injury. Acad Radiol. 2011 Sep;18(9):1101–8.
129. Di Costanzo A, Scarabino T, Trojsi F, Popolizio T, Bonavita S, de Cristofaro M, et al. Recurrent glioblastoma multiforme versus radiation injury: a multiparametric 3-T MR approach. Radiol Med (Torino). 2014 Aug;119(8):616–24.
130. Matsusue E, Fink JR, Rockhill JK, Ogawa T, Maravilla KR. Distinction between glioma progression and post-radiation change by combined physiologic MR imaging. Neuroradiology. 2010 Apr;52(4):297–306.
131. Prat R, Galeano I, Lucas A, Martínez JC, Martín M, Amador R, et al. Relative value of magnetic resonance spectroscopy, magnetic resonance perfusion, and 2-(18F) fluoro-2-deoxy-D-glucose positron emission tomography for detection of recurrence or grade increase in gliomas. J Clin Neurosci Off J Neurosurg Soc Australas. 2010 Jan;17(1):50–3.
132. Verma G, Chawla S, Mohan S, Wang S, Nasrallah M, Sheriff S, et al. Three-dimensional echo planar spectroscopic imaging for differentiation of true progression from pseudoprogression in patients with glioblastoma. NMR Biomed. 2019;32(2):e4042.
133. Kruser TJ, Mehta MP, Robins HI. Pseudoprogression after glioma therapy: a comprehensive review. Expert Rev Neurother. 2013 Apr;13(4):389–403.
134. Albert NL, Weller M, Suchorska B, Galldiks N, Soffietti R, Kim MM, et al. Response Assessment in Neuro-Oncology working group and European Association for Neuro-

Oncology recommendations for the clinical use of PET imaging in gliomas. Neuro-Oncol. 2016;18(9):1199–208.
135. Law I, Albert NL, Arbizu J, Boellaard R, Drzezga A, Galldiks N, et al. Joint EANM/EANO/RANO practice guidelines/SNMMI procedure standards for imaging of gliomas using PET with radiolabelled amino acids and [18F]FDG: version 1.0. Eur J Nucl Med Mol Imaging. 2019;46(3):540–57.
136. Kertels O, Mihovilovic MI, Linsenmann T, Kessler AF, Tran-Gia J, Kircher M, et al. Clinical Utility of Different Approaches for Detection of Late Pseudoprogression in Glioblastoma With O-(2-[18F]Fluoroethyl)-L-Tyrosine PET. Clin Nucl Med. 2019 Sep;44(9):695–701.
137. Oborski MJ, Laymon CM, Lieberman FS, Mountz JM. Distinguishing Pseudoprogression From Progression in High-Grade Gliomas. Clin Nucl Med [Internet]. 2013 May [cited 2018 Sep 5];38(5). Available from: https://www.ncbi.nlm.nih.gov/pmc/articles/PMC3880250/
138. Langleben DD, Segall GM. PET in differentiation of recurrent brain tumor from radiation injury. J Nucl Med Off Publ Soc Nucl Med. 2000 Nov;41(11):1861–7.
139. Horky LL, Hsiao EM, Weiss SE, Drappatz J, Gerbaudo VH. Dual phase FDG-PET imaging of brain metastases provides superior assessment of recurrence versus post-treatment necrosis. J Neurooncol. 2011 May;103(1):137–46.
140. Harat M, Małkowski B, Makarewicz R. Pre-irradiation tumour volumes defined by MRI and dual time-point FET-PET for the prediction of glioblastoma multiforme recurrence: A prospective study. Radiother Oncol J Eur Soc Ther Radiol Oncol. 2016 Aug;120(2):241–7.
141. Matuszak J, Waissi W, Clavier JB, Noël G, Namer IJ. Métastases cérébrales : apport de l'acquisition tardive en TEP/TDM au 18F-FDG pour le diagnostic différentiel entre récurrence tumorale et radionécrose. Médecine Nucl. 2016 May 1;40(3):196.
142. Padma MV, Said S, Jacobs M, Hwang DR, Dunigan K, Satter M, et al. Prediction of pathology and survival by FDG PET in gliomas. J Neurooncol. 2003 Sep;64(3):227–37.
143. Kubota R, Yamada S, Kubota K, Ishiwata K, Tamahashi N, Ido T. Intratumoral distribution of fluorine-18-fluorodeoxyglucose in vivo: high accumulation in macrophages and granulation tissues studied by microautoradiography. J Nucl Med Off Publ Soc Nucl Med. 1992 Nov;33(11):1972–80.
144. Chen W. Clinical applications of PET in brain tumors. J Nucl Med Off Publ Soc Nucl Med. 2007 Sep;48(9):1468–81.
145. Ricci PE, Karis JP, Heiserman JE, Fram EK, Bice AN, Drayer BP. Differentiating recurrent tumor from radiation necrosis: time for re-evaluation of positron emission tomography? AJNR Am J Neuroradiol. 1998 Mar;19(3):407–13.
146. Galldiks N, Law I, Pope WB, Arbizu J, Langen K-J. The use of amino acid PET and conventional MRI for monitoring of brain tumor therapy. NeuroImage Clin. 2017;13:386–94.
147. Chen W, Silverman DHS, Delaloye S, Czernin J, Kamdar N, Pope W, et al. 18F-FDOPA PET imaging of brain tumors: comparison study with 18F-FDG PET and evaluation of diagnostic accuracy. J Nucl Med Off Publ Soc Nucl Med. 2006 Jun;47(6):904–11.
148. Ledezma CJ, Chen W, Sai V, Freitas B, Cloughesy T, Czernin J, et al. 18F-FDOPA PET/MRI fusion in patients with primary/recurrent gliomas: initial experience. Eur J Radiol. 2009 Aug;71(2):242–8.
149. Fueger BJ, Czernin J, Cloughesy T, Silverman DH, Geist CL, Walter MA, et al. Correlation of 6-18F-fluoro-L-dopa PET uptake with proliferation and tumor grade in newly diagnosed and recurrent gliomas. J Nucl Med Off Publ Soc Nucl Med. 2010 Oct;51(10):1532–8.
150. Herrmann K, Czernin J, Cloughesy T, Lai A, Pomykala KL, Benz MR, et al. Comparison of visual and semiquantitative analysis of 18F-FDOPA-PET/CT for recurrence

detection in glioblastoma patients. Neuro-Oncol. 2014 Apr;16(4):603–9.
151. Karunanithi S, Sharma P, Kumar A, Khangembam BC, Bandopadhyaya GP, Kumar R, et al. 18F-FDOPA PET/CT for detection of recurrence in patients with glioma: prospective comparison with 18F-FDG PET/CT. Eur J Nucl Med Mol Imaging. 2013 Jul;40(7):1025–35.
152. Yu J, Zheng J, Xu W, Weng J, Gao L, Tao L, et al. Accuracy of 18F-FDOPA Positron Emission Tomography and 18F-FET Positron Emission Tomography for Differentiating Radiation Necrosis from Brain Tumor Recurrence. World Neurosurg. 2018 Jun 1;114:e1211–24.
153. Wester HJ, Herz M, Weber W, Heiss P, Senekowitsch-Schmidtke R, Schwaiger M, et al. Synthesis and radiopharmacology of O-(2-[18F]fluoroethyl)-L-tyrosine for tumor imaging. J Nucl Med Off Publ Soc Nucl Med. 1999 Jan;40(1):205–12.
154. Ceccon G, Lohmann P, Stoffels G, Judov N, Filss CP, Rapp M, et al. Dynamic O-(2-18F-fluoroethyl)-L-tyrosine positron emission tomography differentiates brain metastasis recurrence from radiation injury after radiotherapy. Neuro-Oncol. 2017 01;19(2):281–8.
155. Galldiks N, Dunkl V, Stoffels G, Hutterer M, Rapp M, Sabel M, et al. Diagnosis of pseudoprogression in patients with glioblastoma using O-(2-[18F]fluoroethyl)-L-tyrosine PET. Eur J Nucl Med Mol Imaging. 2015 Apr;42(5):685–95.
156. Galldiks N, Stoffels G, Filss C, Rapp M, Blau T, Tscherpel C, et al. The use of dynamic O-(2-18F-fluoroethyl)-l-tyrosine PET in the diagnosis of patients with progressive and recurrent glioma. Neuro-Oncol. 2015 Sep;17(9):1293–300.
157. Pauleit D, Floeth F, Hamacher K, Riemenschneider MJ, Reifenberger G, Müller H-W, et al. O-(2-[18F]fluoroethyl)-L-tyrosine PET combined with MRI improves the diagnostic assessment of cerebral gliomas. Brain J Neurol. 2005 Mar;128(Pt 3):678–87.
158. Kebir S, Fimmers R, Galldiks N, Schäfer N, Mack F, Schaub C, et al. Late Pseudoprogression in Glioblastoma: Diagnostic Value of Dynamic O-(2-[18F]fluoroethyl)-L-Tyrosine PET. Clin Cancer Res Off J Am Assoc Cancer Res. 2016 01;22(9):2190–6.
159. Mihovilovic MI, Kertels O, Hänscheid H, Löhr M, Monoranu C-M, Kleinlein I, et al. O-(2-(18F)fluoroethyl)-L-tyrosine PET for the differentiation of tumour recurrence from late pseudoprogression in glioblastoma. J Neurol Neurosurg Psychiatry. 2019 Feb;90(2):238–9.
160. Pöpperl G, Götz C, Rachinger W, Gildehaus F-J, Tonn J-C, Tatsch K. Value of O-(2-[18F]fluoroethyl)- L-tyrosine PET for the diagnosis of recurrent glioma. Eur J Nucl Med Mol Imaging. 2004 Nov;31(11):1464–70.
161. Mehrkens JH, Pöpperl G, Rachinger W, Herms J, Seelos K, Tatsch K, et al. The positive predictive value of O-(2-[18F]fluoroethyl)-L-tyrosine (FET) PET in the diagnosis of a glioma recurrence after multimodal treatment. J Neurooncol. 2008 May;88(1):27–35.
162. Kebir S, Khurshid Z, Gaertner FC, Essler M, Hattingen E, Fimmers R, et al. Unsupervised consensus cluster analysis of [18F]-fluoroethyl-L-tyrosine positron emission tomography identified textural features for the diagnosis of pseudoprogression in high-grade glioma. Oncotarget. 2017 Jan 31;8(5):8294–304.
163. Rachinger W, Goetz C, Pöpperl G, Gildehaus FJ, Kreth FW, Holtmannspötter M, et al. Positron emission tomography with O-(2-[18F]fluoroethyl)-l-tyrosine versus magnetic resonance imaging in the diagnosis of recurrent gliomas. Neurosurgery. 2005 Sep;57(3):505–11; discussion 505-511.
164. Werner J-M, Stoffels G, Lichtenstein T, Borggrefe J, Lohmann P, Ceccon G, et al. Differentiation of treatment-related changes from tumour progression: a direct comparison between dynamic FET PET and ADC values obtained from DWI MRI. Eur J Nucl Med Mol Imaging. 2019 Aug;46(9):1889–901.
165. Grosu A-L, Astner ST, Riedel E, Nieder C, Wiedenmann N, Heinemann F, et al. An interindividual comparison of O-(2-[18F]fluoroethyl)-L-tyrosine (FET)- and L-[methyl-11C]methionine (MET)-PET in patients with brain gliomas and metastases. Int J Radiat

Oncol Biol Phys. 2011 Nov 15;81(4):1049–58.
166. Tsuyuguchi N, Takami T, Sunada I, Iwai Y, Yamanaka K, Tanaka K, et al. Methionine positron emission tomography for differentiation of recurrent brain tumor and radiation necrosis after stereotactic radiosurgery--in malignant glioma. Ann Nucl Med. 2004 Jun;18(4):291–6.
167. De Witte O, Goldberg I, Wikler D, Rorive S, Damhaut P, Monclus M, et al. Positron emission tomography with injection of methionine as a prognostic factor in glioma. J Neurosurg. 2001 Nov;95(5):746–50.
168. Matsuo M, Miwa K, Shinoda J, Tanaka O, Krishna M. Impact of C11-methionine Positron Emission Tomography (PET) for Malignant Glioma in Radiation Therapy: Is C11-methionine PET a superior to Magnetic Resonance Imaging? Int J Radiat Oncol • Biol • Phys. 2011 Oct 1;81(2):S182.
169. Matsuo M, Tanaka H, Yamaguchi T, Nishibori H, Ogawa S. Pseudoprogression of Glioblastoma Multiforme After Chemoradiation Therapy: Diagnosis by 11C-Methionine Positron Emission Tomography (PET). Int J Radiat Oncol • Biol • Phys. 2016 Oct 1;96(2):E102.
170. Tripathi M, Sharma R, Varshney R, Jaimini A, Jain J, Souza MMD, et al. Comparison of F-18 FDG and C-11 methionine PET/CT for the evaluation of recurrent primary brain tumors. Clin Nucl Med. 2012 Feb;37(2):158–63.
171. Terakawa Y, Tsuyuguchi N, Iwai Y, Yamanaka K, Higashiyama S, Takami T, et al. Diagnostic accuracy of 11C-methionine PET for differentiation of recurrent brain tumors from radiation necrosis after radiotherapy. J Nucl Med Off Publ Soc Nucl Med. 2008 May;49(5):694–9.
172. Garcia JR, Cozar M, Baquero M, Fernández Barrionuevo JM, Jaramillo A, Rubio J, et al. The value of 11C-methionine PET in the early differentiation between tumour recurrence and radionecrosis in patients treated for a high-grade glioma and indeterminate MRI. Rev Espanola Med Nucl E Imagen Mol. 2017 Apr;36(2):85–90.
173. Minamimoto R, Saginoya T, Kondo C, Tomura N, Ito K, Matsuo Y, et al. Differentiation of Brain Tumor Recurrence from Post-Radiotherapy Necrosis with 11C-Methionine PET: Visual Assessment versus Quantitative Assessment. PloS One. 2015;10(7):e0132515.
174. Li D-L, Xu Y-K, Wang Q-S, Wu H-B, Li H-S. ^{11}C-methionine and ^{18}F-fluorodeoxyglucose positron emission tomography/CT in the evaluation of patients with suspected primary and residual/recurrent gliomas. Chin Med J (Engl). 2012 Jan;125(1):91–6.
175. Van Laere K, Ceyssens S, Van Calenbergh F, de Groot T, Menten J, Flamen P, et al. Direct comparison of 18F-FDG and 11C-methionine PET in suspected recurrence of glioma: sensitivity, inter-observer variability and prognostic value. Eur J Nucl Med Mol Imaging. 2005 Jan;32(1):39–51.
176. Dandois V, Rommel D, Renard L, Jamart J, Cosnard G. Substitution of 11C-methionine PET by perfusion MRI during the follow-up of treated high-grade gliomas: preliminary results in clinical practice. J Neuroradiol J Neuroradiol. 2010 May;37(2):89–97.
177. Deuschl C, Kirchner J, Poeppel TD, Schaarschmidt B, Kebir S, El Hindy N, et al. 11C-MET PET/MRI for detection of recurrent glioma. Eur J Nucl Med Mol Imaging. 2018;45(4):593–601.
178. Chen W, Cloughesy T, Kamdar N, Satyamurthy N, Bergsneider M, Liau L, et al. Imaging proliferation in brain tumors with 18F-FLT PET: comparison with 18F-FDG. J Nucl Med Off Publ Soc Nucl Med. 2005 Jun;46(6):945–52.
179. Jacobs AH, Thomas A, Kracht LW, Li H, Dittmar C, Garlip G, et al. 18F-fluoro-L-thymidine and 11C-methylmethionine as markers of increased transport and proliferation in brain tumors. J Nucl Med Off Publ Soc Nucl Med. 2005 Dec;46(12):1948–58.

180. Ullrich R, Backes H, Li H, Kracht L, Miletic H, Kesper K, et al. Glioma proliferation as assessed by 3'-fluoro-3'-deoxy-L-thymidine positron emission tomography in patients with newly diagnosed high-grade glioma. Clin Cancer Res Off J Am Assoc Cancer Res. 2008 Apr 1;14(7):2049–55.
181. Choi SJ, Kim JS, Kim JH, Oh SJ, Lee JG, Kim CJ, et al. [18F]3'-deoxy-3'-fluorothymidine PET for the diagnosis and grading of brain tumors. Eur J Nucl Med Mol Imaging. 2005 Jun;32(6):653–9.
182. Schiepers C, Dahlbom M, Chen W, Cloughesy T, Czernin J, Phelps ME, et al. Kinetics of 3'-deoxy-3'-18F-fluorothymidine during treatment monitoring of recurrent high-grade glioma. J Nucl Med Off Publ Soc Nucl Med. 2010 May;51(5):720–7.
183. Wardak M, Schiepers C, Dahlbom M, Cloughesy T, Chen W, Satyamurthy N, et al. Discriminant analysis of ^{18}F-fluorothymidine kinetic parameters to predict survival in patients with recurrent high-grade glioma. Clin Cancer Res Off J Am Assoc Cancer Res. 2011 Oct 15;17(20):6553–62.
184. Dhermain FG, Hau P, Lanfermann H, Jacobs AH, van den Bent MJ. Advanced MRI and PET imaging for assessment of treatment response in patients with gliomas. Lancet Neurol. 2010 Sep;9(9):906–20.
185. Muzi M, Spence AM, O'Sullivan F, Mankoff DA, Wells JM, Grierson JR, et al. Kinetic analysis of 3'-deoxy-3'-18F-fluorothymidine in patients with gliomas. J Nucl Med Off Publ Soc Nucl Med. 2006 Oct;47(10):1612–21.
186. Spence AM, Muzi M, Link JM, O'Sullivan F, Eary JF, Hoffman JM, et al. NCI-sponsored trial for the evaluation of safety and preliminary efficacy of 3'-deoxy-3'-[18F]fluorothymidine (FLT) as a marker of proliferation in patients with recurrent gliomas: preliminary efficacy studies. Mol Imaging Biol MIB Off Publ Acad Mol Imaging. 2009 Oct;11(5):343–55.
187. den Hollander MW, Enting RH, de Groot JC, Solouki MA, den Dunnen WFA, Sluiter WJ, et al. Prospective analysis of serial FLT-PET scanning to discriminate between true and pseudoprogression in glioblastoma. J Clin Oncol. 2014 May 20;32(15_suppl):2009–2009.
188. Brahm CG, den Hollander MW, Enting RH, de Groot JC, Solouki AM, den Dunnen WFA, et al. Serial FLT PET imaging to discriminate between true progression and pseudoprogression in patients with newly diagnosed glioblastoma: a long-term follow-up study. Eur J Nucl Med Mol Imaging. 2018 Jul 21;
189. Enslow MS, Zollinger LV, Morton KA, Kadrmas DJ, Butterfield RI, Christian PE, et al. Comparison of F-18 Fluorodeoxyglucose and F-18 Fluorothymidine Positron Emission Tomography in Differentiating Radiation Necrosis from Recurrent Glioma. Clin Nucl Med. 2012 Sep;37(9):854–61.
190. Gulyás B, Halldin C. New PET radiopharmaceuticals beyond FDG for brain tumor imaging. Q J Nucl Med Mol Imaging Off Publ Ital Assoc Nucl Med AIMN Int Assoc Radiopharmacol IAR Sect Soc Of. 2012 Apr;56(2):173–90.
191. Alkonyi B, Barger GR, Mittal S, Muzik O, Chugani DC, Bahl G, et al. Accurate differentiation of recurrent gliomas from radiation injury by kinetic analysis of α-11C-methyl-L-tryptophan PET. J Nucl Med Off Publ Soc Nucl Med. 2012 Jul;53(7):1058–64.
192. Barajas RF, Krohn KA, Link JM, Hawkins RA, Clarke JL, Pampaloni MH, et al. Glioma FMISO PET/MR Imaging Concurrent with Antiangiogenic Therapy: Molecular Imaging as a Clinical Tool in the Burgeoning Era of Personalized Medicine. Biomedicines. 2016 Oct 31;4(4).
193. Bolcaen J, Descamps B, Deblaere K, Boterberg T, De Vos Pharm F, Kalala J-P, et al. (18)F-fluoromethylcholine (FCho), (18)F-fluoroethyltyrosine (FET), and (18)F-fluorodeoxyglucose (FDG) for the discrimination between high-grade glioma and radiation necrosis in rats: a PET study. Nucl Med Biol. 2015 Jan;42(1):38–45.

194. Beshr R, Isohashi K, Watabe T, Naka S, Horitsugi G, Romanov V, et al. Preliminary feasibility study on differential diagnosis between radiation-induced cerebral necrosis and recurrent brain tumor by means of [18F]fluoro-borono-phenylalanine PET/CT. Ann Nucl Med. 2018 Dec;32(10):702–8.
195. Miyashita M, Miyatake S-I, Imahori Y, Yokoyama K, Kawabata S, Kajimoto Y, et al. Evaluation of fluoride-labeled boronophenylalanine-PET imaging for the study of radiation effects in patients with glioblastomas. J Neurooncol. 2008 Sep;89(2):239–46.
196. Zhang H, Ma L, Wu C, Xu B. Performance of SPECT in the differential diagnosis of glioma recurrence from radiation necrosis. J Clin Neurosci Off J Neurosurg Soc Australas. 2015 Feb;22(2):229–37.
197. Tie J, Gunawardana DH, Rosenthal MA. Differentiation of tumor recurrence from radiation necrosis in high-grade gliomas using 201Tl-SPECT. J Clin Neurosci Off J Neurosurg Soc Australas. 2008 Dec;15(12):1327–34.
198. Caresia AP, Castell-Conesa J, Negre M, Mestre A, Cuberas G, Mañes A, et al. Thallium-201SPECT assessment in the detection of recurrences of treated gliomas and ependymomas. Clin Transl Oncol. 2006 Oct 1;8(10):750–4.
199. Vos MJ, Tony BN, Hoekstra OS, Postma TJ, Heimans JJ, Hooft L. Systematic review of the diagnostic accuracy of 201Tl single photon emission computed tomography in the detection of recurrent glioma. Nucl Med Commun. 2007 Jun;28(6):431–9.
200. Gómez-Río M, Rodríguez-Fernández A, Ramos-Font C, López-Ramírez E, Llamas-Elvira JM. Diagnostic accuracy of 201Thallium-SPECT and 18F-FDG-PET in the clinical assessment of glioma recurrence. Eur J Nucl Med Mol Imaging. 2008 May;35(5):966–75.
201. Jeune FP –Le, Dubois F, Blond S, Steinling M. Sestamibi technetium-99m brain single-photon emission computed tomography to identify recurrent glioma in adults: 201 studies. J Neurooncol. 2006 Apr 1;77(2):177–83.
202. Palumbo B, Lupattelli M, Pelliccioli GP, Chiarini P, Moschini TO, Palumbo I, et al. Association of 99mTc-MIBI brain SPECT and proton magnetic resonance spectroscopy (1H-MRS) to assess glioma recurrence after radiotherapy. Q J Nucl Med Mol Imaging Off Publ Ital Assoc Nucl Med AIMN Int Assoc Radiopharmacol IAR Sect Soc Of. 2006 Mar;50(1):88–93.
203. Amin A, Moustafa H, Ahmed E, El-Toukhy M. Glioma residual or recurrence versus radiation necrosis: accuracy of pentavalent technetium-99m-dimercaptosuccinic acid [Tc-99m (V) DMSA] brain SPECT compared to proton magnetic resonance spectroscopy (1H-MRS): initial results. J Neurooncol. 2012 Feb;106(3):579–87.
204. Alexiou GA, Fotopoulos AD, Papadopoulos A, Kyritsis AP, Polyzoidis KS, Tsiouris S. Evaluation of brain tumor recurrence by (99m)Tc-tetrofosmin SPECT: a prospective pilot study. Ann Nucl Med. 2007 Jul;21(5):293–8.
205. Arora G, Sharma P, Sharma A, Mishra A, Hazari P, Biswas A, et al. 99mTc-Methionine Hybrid SPECT/CT for Detection of Recurrent Glioma. Clin Nucl Med [Internet]. 2018 May 1 [cited 2019 May 9];43(5). Available from: insights.ovid.com
206. Santra A, Kumar R, Sharma P. Use of 99m-technetium-glucoheptonate as a tracer for brain tumor imaging: An overview of its strengths and pitfalls. Indian J Nucl Med IJNM Off J Soc Nucl Med India. 2015;30(1):1–8.
207. Rani N, Singh B, Kumar N, Singh P, Hazari PP, Singh H, et al. Differentiation of Recurrent/Residual Glioma From Radiation Necrosis Using Semi Quantitative 99mTc MDM (Bis-Methionine-DTPA) Brain SPECT/CT and Dynamic Susceptibility Contrast-Enhanced MR Perfusion: A Comparative Study. Clin Nucl Med. 2018 Mar;43(3):e74–81.

Table 1: Description of advanced MRI techniques, metrics, and results of pseudoprogression (PsP) and true progression (TP).

Advanced MRI techniques		Metrics	Results for PsP/TP
Diffusion MRI			
DWI : Diffusion-Weighted MRI	Water diffusion within tissue (displacement of water molecules in brain parenchyma)	**ADC: Apparent Diffusion Coefficient** quantify the mobility of water molecules at the cellular level	**ADC value**: PsP>TP **ADC ratio**: PsP>TP
DTI : Diffusion Tensor Imaging	Direction of water diffusion	**FA: Fractional Anisotropy** measures the fraction of the diffusion that is anisotropic (diffusion asymmetry in a voxel)	**FA value**: TP>PsP **FA ratio**: TP>PsP
Perfusion MRI			
DSC: Dynamic Susceptibility Contrast MRI	T2/T2*-weighted technique measurement of vascular perfusion and permeability Exogenous gadolinium based contrast agent	**rCBF: relative Cerebral Blood Flow** measurement of the lesion blood flow compared to contralateral cerebral tissue (white or grey matter)	**rCBF**: TP>PsP
		rCBV: relative Cerebral Blood Volume measurement of the lesion blood volume compared to contralateral cerebral tissue (white or grey matter)	**rCBV**: TP>PsP
		PH: Peak Height reflects the total blood volume maximal signal intensity	**PH**: TP>PsP
		PSR: percentage of signal intensity recovery reflects capillary permeability	**PSR**: PsP>TP
DCE: Dynamic Contrast Enhanced	T1-based technique measurement of	**K^{trans}: Volume Transfer Constant between plasma and EES**	**K^{trans}**: TP>PsP

MRI	vascular permeability Exogenous gadolinium based contrast agent	reflects gadolinium leakage rate from plasma to EES and microvascular permeability **V_e: Volume of EES** reflects cellularity and necrosis in EES and microvascular permeability **V_p: Vascular plasma volume** reflects blood plasma volume **K_{ep}: Transfer constant from the EES into the plasma** = Ktrans/Ve	 **V_e**: TP≥PsP **V_p**: TP≥PsP **K_{ep}**: TP=PsP
ASL: Arterial Spin Labeling	Brain tissue perfusion Magnetic arterial blood water protons as an endogenous tracer	**CBF: Cerebral Blood Flow** Blood volume through a cerebral region per unit of time	**CBF**: TP>PsP
MRS: **Magnetic Resonance Spectroscopy**	Reflects the distribution of chemical metabolites within a brain tissue volume	**Cho**: Choline **Cr**: Creatinine **Lac**: Lactate **Lip**: Lipid **NAA**: N-acetylaspartate	**Cho/NAA**: TP>PsP **Cho/Cr**: TP>PsP **NAA/Cr**: PsP>TP

Table 2: Review of the apparent diffusion coefficient (ADC) values in the literature for pseudoprogression (PsP) and true progression (TP).

Authors	N	Tumors	Parameters	Values		p value	Threshold	Se	Sp	PPV	NPV	Accuracy
				PsP	TP							
Hein *et al.*, 2004 (54)	18	HGG	ADC ratio	1.82	1.43	<0.001						
			Mean ADC value	1.40	1.18	<0.006						
Asao *et al.*, 2005 (51)	17	HGG	Minimal ADC value	1.04	1.07	> 0.05						
			Mean ADC value	1.68	1.37	>0.05						
			Maximal ADC value	2.30	1.68	0.039						
Sundgren *et a.l*, 2006 (55)	28	Gliomas	Mean ADC value	1.12	1.27	0 .01						
			ADC ratio	1.40	1.54	0.07						
Zeng *et al.*, 2007 (61)	55	HGG	Mean ADC value	1.39	1.20	<0.01						
			ADC ratio	1.69	1.42	<0.01						
Bobek-Billewics *et al.*, 2010 (68)	8	Gliomas	Mean ADC value	1.13	1.06	0.51						
			ADC ratio	1.55	1.55	0.98						
Xu *et al.*, 2010 (53)	35	Gliomas	Mean ADC value	1.54	1.23	0.0002						
			ADC ratio	1.62	1.34	0.0013						
Lee *et al.*, 2012 (52)	20	HGG	Mean ADC value	1.349	1.040	<0.0001	1.200	80	83			81
	22	HGG	Mean ADC value	1.349	1.215	0.289						
Fink *et al.*, 2012 (63)	38	Gliomas	ADC ratio	1.43	1.14	0.035	≤1.28	72	80	91	50	74
Agarwal *et al.*, 2013 (34)	24	HGG	Mean ADC value	1.40	1.37	0.700						
Chu *et al.*, 2013 (71)	30	GBM	Mean ADC value	1.329	1.269	0.616						
Alexiou *et al.*, 2014	30	HGG	ADC ratio	2.12	1.19	0.005	1.27	65	100			

(65)												
Prager *et al.*, 2015 (64)	51 (68)	HGG	Median ADC lesion value ADC ratio Median ADC ROI value	1.62 1.585 1.2	1.39 1.482 1.1	0.001 0.288 0.128	≥1.6	95	63			
Bulik *et al.*, 2015 (66)	24	GBM	Mean ADC value	1.373	1.160	<0.001	1.300	100	100			
Kazda *et al.*, 2016 (67)	39	GBM	Mean ADC value	1.372	1.155	<0.001	1.313	98	100			
Reimer *et al.*, 2017 (60)	35	GBM	Relative ADC			0.014	0.25	86	86			
Jena *et al.*, 2017 (62)	35	Gliomas	Mean ADC value	1.558	1.283	0.015	≤1.507	87	55	84	58	78

ADC: Apparent diffusion coefficient; **GBM**: Glioblastoma; **HGG**: High grade gliomas; **NPV**: Negative Predictive Value; **PPV**: Positive Predictive Value; **PsP**: Pseudoprogression; **ROI**: Region of interest; **TP**: True Progression; **Se**: Sensibility; **Sp**: Specificity

Table 3: Review of the perfusion MRI metrics in the literature and their statistical characteristics

Authors	N	Tumors	Parameters	Values		p	Threshold	Se	Sp	PPV	NPV	Accuracy
				PsP	TP							
Barajas *et al.*, 2009 (115)	57	GBM	Mean rCBV	1.57	2.38	<0.01	1.75	79	72			
			Max rCBV	4.63	8.16	<0.01						
			Min rCBV	0.95	1.61	<0.01						
			Mean rPH	1.25	2.7	<0.01	1.38	89	81			
			Max rPH	1.72	3.09	<0.01						
			Min rPH	0.82	1.31	<0.01						
			Mean rPSR	89.3	80.2	0.01	87.3	78	76			
			Max rPSR	92.5	100	0.05						
			Min rPSR	77.2	68.8	0.04						
Hu *et al.*, 2009 (88)	13	HGG	Min rCBV	0.21	0.55		0.71	92	100			96
			Max rCBV	0.71	4.64							
Gasparetto *et al.*, 2009 (90)	12	HGG	Mean rCBV				1.8	100	87	80	100	92
Bobek-Billewics *et al.*, 2010 (68)	8	Gliomas	Max rCBV	0.78	2.44	<0.001	≥1.7					
			Mean rCBV	0.49	1.46	<0.004	≥1.25					
Tsien *et al.*, 2010 (97)	27	HGG	Mean rCBV	2.3	2.8	0.8						
Kim *et al.*, 2010 (92)	10	HGG	Mean rCBV	2.53	5.72	0.01	3.69	100	100			

Heidemans-Hazelaar *et al.*, 2010 (87)	32	GBM	Mean rCBV			<0.002	2.12	88	83	96	63	
Bisdas *et al.*, 2011 (103)	18	HGG	Median K^{trans} Median V_e Median K_{ep}	0.15 0.34 0.34	0.43 0.56 0.45	0.0051 NS NS	>0.19	100	83			
Gahramanov *et al.*, 2011 (91)	14	GBM	Mean rCBV	0.7	2.7	NA	1.75					
Kong *et al.*, 2011 (100)	59	GBM	Mean rCBV	1.49	2.85	0.003	>1.49	81	78			
Fink *et al.*, 2012 (63)	38	Gliomas	CBV ratio	1.31	3.62	<0.001	≥2.08	86	90	96	69	87
Hu *et al.*, 2012 (89)	25	GBM	Mean rCBV				1.0	100	100			100
Young *et al.*, 2013 (93)	20	GBM	Median rCBV Mean rPH Mean PSR	1.50 1.34 1.01	2.75 3.04 0.84	0.009 <0.001 <0.039	≤1.8 ≤2.4 ≤1.7 ≥0.9	100 69 100 100	75 100 100 63			
Larsen *et al.*, 2013 (15)	14	HGG	Mean CBV Mean CBF	1.3 11.9	10.9 28.1	NA NA	2.0	100	100			
Seeger *et al.*, 2013 (85)	40	HGG	Mean rCBF (DSC) Mean rCBF (ASL) Mean rCBV Median K^{trans} Maximum K^{trans}	1.66 1.66 1.73 0.03 0.047	4.01 2.41 3.91 0.05 0.08	<0.01 0.063 0.01 0.07 0.046	2.24 2.18 2.15 >0.058	77 54 81 62	85 85 77 80			80 69 79 69

			V_e	0.15	0.27	0.10						
Alexiou *et al.*, 2014 (65)	30	HGG	Mean rCBV	1.68	6.71	0.000	2.2	100	100			
D'Souza *et al.*, 2014 (86)	29	HGG	Mean rCBV	3.01	0.8	NA						
Shin *et al.*, 2014 (98)	31	Gliomas	Mean rCBV	2.11	2.55	0.511	2.33	72	70			
			Mean rK^{trans}	1.69	2.52	0.399	2.1	61	80			
Yun *et al.*, 2015 (104)	33	GBM	Mean K^{trans}	0.23	0.44	0.004	0.347	59	94	91	68	76
			V_e	0.75	1.26	0.034	0.570	88	56	68	82	
			V_p	0.11	0.14	0.119						
Thomas *et al.*, 2015 (105)	37	GBM	Mean V_p	2.4	5.3	0.0002	>3.7	85	79			
			90^{th} percentile V_p	3.2	6.6	>0.0001	>3.9	85	92			
			Mean K^{trans}	3.5	7.4	0.002	>3.6	69	79			
			90^{th} percentile K^{trans}	4.2	9.1	0.0004						
Prager *et al.*, 2015 (64)	51 (68)	HGG	Median rCBVlesion	0.88	1.76	0.028	<1.07	75	100			
			Median rCBVroi	1.625	2.575	0.032	<1.74	75	93			
			Median rPSRroi	0.87	0.80	0.467						
Wang *et al.*, 2016 (74)			Max rCBV	2.90	4.75	0.007	4.06	62	80			
Jena *et al.*, 2017 (62)	35	Gliomas	Mean rCBV	1.82	2.41	0.082	≥1.71					77
Boxerman *et al.*,	25	HGG	Mean rCBV	2.4	2.2	0.67	>2.4	67	40			

2017 (96)												

GBM: Glioblastoma; **HGG**: High Grade Glioma; $\mathbf{K_{ep}}$: Transfer constant from the extracellular-extravascular space into the plasma; $\mathbf{K^{trans}}$: Volume Transfer Constant; **NPV**: Negative Predictive Value; **PPV**: Positive Predictive Value; **PsP**: Pseudoprogression; **rCBF**: relative Cerebral Blood Flow; **rCBV**: relative Cerebral Blood Volume; **ROI**: Regio of Interest; **rPH**: relative Peak Height; **rPSR**: relative Percentage of Signal intensity Recovery; **TP**: True Progression; **Se**: Sensibility; **Sp**: Specificity; $\mathbf{V_e}$: Volume of extravascular-extracellular space; $\mathbf{V_p}$: Vascular plasma volume

Table 4: Review of the different publications regarding MRS and the reported threshold values, sensitivity (Se), specificity (Sp), positive predictive value (PPV), negative predictive value (NPV), and accuracy

Parameters	Authors	Values		p	Threshold	Se	Sp	PPV	NPV	Accuracy
		PsP	TP							
Cho/NAA	Plotkin *et al.*, 2004 (127)	0.74	1.51	<0.0001	1.17	89	83			88
	Weybright *et al.*, 2005 (125)	1.31	3.48	<0.0001	1.8					
	Zeng *et al.*, 2007 (61)	1.55	3.52	<0.01						
	Smith *et al.*, 2009 (124)	1.43	3.20	0.0007		85	69	81	75	
	Bobek-Billewicz *et al.*, 2010 (68)	2.11	1.9	0.51						
	Elias *et al.*, 2011 (128)	1.39	2.81	0.0004						
	Fink *et al.*, 2012 (63)	0.84	2.87	0.002						
	Seeger *et al.*, 2013 (85)	1.47	2.20	0.20						
	Anbarloui *et al.*, 2015 (123)	1.46	2.72	<0.01	>1.8	84	75			81
	Bulik *et al.*, 2015 (66)	0.77	2.00	<0.001	≥1.4	100	92			
	Kazda *et al.*, 2016 (67)	0.74	2.13	<0.001	≥1.3	100	95			
Cho/Cr	Plotkin *et al.*, 2004 (127)	0.95	1.38	0.030	1.11	89	83			88
	Weybright *et al.*, 2005 (125)	1.57	2.52	<0.0001	1.8					
	Zeng *et al.*, 2007 (61)	1.61	2.82	<0.01	2.5	78	86			

	Nakajima *et al.*, 2009 (126)	2.25	3.17	NS						
	Smith *et al.*, 2009 (124)	1.57	2.36	0.0001						
	Bobek-Billewicz *et al.*, 2010 (68)	1.84	2.23	0.2441						
	Elias *et al.*, 2011 (128)	1.34	2.16	0.15						
	Fink *et al.*, 2012 (63)	1.57	2.57	0.021						
	Seeger *et al.*, 2013 (85)	1.30	1.66	0.047	>1.12	85	50			72
	D'Souza *et al.*, 2014 (86)	1.26	2.27	NA	≥0.7	83	42			
	Bulik *et al.*, 2015 (66)	0.82	0.86	0.317	≥1.405					91
	Jena *et al.*, 2017 (62)	1.63	3.47	0.002	≥0.7	75	63			
	Kazda *et al.*, 2016 (67)	0.64	0.89	0.013						
NAA/Cr	Plotkin *et al.*, 2004 (127)	1.44	0.99	0.212						
	Weybright *et al.*, 2005 (125)	1.22	0.79	<0.0001						
	Zeng *et al.*, 2007 (61)	1.10	0.84	<0.01						
	Smith *et al.*, 2009 (124)	1.14	0.85	0.0183						
	Elias *et al.*, 2011 (128)	1.36	0.85	0.0033						
	Seeger *et al.*, 2013 (85)	0.51	1.01	0.051						
	Bulik *et al.*, 2015 (66)	0.99	0.45	<0.001	≤0.7	94	92			

	Kazda *et al.*, 2016 (67)	0.99	0.41	<0.001	≤0.7	97	95			
Cho/Lip	Anbarloui *et al.*, 2015 (123)	0.6	2.78	<0.01	>1.0	84	75			81
Lac/Cr	Zeng *et al.*, 2007 (61)	0.45	1.28	0.01						
Lip/Cr	Zeng *et al.*, 2007 (61)	0.54	0.14	0.01						
Lac/Cho	Nakajima *et al.*, 2009 (126)	2.35	0.63	<0.01	1.05	89	100			
(Lac+Lip)/Cr	Bulik *et al.*, 2015 (66)	0.88	4.43	0.004	≥1.9	92	75			
	Kazda *et al.*, 2016 (67)	1.13	2.69	0.005	≥1.6	76	68			
Lac+Lip	Bulik *et al.*, 2015 (66)	3.50	10.77	0.004	≥4.8	100	67			
Cho	Bulik *et al.*, 2015 (66)	2.88	2.41	0.739	≤2.9	69	42			
NAA	Bulik *et al.*, 2015 (66)	2.88	1.19	<0.001	≤1.5	75	100			
Cr	Bulik *et al.*, 2015 (66)	2.74	2.49	0.243	≤2.6	56	67			

Cho:Choline; **Cr**:Creatinine; **Lac**:Lactates; **Lip**:Lipids; **NAA**:N-acetylaspartate; **NPV**: Negative Predictive Value; **PPV**: Positive Predictive Value; **PsP**: Pseudoprogression; **TP**: True Progression; **Se**: Sensibility; **Sp**: Specificity

Table 5: Different tracers and metrics of positron-emission tomography (PET).

PET tracers		Metrics	TP/PsP
FDG	2-deoxy-2-[fluorine-18]fluoro- D-glucose	**SUV:** standardized uptake value	**TP>PsP**
FDOPA	^{18}F-fluoro-L-dopa	**T/N:** tumor uptake to normal hemispheric tissue uptake	**TP>PsP**
FET	O-(2-[^{18}F]fluoroethyl)-L-tyrosine	**T/S:** tumor uptake to striatum uptake	**TP>PsP**
MET	^{11}C-methyl-L-methionine	**L/N:** lesion uptake to normal brain tissue uptake	**TP>PsP**
FLT	3'-deoxy-3'[(18)F]-fluorothymidine	**L/R:** lesion uptake to contralateral cerebral white matter uptake	**TP>PsP**
Choline	^{11}C-Choline	**TBR:** tumor-to-brain ratio	**TP>PsP**
FMISO	^{18}F-Fluoromisonidazole	**TNR:** tumor-to-normal brain ratio	**TP>PsP**
MLT	^{11}C-Methyl-L-Tryptophan PET	**SUV/BG:** standardized uptake value/background	**TP>PsP**
FCho	^{18}F-fluoromethylcholine	**TTP:** time to peak	**PsP>TP**
FBPA	4-borono-2-^{18}F-fluoro-phenylalanine		

PET: Positrion Emisson Tomography; **PsP:** Pseudoprogression; **TP**: True Progression

Figure 1: Clinical decisional diagram between pseudoprogression (PsP) and true progression (TP)

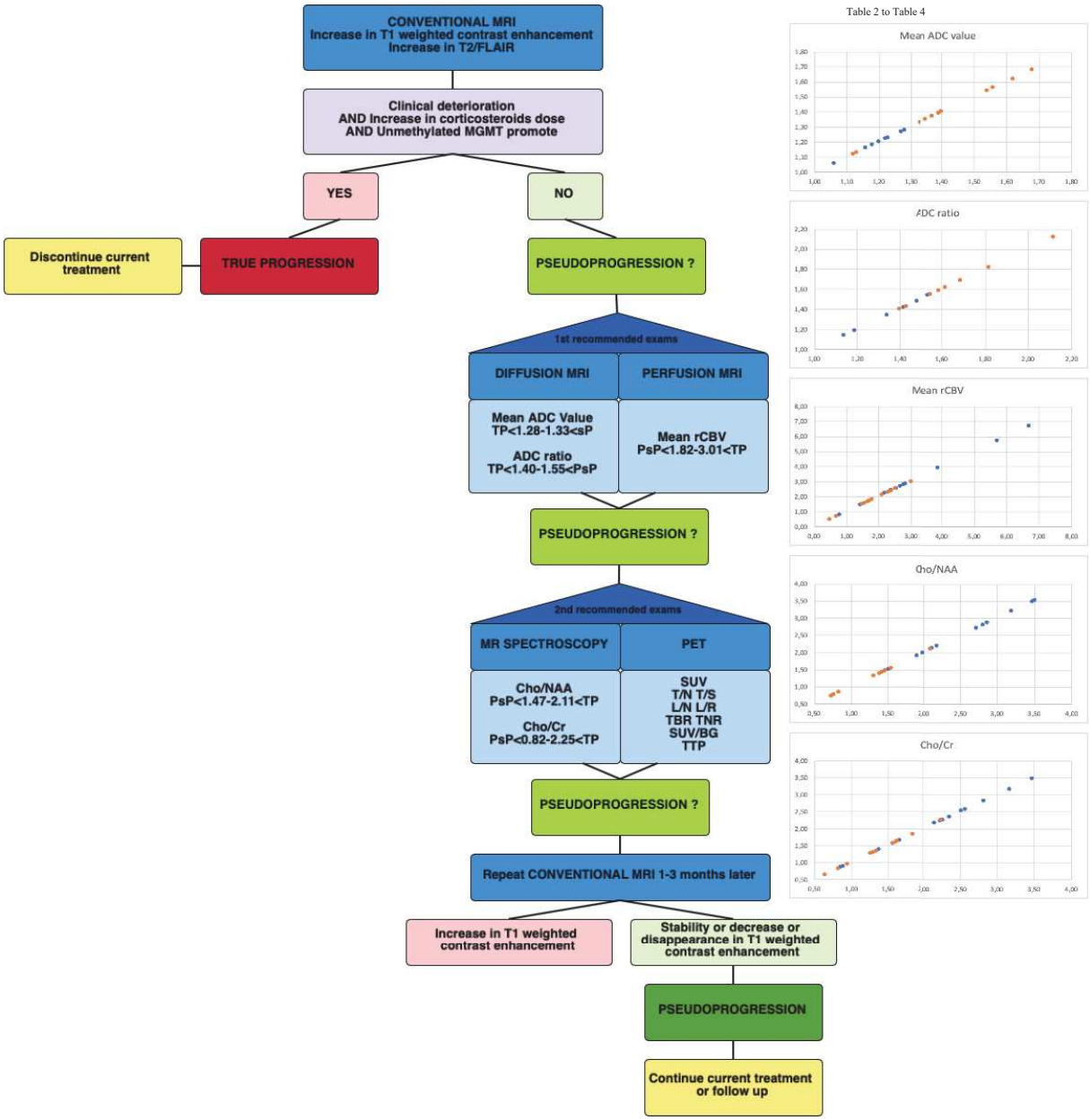

Measurements of volumetric tumor size in glioblastoma: 3D diameters volume measurements versus delineated volume measurements: a study on 114 MRIs

Résumé

Introduction L'évaluation de la réponse thérapeutique des glioblastomes (GBM) est essentiellement basée sur l'évolution de la taille tumorale, mesurée en deux dimensions, selon les critères RANO. Cette approche en deux dimensions reste cependant discutable. Plusieurs approches volumétriques ont été étudiées pour améliorer l'estimation de la taille tumorale. Cette étude a comparé deux méthodes d'estimation du volume de différents compartiments tumoraux chez des patients atteints d'un GBM.

Méthode Le volume de la prise de contraste (CE), de la nécrose (NEC), de la tumeur (CE + NEC + lit opératoire) (GTV) et de l'œdème (FLAIR) a été déterminé sur 114 IRM de 57 patients atteints d'un GBM par deux méthodes d'estimation : par le calcul du volume d'une ellipse (méthode de calcul) et par contourage manuel (méthode de mesure). Le coefficient de corrélation intra-classe (ICC) et le coefficient de corrélation de Pearson ont défini la corrélation entre les deux méthodes (représentée par le graphe de Bland-Altman). La concordance entre les deux méthodes pour classer les patients selon les critères RANO a été déterminée par le coefficient Kappa de Cohen. Une analyse de survie a été effectuée en utilisant le test du Log Rank et une régression de Cox.

Résultats Une forte corrélation a été retrouvée entre les deux méthodes d'estimation pour CE, NEC, GTV et FLAIR ($r \geq 0.90$, $p < 0.001$). L'ICC a démontré une bonne corrélation inter-observateur pour GTV et FLAIR, une corrélation modérée pour NEC and une faible corrélation pour CE. Le coefficient Kappa était de 0.66 (95%CI : 0.45-0.87, $p < 0.001$) suggérant une bonne concordance entre les deux méthodes pour classer les patients selon les critères RANO. La survie globale médiane ne différait pas entre les deux méthodes pour les patients présentant une pseudoprogression ou une vraie progression.

Conclusion Cette étude a montré que la méthode d'estimation du volume tumoral par le calcul, via la formule d'une ellipse, pouvait être utilisée en routine clinique pour le suivi des patients atteints d'un GBM à la place du contourage manuel.

Mots clés

Délinéation, Ellipse, Glioblastome, RANO, Volume, Survie globale

Measurements of volumetric tumor size in glioblastoma: 3D diameters volume measurements versus delineated volume measurements: a study on 114 MRIs

Clara Le Fèvre[1], MSc, Hélène Cebula[2], MD MSc, Alicia Thiery[3], MD MSc, Delphine Antoni[1.4], MD MSc, Roland Schott[5], MD, MSc, François Proust[2], MD PhD, Jean-Marc Constans [6], MD PhD, Georges Noël[1.4.*], MD PhD.

[1] Department of radiotherapy, comprehensive cancer center Paul Strauss, UNICANCER, 3 rue de la porte de l'Hôpital, 67065 Strasbourg Cedex, France.

[2] Departement of Neurosurgery, Hautepierre University Hospital, 1, avenue Molière, 67200 Strasbourg, France

[3] Department of public health, comprehensive cancer center Paul Strauss, UNICANCER, 3 rue de la porte de l'Hôpital, 67065 Strasbourg Cedex, France.

[4] Strasbourg University, CNRS, IPHC UMR 7178, Centre Paul Strauss, UNICANCER, 67000 Strasbourg, France.

[5] Departement of medical oncology, comprehensive cancer center Paul Strauss, UNICANCER, 3 rue de la porte de l'Hôpital, 67065 Strasbourg Cedex, France.

[6] Department of Radiology, Amiens-Picardie University Hospital, 1 rond-point du Professeur Christian Cabrol, 80054 Amiens Cedex 1, France.

*: Corresponding author: Pr Georges NOEL, same address, gnoel@strasbourg.unicancer.fr

Abstract

Introduction In glioblastoma (GBM), the response to treatment assessment is essentially based on the 2D tumor size evolution according to the RANO criteria but remains disputable. Various volumetric approaches were evaluated for a more accurate estimation of tumor size but were difficult to use. This study compared two volume measurement methods to determine the size of different GBM regions of interest.

Methods: The contrast-enhancing area (CE), the necrotic area (NEC), the gross target volume (GTV) volume and the volume of the edema area (FLAIR) on 114 MRIs from 57 GBM patients were determined with two methods: the ellipsoid formula (the calculated method) and by manual delineation (the measured method). The correlation between the two methods was analyzed with the intraclass correlation coefficient (ICC) and the Pearson correlation coefficients and was represented by Bland-Altman plots. The agreement of the patients' RANO response to treatment category of the two methods was assessed using a Cohen's weighted kappa statistic. A survival analysis was performed using a log-rank test, and a Cox regression analysis was performed to compare the two measurement methods to predict OS.

Results A high correlation was observed between the calculated and measured volume for the CE, the NEC, the GTV and the FLAIR ($r \geq 0.90$, $p < 0.001$ for each). The ICC showed a good inter-rater reliability for the GTV and the FLAIR, a moderate inter-rater reliability for the NEC and a poor inter-rater reliability for the CE. The kappa coefficient value was 0.66 (95% CI: 0.45-0.87, $p < 0.001$), revealing a high agreement between the two methods. The median OS of patients with progression and those without progression did not differ between the two methods.

Conclusion This study revealed that the calculated volume (obtained with the ellipsoid formula) could be used in clinical practice to estimate GBM volume size and to evaluate tumor size evolution instead of manual delineation GBM volume determination.

Key words

Delineation, Ellipse, Glioblastoma, RANO, Volume, Overall survival

Introduction

Glioblastoma (GBM) is the most common and aggressive brain tumor in adults (1,2). Although the prognosis of GBM patients improved with the introduction of adjuvant chemoradiotherapy protocol, it remains poor, with a median overall survival (OS) of 15-18 months (1,3–5).

The evaluation of the response to treatment is essentially based on tumor size evolution, which is often used as an endpoint of clinical studies (2,6–8). Traditionally, tumor size is estimated by a cross-sectional 2D method with the product of the largest perpendicular diameters on T1-weighted contrast-enhanced MRI rather than a 1D method (9). In the response to treatment assessment, the RANO criteria included the tumor size evolution in 2D obtained by calculating the sum of the product of the largest diameters on measurable lesions (at least 10 mm). The RANO criteria ranked a tumor as “progression disease” when the 2D size increased at least 25% or when the T2-FLAIR lesion increased but was without measurement guidelines (10).

This size measurement method was criticized because GBM is usually an irregular tumor with a cystic area, a surgical cavity, hemorrhage and no sharp demarcation that could compromise the size estimation and lead to error in therapeutic decisions (11–13). Consequently, the volumetric approach seemed to be more appropriate to obtain a better estimation of tumor size with more accuracy (11). Therefore, the modified RANO criteria and Ellingson *et al.* proposed a volumetric evaluation with at least a 40% increase in the total volume of the tumor to conclude “progression disease”, but no detail of the measurement method was described (14,15). Many possibilities are available to measure the volume of a tumor: manual delineation, semi-automated, automated or calculation methods (16). With improvements in imaging techniques, higher resolution and the availability in routine, complex tumors such as GBM are easily and precisely measured in size. However, according to the method of measurement, the time needed to reach results is highly variable (12,17).

This study compared two methods of volume measurement to estimate the size of different GBM regions of interest in adult patients.

Methods

This study was approved by the center's institutional review board.

Population

One hundred and fourteen MRIs from 57 patients were examined in this retrospective single-center study. All patients included had pathologically proven GBM and were treated by surgery and chemoradiotherapy (CRT) with temozolomide according to the EORTC/NCIC protocol (10). Patient ages ranged from 24 to 81 years with a median age of 62 years. Forty patients (70%) were male and 17 patients (30%) were female. All patients experienced a suspicion of progression after CRT. Fifty-seven pairs of MRIs were evaluated corresponding to 57 MRIs performed before CRT and 57 MRIs where a suspicion of progression was diagnosed. The examination was performed on a Siemens Magneton AERA XJ 1.5T MRI (Siemens®, München, Germany) and included T1-weighted images before administration of the contrast agent, T1-weighted contrast-enhanced 3D magnetization prepared rapid gradient echo (MPRAGE) sequence and a fluid-attenuation inversion recovery on T2-weighted images (T2-FLAIR). MRI showing a suspicion of progression was performed at a mean of 23.6 weeks after the completion of CRT.

Recorded data

For each MRI, the volume of different GBM regions of interest was evaluated (Figure 1). On the T1-weighted contrast-enhanced MPRAGE sequence, the contrast-enhancing area (CE), the necrotic area (NEC) and the gross target volume (GTV) which included the CE, the NEC and the surgical cavity, were obtained. On the T2-FLAIR sequence, the volume of the edema area (FLAIR) was measured. On the MRI performed before CRT, one, two or three CE areas were

seen in 48, five and four patients, respectively. On MRI showing a suspicion of progression, one, two, three or four CE areas were viewable in 37, 10, 7 and three patients, respectively.

Two methods of volume measurements were used to define the volume of different GBM regions of interest and compared.

The calculated volume (CV) for each compartment of the tumor was obtained with the ellipsoid volume formula: $\pi/6*D1*D2*D3$, where D1, D2 and D3 corresponded to the largest diameter of the compartment in three-dimensional plans:

The measured volume (MV) resulted from the manual delineation in all MRI slices, (slice per slice) of each compartment computed with FocalSim™ (Elekta®, Stockholm, Sweden) contouring software. After contouring, the volume was automatically calculated by the software for each compartment.

For patients with multifocal lesions, all lesions were measured with the two methods separately and summed for the comparison. For the CE, the analyzed volume corresponded to the sum of the measurable lesions (which had at least two diameters greater than 10 mm) according to the RANO criteria.

The measurements were performed in a blinded fashion by a radiation oncologist resident with 6 years of experience (CL) and approved in a blinded fashion by two reviewers with over 20-years of experience, a radiation oncologist (GN) and a neuroradiologist (JMC).

Evaluation of the response according to the RANO criteria

Only for the response to treatment classification was the MRI showing the best response to treatment examined in seven patients (data not shown).

Complete response (CR), partial response (PR), stable disease (SD) or progressive disease (PD), defined according to the RANO (10) and the modified RANO criteria (15), were applied only on the CE comparing the MRI performed before CRT and the MRI showing a suspicion of progression for 50 patients and the MRI showing the best response after treatment and the MRI

showing a suspicion of progression for seven patients (9–11,14,18,19). For each patient, the classification based on the CV and the classification based on the MV were compared. CR, PR, SD and PD were defined according to Ellingson *et al.* (14).

Statistical analysis

The comparison was performed in volume (cm^3) and percent variations between the two methods of measurement. The correlation between the two volume measurement methods for each compartment was analyzed with Pearson correlation coefficients and 95% confidence intervals (95%CIs). For each type of compartment, the intraclass correlation coefficient (ICC) estimated the interrater reliability of measurements as follows: poor reliability when the ICC was below 0.50, moderate reliability when the ICC was between 0.50 and 0.75, good reliability when the ICC was between 0.75 and 0.90 and excellent reliability when the ICC was above 0.90. The comparison of the two measurement methods was represented by a Bland-Altman plot for each compartment. The agreement of the patient's response to treatment category of the two volume measurement methods was assessed using Cohen's weighted kappa statistic with the 95%CI with the kappa value ranging from -1 to +1. A kappa value between 0.01 and 0.20 indicated no or slight agreement, between 0.21 and 0.40 indicated fair agreement, between 0.41 and 0.60 indicated moderate agreement, between 0.61 and 0.80 indicated substantial agreement and between 0.81 and 1.00 indicated almost perfect agreement.

A survival analysis was performed to evaluate the impact of the volume measurement methods on OS according to the response to treatment expressed by the radiological RANO classification (CE volume evolution). Patients were classified as PD or non-PD (CR, PR or SD). OS was determined from the date of pathological diagnosis to death or the last follow-up. OS in PD and non-PD patients was estimated by a log-rank test, and Kaplan-Meier survival curves were drawn for each group according to the measurement methods. A Cox regression analysis was

performed to compare the two measurement methods to predict OS, with the determination of hazard ratios (HRs) and their 95% confidence intervals (95%CIs).

Statistical calculations were performed with R version 3.6.1 software (www.r-project.org).

Results

Calculated volume (CV) versus measured volume (MV)

The analysis of the calculated and measured volume is summarized in Table 1.

The mean CV of the CE, the NEC, the GTV and the FLAIR was 41.6 cm^3, 17.5 cm^3, 58.7 cm^3 and 179.2 cm^3, respectively. The mean MV of the CE, the NEC, the GTV and the FLAIR was 15.5 cm^3, 7.3 cm^3, 47.6 cm^3 and 132.3 cm^3, respectively. The mean difference between CV and MV for the CE, the NEC, the GTV and the FLAIR was 26.1 cm^3 (-0.2-117.3), 10.1 cm^3 (-0.1-95.9), 11.1 cm^3 (-28.9-67.0) and 46.9 cm^3 (-53.3-222.5), respectively, corresponding to a mean percentage difference of 174.9%, 150.3%, 26.1% and 38.2%, respectively. CV was significantly larger than MV for each tumor compartment (CE $p<0.001$, NEC $p=0.01$, GTV $p=0.05$ and FLAIR $p=0.01$).

A high correlation was observed between the CV and MV for the CE ($r=0.91$, 95% CI: 0.87-0.94, $p<0.001$), the NEC ($r=0.94$, 95% CI: 0.91-0.96, $p<0.001$), the GTV ($r=0.90$, 95% CI: 0.85-0.93, $p<0.001$) and the FLAIR ($r=0.95$, 95% CI: 0.93-0.97, $p<0.001$) (Figures 2 and 3).

For the CE, the NEC, the GTV, and the FLAIR, the ICC was 0.33 (95% CI: 0.16-0.49), 0.56 (95% CI: 0.42-0.67), 0.82 (95% CI: 0.75-0.87) and 0.84 (95% CI: 0.78-0.89), respectively, with a good inter-rater reliability for the GTV and the FLAIR, a moderate inter-rater reliability for the NEC and a poor inter-rater reliability for the CE.

Response assessment agreement according to the RANO criteria

For the CE estimated with CV method, one, three, 23 and 30 patients were classified as CR, PR, SD and PD, respectively. For the CE estimated with the MV method, one, 0, 19 and 37 patients were classified as CR, PR, SD and PD, respectively (Table 2). A total of 41 (72%)

patients were classified in the same category with the CV method and the MV method (Table 3). The kappa coefficient value between the CV and MV was 0.66 (95% CI:0.45-0.87, p<0.001), revealing substantial agreement between the two volume measurement methods to classify patients according to the response to treatment into four groups.

Survival analysis

With the CV method, 30 patients were classified as PD, and 27 patients were classified as non-PD; with the MV method, 37 patients were classified as PD, and 20 patients were classified as non-PD (p<0.001). With the CV method, 20 patients died in the PD group, and 20 patients died in the non-PD group. With the MV method, 27 patients died in the PD group, and 13 patients died in the non-PD group. According to the CV or MV method, there was no significant difference in the median OS for PD patients (20.3 months and 19.5 months, respectively; HR=1.096, 95%CI 0.615-1.954, p=0.756), and for non-PD patients, with a median OS of 20.4 months and 22.0 months, respectively (HR=0.890, 95%CI: 0.442-1.790, p=0.743) (Figure 4).

Discussion

To our knowledge, this study was the first to compare GBM evolution size on MRI with two methods of volume measurements. The investigations revealed that the CV, with an ellipsoid volume simple formula based on tumor diameters, and the MV obtained by manual contouring, had a high correlation for all tumor compartments, although inter-method variability was shown mainly for the NEC and the CE. The agreement between the two volume measurement methods to classify patients based on CE changes according to the response to treatment was high, with no difference in OS for patients with or without PD, suggesting that the CV method could be used as an alternative method to evaluate tumor volume.

For the MV method, we used manual delineation and not a semiautomated or an automated segmentation method. Although this method was time consuming, tumor segmentation was a complex task that needed much experience and competency for the appreciation of mixed areas,

cystic and surgical cavities, necrosis, shape, and border enhancement that were not always well defined and reproducible from one software to another with automated methods (20).

The GBM response to treatment was routinely evaluated by conventional MRI, with the change in tumor size comparing the pretreatment (baseline) MRI or the MRI showing the best response to the last MRI. For a standardized response evaluation, the RANO criteria, including radiological, clinical criteria and the use of corticosteroids, were used to classify patients into four groups according to the response (CR, PR, SD and PD) (10). Radiological criteria were based on contrast-enhancing lesion and FLAIR and excluded cystic and surgical cavities. However, some limitations persisted. The assessment of contrast-enhancing lesions was based on the change in the sum of the product of the largest diameters of each contrast-enhancing lesion (cross-sectional area in 2D), not on a volumetric approach. The FLAIR lesion assessment was not defined with a percentage of change and was neuroradiologist appreciation-dependent (21). The baseline MRI was the postsurgical MRI, which could present some artifacts such as postsurgical bleeding, vascular permeability modifications or image modifications due to high steroids dose given immediately postsurgery. After chemoradiotherapy, the MRI could be modified with the use of high steroid dose too. Moreover, imaging modifications could appear between the postoperative MRI and the MRI used for the radiotherapy delineation performed sometimes several weeks after surgery (22). In this study, pre-CRT MRI (dosimetric MRI) was chosen as the baseline. It was the most representative of the lesion before the CRT.

Ellingson *et al*. proposed modified RANO criteria to evaluate the radiological response with a volumetric approach (14). They removed the FLAIR evaluation from the criteria and considered only contrast-enhancing lesions. Moreover, the authors proposed the postradiation MRI as baseline instead of postsurgical MRI. A FLAIR analysis was not carried out, and radiological criteria for the patient's categorization of response were based only on contrast-enhancing lesion evolution in size. In the current study, the classification of patients was exclusively based

on CE volume changes, not on FLAIR changes. As described in the literature, FLAIR tumor progression evaluation was too complex, subjective and controversial to be integrated into patients' classification criteria. For the CV, an ellipsoid volume formula was chosen rather than a spheroid and rectangular model to estimate the tumor volume for more accuracy (23).

The 2D measurement corresponding to the sum of the product of the largest diameters was very simple and fast to use and was adapted routine clinical practice without the need for specific software (17). However, the intra- and inter-observer variabilities were high, and measurements could lack of objectivity (24,25). The measurement was based only on a single axial MRI slice, which showed the largest diameters of the tumor compared to the volume approach based on the analysis of the overall MRI slices. Moreover, the 2D measurement indirectly included the cystic and surgical cavity, although the RANO criteria stated their exclusion (28). With the recent development of novel therapies causing pseudoresponse and pseudoprogression, assessment of the treatment response needed more accuracy and reliability and less inter-observer variability (29). For this reason, a volumetric approach sparked interest, particularly for GBM (26). Indeed, because GBM was a heterogeneous, irregular tumor in shape and often containes necrotic and cystic areas, measurement based only on one axial slice might be intrinsically less precise (11–13). With a volumetric measurement, all axial slices were taken into account respecting GBM demarcation and allowing the exclusion of cystic and necrotic areas (12). However, the volumetric measurement was challenging because of the time needed and because of borders definitions needing experienced physicians (12,17). The volume precision depended on the method of measurement (manual, semiautomated, automated) and to the MRI resolution (11,17,26). The initial volume evaluation seemed to have a high importance in evaluating GBM (30). Furthermore, Schmitt *et al.* highlighted the importance of the reproducibility of scanning conditions to evaluate changes in tumor size and concluded slice thicknesses larger than 3mm induced maximal errors, especially in cases of small lesions and

axial plane rotation. The volumetric method was less affected by scanning conditions than the 2D method (31).

Some GBM measurement methods were compared in the literature, with discordant results. The 2D method remained easier than volumetric methods. However, a volumetric analysis could provide a better estimation of the tumor response, with more reproducibility and less inter-rater variability than 1D and 2D measurements (19,32–34). Some authors demonstrated a high correlation between 2D measurement methods and 3D or semiautomated volume measurement methods (11,32,35,36). However, the 2D assessment remained disputable: Dempsey *et al.* showed that, although the 2D and 3D measurements were well correlated, the 2D measurements were larger than the 3D measurements, and the 3D measurements better predicted survival (28). Therefore, the 2D measurement method was not analyzed in this study with a focus on a volumetric analysis.

Some authors questioned the volume measurement comparison. For GBM volume determination with the use of a formula, the ellipsoid model appeared more accurate than spheroid and rectangular models but remained insufficient compared to computer-assisted methods, with a higher intra- and inter-rater variability and less reproducibility and sensitivity to analyze early progression and small lesion evolution (23,25). Concerning the manual segmentation method, some authors concluded its equivalence with automated and semiautomated segmentation methods, (18,37,38) but most of these conclusions were debatable. According to Shah *et al.,* the correlation between the 3D measurement method and the volumetric method was low (r=0.50) (36). The estimation of volume changes with the manual method seemed higher than that with software methods (16). Huber *et al.* studied segmentation methods for detecting progression in terms of absolute changes in volume (delta) and regional subtractions (regional volume changes) and showed that only the delta CE could predict progression (p=0.005). Manual segmentation was amenable to bias, whereas

segmentation assistance improved homogeneity and was less time consuming. However, automated segmentation had doubtful precision, and an expert MRI evaluation was more accurate (24). Manual segmentation and volume formulas were compared with computer-assisted methods, but no study comparing manual segmentation and the ellipsoid formula was found in the literature.

Menze *et al.* showed high disagreement between different raters in manual segmentation, with a Dice score ranging from 74% to 85%. Indeed, the use of semiautomated and automated segmentation software for tumor contouring was gradually more often used in clinical routine to improve clinical decisions and performed volumetric assessment faster, more reliable and more reproducible than manual contouring (16–18,39–41). However, the lack of standardization and availability remained an issue (42). Semiautomated segmentation software tended to be more accurate than automated segmentation software, but with less objectivity (43). Although semiautomated software had proved their high agreements (42), Menze *et al.* highlighted the variability between software to segment different tumor subregions, with the need to fuse software for an optimal segmentation (20). Moreover, semiautomated segmentation software offered a higher reliability for some tumor subregions (44) as in the study by Huber *et al.*, which showed a higher intra-rater reliability for FLAIR volume than for CE volume with lower precision errors (29).

The determination of a reliable tumor size and the percent of changes in tumor size appeared highly relevant in clinical practice. Quantitative changes in volume could predict OS and PFS (45). Buemi *et al.* demonstrated that the CE volume percentage change was able to predict PFS ($p=0.01$), with a cutoff of 55% changes (46). Huang *et al.* concluded that the percentage of CE volume changes defined with computer assistance was correlated with OS and PFS using a 52% percentage change cutoff and a 7.8 cm^3 threshold for the median residual enhancing (47). In addition to the conventional MRI analysis, tumor size determination using advanced MRI

appeared promising (48). Gzell *et al.* revealed that a decrease in survival was associated with a 5% or greater increase in the CE and surgical cavity at three and five months after CRT (49). In this study, an increase of ≥5%, ≥10%, ≥25%, ≥40% and ≥55% of the CE was not associated with survival with the CV method (p=0.780, p=0.578, p=0.794, p=0.709 and p=0.837 respectively) or the MV method (p=0.987, p=0.987, p=0.798, p=0.441 and p=0338 respectively).

To further improve the assessment of GBM, machine learning models were developed (50). In fact, an MRI containing over a million voxels that constituted a complex "big data" management and deep learning methods for segmentation, survival prediction or brain tumor gradation was to develop (51,52). Therefore, quantitative features as textural and geometric data could be explored, combined with genomics, proteomics and clinical data and compiled into diagnostic, prognostic, and therapeutic models (53).

Conclusion

The GBM evaluation should be not ambiguous or complex for clinical management and clinical trials, and a volume approach seemed more realistic. The current study showed a high concordance between manual segmentation and the ellipsoid formula to define the GTV, the CE, the FLAIR and the NEC volumes with a good agreement to classify the patient response to treatment according to the four RANO groups, allowing the use of the ellipsoid formula in clinical practice. However, the inter-rater variability for CE volume definition was relatively high, so the treatment response categorization of patients should be performed with caution using this formula. For that semi-automated method should be evaluated.

Bibliography

1. Ostrom QT, Gittleman H, Stetson L, Virk SM, Barnholtz-Sloan JS. Epidemiology of gliomas. Cancer Treat Res. 2015;163:1–14.
2. Ahmed R, Oborski MJ, Hwang M, Lieberman FS, Mountz JM. Malignant gliomas: current perspectives in diagnosis, treatment, and early response assessment using advanced quantitative imaging methods. Cancer Manag Res. 2014;6:149–70.
3. Ostrom QT, Gittleman H, Farah P, Ondracek A, Chen Y, Wolinsky Y, et al. CBTRUS statistical report: Primary brain and central nervous system tumors diagnosed in the United States in 2006-2010. Neuro-Oncol. 2013 Nov;15 Suppl 2:ii1-56.
4. Seystahl K, Wick W, Weller M. Therapeutic options in recurrent glioblastoma--An update. Crit Rev Oncol Hematol. 2016 Mar;99:389–408.
5. Stupp R, Mason WP, van den Bent MJ, Weller M, Fisher B, Taphoorn MJB, et al. Radiotherapy plus concomitant and adjuvant temozolomide for glioblastoma. N Engl J Med. 2005 Mar 10;352(10):987–96.
6. Ellingson BM, Wen PY, Cloughesy TF. Evidence and context of use for contrast enhancement as a surrogate of disease burden and treatment response in malignant glioma. Neuro-Oncol. 2018 27;20(4):457–71.
7. Jiang X, Xu J, Gore JC. Quantitative temporal diffusion spectroscopy as an early imaging biomarker of radiation therapeutic response in gliomas: A preclinical proof of concept. Adv Radiat Oncol. 2019 Jun;4(2):367–76.
8. Mazzocco P, Barthélémy C, Kaloshi G, Lavielle M, Ricard D, Idbaih A, et al. Prediction of Response to Temozolomide in Low-Grade Glioma Patients Based on Tumor Size Dynamics and Genetic Characteristics. CPT Pharmacomet Syst Pharmacol. 2015 Dec;4(12):728–37.
9. Galanis E, Buckner JC, Maurer MJ, Sykora R, Castillo R, Ballman KV, et al. Validation of neuroradiologic response assessment in gliomas: measurement by RECIST, two-dimensional, computer-assisted tumor area, and computer-assisted tumor volume methods. Neuro-Oncol. 2006 Apr;8(2):156–65.
10. Wen PY, Macdonald DR, Reardon DA, Cloughesy TF, Sorensen AG, Galanis E, et al. Updated response assessment criteria for high-grade gliomas: response assessment in neuro-oncology working group. J Clin Oncol Off J Am Soc Clin Oncol. 2010 Apr 10;28(11):1963–72.
11. Wang M-Y, Cheng J-L, Han Y-H, Li Y-L, Dai J-P, Shi D-P. Measurement of tumor size in adult glioblastoma: classical cross-sectional criteria on 2D MRI or volumetric criteria on high resolution 3D MRI? Eur J Radiol. 2012 Sep;81(9):2370–4.
12. Henson JW, Ulmer S, Harris GJ. Brain tumor imaging in clinical trials. AJNR Am J Neuroradiol. 2008 Mar;29(3):419–24.
13. Henker C, Hiepel MC, Kriesen T, Scherer M, Glass Ä, Herold-Mende C, et al. Volumetric assessment of glioblastoma and its predictive value for survival. Acta Neurochir (Wien). 2019 Jun 28;
14. Ellingson BM, Wen PY, Cloughesy TF. Modified Criteria for Radiographic Response Assessment in Glioblastoma Clinical Trials. Neurother J Am Soc Exp Neurother. 2017;14(2):307–20.
15. Wen PY, Chang SM, Van den Bent MJ, Vogelbaum MA, Macdonald DR, Lee EQ. Response Assessment in Neuro-Oncology Clinical Trials. J Clin Oncol Off J Am Soc Clin Oncol. 2017 Jul 20;35(21):2439–49.
16. Ertl-Wagner BB, Blume JD, Peck D, Udupa JK, Herman B, Levering A, et al. Reliability of tumor volume estimation from MR images in patients with malignant glioma. Results from the American College of Radiology Imaging Network (ACRIN) 6662 Trial. Eur Radiol. 2009 Mar;19(3):599–609.

17. Kickingereder P, Isensee F, Tursunova I, Petersen J, Neuberger U, Bonekamp D, et al. Automated quantitative tumour response assessment of MRI in neuro-oncology with artificial neural networks: a multicentre, retrospective study. Lancet Oncol. 2019 May;20(5):728–40.
18. Chow DS, Qi J, Guo X, Miloushev VZ, Iwamoto FM, Bruce JN, et al. Semiautomated volumetric measurement on postcontrast MR imaging for analysis of recurrent and residual disease in glioblastoma multiforme. AJNR Am J Neuroradiol. 2014 Mar;35(3):498–503.
19. Pichler J, Pachinger C, Pelz M, Kleiser R. MRI assessment of relapsed glioblastoma during treatment with bevacizumab: volumetric measurement of enhanced and FLAIR lesions for evaluation of response and progression--a pilot study. Eur J Radiol. 2013 May;82(5):e240-245.
20. Menze BH, Jakab A, Bauer S, Kalpathy-Cramer J, Farahani K, Kirby J, et al. The Multimodal Brain Tumor Image Segmentation Benchmark (BRATS). IEEE Trans Med Imaging. 2015 Oct;34(10):1993–2024.
21. Pope WB, Hessel C. Response assessment in neuro-oncology criteria: implementation challenges in multicenter neuro-oncology trials. AJNR Am J Neuroradiol. 2011 May;32(5):794–7.
22. De Barros A, Attal J, Roques M, Nicolau J, Sol J-C, Cohen-Jonathan-Moyal E, et al. Impact on survival of early tumor growth between surgery and radiotherapy in patients with de novo glioblastoma. J Neurooncol. 2019 May;142(3):489–97.
23. Iliadis G, Selviaridis P, Kalogera-Fountzila A, Fragkoulidi A, Baltas D, Tselis N, et al. The importance of tumor volume in the prognosis of patients with glioblastoma: comparison of computerized volumetry and geometric models. Strahlenther Onkol Organ Dtsch Rontgengesellschaft Al. 2009 Nov;185(11):743–50.
24. Huber T, Alber G, Bette S, Kaesmacher J, Boeckh-Behrens T, Gempt J, et al. Progressive disease in glioblastoma: Benefits and limitations of semi-automated volumetry. PloS One. 2017;12(2):e0173112.
25. Sorensen AG, Patel S, Harmath C, Bridges S, Synnott J, Sievers A, et al. Comparison of diameter and perimeter methods for tumor volume calculation. J Clin Oncol Off J Am Soc Clin Oncol. 2001 Jan 15;19(2):551–7.
26. Sorensen AG, Batchelor TT, Wen PY, Zhang W-T, Jain RK. Response criteria for glioma. Nat Clin Pract Oncol. 2008 Nov;5(11):634–44.
27. van den Bent MJ, Vogelbaum MA, Wen PY, Macdonald DR, Chang SM. End point assessment in gliomas: novel treatments limit usefulness of classical Macdonald's Criteria. J Clin Oncol Off J Am Soc Clin Oncol. 2009 Jun 20;27(18):2905–8.
28. Dempsey MF, Condon BR, Hadley DM. Measurement of tumor "size" in recurrent malignant glioma: 1D, 2D, or 3D? AJNR Am J Neuroradiol. 2005 Apr;26(4):770–6.
29. Huber T, Alber G, Bette S, Boeckh-Behrens T, Gempt J, Ringel F, et al. Reliability of Semi-Automated Segmentations in Glioblastoma. Clin Neuroradiol. 2017 Jun;27(2):153–61.
30. Henker C, Kriesen T, Glass Ä, Schneider B, Piek J. Volumetric quantification of glioblastoma: experiences with different measurement techniques and impact on survival. J Neurooncol. 2017 Nov;135(2):391–402.
31. Schmitt P, Mandonnet E, Perdreau A, Angelini ED. Effects of slice thickness and head rotation when measuring glioma sizes on MRI: in support of volume segmentation versus two largest diameters methods. J Neurooncol. 2013 Apr;112(2):165–72.
32. Wang M-Y, Cheng J-L, Han Y-H, Li Y-L, Dou S-W, Yan F-S, et al. Comparison of volumetric methods for tumor measurements on two and three dimensional MRI in adult glioblastoma. Neuroradiology. 2011 Aug;53(8):565–9.
33. Kanaly CW, Ding D, Mehta AI, Waller AF, Crocker I, Desjardins A, et al. A novel method for volumetric MRI response assessment of enhancing brain tumors. PloS One. 2011 Jan 26;6(1):e16031.

34. Kanaly CW, Mehta AI, Ding D, Hoang JK, Kranz PG, Herndon JE, et al. A novel, reproducible, and objective method for volumetric magnetic resonance imaging assessment of enhancing glioblastoma. J Neurosurg. 2014 Sep;121(3):536–42.
35. Gahrmann R, van den Bent M, van der Holt B, Vernhout RM, Taal W, Vos M, et al. Comparison of 2D (RANO) and volumetric methods for assessment of recurrent glioblastoma treated with bevacizumab-a report from the BELOB trial. Neuro-Oncol. 2017 01;19(6):853–61.
36. Shah GD, Kesari S, Xu R, Batchelor TT, O'Neill AM, Hochberg FH, et al. Comparison of linear and volumetric criteria in assessing tumor response in adult high-grade gliomas. Neuro-Oncol. 2006 Jan;8(1):38–46.
37. Meier R, Knecht U, Loosli T, Bauer S, Slotboom J, Wiest R, et al. Clinical Evaluation of a Fully-automatic Segmentation Method for Longitudinal Brain Tumor Volumetry. Sci Rep. 2016 Mar 22;6:23376.
38. Porz N, Bauer S, Pica A, Schucht P, Beck J, Verma RK, et al. Multi-modal glioblastoma segmentation: man versus machine. PloS One. 2014;9(5):e96873.
39. Yushkevich PA, Piven J, Hazlett HC, Smith RG, Ho S, Gee JC, et al. User-guided 3D active contour segmentation of anatomical structures: significantly improved efficiency and reliability. NeuroImage. 2006 Jul 1;31(3):1116–28.
40. Zhuge Y, Krauze AV, Ning H, Cheng JY, Arora BC, Camphausen K, et al. Brain tumor segmentation using holistically nested neural networks in MRI images. Med Phys. 2017 Oct;44(10):5234–43.
41. Egger J, Kapur T, Fedorov A, Pieper S, Miller JV, Veeraraghavan H, et al. GBM volumetry using the 3D Slicer medical image computing platform. Sci Rep. 2013;3:1364.
42. Fyllingen EH, Stensjøen AL, Berntsen EM, Solheim O, Reinertsen I. Glioblastoma Segmentation: Comparison of Three Different Software Packages. PloS One. 2016;11(10):e0164891.
43. Heckel F, Moltz JH, Tietjen C, Hahn HK. Sketch-Based Editing Tools for Tumour Segmentation in 3D Medical Images. Comput Graph Forum. 2013;32(8):144–57.
44. Tixier F, Um H, Young RJ, Veeraraghavan H. Reliability of tumor segmentation in glioblastoma: Impact on the robustness of MRI-radiomic features. Med Phys. 2019 May 27;
45. Ellingson BM, Cloughesy TF, Lai A, Nghiemphu PL, Mischel PS, Pope WB. Quantitative volumetric analysis of conventional MRI response in recurrent glioblastoma treated with bevacizumab. Neuro-Oncol. 2011 Apr;13(4):401–9.
46. Buemi F, Guzzardi G, Del Sette B, Sponghini AP, Matheoud R, Soligo E, et al. Apparent diffusion coefficient and tumor volume measurements help stratify progression-free survival of bevacizumab-treated patients with recurrent glioblastoma multiforme. Neuroradiol J. 2019 Aug;32(4):241–9.
47. Huang RY, Rahman R, Hamdan A, Kane C, Chen C, Norden AD, et al. Recurrent glioblastoma: volumetric assessment and stratification of patient survival with early posttreatment magnetic resonance imaging in patients treated with bevacizumab. Cancer. 2013 Oct 1;119(19):3479–88.
48. Hwang EJ, Cha Y, Lee AL, Yun TJ, Kim TM, Park C-K, et al. Early response evaluation for recurrent high grade gliomas treated with bevacizumab: a volumetric analysis using diffusion-weighted imaging. J Neurooncol. 2013 May;112(3):427–35.
49. Gzell CE, Wheeler HR, McCloud P, Kastelan M, Back M. Small increases in enhancement on MRI may predict survival post radiotherapy in patients with glioblastoma. J Neurooncol. 2016;128(1):67–74.
50. Hu LS, Yoon H, Eschbacher JM, Baxter LC, Dueck AC, Nespodzany A, et al. Accurate Patient-Specific Machine Learning Models of Glioblastoma Invasion Using Transfer Learning. AJNR Am J Neuroradiol. 2019 Mar;40(3):418–25.

51. Shaver MM, Kohanteb PA, Chiou C, Bardis MD, Chantaduly C, Bota D, et al. Optimizing Neuro-Oncology Imaging: A Review of Deep Learning Approaches for Glioma Imaging. Cancers. 2019 Jun;11(6):829.
52. Juan-Albarracín J, Fuster-Garcia E, García-Ferrando GA, García-Gómez JM. ONCOhabitats: A system for glioblastoma heterogeneity assessment through MRI. Int J Med Inf. 2019 Aug;128:53–61.
53. Chaddad A, Kucharczyk MJ, Daniel P, Sabri S, Jean-Claude BJ, Niazi T, et al. Radiomics in Glioblastoma: Current Status and Challenges Facing Clinical Implementation. Front Oncol. 2019;9:374.

Table 1: Calculated volume (CV) and measured volume (MV) and difference between the two measurement methods for the CE, the NEC, the GTV, and the FLAIR compartments for the 114 MRIs: the 57 MRIs before CRT and the 57 MRIs showing a suspicion of progression

	Calculated volume (CV) (diameters 3D) (cm^3)	Measured volume (MV) (delineation) (cm^3)	Difference CV-MV (cm^3)	((CV-MV)/CV)*100 (%)		CV (diameters 3D) (cm^3)	MV (delineation) (cm^3)	Difference CV-MV (cm^3)	((CV-MV)/CV)*100 (%)
CE total					**CE before CRT**				
Mean	**41.6**	**15.5**	**26.1**	**174.9**	**Mean**	**37.1**	**12.6**	**24.9**	**196.6**
Median	**27.9**	**11.2**	**17.9**	**162.1**	**Median**	**26.7**	**9.2**	**18.7**	**189.3**
Range	**0.6-167.6**	**0.3-66.0**	**-0.2-117.3**	**-26.1-398.5**	**Range**	**2.4-167.6**	**1.2-66.0**	**0.8-117.3**	**6.9-398.5**
					CE at suspicion of progression				
					Mean	**46.1**	**18.3**	**27.8**	**153.2**
					Median	**31.0**	**11.5**	**17.5**	**145.3**
					Range	**0.6-159.6**	**0.3-60.7**	**-0.2-115.3**	**-26.10392.1**
NEC total					**NEC before CRT**				
Mean	**17.5**	**7.3**	**10.1**	**150.3**	**Mean**	**15.4**	**5.9**	**9.6**	**165.4**
Median	**6.3**	**2.4**	**3.0**	**111.3**	**Median**	**3.6**	**1.5**	**1.7**	**125.6**
Range	**0.0-128.1**	**0.0-42.4**	**-0.1-95.9**	**-10.7-789.3**	**Range**	**0.0-128.1**	**0.0-39.8**	**-0.1-95.9**	**-10.7-789.3**
					NEC at suspicion of progression				
					Mean	**19.5**	**8.8**	**10.7**	**139.9**
					Median	**9.9**	**3.6**	**5.3**	**100.8**
					Range	**0.0-106.6**	**0.0-42.4**	**0.0-70.3**	**20.8-615.8**
GTV total					**GTV before CRT**				
Mean	**58.7**	**47.6**	**11.1**	**26.1**	**Mean**	**54.7**	**42.8**	**11.9**	**30.5**
Median	**52.7**	**39.8**	**8.8**	**22.1**	**Median**	**47.0**	**36.4**	**9.0**	**26.4**
Range	**1.2-145.8**	**1.0-128.2**	**-28.9-67.0**	**-68.8-207.2**	**Range**	**5.1-145.0**	**4.1-107.9**	**-12.7-53.6**	**-24.1-117.6**
					GTV at suspicion of progression				
					Mean	**62.2**	**52.4**	**10.3**	**21.7**
					Median	**55.6**	**53.2**	**6.00**	**15.0**
					Range	**1.2-145.8**	**1.0-128.2**	**-28.9-67.0**	**-68.8-207.2**
FLAIR total					**FLAIR before CRT**				
Mean	**179.2**	**132.3**	**46.9**	**38.2**	**Mean**	**129.7**	**95.9**	**33.8**	**38.5**
Median	**142.0**	**110.8**	**32.4**	**34.2**	**Median**	**94.5**	**73.4**	**23.9**	**32.1**
Range	**13.7-722.9**	**13.6-520.2**	**-53.3-222.5**	**-34.5-172.2**	**Range**	**13.7-505.3**	**13.6-339.3**	**-50.4-189.1**	**-34.5-172.1**
					FLAIR at suspicion of progression				
					Mean	**228.7**	**168.8**	**59.9**	**37.9**
					Median	**200.1**	**146.3**	**50.6**	**39.0**
					Range	**30.7-722.9**	**21.3-520.2**	**-53.3-222.5**	**-29.5-113.3**

CE: Contrast-Enhancement; **GTV**: Gross Target Volume **; NEC**: Necrosis Area

Table 2: RANO response assessment category according to volume measurement methods based on the contrast-enhancing tumor size

Measurement methods	RANO response category (n)			
	CR	PR	SD	PD
CE Calculated volume (diameters 3D)	1	3	23	30
CE Measured volume (delineation)	1	0	19	37

CE: Contrast-Enhancement ; **CR**: Complete Response ; **PD**: Progressive Disease; **PR**: Partial Response ; **SD**: Stable Disease

Table 3: Agreement in the RANO response assessment category between the two methods

RANO response assessment category		CE Measured volume (manual delineation)				
		CR	PR	SD	PD	Total
CE Calculated volume (ellipsoid formula)	CR	1	0	0	0	1
	PR	0	0	3	0	3
	SD	0	0	13	10	23
	PD	0	0	3	27	30
	Total	1	0	19	37	57

CE: Contrast-Enhancement ; **CR**: Complete Response ; **PD**: Progressive Disease; **PR**: Partial Response ; **SD**: Stable Disease

Figure 1: Manual segmentation of the GTV, the CE, the NEC and the FLAIR on T1-weighted contrast-enhanced MRI and T2-Flair MRI sequences

A **B**

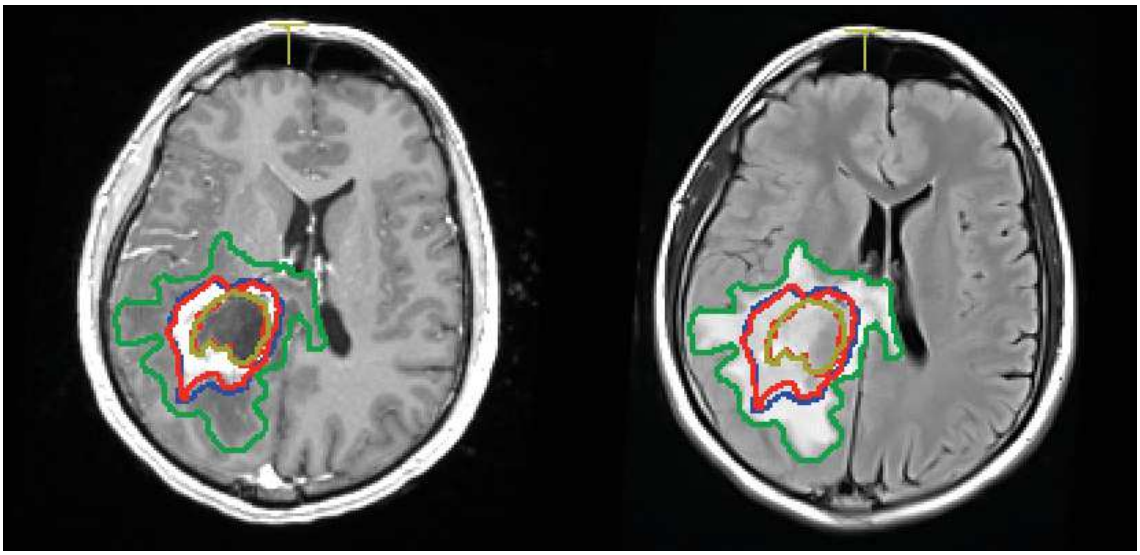

GTV (gross target volume) in blue, **CE** (contrast-enhanced region) in red, **NEC** (necrosis areas) in yellow, **FLAIR** in green in axial slice of **A**: T1-weighetd contrast-enhanced MRI sequence, **B**: T2-Flair MRI sequence

Figure 2: Plots of the calculated volume (CV) versus the measured volume (MV) (cm^3) for the 114 MRIs for the GTV, the FLAIR, the CE and the NEC

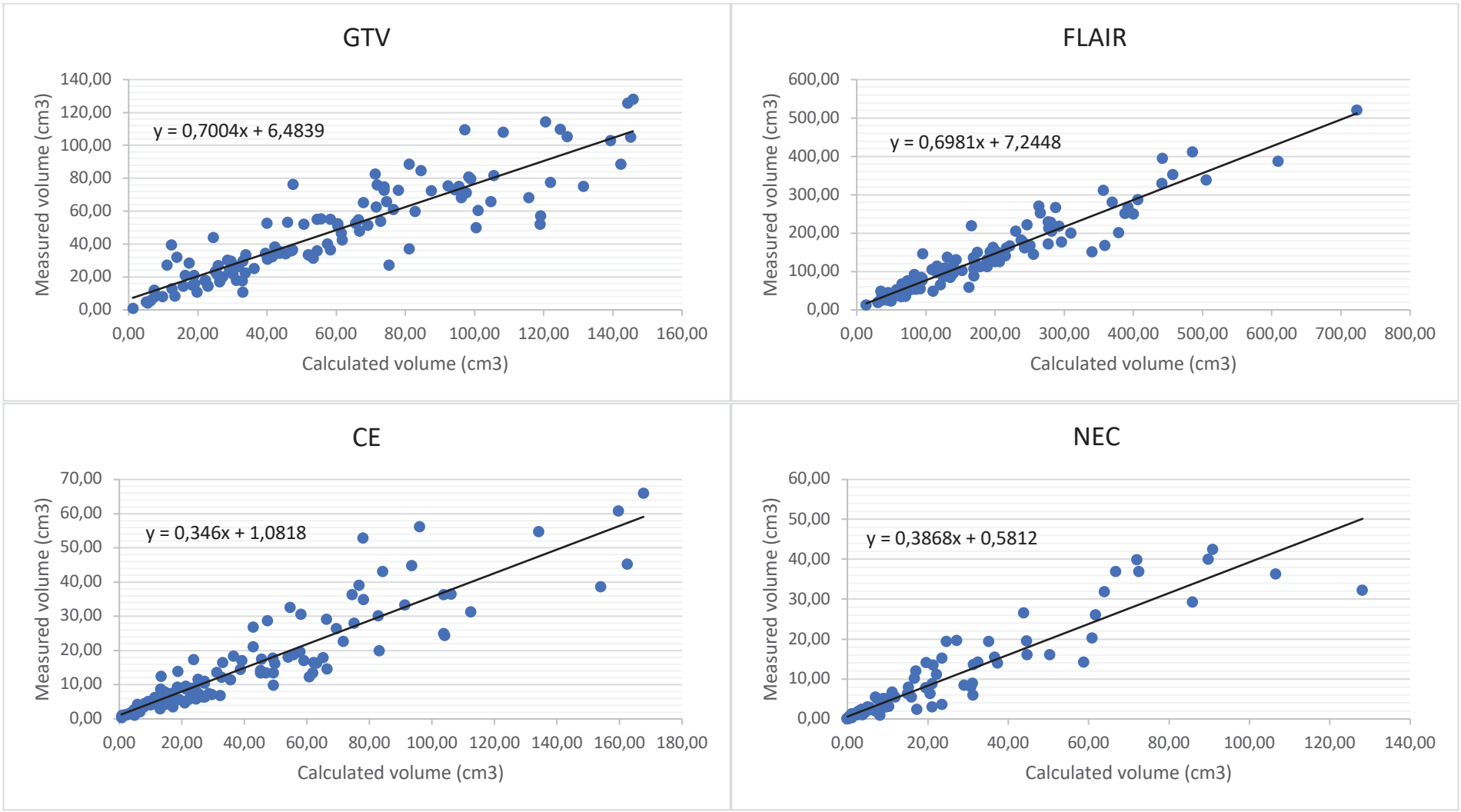

CE: Contrast-Enhancement; **GTV**: Gross Target Volume; **NEC**: Necrosis Area

Figure 3 : Plots of the difference between the calculated volume (CV) and the measured volume (MV) (cm^3)(Bland Altman plot)

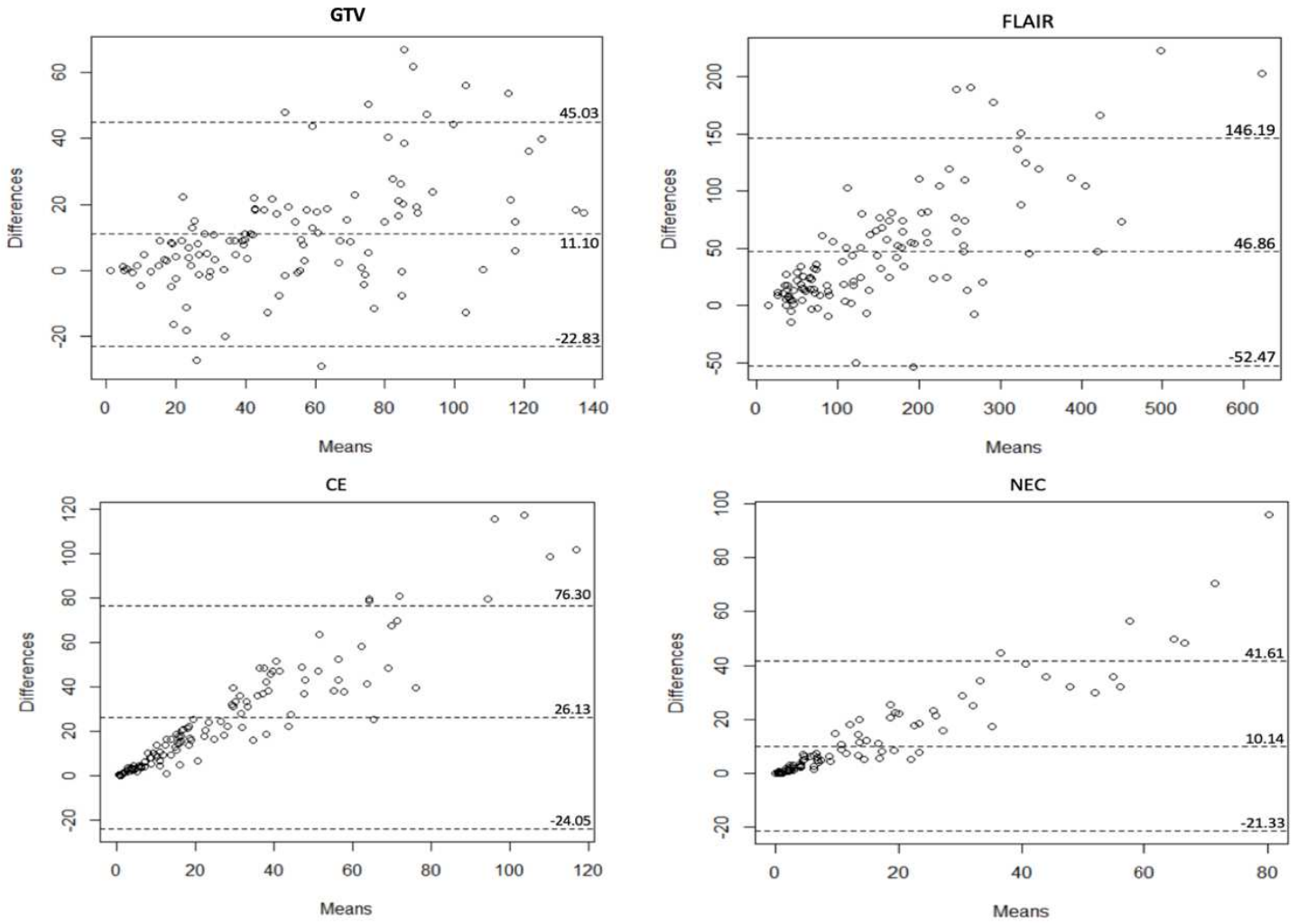

CE: Contrast-Enhancement; **GTV**: Gross Target Volume**; NEC**: Necrosis Area

Figure 4: Overall survival (OS) according to the volume measurement methods for A: patients considered non-PD and B: patients considered PD.

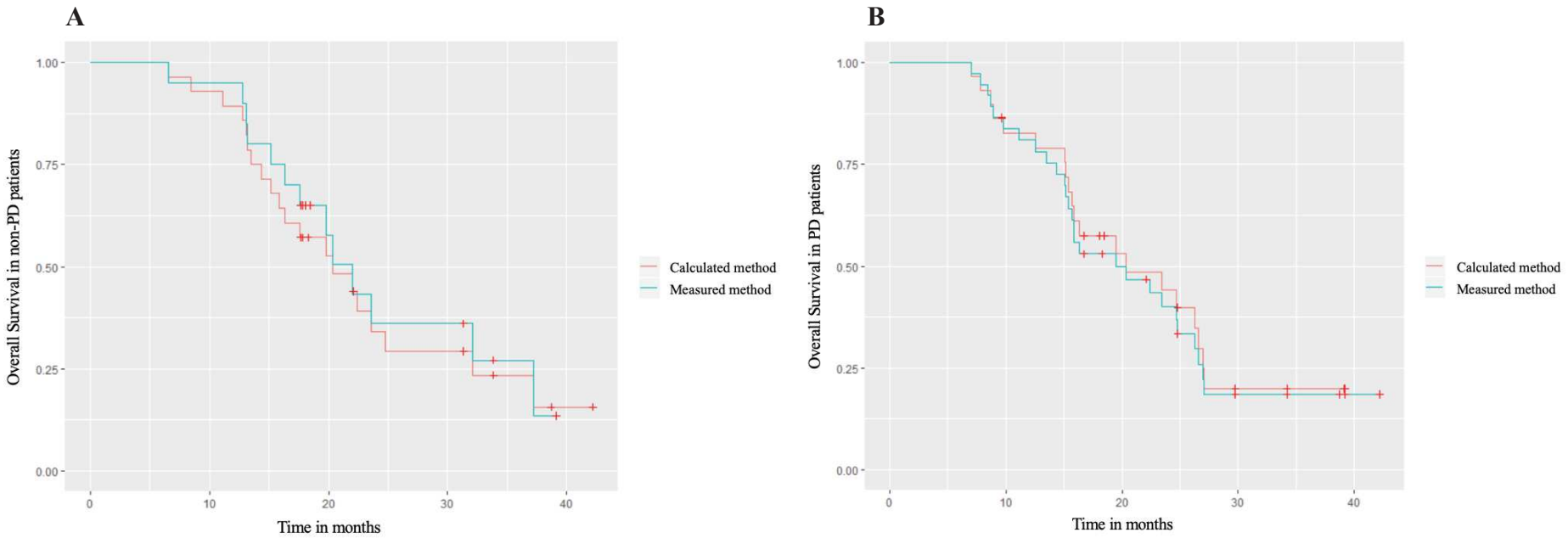

PD: progressive disease

Predictive factors of pseudoprogression versus true progression in patients treated with surgery and chemoradiotherapy for glioblastoma: A retrospective study of 57 patients.

Résumé

Introduction Le diagnostic de pseudoprogression (PsP) au cours du suivi des patients atteints d'un glioblastome (GBM) est un vrai dilemme. Actuellement, aucun facteur prédictif universel n'a été mis en évidence. Le but de cette étude était d'identifier des facteurs prédictifs de PsP afin d'aider le clinicien à la décision thérapeutique.

Méthodes Les patients suivis pour un GBM prouvé histologiquement, et traités par une chirurgie optimale et une chimioradiothérapie, selon le protocole EORTC/NCIC, ont été inclus. Les données cliniques, histologiques, radiologiques et d'irradiation ont été analysées au moment de l'IRM dosimétrique (baseline) et au moment de l'IRM montrant une progression (IRM progression). Les patients ont été classés dans le groupe PsP ou dans le groupe vraie progression (TP) selon les données de l'IRM qui a suivi l'IRM progression. Une analyse de corrélation a été effectuée avec les variables ayant une p valeur ≤0.200 en analyse univariée. Le modèle multivarié incluait les variables ayant un coefficient de corrélation r compris entre -0.5 et 0.5.

Résultats Cinquante-sept patients ont été inclus dans l'étude, 44 (77%) dans le groupe TP et 13 (23%) dans le groupe PsP. En analyse univariée, les potentiels facteurs prédictifs de PsP étaient : l'absence d'épilepsie au moment de l'IRM dosimétrique (p=0.042), et sa stabilité (p=0.032), la méthylation du promoteur de MGMT (p=0.044), la mutation d'ATRX (p=0.043), la diminution de la taille de la nécrose en deux dimensions (p=0.041) et en trois dimensions (p=0.024), la $V_{80\%}$ et la D_{min} du volume incluant la prise de contraste, la nécrose et la cavité chirurgicale, sur l'IRM progression (p=0.023 and p=0.017), et du volume de la prise de contraste seule (p=0.039 and p=0.029). En analyse multivariée, les facteurs prédictifs de PsP étaient : la $V_{80\%}$ du volume de l'œdème sur l'IRM progression (p=0.027), le nombre de prises

de contraste sur l'IRM progression (p=0.035) et la classe de réponse thérapeutique selon RANO (p=0.019).

Conclusion

Actuellement le diagnostic de certitude de PsP nécessite une confirmation histologique. Cependant, en routine clinique, l'analyse des IRM conventionnelles de suivi est le plus souvent utilisée. L'étude a identifié des facteurs prédictifs potentiels de PsP qu'il conviendrait de confirmer par une analyse prospective, complétée de données d'imagerie et de données génétiques.

Mots clés

Glioblastome, IRM, MGMT, Progression, Pseudoprogression, RANO

Predictive factors of pseudoprogression versus true progression in patients treated with surgery and chemoradiotherapy for glioblastoma: A retrospective study of 57 patients.

Clara Le Fèvre[1], MSc, Hélène Cebula[2], MD MSc, Benoit Lhermitte[3], MD, MSc, Isabelle Chambrelant[1], MSc, Roland Schott[4], MD, MSc, Delphine Antoni[1,5], MD MSc, Alicia Thiery[6], MD MSc, Jean-Marc Constans[7], MD PhD, Georges Noël[1,5,*], MD PhD.

[1] Department of radiotherapy, comprehensive cancer center Paul Strauss, UNICANCER, 3 rue de la porte de l'Hôpital, 67065 Strasbourg Cedex, France

[2] Departement of Neurosurgery, Hautepierre University Hospital, 1, avenue Molière, 67200 Strasbourg, France

[3] Département of Pathology, Hautepierre University Hospital, 1, avenue Molière, 67200 Strasbourg, France

[4] Departement of medical oncology, comprehensive cancer center Paul Strauss, UNICANCER, 3 rue de la porte de l'Hôpital, 67065 Strasbourg Cedex, France.

[5] Strasbourg University, CNRS, IPHC UMR 7178, Centre Paul Strauss, UNICANCER, 67000 Strasbourg, France

[6] Department of public health, comprehensive cancer center Paul Strauss, UNICANCER, 3 rue de la porte de l'Hôpital, 67065 Strasbourg Cedex, France

[7] Department of Radiology, Amiens-Picardie University Hospital, 1 rond-point du Professeur Christian Cabrol, 80054 Amiens Cedex 1, France

*: correspondent author, same address, gnoel@strasbourg.unicancer.fr

Short title: predictive factors of pseudoprogression in GBM

Abstract

Purpose: Glioblastoma (GBM) remains the most common malignant brain primary tumor in adults. The diagnosis of pseudoprogression (PsP) during follow-up is a real dilemma, and actually, no universal predictive factor of PsP has been found. The aim of this study was to determine predictive factors of PsP to help the clinician to distinguish PsP from true progression (TP) in GBM patients.

Materials and Methods: Adult patients with histopathological confirmation of GBM treated with optimal surgery and standard chemoradiotherapy (CRT) according to the EORTC/NCIC protocol were included. Clinical, radiological, histopathological, and radiation data were analyzed at the time of the dosimetric magnetic resonance imaging (MRI) performed before CRT (baseline) and of the progression MRI showing a suspicion of progression. Patients were classified into the PsP group or in TP group according to the conclusion of the local multidisciplinary tumor board at the time of the MRI following the progression MRI. In parallel, patients' data were analyzed according to the RANO criteria. An analysis of correlation was performed with the variables of *P* value ≤0.200 in univariate analysis. The multivariate model included variables such as the *r* correlation coefficient $-0.5 \leq r \leq 0.5$.

Results: A total of 57 patients were included in the study, 44 (77%) in the TP group and 13 (23%) in the PsP group. The univariate analysis identified potential predictive factors of PsP: the absence of epilepsy at the time of the dosimetric MRI (p=0.042) and its stable evolution (p=0.032), the MGMT promotor methylation (p=0.044) and the ATRX mutation (p=0.043), the decrease of the necrotic areas evaluated in two dimensions (p=0.041) and in three dimensions (p=0.024), the $V_{80\%}$ and the D_{min} of the volume including the contrast-enhanced lesions, the necrotic areas, and the surgical cavity in the progression MRI (p=0.023 and p=0.017, respectively) and the volume of the contrast-enhanced lesions alone (p=0.039 and p=0.029, respectively). In multivariate analysis, predictive factors of PsP were the $V_{80\%}$ of edema areas

volume (p=0.027), the number of contrast-enhanced lesions at the time of progression MRI (p=0.035), and the RANO response group (p=0.019).

Conclusion: Currently, the only method of diagnosing PsP with certainty is histopathological confirmation. But in clinical routine, the analysis of conventional MRIs during the follow-up is the most used. This study identified potential predictive factors of PsP, which remain to be confirmed with a prospective study and supplementary data on advanced MRIs and genetic analysis.

Key words

Glioblastoma, MGMT, MRI, Progression, Pseudoprogression, RANO

Introduction

Glioblastoma (GBM) remains the most common malignant brain primary tumor in adults (1). Since the introduction of concomitant chemoradiotherapy (CRT) with daily temozolomide (TMZ) and adjuvant TMZ following maximal surgery as the gold standard, the median overall survival (OS) rate has increased and reaches 15 to 18 months (1–5). However, more patients experience pseudoprogression (PsP) after CRT compared with those who receive radiotherapy (RT) alone (4), with a rate of 36% in a recent meta-analysis (6). Usually, PsP occurs within 6 months after CRT and is considered a transient new or enlargement contrast enhancement in T1-weighted contrast-enhanced magnetic resonance imaging (MRI), mimicking true progression (TP) (7–19). The diagnosis of PsP versus TP is a real dilemma and affects the therapeutic decision. In the case of PsP, it is recommended to continue the current treatment or follow-up, but in the case of TP, the treatment must be changed (7,20,21).

To help with medical decision making, standardized criteria such as the Macdonald criteria (22) or RANO criteria (23) have been edited and based on clinical and MRI criteria. Moreover, advanced imaging modalities such as diffusion MRI, perfusion MRI, MR spectroscopy (MRS), or positron emission tomography (PET); histopathology; and genomic features can complete classical clinical and radiological data to orientate the diagnosis (24–26). Currently, no specific factor has been found that can diagnose PsP with certainty, and no single imaging feature or a combination of features has been validated to differentiate PsP and TP, because of the lack of standardized imaging procedures (27). Moreover, the definition of PsP in clinical trials has remained heterogeneous (21).

The aim of this study was to attempt to determine predictive factors of PsP to help the clinician distinguish PsP from TP in GBM patients treated by maximal debulking surgery, CRT, and adjuvant chemotherapy according to the EORTC/NCIC protocol (4).

Methods

This study was approved by the center's institutional review board.

Patients selection

A total of 139 patients with newly diagnosed and histologically confirmed GBM were identified between 2015 and 2017 and reviewed in this single-center retrospective study. Inclusion criteria consisted of 1) age 18 years or older, 2) histopathological confirmation of GBM, 3) completion of entire course of CRT with TMZ after surgery according to the EORTC/NCIC protocol, and 4) MRI follow-up until progression. Thirty-eight patients were excluded because of hypofractionated RT schedules, 15 for another chemotherapy protocol (bevacizumab), eight died before progression, seven had no progression at the time of data collection, five were lost to follow-up, five had gliosarcoma histological conclusion, three had no MRI examination during the follow-up, and one had a history of cerebral irradiation. Finally, 57 patients were included in the study (Appendix 1). They were followed until December 22, 2018, with a minimum follow-up of 1 year.

Data recorded

Data were recorded at the time the dosimetric MRI was performed for the RT planification before the CRT and at the time of progression MRI, defined as the MRI showing a suspicion of progression during the follow-up.

Clinical data

General patient characteristics are summarized in Table 1. Neurological data were characterized according to the CTCAE v4.0 and are presented in Appendix 2. The median age of the patients was 62 years (range, 24-81 years), and 17 patients (30%) were female. At the time of dosimetric MRI, the Karnofsky Performance Status (KPS) was 90-100% and 70-80% in 27 (47%) and 30 (53%) patients, respectively. At the time of progression MRI, the KPS status was 90-100%, 70-80%, and ≤60% in 15 (26%), 30 (53%), and 12 (21%) patients, respectively.

Radiological data

All MRIs were performed on a Siemens Magneton AERA XJ 1.5T MRI (Siemens®, Muenchen, Germany) and included at least T1-weighted images, T1-weighted contrast-enhanced three-dimensional (3D) magnetization prepared rapid gradient echo (MPRAGE) sequence, and fluid-attenuation inversion recovery on T2-weighted images (T2-FLAIR). Radiological data are summarized in Table 1. The comparison between the dosimetric MRI and the progression MRI showed that mass effect, contrast enhancement, sharp demarcation, and contact with the dura were unchanged. However, contact with the ventricle and ependymal propagation were significantly larger at the time of progression MRI ($p = 0.002$ and $p < 0.001$ respectively). On the progression MRI, progression images were multifocal in 23 (40%) patients and unifocal in 34 (60%) patients. The progression was considered local in 49 (86%) cases and distant in 8 (14%) cases. Fourteen (25%) patients presented one to three new lesions.

On T1-weighted contrast-enhanced MPRAGE sequence, several volumes were defined: 1) the gadolinium contrast-enhanced lesions corresponding to the hypersignal area of gadolinium contrast enhancement (CEL), 2) the necrosis area corresponding to the hyposignal area (NEC), and 3) the contrast-enhanced gross target volume (GTV_{GADO}) including CEL, NEC, and the surgical cavity. On T2-FLAIR sequence, the volume of the edema area (GTV_{FLAIR}) was defined. The CEL, NEC, GTV_{GADO}, and GTV_{FLAIR} were manually delineated with the software FocalSim™ (Elekta®, Stockholm, Sweden) on all MRI axial slices, slice per slice. On the dosimetric MRI, tumor compartments were named CEL_{ref}, NEC_{ref}, $GTV_{GADOref}$, and $GTV_{FLAIRref}$. On the progression MRI, tumor compartments were named CEL_P, NEC_P GTV_{GADOP}, and GTV_{FLAIRP}. Each tumor compartment size was analyzed with a two-dimensional (2D) method (as in RANO criteria) and with two methods of volume determination: the calculated volume (CV) and the measured volume (MV). The 2D method corresponded to the product of the largest diameters of the tumor compartment on MRI axial slices, D1*D2, with D1 and D2 corresponding to largest diameter of the compartment in two

dimensional plans, in cm^2. The CV method corresponded to an ellipsoid formula (π/6*D1*D2*D3), with D1, D2, and D3 corresponding to the largest diameter of the compartment in 3D plans, in cm^3. The MV method corresponded to the volume calculated automatically by the software FocalSim™ and derived from the compartment manual delineation. The 2D, CV, and MV size of GTV_{GADO}, GTV_{FLAIR}, CEL, and NEC and their evolution are summarized in Table 2 and Figure 1.

Treatments

Treatment data are summarized in Table 1. Following surgery, all patients benefited from the EORTC/NCIC protocol (4). The surgery consisted of a biopsy, a partial resection, or a complete resection in 15 (26%), 24 (42%), and 18 (32%) cases, respectively. Complete surgery was defined as more than 90% resected tumor evaluated in a 48-h postoperative MRI. MGMT status was available for all patients, and 25 (44%) patients had the methylated MGMT promoter, and isocitrate dehydrogenase (IDH) status was available for 55 patients (mutated in 2 cases).

RT delivered a total dose of 60 Gy in 30 fractions of 2 Gy per fraction given once daily for 5 days per week. The RT was administered using Primus® (Siemens®, Muenchen, Germany) for conformal three-dimensional RT technique (3D-RT) or Clinac® (Varian®, Palo Alto, USA), Tomotherapy® (Accuray®, Madison, USA), or Novalis® (Varian®, Palo Alto, USA) for intensity-modulated radiation therapy. Target volumes were delineated on the dosimetric MRI. The gross target volume (GTV) included contrast-enhanced lesions and surgery cavity. The clinical target volume (CTV) included the GTV with a 10-mm margin and T2/FLAIR hyperintensity, and the planning target volume (PTV) corresponded to the CTV plus a 3- to 5-mm margin. The radiation therapy and dosimetry characteristics are summarized in Table 1. The mean CTV and PTV volume were 165.2 ± 75.8 cm^3 and 229.7 ± 97.2 cm^3, respectively. Dosimetric data were recorded from ARTIVIEW™ software (Aquilab®, Loos, France). The application of the radiation therapy planning dose plan on the progression MRI showed the

mean percentage of volume inside the 80% isodose ($V_{80\%}$) and the mean minimum received dose (D_{min}) were 98.3 ± 6.04% and 46.7 ± 18.9 Gy for GTV_{GADOP}, 89.7 ± 13.5% and 28.0 ± 22.0 Gy for GTV_{FLAIRP}, and 96.9 ± 9.0% and 49.7 ± 19.1 Gy for CEL_P, respectively.

Simultaneously to RT, patients received daily TMZ. Adjuvant TMZ was administered 4 weeks after during 5 days on 28 days for six provisional cycles. All patients had received the full CRT according to the EORTC/NCIC protocol and had completed a median of 3 cycles (0-6) of adjuvant TMZ. The median interval between the completion of CRT and the progression MRI was 13.4 weeks (–1.3 to 82.6), and the progression MRI was the first follow-up MRI in 35 (61%) cases. At the time of the progression MRI, 40 (70%) patients pursued adjuvant TMZ treatment, one (2%) patient received support care, and 16 (28%) had no treatment.

Definition of response to treatment according to RANO

Patient response to treatment was analyzed according to the RANO criteria and modified RANO criteria (23,28). Each patient was classified as having complete response (CR), partial response (PR), stable disease (SD), or progressive disease (PD) (Appendix 3). The dosimetric MRI was chosen as baseline. To determine the GBM response to treatment according to RANO, the progression MRI was compared with the dosimetric MRI or with the MRI demonstrating the best response to treatment for patients with several MRIs performed between the dosimetric MRI and the progression MRI. Within the first 12 weeks after CRT, progression was defined with radiological or histological data. Beyond 12 weeks after CRT, the definition of progression was based on clinical and radiological criteria (Appendix 4). RANO criteria results are summarized in Table 1. According to RANO criteria, 18 (32%) patients were in SD and 39 (68%) in PD.

Patients group*s: *PsP or TP

All patients in this study experienced a suspicion of progression during the follow-up at the so-called progression MRI. GBM patients were classified as PsP or TP after confirmation with the

MRI following the progression MRI. PsP was considered a stable, decrease in, or disappearance of the contrast-enhanced lesions that were identified as having progressed on the progression MRI, and TP corresponded to an increase of the contrast-enhanced lesions. This radiological conclusion was confirmed by conclusion of the local multidisciplinary tumor board. If patients had benefited from a second line of chemotherapy after the progression MRI (i.e., without second MRI confirmation), they were considered as having TP.

Survival analysis

The OS and time to progression (TTP) were determined from the date of the GBM histopathological diagnosis to the date of death or last follow-up and to the date of progression, respectively.

Statistical analysis

Statistical calculations were performed with R version 3.6.1 software (R foundation for Statistical Computing, Vienna, Austria; www.r-project.org).

Quantitative variables were expressed as the mean and standard deviation (SD) or as the median with minimum and maximum. Qualitative variables were expressed as counts and percentages. In the univariate analysis, for the quantitative variables, a Student's *t*-test was performed when the distribution was Gaussian. In the opposite case, a Mann-Whitney test was conducted. The distribution of the variables was assessed by a Shapiro-Wilk test. For the qualitative variables, a Pearson's chi-square test was performed in the case of sufficient theoretical count. Otherwise, a Fischer's exact test was executed.

Before the multivariate analysis, a correlation analysis was performed as the first step for the variables with a p value ≤ 0.200 in the univariate analysis with a correlation matrix. Then, a multivariate analysis model was constructed with variables with a p value ≤ 0.200 in univariate analysis and an r correlation coefficient of $-0.5 \leq r \leq 0.5$. Results from the multivariate analysis

identified significant predictive factors of PsP. The beta coefficient of those factors was used to estimate the probability of PsP according to the following formula (29):

PsP probability = □□+ (□$_1$*variable$_1$) + (□□$_2$*variable$_2$) + (…) + (□$_n$*variable$_n$).

OS and TTP were analyzed with the Kaplan-Meier method and with the log-rank test for the comparison between the PsP and TP groups.

Results

Characteristics of the patients in the PsP and TP groups are summarized in Tables 1 to 3.

According to the progression MRI, 33 (58%) patients were classified in the TP group and 24 (52%) patients in the PsP group, whereas with the MRI following the progression MRI, a total of 44 (77%) patients were classified in the TP group and 13 (23%) in the PsP group (Table 3). Eleven (25%) patients in the TP group and no patients in the PsP group experienced a suspicious progression within the first 12 weeks (p = 0.053). The mean and the median time intervals between the progression MRI and the next MRI were 7.7 and 2.8 months (range: 0.4-4.7) in the TP group and 2.6 and 3.0 months (range: 1.1-9.8) in the PsP group, respectively, without a significant difference (p = 0.718).

The univariate analysis is summarized in Table 4. Among the clinical symptoms, only epilepsy differed between the TP and PsP groups. At the time of the dosimetric MRI, 18 (41%) patients in the TP group and one (8%) patient in the PsP group presented with epilepsy (p = 0.042). Between the dosimetric MRI and the progression MRI, stabilization, worsening, and improvement of epilepsy differed significantly between both groups (p = 0.032).

GBM histological examination revealed that 17 (39%) and 8 (61%) patients in the TP and PsP groups, respectively, had a methylation of the MGMT promotor (p = 0.044). No patient in the TP group and two (15%) patients in the PsP group had an ATRX mutation (p = 0.043).

Between the dosimetric and the progression MRI, only two radiological features differed significantly between the groups: 2D NEC and CV NEC size (p = 0.041 and p = 0.024,

respectively). An increase in 2D NEC size was observed in 18% of patients in the TP group and in 9% of patients in the PsP group. An increase in CV NEC size was observed in 33% of patients in the TP group and in 20% of patients in the PsP group.

Dosimetric data revealed that the GTV_{GADOP} and the CEL_P volume included in the 80% isodose were significantly higher in the PsP group versus the TP group ($p = 0.023$ and $p = 0.039$, respectively), as was the D_{min} in these volumes ($p = 0.017$ and $p = 0.029$, respectively).

In the PsP group, four (31%) patients did not experience TP at the point date. For the other patients, TP was definitively diagnosed at a mean of 10.1 ± 5.4 months after the progression MRI.

Predictive risk factors of PsP

Variables with p-value ≤0.200 in the univariate analysis were included in the correlation matrix (Figure 2). Because of high correlation ($r \geq 0.5$ or $r \leq -0.5$), some variables were excluded from the multivariate analysis. Results of the multivariate analysis are summarized in Table 4. The $V_{80\%}$ of GTV_{FLAIRP}, the number of CEL_P, and the 2D RANO classification were identified as predictive factors for PsP. The $V_{80\%}$ of GTV_{FLAIRP} was 94.2% (range, 49.2-100.0%) in the TP group and 99.4% (range, 81.8-100.0%) in the TP group ($p = 0.027$). The number of CEL_P was one, two, three, or four in 27 (61%), seven (16%), seven (16%), and three (7%) patients in the TP group and 10 (77%), three (23%), zero, and zero patients in the PsP group, respectively ($p = 0.035$). Using the 2D RANO criteria, PD and SD were determined in 28 (64%) and 16 (36%) patients in the TP group and 11 (85%) and two (15%) patients in the PsP group, respectively ($p = 0.019$).

The predictive score evaluating the PsP probability was PsP probability = –8.01267 + 0.09992* ($V_{80\%}$ of GTV_{FLAIRP}) – 1.30864* (number of CEL_P) – 2.17519* (2D RANO classification) (1 = SD; 0 = PD).

Survival analysis

Figure 3 reports the survival features of the TP and PsP groups. At the point date, 40 (70%) patients had died, 35 (80%) in the TP group and 5 (38%) in the PsP group (p = 0.012). The median OS was significantly different between the TP (16.4 months; 95% confidence interval [CI] 16.3-26.4 months) and PsP (NA; 95% CI 24.0-31.8 months) groups (p = 0.004). The TTP did not differ significantly between the TP (6.4 months; 95% CI 5.8-9.2) and PsP (6.1 months; 95% CI 5.9-9.0) groups (p = 0.3).

If patients were classified into four groups according to the local multidisciplinary tumor board conclusion and RANO category (i.e., TP/PD, TP/SD, PsP/PD, and PsP/SD; Table 3), the median OS was 17.1 months (95% CI 15.2-26.7), 15.4 months (95% CI 13.3-24.9), not reached (95% CI 23.7-NR), and 24.0 months (95% CI 24.0-NR), respectively (Figure 3).

Discussion

The aim of this study was to identify predictive factors of PsP to improve the treatment management of GBM patients. In the current study, the PsP incidence of 23% was consistent with the literature data (6). The number of CEL_P, $V_{80\%}$ of GTV_{FLAIRP}, and 2D RANO classification appeared to be relevant predictive factors of PsP in multivariate analysis.

Data in the literature about predictive factors of PsP are discordant, and studied factors are heterogeneous. The univariate analysis of the present study retrieved 10 predictive factors of PsP. The initial epilepsy was significantly more frequent in the TP group (p = 0.042), but its pejorative evolution was more frequent in the case of PsP (p = 0.032). To our knowledge, this factor was not already described in the literature. The MGMT promotor methylation and ATRX mutation were identified as predictive factors of PsP (p = 0.044 and p = 0.043, respectively) as already demonstrated in the literature (9,12,25,30–37). According to Balana et al., patients with methylated MGMT promotor would have 3.5-fold increased risk of having PsP than TP in the case of MRI suggesting progression (33). In the study by Li et al., the probability of PsP in the case of images of progression was 1.9 times that in the case of MGMT promoter methylation

(32). However, few studies have demonstrated that MGMT status is not associated with PsP (38,39). In the current study, only the evolution of the NEC size seemed to be an imaging biomarker of PsP ($p = 0.041$ for 2D and $p = 0.024$ for CV), a factor not found in the literature. All patients included in this study benefited from radiation therapy, with 60 Gy in 30 fractions. The $V_{80\%}$ and the D_{min} of GTV_{GADOP} and CEL_P were significantly different between the PsP and TP group. In the literature, the radiation dose was not predictive of PsP in several studies (8,38,40–42), except in the Yang et al. study, where high-dose RT significantly increased the PsP rate (43). In the analysis by Taal et al., the irradiated volume did not differ between patients with TP, PsP, or without progression (44).

Other biomarkers were studied in the literature without significant results in this study. The median patient age between the two groups did not differ significantly and was 62 years in the TP group and 60 years in the PsP group ($p = 0.366$). This observation has already been described in the literature (33,40–42). However, Tall et al. showed that patients with TP were significantly older than those with PsP (55 versus 46 years; $p = 0.034$) (44). Gender was not identified as a predictive factor of PsP ($p = 1.000$) as in other studies (32,33,42), even if Jang et al. showed that female patients more frequently developed PsP than male patients did ($p = 0.03$) (39). Clinical parameters, such as KPS status ($p = 0.172$), did not support the PsP diagnosis, as already reported in several studies (33,40,41,44). Neurological deterioration was not identified as a predictive factor in the current study ($p = 0.123$), as in the literature (33,41,44). However, Rowe et al. showed that patients with TP presented significantly more clinical deterioration than patients with PsP ($p = 0.046$) (9). Other potential clinical predictive factors of PsP were studied in the literature without significant results, such as Recursive Partitioning Analysis score (41) and Mini-Mental State Examination score (33). The consumption of anticonvulsants did not differ between the two groups initially ($p = 0.060$) nor at the time of progression ($p = 0.123$), as also seen in the study by Balana et al. ($p = 0.55$) (33). Contrary to Balana et al., who

demonstrated that the dose of dexamethasone at the start of concurrent CRT was a factor associated with PsP (33), and Rowe et al., who concluded that the increase in steroids could differentiate PsP and TP (9), the current study did not relate steroid consumption variation with PsP or TP. This was consistent with previous published conclusions (45). The current study is in accordance with most other researchers in that the extent of surgery did not influence the occurrence of PsP (32,33,38,40–42,44,45). However, Gerstner et al. demonstrated on univariate analysis that the extent of surgery was significantly associated with PsP ($p = 0.04$) (46). The interval between surgery and CRT was not significantly different between TP and PsP (46 versus 42 days; $p = 0.859$), as in the Kang et al. study (42), and the interval between the end of CRT and suspicious progression also did not differ (14.4 versus 13.4 weeks; $p = 0.746$), which is in contrast to the study by Jang et al., who found that this interval was shorter in the PsP group than in the TP group (82 versus 124 days; $p = 0.02$) (39). Consistent with other papers, IDH, TP53, and epidermal growth factor receptor did not differ significantly between the TP and PsP group in this study (33,39). Other authors suggested that IDH could be a molecular biomarker for PsP (32,33,47) as p53 overexpression (42). The size and the evolution of the size of the GBM compartments, other than NEC, did not influence the diagnosis of PsP nor the GBM radiological characteristics and tumor location. Frequently, contrast enhancement was considered a treatment response marker, even if there was a lack of standardization. Interpretation of imaging results is difficult because clinical and molecular parameters could interact with outcomes and create biases in the comparison of studies (48). In the literature, tumor location (33,41), initial tumor volume (41), and tumor size at T1 gadolinium and T2/FLAIR MRI (9,33) were not markers of PsP. Researchers have shown significant correlations between TP and contact with dura, contact with ventricle, and pattern of contrast enhancement but not for multifocal lesion and ependymal spread (49).

In the multivariate analysis, three factors were predictive of PsP. The $V_{80\%}$ of GTV_{FLAIRP} was identified as a predictive factor of PsP, with 5.8% and 0.63% of the GTV_{FLAIRP} outside the isodose 80% in the TP and PsP groups, respectively. Those results suggested that the edema inside the 80% isodose corresponded to ab RT reaction, whereas the edema outside the 80% was evidence of the presence of tumor cells. Choi et al. demonstrated that the inclusion of the edema volume into the RT target volume did not increase the occurrence of PsP (50). Huber et al. suggested that FLAIR volume changes during the follow-up could be more suitable and specific for the detection of TP than contrast-enhanced volume changes (51). Other authors showed that the FLAIR signal decreased in 30% of PsP patients, but no decrease in FLAIR signal was observed in TP patients, undermining the potential predictive factors of FLAIR signal in PsP (9). In the present study, 23% of patients with PsP and 16% of patients with TP had a decrease in FLAIR signal ($p = 0.216$). The number of CEL_P appeared to be a predictive factor of PsP in the present study ($p = 0.035$), and 34% and 15% of patients in the TP and PsP groups experienced new lesions, respectively ($p = 0.304$). Those results raise questions about the importance of the number of contrast-enhanced lesions instead of the volume of lesions. The last predictive factor of PsP in the multivariate analysis was the RANO criteria conclusion, which has not been, to our knowledge, discussed in the literature. In this study, with RANO criteria, 39 (68%) patients were determined as PD, of whom 28 (72%) were in the TP group and 11 (28%) were in the PsP group; 18 (32%) patients were determined as SD, of whom 16 (89%) were in the TP group and 2 (11%) were in the PsP group ($p = 0.191$). Among the patients in the PsP group, two had new contrast-enhanced lesions, and TP appeared at 6 and 10 months, respectively, after the progression MRI. These results suggest that in the case of PD according to RANO criteria, TP was highly suspicious. In the case of SD, follow-up should be continued. From this finding, a radiological interpretation, without RANO evaluation, could wrongly conclude TP.

RANO criteria constitute an international reference for the response assessment in GBM. However, RANO criteria have some limitations: the lack of objective FLAIR assessment definition (52,53), the lack of objective neurological deterioration definition (54), and the lack of objective corticosteroid dose threshold. In this study, to be more reproducible, clinical criteria and corticosteroid dose consumption were defined as described in appendix 4. Tumor size and its evolution were often used as endpoints in studies with 2D size measurements. However, GBM is often irregular and sharp with cystic area, surgical cavity, necrosis areas, and new contrast-enhancing spots that could lead to size estimation error (55). Therefore, a volumetric approach seems to be more appropriate, and automated contour techniques have increased the accuracy of volume definition (56). With the RANO criteria, the baseline MRI was the postsurgical MRI, and with the modified RANO criteria, the baseline MRI was the postradiation MRI. Those two MRIs had limitations, such as postsurgical bleeding, vascular permeability modifications, and image modification due to a high dose of steroids in the immediate postsurgery period or GBM regrowth before CRT (57). However, authors have shown that an early MRI evaluation at 30 Gy and 60 Gy could lead to early detection of TP and could be an interesting point of discussion in terms of treatment modification (58). In this study, the pre-CRT MRI (dosimetric MRI) was chosen as the baseline because it was considered the most representative of the lesion before CRT to allow appreciation of the GBM response to treatment and to differentiate PsP and TP.

Several authors have studied the potential predictive factors of PsP, but results remain divergent and contradictory. Most studies were retrospective and did not use standardized and comparable imaging protocols. In clinical trials, the criteria used to define PsP as well as the time point to evaluation were often different (21,59,60). Currently, the differentiation between PsP and TP remains a real challenge; in particular, new therapeutics and a robust model correlating clinical, genetic, molecular, and radiological data are needed (61–63). In addition to conventional

imaging, combined and advanced imaging seems promising, with the need for standardization and homogenization of the methodology, acquisition protocols, and analytical approaches (24,27,64–67). No single imaging features or combination of features have been validated for differentiating PsP and TP (27). New therapeutics, which affect MRI, further complicate the PsP diagnosis. Moreover, contrast-enhanced image signal MRI is dependent on contrast dose, injection timing, magnetic field strength, and choice of image sequences (68). Conventional MRI has become limited in response assessment and disease progression monitoring. Some authors have proposed advanced imaging, now routinely available, to determine noninvasive imaging markers and improve the PsP diagnosis to improve patient outcomes (64,65). In addition to bringing structural and anatomical information, advanced MRI provides cellular, biological, and metabolic information (66). Diffusion MRI, perfusion MRI, MRS, and positron emission tomography have their place in the PsP diagnosis. A meta-analysis, including 941 patients with GBM, showed that advanced MRI techniques had higher diagnostic accuracy than conventional MRI for the distinction of PsP and TP with a sensitivity and specificity of 71-92% and 85-95% versus 68% and 77%, respectively. MRS had the best accuracy, with a sensitivity and specificity of 91% and 95%, respectively, followed by perfusion MRI with dynamic contrast-enhanced MRI (24). The combination of advanced modalities in multiparametric imaging improves accuracy but requires training, clinical trial data, and standardization as well. To improve GBM assessment, machine-learning models could be interesting, as clinical data, radiomics, proteomics, and genomics constitute complex “big data” to manage and analyze, in order to perform diagnostic, prognostic, and therapeutic models (69–72). Some authors have developed machine-learning algorithms to differentiate TP and PsP, with promising results (39,61–63,73). Neal et al. developed a model-based metric of therapy response based on T1 contrast-enhanced MRI and used linear, 4D spherical and 4D anatomic models to distinguish

PsP from TP, with a sensitivity of 79%, a specificity of 59%, a positive predictive value of 50%, and a negative predictive value of 93% (67).

Potential biases and limitations affected the interpretation and extrapolation of the results. First, this was a retrospective study with a relatively small number of patients, which could have affected the statistical results. In fact, the high number of variables analyzed in the multivariate analysis versus the number of patients included could be responsible for the decrease in statistical power. However, in the literature, the number of included patients was not elevated, with a mean of 73 and a median of 75 (30–42,44–46,49,50). Second, the PsP or TP group attribution is disputable. The diagnosis of PsP or TP was not histopathological, except in two cases. The GTV_{FLAIR} analysis should be done with caution because corticosteroid treatment, which is frequent in patients, could affect brain edema. Moreover, the suspicious progression did not appear on the same follow-up MRI in all patients of the study. Furthermore, because patients did not receive the same number of adjuvant TMZ cycles, assignment to the PsP or TP groups could be disputed.

Conclusion

PsP doubt is a common situation in clinical routine management of GBM. This study identified 10 predictive factors of PsP in univariate analysis and three in multivariate analysis. We proposed a formula to calculate the potential probability of PsP. Those results remain to be confirmed with a prospective study with supplementary data on advanced MRI and genetic analysis.

Bibliography

1. Ostrom QT, Gittleman H, Stetson L, Virk SM, Barnholtz-Sloan JS. Epidemiology of gliomas. Cancer Treat Res. 2015;163:1–14.
2. Ostrom QT, Gittleman H, Farah P, Ondracek A, Chen Y, Wolinsky Y, et al. CBTRUS statistical report: Primary brain and central nervous system tumors diagnosed in the United States in 2006-2010. Neuro-Oncol. 2013 Nov;15 Suppl 2:ii1-56.
3. Stupp R, Hegi ME, Mason WP, van den Bent MJ, Taphoorn MJB, Janzer RC, et al. Effects of radiotherapy with concomitant and adjuvant temozolomide versus radiotherapy alone on survival in glioblastoma in a randomised phase III study: 5-year analysis of the EORTC-NCIC trial. Lancet Oncol. 2009 May;10(5):459–66.
4. Stupp R, Mason WP, van den Bent MJ, Weller M, Fisher B, Taphoorn MJB, et al. Radiotherapy plus concomitant and adjuvant temozolomide for glioblastoma. N Engl J Med. 2005 Mar 10;352(10):987–96.
5. Seystahl K, Wick W, Weller M. Therapeutic options in recurrent glioblastoma--An update. Crit Rev Oncol Hematol. 2016 Mar;99:389–408.
6. Abbasi AW, Westerlaan HE, Holtman GA, Aden KM, van Laar PJ, van der Hoorn A. Incidence of Tumour Progression and Pseudoprogression in High-Grade Gliomas: a Systematic Review and Meta-Analysis. Clin Neuroradiol. 2018 Sep;28(3):401–11.
7. Wick W, Chinot OL, Bendszus M, Mason W, Henriksson R, Saran F, et al. Evaluation of pseudoprogression rates and tumor progression patterns in a phase III trial of bevacizumab plus radiotherapy/temozolomide for newly diagnosed glioblastoma. Neuro-Oncol. 2016;18(10):1434–41.
8. Brandsma D, Stalpers L, Taal W, Sminia P, van den Bent MJ. Clinical features, mechanisms, and management of pseudoprogression in malignant gliomas. Lancet Oncol. 2008 May;9(5):453–61.
9. Rowe LS, Butman JA, Mackey M, Shih JH, Cooley-Zgela T, Ning H, et al. Differentiating pseudoprogression from true progression: analysis of radiographic, biologic, and clinical clues in GBM. J Neurooncol. 2018 May 16;
10. Chaskis C, Neyns B, Michotte A, De Ridder M, Everaert H. Pseudoprogression after radiotherapy with concurrent temozolomide for high-grade glioma: clinical observations and working recommendations. Surg Neurol. 2009 Oct;72(4):423–8.
11. Chang JH, Kim C-Y, Choi BS, Kim YJ, Kim JS, Kim IA. Pseudoprogression and pseudoresponse in the management of high-grade glioma : optimal decision timing according to the response assessment of the neuro-oncology working group. J Korean Neurosurg Soc. 2014 Jan;55(1):5–11.
12. Zikou A, Sioka C, Alexiou GA, Fotopoulos A, Voulgaris S, Argyropoulou MI. Radiation Necrosis, Pseudoprogression, Pseudoresponse, and Tumor Recurrence: Imaging Challenges for the Evaluation of Treated Gliomas. Contrast Media Mol Imaging. 2018;2018:6828396.
13. Nasseri M, Gahramanov S, Netto JP, Fu R, Muldoon LL, Varallyay C, et al. Evaluation of pseudoprogression in patients with glioblastoma multiforme using dynamic magnetic resonance imaging with ferumoxytol calls RANO criteria into question. Neuro-Oncol. 2014 Aug;16(8):1146–54.
14. Jefferies S, Burton K, Jones P, Burnet N. Interpretation of Early Imaging after Concurrent Radiotherapy and Temozolomide for Glioblastoma. Clin Oncol. 2007 Apr 1;19(3):S33.
15. Radbruch A, Fladt J, Kickingereder P, Wiestler B, Nowosielski M, Bäumer P, et al. Pseudoprogression in patients with glioblastoma: clinical relevance despite low incidence. Neuro-Oncol. 2015 Jan;17(1):151–9.

16. Tran DKT, Jensen RL. Treatment-related brain tumor imaging changes: So-called "pseudoprogression" vs. tumor progression: Review and future research opportunities. Surg Neurol Int. 2013;4(Suppl 3):S129-135.
17. Larsen VA, Simonsen HJ, Law I, Larsson HBW, Hansen AE. Evaluation of dynamic contrast-enhanced T1-weighted perfusion MRI in the differentiation of tumor recurrence from radiation necrosis. Neuroradiology. 2013 Feb;55(3):361–9.
18. Ellingson BM, Wen PY, van den Bent MJ, Cloughesy TF. Pros and cons of current brain tumor imaging. Neuro-Oncol. 2014 Oct;16 Suppl 7:vii2-11.
19. Dietrich J, Winter SF, Klein JP. Neuroimaging of Brain Tumors: Pseudoprogression, Pseudoresponse, and Delayed Effects of Chemotherapy and Radiation. Semin Neurol. 2017;37(5):589–96.
20. Peca C, Pacelli R, Elefante A, Del MBDC, Vergara P, Mariniello G, et al. Early clinical and neuroradiological worsening after radiotherapy and concomitant temozolomide in patients with glioblastoma: tumour progression or radionecrosis? Clin Neurol Neurosurg. 2009 May;111(4):331–4.
21. Yoo R-E, Choi SH. Recent Application of Advanced MR Imaging to Predict Pseudoprogression in High-grade Glioma Patients. Magn Reson Med Sci MRMS Off J Jpn Soc Magn Reson Med. 2016;15(2):165–77.
22. Macdonald DR, Cascino TL, Schold SC, Cairncross JG. Response criteria for phase II studies of supratentorial malignant glioma. J Clin Oncol Off J Am Soc Clin Oncol. 1990 Jul;8(7):1277–80.
23. Wen PY, Macdonald DR, Reardon DA, Cloughesy TF, Sorensen AG, Galanis E, et al. Updated response assessment criteria for high-grade gliomas: response assessment in neuro-oncology working group. J Clin Oncol Off J Am Soc Clin Oncol. 2010 Apr 10;28(11):1963–72.
24. van Dijken BRJ, van Laar PJ, Holtman GA, van der Hoorn A. Diagnostic accuracy of magnetic resonance imaging techniques for treatment response evaluation in patients with high-grade glioma, a systematic review and meta-analysis. Eur Radiol. 2017 Oct;27(10):4129–44.
25. Brandes AA, Franceschi E, Tosoni A, Blatt V, Pession A, Tallini G, et al. MGMT promoter methylation status can predict the incidence and outcome of pseudoprogression after concomitant radiochemotherapy in newly diagnosed glioblastoma patients. J Clin Oncol Off J Am Soc Clin Oncol. 2008 May 1;26(13):2192–7.
26. Gutman DA, Cooper LAD, Hwang SN, Holder CA, Gao J, Aurora TD, et al. MR imaging predictors of molecular profile and survival: multi-institutional study of the TCGA glioblastoma data set. Radiology. 2013 May;267(2):560–9.
27. Lieberman F. Glioblastoma update: molecular biology, diagnosis, treatment, response assessment, and translational clinical trials. F1000Research [Internet]. 2017 Oct 26 [cited 2018 Sep 3];6. Available from: https://www.ncbi.nlm.nih.gov/pmc/articles/PMC5658706/
28. Ellingson BM, Wen PY, Cloughesy TF. Modified Criteria for Radiographic Response Assessment in Glioblastoma Clinical Trials. Neurother J Am Soc Exp Neurother. 2017;14(2):307–20.
29. Raharimanantsoa M, Zingg T, Thiery A, Brigand C, Delhorme J-B, Romain B. Proposal of a new preliminary scoring tool for early identification of significant blunt bowel and mesenteric injuries in patients at risk after road traffic crashes. Eur J Trauma Emerg Surg Off Publ Eur Trauma Soc. 2018 Oct;44(5):779–85.
30. Van Mieghem E, Wozniak A, Geussens Y, Menten J, De Vleeschouwer S, Van Calenbergh F, et al. Defining pseudoprogression in glioblastoma multiforme. Eur J Neurol. 2013 Oct;20(10):1335–41.
31. de Wit MCY, de Bruin HG, Eijkenboom W, Sillevis Smitt P a. E, van den Bent MJ. Immediate post-radiotherapy changes in malignant glioma can mimic tumor progression.

Neurology. 2004 Aug 10;63(3):535–7.
32. Li H, Li J, Cheng G, Zhang J, Li X. IDH mutation and MGMT promoter methylation are associated with the pseudoprogression and improved prognosis of glioblastoma multiforme patients who have undergone concurrent and adjuvant temozolomide-based chemoradiotherapy. Clin Neurol Neurosurg. 2016 Dec;151:31–6.
33. Balaña C, Capellades J, Pineda E, Estival A, Puig J, Domenech S, et al. Pseudoprogression as an adverse event of glioblastoma therapy. Cancer Med. 2017 Dec;6(12):2858–66.
34. Soike MH, McTyre ER, Shah N, Puchalski RB, Holmes JA, Paulsson AK, et al. Glioblastoma radiomics: can genomic and molecular characteristics correlate with imaging response patterns? Neuroradiology. 2018 Oct;60(10):1043–51.
35. Thomas AA, Arevalo-Perez J, Kaley T, Lyo J, Peck KK, Shi W, et al. Dynamic contrast enhanced T1 MRI perfusion differentiates pseudoprogression from recurrent glioblastoma. J Neurooncol. 2015 Oct;125(1):183–90.
36. Galldiks N, Dunkl V, Stoffels G, Hutterer M, Rapp M, Sabel M, et al. Diagnosis of pseudoprogression in patients with glioblastoma using O-(2-[18F]fluoroethyl)-L-tyrosine PET. Eur J Nucl Med Mol Imaging. 2015 Apr;42(5):685–95.
37. Yoon RG, Kim HS, Paik W, Shim WH, Kim SJ, Kim JH. Different diagnostic values of imaging parameters to predict pseudoprogression in glioblastoma subgroups stratified by MGMT promoter methylation. Eur Radiol. 2017 Jan;27(1):255–66.
38. Young RJ, Gupta A, Shah AD, Graber JJ, Zhang Z, Shi W, et al. Potential utility of conventional MRI signs in diagnosing pseudoprogression in glioblastoma. Neurology. 2011 May 31;76(22):1918–24.
39. Jang B-S, Jeon SH, Kim IH, Kim IA. Prediction of Pseudoprogression versus Progression using Machine Learning Algorithm in Glioblastoma. Sci Rep. 2018 Aug 21;8(1):12516.
40. Lee WJ, Choi SH, Park C-K, Yi KS, Kim TM, Lee S-H, et al. Diffusion-weighted MR imaging for the differentiation of true progression from pseudoprogression following concomitant radiotherapy with temozolomide in patients with newly diagnosed high-grade gliomas. Acad Radiol. 2012 Nov;19(11):1353–61.
41. Tsien C, Galbán CJ, Chenevert TL, Johnson TD, Hamstra DA, Sundgren PC, et al. Parametric response map as an imaging biomarker to distinguish progression from pseudoprogression in high-grade glioma. J Clin Oncol Off J Am Soc Clin Oncol. 2010 May 1;28(13):2293–9.
42. Kang H-C, Kim C-Y, Han JH, Choe GY, Kim JH, Kim JH, et al. Pseudoprogression in patients with malignant gliomas treated with concurrent temozolomide and radiotherapy: potential role of p53. J Neurooncol. 2011 Mar;102(1):157–62.
43. Yang I, Aghi MK. New advances that enable identification of glioblastoma recurrence. Nat Rev Clin Oncol. 2009 Nov;6(11):648–57.
44. Taal W, Brandsma D, de Bruin HG, Bromberg JE, Swaak-Kragten AT, Smitt PAES, et al. Incidence of early pseudo-progression in a cohort of malignant glioma patients treated with chemoirradiation with temozolomide. Cancer. 2008 Jul 15;113(2):405–10.
45. Roldán GB, Scott JN, McIntyre JB, Dharmawardene M, de Robles PA, Magliocco AM, et al. Population-based study of pseudoprogression after chemoradiotherapy in GBM. Can J Neurol Sci J Can Sci Neurol. 2009 Sep;36(5):617–22.
46. Gerstner ER, McNamara MB, Norden AD, Lafrankie D, Wen PY. Effect of adding temozolomide to radiation therapy on the incidence of pseudo-progression. J Neurooncol. 2009 Aug;94(1):97–101.
47. Kebir S, Rauschenbach L, Gielen GH, Schäfer N, Tzaridis T, Scheffler B, et al. Recurrent pseudoprogression in isocitrate dehydrogenase 1 mutant glioblastoma. J Clin

Neurosci Off J Neurosurg Soc Australas. 2018 Jul;53:255–8.
48. Ellingson BM, Wen PY, Cloughesy TF. Evidence and context of use for contrast enhancement as a surrogate of disease burden and treatment response in malignant glioma. Neuro-Oncol. 2018 27;20(4):457–71.
49. Bette S, Barz M, Huber T, Straube C, Schmidt-Graf F, Combs SE, et al. Retrospective Analysis of Radiological Recurrence Patterns in Glioblastoma, Their Prognostic Value And Association to Postoperative Infarct Volume. Sci Rep. 2018 Mar 14;8(1):4561.
50. Choi SH, Kim JW, Chang JS, Cho JH, Kim SH, Chang JH, et al. Impact of Including Peritumoral Edema in Radiotherapy Target Volume on Patterns of Failure in Glioblastoma following Temozolomide-based Chemoradiotherapy. Sci Rep. 2017 08;7:42148.
51. Huber T, Alber G, Bette S, Boeckh-Behrens T, Gempt J, Ringel F, et al. Reliability of Semi-Automated Segmentations in Glioblastoma. Clin Neuroradiol. 2017 Jun;27(2):153–61.
52. Yang D. Standardized MRI assessment of high-grade glioma response: a review of the essential elements and pitfalls of the RANO criteria. Neuro-Oncol Pract. 2016 Mar 1;3(1):59–67.
53. Pope WB, Hessel C. Response assessment in neuro-oncology criteria: implementation challenges in multicenter neuro-oncology trials. AJNR Am J Neuroradiol. 2011 May;32(5):794–7.
54. Wen PY, Chang SM, Van den Bent MJ, Vogelbaum MA, Macdonald DR, Lee EQ. Response Assessment in Neuro-Oncology Clinical Trials. J Clin Oncol Off J Am Soc Clin Oncol. 2017 Jul 20;35(21):2439–49.
55. Voss M, Franz K, Steinbach JP, Fokas E, Forster M-T, Filipski K, et al. Contrast enhancing spots as a new pattern of late onset pseudoprogression in glioma patients. J Neurooncol. 2019 Mar;142(1):161–9.
56. Wang M-Y, Cheng J-L, Han Y-H, Li Y-L, Dai J-P, Shi D-P. Measurement of tumor size in adult glioblastoma: classical cross-sectional criteria on 2D MRI or volumetric criteria on high resolution 3D MRI? Eur J Radiol. 2012 Sep;81(9):2370–4.
57. De Barros A, Attal J, Roques M, Nicolau J, Sol J-C, Cohen-Jonathan-Moyal E, et al. Impact on survival of early tumor growth between surgery and radiotherapy in patients with de novo glioblastoma. J Neurooncol. 2019 May;142(3):489–97.
58. Leitzen C, Wilhelm-Buchstab T, Schmeel LC, Garbe S, Greschus S, Müdder T, et al. MRI during radiotherapy of glioblastoma : Does MRI allow for prognostic stratification? Strahlenther Onkol Organ Dtsch Rontgengesellschaft Al. 2016 Jul;192(7):481–8.
59. van den Bent MJ, Vogelbaum MA, Wen PY, Macdonald DR, Chang SM. End point assessment in gliomas: novel treatments limit usefulness of classical Macdonald's Criteria. J Clin Oncol Off J Am Soc Clin Oncol. 2009 Jun 20;27(18):2905–8.
60. Delgado-López PD, Riñones-Mena E, Corrales-García EM. Treatment-related changes in glioblastoma: a review on the controversies in response assessment criteria and the concepts of true progression, pseudoprogression, pseudoresponse and radionecrosis. Clin Transl Oncol Off Publ Fed Span Oncol Soc Natl Cancer Inst Mex. 2018 Aug;20(8):939–53.
61. Elshafeey N, Kotrotsou A, Hassan A, Elshafei N, Hassan I, Ahmed S, et al. Multicenter study demonstrates radiomic features derived from magnetic resonance perfusion images identify pseudoprogression in glioblastoma. Nat Commun. 2019 Jul 18;10(1):3170.
62. Ismail M, Hill V, Statsevych V, Huang R, Prasanna P, Correa R, et al. Shape Features of the Lesion Habitat to Differentiate Brain Tumor Progression from Pseudoprogression on Routine Multiparametric MRI: A Multisite Study. AJNR Am J Neuroradiol. 2018 Dec;39(12):2187–93.
63. Galldiks N, Kocher M, Langen K-J. Pseudoprogression after glioma therapy: an update. Expert Rev Neurother. 2017 Nov;17(11):1109–15.
64. Masch WR, Wang PI, Chenevert TL, Junck L, Tsien C, Heth JA, et al. Comparison of

Diffusion Tensor Imaging and Magnetic Resonance Perfusion Imaging in Differentiating Recurrent Brain Neoplasm From Radiation Necrosis. Acad Radiol. 2016 May;23(5):569–76.
65. Shukla G, Alexander GS, Bakas S, Nikam R, Talekar K, Palmer JD, et al. Advanced magnetic resonance imaging in glioblastoma: a review. Chin Clin Oncol. 2017 Aug;6(4):40.
66. Hyare H, Thust S, Rees J. Advanced MRI Techniques in the Monitoring of Treatment of Gliomas. Curr Treat Options Neurol. 2017 Mar;19(3):11.
67. Neal ML, Trister AD, Ahn S, Baldock A, Bridge CA, Guyman L, et al. Response classification based on a minimal model of glioblastoma growth is prognostic for clinical outcomes and distinguishes progression from pseudoprogression. Cancer Res. 2013 May 15;73(10):2976–86.
68. Thust SC, van den Bent MJ, Smits M. Pseudoprogression of brain tumors. J Magn Reson Imaging JMRI. 2018 May 7;
69. Chaddad A, Kucharczyk MJ, Daniel P, Sabri S, Jean-Claude BJ, Niazi T, et al. Radiomics in Glioblastoma: Current Status and Challenges Facing Clinical Implementation. Front Oncol. 2019;9:374.
70. Hu LS, Yoon H, Eschbacher JM, Baxter LC, Dueck AC, Nespodzany A, et al. Accurate Patient-Specific Machine Learning Models of Glioblastoma Invasion Using Transfer Learning. AJNR Am J Neuroradiol. 2019 Mar;40(3):418–25.
71. Shaver MM, Kohanteb PA, Chiou C, Bardis MD, Chantaduly C, Bota D, et al. Optimizing Neuro-Oncology Imaging: A Review of Deep Learning Approaches for Glioma Imaging. Cancers. 2019 Jun;11(6):829.
72. Juan-Albarracín J, Fuster-Garcia E, García-Ferrando GA, García-Gómez JM. ONCOhabitats: A system for glioblastoma heterogeneity assessment through MRI. Int J Med Inf. 2019 Aug;128:53–61.
73. Zhang J, Yu H, Qian X, Liu K, Tan H, Yang T, et al. Pseudo progression identification of glioblastoma with dictionary learning. Comput Biol Med. 2016 01;73:94–101.

Table 1: General, clinical, histological, radiological, and dosimetric characteristics and RANO category

General characteristics				
	Total (n=57)	**TP (n=44)**	**PsP (n=13)**	**p value**
Age (years)				
Mean	61	62	57	0.366
Median	62	62	60	
Range	24-81	33-81	24-70	
Sex no. (%)				
Male	40 (70%)	31 (70%)	9 (69%)	1.000
Female	17 (30%)	13 (30%)	4 (31%)	
GBM location no. (%)				
Frontal	15 (26%)	9 (20%)	6 (46%)	0.587
Temporal	15 (26%)	14 (32%)	1 (8%)	
Parietal	9 (16%)	7 (16%)	2 (15%)	
Brainstem	1 (2%)	1 (2%)	0 (0%)	
Corpus callosum	1 (2%)	1 (2%)	0 (0%)	
Multi	17 (28%)	12 (28%)	4 (31%)	
Extent of surgery no. (%)				
Complete	18 (32%)	13 (30%)	5 (38%)	0.851
Partial	24 (42%)	19 (43%)	5 (38%)	
Biopsy	15 (26%)	12 (27%)	3 (23%)	
Interval between surgery and CRT (days)				
Mean	45.6	45.8	45.2	0.859
Median	45.0	45.5	42.0	
Range	19.0-69.0	19.0-69.0	28.0-68.0	
Corticosteroids before CRT no. (%)				
Yes	10 (18%)	8 (8%)	2 (15%)	1.000
Mean dose (mg)	58	58	68	
Range	(20-100)	(20-100)	(28-80)	
No	47 (82%)	36 (82%)	11 (85%)	
Anticonvulsants before CRT no. (%)				
Yes	22 (39%)	24 (55%)	11 (85%)	0.060
No	35 (61%)	20 (45%)	2 (15%)	
WHO performance status before CRT no. (%)				
0	9 (16%)	6 (14%)	3 (23%)	0.251
1-2	48 (84%)	38 (86%)	10 (77%)	
3-4	0 (0%)	0 (0%)	0 (0%)	
KPS status before CRT no. (%)				
90-100	27 (47%)	18 (41%)	9 (69%)	0.233
70-80	30 (53%)	26 (59%)	4 (31%)	
Corticosteroids at progression no. (%)				
Yes	30 (53%)	24 (55%)	6 (46%)	0.829
Mean dose (mg)	66	69	53	
Range	(20-120)	(20-120)	(20-80)	
No	27 (47%)	20 (45%)	7 (54%)	
Anticonvulsants at progression no. (%)				
Yes	29 (51%)	25 (57%)	4 (31%)	0.123
No	28 (49%)	19 (43%)	9 (69%)	
WHO performance status at progression no. (%)				
0	9 (16%)	6 (14%)	3 (23%)	0.932
1-2	40 (70%)	31 (70%)	9 (69%)	
3-4	8 (14%)	7 (16%)	1 (8%)	
KPS status at progression no. (%)				
90-100	15 (26%)	9 (20%)	6 (46%)	0.172
70-80	30 (53%)	25 (57%)	5 (38%)	
≤60	12 (21%)	10 (23%)	2 (15%)	
Number of TMZ cycles at the time of progression no. (%)				0.961

0 -3	38 (67%)	28 (64%)	10 (77%)	
4-6	19 (33%)	16 (36%)	3 (23%)	
Mean	3	3	3	
Median	3	3	3	
Range	0-6	0-6	0-6	
Type of treatment at the time of progression no. (%)				
Support care	1 (2%)	1 (2%)	0 (0%)	0.797
TMZ	40 (70%)	30 (68%)	10 (77%)	
No treatment (follow up)	16 (28%)	13 (30%)	3 (28%)	
MRI follow-up number at progression no. (%)				
1	35 (61%)	25 (57%)	10 (77%)	0.513
2-3	13 (23%)	11 (25%)	2 (15%)	
>3	9 (16%)	8 (18%)	1 (8%)	
Interval between end of CRT and progression (weeks)				
Mean	23.6	25.2	18.3	
Median	13.4	14.4	13.4	
Range	-1.3-82.6	-1.3-82.6	12.0-56.4	0.746
<12 weeks	11 (19%)	11 (25%)	0 (0%)	
12-24 weeks	28 (49%)	17 (39%)	11 (84%)	
24-48 weeks	9 (16%)	8 (18%)	1 (8%)	
>48 weeks	9 (16%)	8 (18%)	1 (8%)	
Histological characteristics				
MGMT promotor methylation status no. (%)				
Methylated	25 (44%)	17 (39%)	8 (61%)	**0.044**
Unmathylated	31 (54%)	27 (61%)	4 (31%)	
Unknown	1 (2%)	0 (0%)	1 (8%)	
IDH Mutation no. (%)				
Wildtype	53 (92%)	42 (96%)	11 (84%)	0.221
Mutated	2 (4%)	1 (2%)	1 (8%)	
Unknown	2 (4%)	1 (2%)	1 (8%)	
Ki67 index (%)				
Mean	30%	30%	35%	
Median	20%	20%	35%	0.590
Range	10%-60%	10%-60%	20%-50%	
Unknown	38	27	11	
Tumor cells proportion (ù)				
Mean	60%	60%	60%	
Median	70%	70%	60%	0.600
Range	10%-100%	10%-100%	40%-90%	
Unknown	6 (11%)	4 (9%)	2 (15%)	
TP53 overexpression no. (%)				
≤10%	44 (77%)	35 (79%)	9 (70%)	0.569
>10%	8 (14%)	6 (14%)	2 (15%)	
Unknown	5 (9%)	3 (7%)	2 (15%)	
ATRX mutation no. (%)				
Yes	2 (4%)	0 (0%)	2 (15%)	**0.043**
No	47 (82%)	38 (86%)	9 (70%)	
Unknown	8 (14%)	6 (14%)	2 (15%)	
EGFR amplification no. (%)				
Yes	32 (56%)	25 (57%)	7 (54%)	1.000
No	16 (28%)	12 (28%)	4 (31%)	
Unknown	9 (16%)	7 (15%)	2 (15%)	
Radiological characteristics				
Mass effect before CRT				
Yes	39 (68%)	31 (70%)	8 (62%)	0.789
No	18 (32%)	13 (30%)	5 (38%)	
Contrast enhancement before CRT				
Homogeneous	7 (12%)	6 (14%)	1 (8%)	1.000
Non homogeneous	50 (88%)	38 (86%)	12 (92%)	
Sharp demarcation before CRT				
Yes	47 (82%)	37 (84%)	10 (77%)	0.680

No	10 (18%)	7 (16%)	3 (23%)	
Dura contact before CRT				
Yes	47 (82%)	35 (80%)	12 (92%)	0.426
No	10 (18%)	9 (20%)	1 (8%)	
Ventricle contact before CRT				
Yes	32 (56%)	27 (61%)	5 (38%)	0.253
No	25 (44%)	17 (39%)	8 (62%)	
Ependymal propagation before CRT				
Yes	24 (58%)	21 (48%)	3 (23%)	0.200
No	33 (42%)	23 (52%)	10 (77%)	
Number of CEL before CRT no. (%)				
1	48 (84%)	36 (82%)	12 (92%)	
2	5 (9%)	5 (11%)	0 (0%)	0.673
3	4 (7%)	3 (7%)	1 (8%)	
4	0 (0%)	0 (0%)	0 (0%)	
Number of NEC before CRT no. (%)				
0	16 (28%)	11 (25%)	5 (38%)	
1	37 (65%)	29 (66%)	8 (62%)	0.526
2	4 (7%)	4 (9%)	0 (0%)	
3	0 (0%)	0 (0%)	0 (0%)	
Mass effect at progression				
Yes	41 (72%)	32 (73%)	9 (69%)	1.000
No	16 (28%)	12 (27%)	4 (31%)	
Contrast enhancement at progression				
Homogeneous	7 (12%)	6 (14%)	1 (8%)	1.000
Non homogeneous	50 (88%)	38 (86%)	12 (92%)	
Sharp demarcation at progression				
Yes	47 (82%)	35 (80%)	12 (92%)	0.426
No	10 (18%)	9 (20%)	1 (8%)	
Dura contact at progression				
Yes	46 (81%)	34 (77%)	12 (92%)	0.426
No	11 (19%)	10 (23%)	1 (8%)	
Ventricle contact at progression				
Yes	42 (74%)	34 (77%)	8 (62%)	0.439
No	15 (26%)	10 (23%)	5 (38%)	
Ependymal propagation at progression				
Yes	38 (67%)	31 (70%)	7 (54%)	0.435
No	19 (33%)	13 (30%)	6 (46%)	
Number of CEL at progression no. (%)				
1	37 (65%)	27 (61%)	10 (77%)	
2	10 (18%)	7 (16%)	3 (23%)	0.186
3	7 (12%)	7 (16%)	0 (0%)	
4	3 (5%)	3 (7%)	0 (0%)	
Number of NEC at progression no. (%)				
0	10 (17%)	7 (16%)	3 (23%)	
1	41 (72%)	31 (70%)	10 (77%)	0.791
2	4 (7%)	4 (9%)	0 (0%)	
3	2 (4%)	2 (5%)	0 (0%)	
Number of new CEL at progression no. (%)				
0	43 (75%)	32 (73%)	11 (85%)	
1	9 (16%)	7 (16%)	2 (15%)	0.331
2	3 (5%)	3 (7%)	0 (0%)	
3	2 (4%)	2 (4%)	0 (0%)	
Progression no. (%)				
Unifocal	34 (60%)	24 (56%)	10 (77%)	0.204
Multifocal	23 (40%)	20 (45%)	3 (23%)	
Progression no. (%)				
Local	49 (86%)	36 (82%)	13 (100%)	0.177
Distant	8 (14%)	8 (18%)	0 (0%)	
Radiation therapy and dosimetry characteristic				
Radiotherapy technique no. (%)				
3D	25 (44%)	20 (45%)	5 (38%)	0.898
IMRT	32 (56%)	24 (55%)	8 (62%)	
CTV volume (cm^3)				0.618
Mean	165.2	159.7	184.1	

Median	169.1	169.3	165.5	
Range	59.5-388.0	61.9-388.0	59.5-337.4	
PTV volume (cm^3)				
Mean	229.7	222.9	252.9	0.504
Median	233.0	231.6	248.3	
Range	88.5-510.8	88.5-510.8	92.0-441.5	
V80% GTV_{GADOP} (%)				
Mean	98.2	97.7	100.	
Median	100.0	100.0	100.00	**0.023**
Range	65.2-100.0	65.2-100.0	100.0-100.0	
N outside isodose 80%-Mean V80%	14 (25%)-92.9	14 (32%)-92.9	0	
Dmin GTV_{GADOP} (Gy)				
Mean	46.7	43.7	56.9	**0.017**
Median	58.0	56.0	58.7	
Range	1.1-61.8	1.1-59.7	43.1-61.8	
V80% GTV_{FLAIRP} (%)				
Mean	89.7	87.9	95.6	0.080
Median	96.9	94.2	99.4	
Range	49.2-100.0	49.2-100.0	81.8-100.0	
Dmin GTV_{FLAIRP} (Gy)				
Mean	28.0	26.2	34.1	0.189
Median	23.2	21.1	36.5	
Range	1.1-60.3	1.1-59.1	1.7-60.3	
Progression GTV_{FLAIRP} in the isodose 80% no. (%)				0.263
Yes	17 (30%)	11 (25%)	6 (46%)	
No	40 (70%)	33 (75%)	7 (54%)	
V80% CEL_P (%)				
Mean	96.9	96.0	100.0	
Median	100.0	100.0	100.0	**0.039**
Range	47.6-100.0	47.6-100.0	100.0-100.0	
N outside isodose 80%-Mean V80%	12 (21%)-85.53	12 (27%)-85.53	0	
Dmin CEL_P (Gy)				
Mean	49.7	47.4	57.2	**0.029**
Median	58.7	58.1	59.2	
Range	1.0-61.9	1.0-59.8	45.0-61.9	
RANO criteria				
Clinical deterioration at progression no. (%)				0.123
Yes	29 (51%)	25 (57%)	4 (31%)	
No	28 (49%)	19 (43%)	9 (69%)	
WHO performance status no. (%)				0.343
PD	26 (46%)	22 (50%)	4 (31%)	
CR/PR/SD	31 (54%)	22 (50%)	9 (69%)	
KPS status no. (%)				0.510
PD	19 (33%)	16 (36%)	3 (23%)	
CR/PR/SD	38 (67%)	28 (64%)	10 (77%)	
Corticosteroids no. (%)				0.814
PD	26 (46%)	21 (48%)	5 (38%)	
PR/SD	6 (10%)	5 (11%)	1 (8%)	
CR	25 (44%)	18 (41%)	7 (54%)	
New lesions no. (%)				0.304
Yes	17 (30%)	15 (34%)	2 (15%)	
No	40 (70%)	29 (66%)	11 (85%)	
Progression CEL in isodose 80% no. (%)				0.051
Yes	45 (79%)	32 (73%)	13 (100%)	
No	12 (21%)	12 (27%)	0 (0%)	
2D CEL size evolution no. (%)				0.703
CR	1 (2%)	1 (2%)	0 (0%)	
PR	2 (4%)	1 (2%)	1 (8%)	
SD	24 (42%)	19 (43%)	5 (38%)	
PD	30 (52%)	23 (53%)	7 (54%)	
CV CEL size evolution no. (%)				0.752
CR	1 (2%)	1 (2%)	0 (0%)	
PR	3 (5%)	2 (5%)	1 (8%)	
SD	23 (40%)	17 (39%)	6 (46%)	

PD	30 (53%)	24 (54%)	6 (46%)	
MV CEL size evolution no. (%)				
CR	1 (2%)	1 (2%)	0 (0%)	0.482
SD	19 (33%)	13 (30%)	6 (46%)	
PD	37 (65%)	30 (68%)	7 (54%)	
2D GTV_{FLAIR} size evolution no. (%)				
Increase	45 (79%)	34 (77%)	11 (85%)	0.713
Decrease	12 (21%)	10 (23%)	2 (15%)	
CV GTV_{FLAIR} size evolution no. (%)				
Increase	46 (81%)	36 (82%)	10 (77%)	0.700
Decrease	11 (19%)	8 (18%)	3 (23%)	
MV GTV_{FLAIR} size evolution no. (%)				
Increase	49 (86%)	39 (89%)	10 (77%)	0.365
Decrease	8 (14%)	5 (11%)	3 (33%)	
Progression occurring within 12 weeks after CRT no. (%)				0.053
Yes	11 (19%)	11 (25%)	0 (0%)	
No	46 (81%)	33 (75%)	13 (100%)	
RANO 2D conclusion no. (%)				
PD	39 (68%)	28 (64%)	11 (85%)	0.191
SD	18 (32%)	16 (36%)	2 (15%)	
RANO CV conclusion no. (%)				
PD	40 (70%)	29 (66%)	11 (85%)	0.304
SD	17 (30%)	15 (34%)	2 (15%)	
RANO MV conclusion no. (%)				
PD	41 (72%)	30 (85%)	11 (68%)	0.313
SD	16 (28%)	14 (15%)	2 (32%)	

ATRX: Alpha-Thalassemia/mental Retardation syndrome X-linked, **CEL:** contrast enhanced lesion, **CR:** Complete Response, **CRT:** Chemoradiotherapy, **CTV:** Clinical Target Volume, **CV:** Calculated Volume, **EGFR:** Epidermal Growth Factor Receptor, **GBM:** Glioblastoma, **GTV:** Gross Target Volume, **IDH:** Isocitrate Deshydrogenase, **IMRT:** Intensity Modulated Radiation Therapy, **KPS:** Karnofsky Performance Status, **MGMT:** Methylguanine-Methyltransferase, **MV:** Measured Volume, **NEC:** Necrosis Area, **PD:** Progressive Disease, **PR:** Partial Response, **PTV:** Planning Target Volume, **SD:** Stable Disease, **TMZ:** Temozolomide, **TP53:** Tumor Protein 53, **WHO:** World Health Classification

Table 2: 2D, CV and MV size of GTV_{GADO}, GTV_{FLAIR} , CEL, and NEC and evolution between dosimetric and progression MRIs

Radiological characteristics	Dosimetric MRI characteristics				Progression MRI characteristics				Lesion size evolution: Dosimetric MRI versus progression MRI (%)				
	Total (n=57)	TP (n=44)	PsP (n=13)	p value	Total (n=57)	TP (n=44)	PsP (n=13)	p value		Total (n=57)	TP (n=44)	PsP (n=13)	p value
GTV_{GADO} 2D size (cm^2)									**GTV_{GADO} 2D**				
Mean	23.9	22.9	27.1		35.3	35.0	36.4		**Mean**	67.5	67.9	66.1	
Median	21.1	20.4	23.9	0.391	33.5	34.1	31.0	0.808	**Median**	53.2	58.6	49.6	0.529
Range	4.3-54.5	4.3-54.5	7.7-54.5		1.9-80.5	1.9-80.5	14.9-72.5		**Range**	-87.0-412.3	-87.0-218.9	-25.0-412.3	
									Decrease no. (%)	13 (23%)	10 (23%)	3 (23%)	
GTV_{GADO} CV size (cm^3)									**GTV_{GADO} CV**				
Mean	54.7	53.4	59.3		62.2	65.3	51.9		**Mean**	42.1	55.4	-3.2	
Median	47.0	43.9	57.4	0.714	55.6	59.3	29.6	0.332	**Median**	2.8	17.6	-22.5	0.118
Range	5.1-145.0	5.1-145.0	13.3-126.7		1.20145.8	1.2-145.8	11.0-122.0		**Range**	-96.4-479.2	-96.4-479.2	-77.5-157.8	
									Decrease no. (%)	26 (46%)	18 (41%)	8 (62%)	
GTV_{GADO} MV(cm^3)									**GTV_{GADO} MV**				
Mean	42.8	41.2	48.2		52.4	53.9	47.2		**Mean**	51.8	54.5	42.4	
Median	36.4	35.9	40.2	0.628	53.3	55.1	32.1	0.667	**Median**	22.0	23.0	5.7	0.430
Range	4.1-107.9	4.1-105.1	8.4-107.9		1.0-128.2	1.0-128.2	16.0-84.8		**Range**	-95.3-424.0	-95.3-323.6	-60.0-424.0	
									Decrease no. (%)	20 (35%)	14 (32%)	6 (46%)	
GTV_{FLAIR} 2D size (cm^2)									**GTV_{FLAIR} 2D**				
Mean	40.4	41.2	37.9		60.2	62.7	51.5		**Mean**	64.7	66.8	57.7	
Median	36.8	37.9	33.8	0.659	56.7	60.0	48.8	0.255	**Median**	30.4	32.1	26.7	0.814
Range	6.1-115.2	14.8-115.2	6.1-83.1		13.1-150.3	13.8-150.3	13.1-105.3		**Range**	-54.9-265.5	-36.4-265.5	-54.9-261.6	
									Decrease no. (%)	13 (23%)	11 (25%)	2 (15%)	
GTV_{FLAIR} CV size (cm^3)									**GTV_{FLAIR} CV**				
Mean	129.7	134.8	112.5		228.7	243.3	179.4		**Mean**	109.7	112.4	100.9	
Median	94.5	93.1	95.8	0.631	200.2	206.6	144.2	0.158	**Median**	51.7	59.5	32.5	0.464
Range	13.7-505.4	31.1-505.4	13.7-296.1		30.7-722.9	36.5-722.9	30.7-441.5		**Range**	-57.3-568.2	-29.1-568.2	-57.3-494.1	
									Decrease no. (%)	10 (18%)	7 (16%)	3 (23%)	
GTV_{FLAIR} MV (cm^3)									**GTV_{FLAIR} MV**				
Mean	95.9	98.5	86.9		168.8	180.5	129.3		**Mean**	112.0	122.3	77.3	
Median	73.4	71.0	86.4	0.800	146.3	165.7	130.8	0.164	**Median**	53.3	56.3	28.8	0.216
Range	13.6-339.3	19.1-339.3	13.6-176.8		21.3-520.2	26.0-520.2	21.3-330.3		**Range**	-67.1-899.3	-31.5-899.3	-67.1-428.7	
									Decrease no. (%)	10 (18%)	7 (16%)	3 (15%)	
Sum of CEL size 2D (ML) (cm^2)									**CEL 2D (ML)**				
Mean	17.4	17.0	18.7		20.2	20.3	20.1		**Mean**	39.8	48.0	12.2	
Median	16.6	15.5	17.8	0.686	17.5	18.4	14.2	0.873	**Median**	10.3	10.4	8.5	0.506
Range	2.7-51.9	3.5-51.9	2.7-44.22		1.9-50.8	1.9-50.8	1.9-48.0		**Range**	-78.8-519.9	-78.8-519.9	-71.6-117.4	
									Decrease no. (%)	24 (42%)	18 (41%)	6 (46%)	
Sum of CEL size CV (ML) (cm^3)									**CEL CV (ML)**				
Mean	37.1	36.5	39.4		46.1	47.0	42.9		**Mean**	90.8	112.4	17.7	
Median	26.7	26.0	28.5	0.566	31.0	33.2	27.1	0.844	**Median**	22.7	16.3	22.7	0.414
Range	2.5-167.7	2.5-167.7	3.2-106.0		0.7-159.6	1.250.7-159.6	1.0-103.9		**Range**	-92.1-1262.6	-89.9-1262.6	-92.1-216.7	
									Decrease no. (%)	25 (44%)	19 (43%)	6 (46%)	
Sum of CEL size MV (ML) (cm^3)									**CEL MV (ML)**				
Mean	12.7	13.0	11.5		18.3	18.8	16.7		**Mean**	87.9	99.1	49.8	
Median	9.2	9.0	12.2	0.849	11.5	12.5	10.4	0.785	**Median**	40.5	45.5	11.8	0.537
Range	1.2-66.0	1.2-66.0	1.5-36.4		0.3-60.7	0.3-60.7	1.0-52.8		**Range**	-87.0-819.2	-87.0-819.0	-80.0-331.1	
									Decrease no. (%)	20 (35%)	14 (32%)	6 (46%)	
Sum of CEL size 2D (all) (cm^2)									**CEL 2D (all)**				
Mean	17.4	17.0	18.7		20.4	20.5	20.1		**Mean**	40.3	48.4	13.1	
Median	16.6	15.5	17.8	0.686	17.5	18.4	14.2	0.800	**Median**	10.3	10.4	8.5	0.556
Range	2.7-51.9	3.5-51.9	2.7-44.2		1.9-50.8	1.9-50.8	2.6-48.0		**Range**	-78.8-519.9	-78.8-519.9	-71.6-117.4	
Sum of CEL size CV (all) (cm^3)									**CEL CV (all)**				
Mean	37.1	36.5	39.4		46.16	47.1	42.9		**Mean**	89.8	111.1	17.9	
Median	26.7	26.0	28.5	0.566	31.03	33.2	27.1	0.829	**Median**	22.7	16.3	22.7	0.458
Range	2.5-167.7	2.5-167.7	3.3-106.0		1.09-159.57	1.1-159.6	1.4-104.0		**Range**	-93.0-1262.6	-93.0-1262.6	-89.0-216.7	

Sum of CEL size MV (all) (cm^3)									**CEL MV (all)**				
Mean	12.7	13.0	11.5	0.849	18.4	18.9	16.7	0.771	**Mean**	87.9	98.8	50.7	0.614
Median	9.2	9.0	12.2		12.3	12.9	10.4		**Median**	40.5	45.5	11.8	
Range	1.2-66.0	1.2-66.0	1.5-36.4		0.7-60.7	0.7-60.7	1.4-52.8		**Range**	-85.7-819.2	-85.7-819.2	-80.0-331.1	
Sum of NEC size 2D (cm^2)									**NEC 2D**				
Mean	7.8	7.6	8.7	0.484	9.6	10.5	6.4	0.147	**Mean**	84.3	110.6	-18.4	**0.041**
Median	3.5	3.9	2.4		6.5	7.2	4.4		**Median**	0.00	9.3	-18.8	
Range	0.0-42.2	0.0-42.2	0.0-37.0		0.0-40.3	0.0-40.3	0.0-26.8		**Range**	-100.0-1297.1	-100.0-1297.1	-100.0-89.3	
									Appearance no. (%)	8 (14%)	5 (11%)	3 (23%)	
									Decrease no. (%)	19 (33%)	13 (30%)	6 (46%)	
Sum of NEC size CV (cm^3)									**NEC CV**				
Mean	15.4	14.9	17.4	0.520	19.5	22.0	11.3	0.153	**Mean**	204.4	262.1	-20.7	**0.024**
Median	3.6	4.7	3.2		9.9	13.2	5.5		**Median**	0.0	20.1	-32.8	
Range	0.0-128.2	0.0-128.2	0.0-85.8		0.0-106.6	0.0-106.6	0.0-50.3		**Range**	-100.0-3520.9	-100.0-3520.9	-100.0-75.2	
									Appearance no. (%)	8 (14%)	5 (11%)	3 (23%)	
									Decrease no. (%)	17 (30%)	11 (25%)	6 (46%)	
Sum of NEC size MV (cm^3)									**NEC MV**				
Mean									**Mean**	279.7	354.8	-13.1	
Median	5.9	5.9	5.7	0.584	8.8	9.9	5.3	0.208	**Median**	0.7	12.5	-16.9	0.052
Range	1.5	1.5	1.6		3.6	4.5	2.7		**Range**	-100.0-4105.6	-100.0-4105.6	-100.0-71.0	
	0.0-39.8	0.0-39.8	0.0-29.2		0.0-42.4	0.0-42.4	0.0-19.4		**Appearance no. (%)**	8 (14%)	5 (11%)	3 (23%)	
									Decrease no. (%)	14 (25%)	9 (20%)	5 (38%)	
Proportion of CEL in (CEL+NEC) 2D (%)									**Proportion of CEL in (CEL+NEC) 2D evolution (%)**				
Mean	76.2	75.3	79.0	0.591	74.5	73.2	78.9	0.208	**Mean**	-1.7	-2.2	-0.0	0.701
Median	77.6	73.2	83.1		73.1	71.8	76.0		**Median**	0.0	-1.1	0.0	
Range	32.0-100.0	32.0-100.0	49.4-100.0		39.5-100.0	39.5-100.0	59.9-100.0		**Range**	-40.7-34.5	-40.7-34.5	-31.9-26.3	
Proportion of CEL in (CEL+NEC) CV (%)									**Proportion of CEL in (CEL+NEC) CV evolution (%)**				
Mean	80.2	79.5	82.7	0.520	77.5	76.0	82.6	0.188	**Mean**	-2.7	-3.5	-0.1	0.546
Median	82.7	81.7	91.4		78.2	76.1	79.4		**Median**	-1.0	-2.0	0.0	
Range	24.6-100.0	24.6-100.0	49.9-100.0		26.5-100.0	26.5-100.0	64.5-100.0		**Range**	-61.9-45.9	-61.9-45.9	-25.3-28.6	
Proportion of CEL in (CEL+NEC) MV (%)									**Proportion of CEL in (CEL+NEC) MV evolution (%)**				
Mean	78.2	77.7	80.1	0.527	76.1	74.4	81.8	0.182	**Mean**	-2.1	-3.3	1.7	0.487
Median	77.2	77.2	77.2		76.0	74.0	79.7		**Median**	0.0	-0.0	0.9	
Range	31.9-100.0	31.9-100.0	37.7-100.0		19.4-100.0	19.4-100.0	65.2-100.0		**Range**	-74.4-42.1	-74.4-32.8	-34.8-42.1	
Proportion of NEC in (CEL+NEC) 2D (%)									**Proportion of NEC in (CEL+NEC) 2D evolution (%)**				
Mean	23.9	24.7	21.1	0.591	25.5	26.8	21.1	0.208	**Mean**	1.7	2.2	0.0	0.701
Median	22.4	26.8	16.9		26.9	28.2	24.0		**Median**	0.0	1.1	0.0	
Range	0.0-68.0	0.0-68.0	0.0-50.6		0.0-60.5	0.0-60.5	0.0-40.1		**Range**	-34.5-40.6	-34.5-40.6	-26.3-31.9	
Proportion of NEC in (CEL+NEC) CV (%)									**Proportion of NEC in (CEL+NEC) CV evolution (%)**				
Mean	19.8	20.5	17.3	0.520	22.5	24.0	17.4	0.188	**Mean**	2.7	3.5	0.1	0.546
Median	17.3	18.3	8.6		21.8	24.0	20.6		**Median**	1.0	2.0	0.0	
Range	0.0-75.4	0.0-75.4	0.0-50.1		0.0-73.5	0.0-73.5	0.0-35.6		**Range**	-45.9-61.9	-45.9-61.9	-28.6-25.3	
Proportion of NEC in (CEL+NEC) MV (%)									**Proportion of NEC in (CEL+NEC) MV evolution (%)**				
Mean	21.8	22.3	19.9	0.527	23.9	25.6	18.3	0.182	**Mean**	2.1	3.3	-1.7	0.450
Median	22.8	22.8	22.8		24.0	26.0	20.3		**Median**	0.0	-32.8-74.4	-0.9	
Range	0.0-68.1	0.0-68.1	0.0-62.3		0.0-80.6	0.0-80.6	0.0-34.8		**Range**	-42.1-74.4		-42.1-34.8	
									Monthly growth rate of GTV_{GADO} (%)				
									Mean	62.6	67.0	47.5	0.295
									Median	50.2	52.8	40.7	
									Range	3.5-319.8	3.5-319.8	17.3-122.8	
									Monthly growth rate of GTV_{FLAIR} (%)				0.230

									Mean **Median** **Range**	79.7 53.1 1.4-495.7	87.0 56.1 1.4-495.7	55.1 44.4 16.5-151.6	
									Monthly growth rate of CEL (ML) (%) **Mean** **Median** **Range**	 65.8 41.9 9.1-509.6	 71.6 43.3 9.1-509.6	 46.4 41.4 17.9-115.1	0.457
									Monthly growth rate of CEL (all) (%) **Mean** **Median** **Range**	 67.2 43.7 9.1-509.6	 73.2 44.1 9.1-509.6	 46.7 41.4 18.5-115.1	0.371
									Monthly growth rate of NEC (%) **Mean** **Median** **Range**	 80.5 34.1 -8.3-722.6	 93.6 40.7 -8.3-722.6	 25.0 24.4 -8.3-42.4	0.070

CEL: contrast enhanced lesion; **CV**: Calculated Volume; **MV**: Measured Volume; **NEC:** Necrosis Area

Table 3: True progression (TP) and pseudoprogression (PsP) groups:
A: progression MRI versus MRI following progression MRI
B: RANO category versus MRI following progression MRI

A		Following MRI		
		TP	PsP	Total
Progression MRI	TP	31	2	33
	PsP	13	11	24
	Total	44	13	57
B		**Following MRI**		
		TP	**PsP**	**Total**
RANO	PD	28	11	39
	SD	16	2	18
	Total	44	13	57

Table 4: Predictive factors of PsP in univariate and multivariate analysis

Univariate analysis	Univariate analysis p value	Multivariate analysis p value
KPS status at the time of the progression MRI	0.172	-
Epilepsy at the time of the dosimetric MRI	**0.042**	-
Evolution of epilepsy between the dosimetric MRI and the progression MRI	**0.032**	0.999
Anticonvulsant drugs at the time of the dosimetric MRI	0.060	-
Anticonvulsant drugs at the time of the progression MRI	0.123	-
Clinical deterioration between the dosimetric MRI and the progression MRI	0.123	0.157
MGMT promotor methylation status	**0.044**	0.256
ATRX mutation status	**0.043**	0.999
Ependymal propagation at the time of the dosimetric MRI	0.200	0.286
Local/ distant progression	0.177	-
Number of CEL_P	0.186	**0.035**
CV GTV_{FLAIRP} size	0.158	0.703
MV GTV_{FLAIRP} size	0.164	-
2D NEC_P size	0.147	-
CV NEC_P size	0.143	-
CV GTV_{GADO} size evolution between the dosimetric MRI and the progression MRI	0.118	-
2D NEC size evolution between the dosimetric MRI and the progression MRI	**0.041**	-
CV NEC size evolution between the dosimetric MRI and the progression MRI	**0.024**	-
MV NEC size evolution between the dosimetric MRI and the progression MRI	0.052	-
Proportion of CV CEL_P in (CEL_P+NEC_P)	0.188	0.488
Proportion of MV CEL_P in (CEL_P+NEC_P)	0.182	-
Proportion of CV NEC_P in (CEL_P+NEC_P)	0.188	-
Proportion of MV NEC_P in (CEL_P+NEC_P)	0.182	-
Monthly growth rate of NEC	0.070	-
$V_{80\%}$ GTV_{GADOP}	**0.023**	-
D_{min} GTV_{GADOP}	**0.017**	-
$V_{80\%}$ GTV_{FLAIRP}	0.080	**0.027**
D_{min} GTV_{FLAIRP}	0.189	-
$V_{80\%}$ CEL_P	**0.039**	0.995
D_{min} CEL_P	**0.029**	-
CEL_P in the 80% isodose (yes/no)	0.051	-
Progression occurring within the 12 weeks after CRT	0.053	-
2D RANO classification	0.191	**0.019**

ATRX: Alpha-Thalassemia/mental Retardation syndrome X-linked; **CEL:** contrast enhanced lesion; **CRT**: Chemoradiotherapy; **CV**: Calculated Volume; **MGMT**: Methylguanine-Methyltransferase; **MV**: Measured Volume**; NEC:** Necrosis Area

Figure 1: 2D, CV and MV tumor size evolution in TP and PsP groups between dosimetric MRI and progression MRI

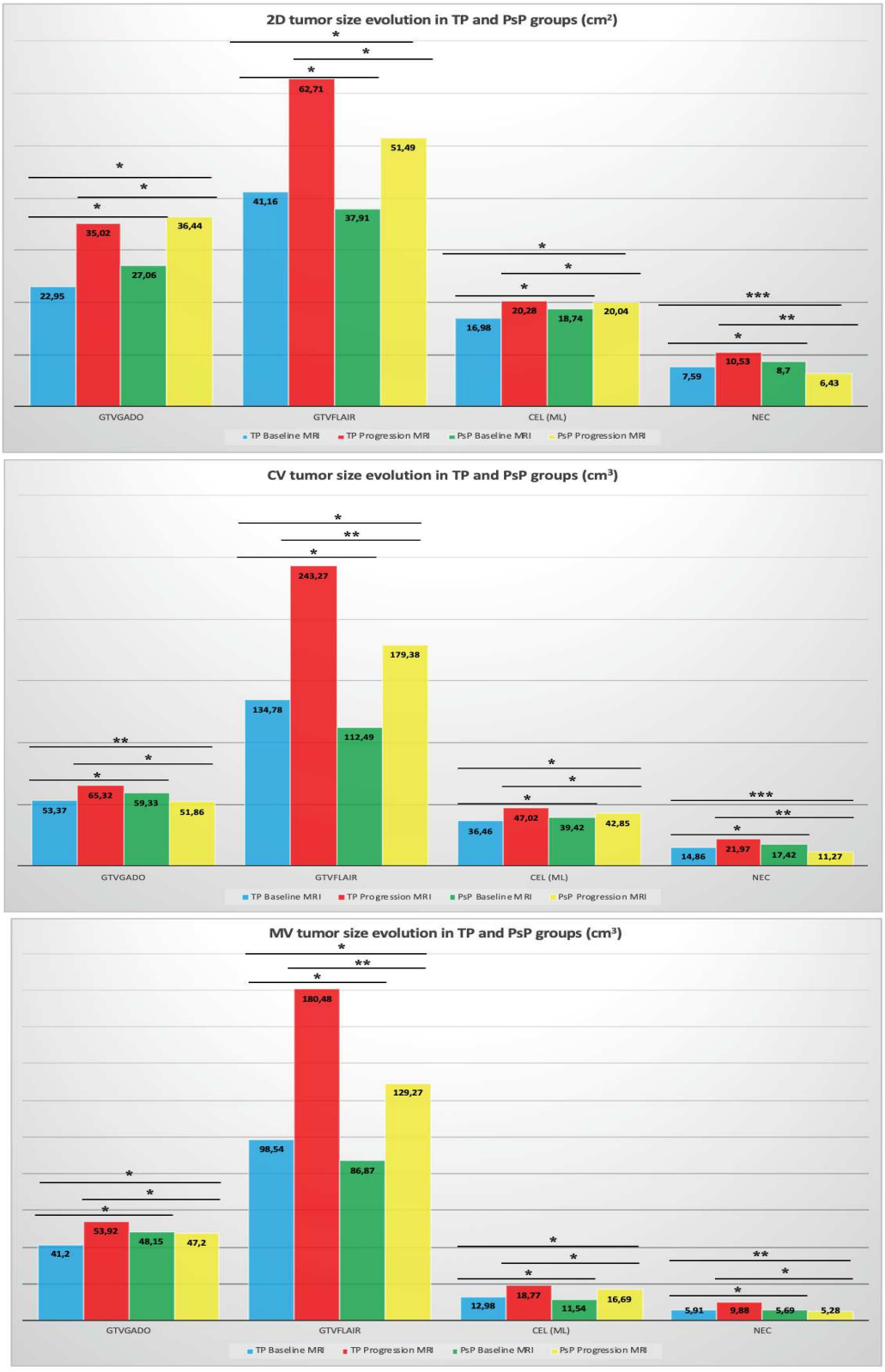

CV: Calculated Volume; **MV**: Measured Volume; **PsP**: Pseusoprogression; **TP**: True Progression
*: p value>0.200; **: p value>0.050; ***: p value<0.050

Figure 2: Matrix of correlation with the following criteria

For clinical characteristics: the KPS status at the time of progression MRI (p=0.172), the epilepsy status at the time of the dosimetric MRI (p=0.042) and the epilepsy evolution between the dosimetric MRI and the progression MRI (p=0.032), the anticonvulsants consumption at the time of the dosimetric MRI (p=0.060) and at the progression MRI (p=0.123), the clinical deterioration between the dosimetric MRI and the progression MRI (p=0,123).

For histological characteristics: MGMT promotor methylation status (p=0.044) and ATRX mutation status (p=0.043).

For radiological characteristics: the ependymal propagation at the time of the dosimetric MRI (p=0.200), the local or distant progression features (p=0.177) and the number of CEL_P (p=0.186), the CV (p=0.158) and MV (p=0.164) GTV_{FLAIRP} size, the 2D (p=0.147) and CV (p=0.153) NEC_P size, the evolution of the CV GTV_{GADO} (p=0.118), of the 2D (p=0.041), CV (p=0.024) and MV (p=0.052) NEC between the dosimetric MRI and the progression MRI, the proportion of CV (p=0.188) and MV (p=0.182) NEC_P in (CEL_P+NEC_P) and the proportion of CV (p=0.188) and MV (p=0.182) CEL_P in (CEL_P+NEC_P) and the monthly growth rate of NEC (p=0.07).

For dosimetric data: the $V_{80\%}$ of GTV_{GADOP} (p=0.023), GTV_{FLAIRP} (p=0.080) and CEL_P (p=0.039), the D_{min} of GTV_{GADOP} (p=0.017), GTV_{FLAIRP} (p=0.189) and CEL_P (p=0.029), the CEL_P in 80% isodose or not (p=0.049).

For RANO data: the 2D RANO classification (p=0.191) and the progression occurring within the 12 weeks after CRT or not (p=0.053).

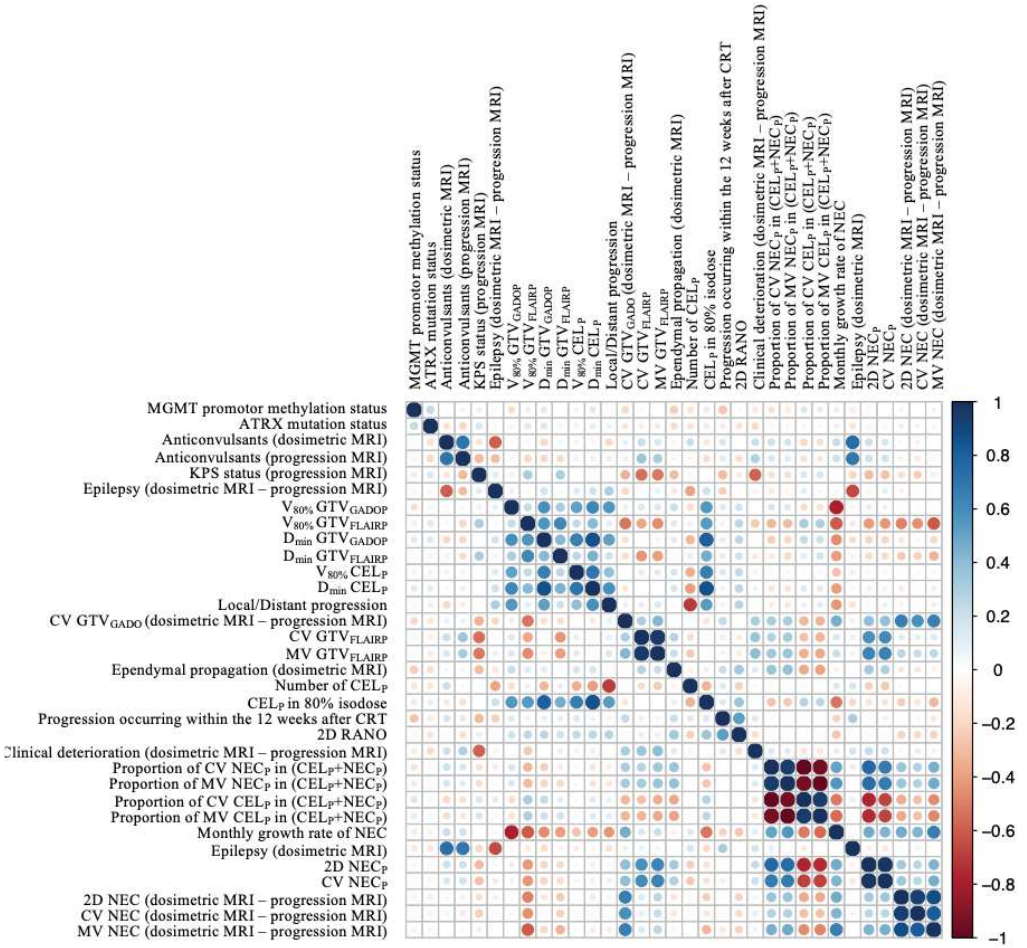

ATRX: Alpha-Thalassemia/mental Retardation syndrome X-linked; **CEL:** contrast enhanced lesions**; CV**: Calculated Volume; **KPS**: Karnofsky Performance Status; **MGMT**: Methylguanine-Methyltransferase; **MV**: Measured Volume; **NEC:** Necrosis Area

Figure 3: Overall survival (OS) and time to progression (TTP) in months in true progression (TP) and pseudoprogression (PsP) groups
A: OS since the date of diagnosis in the general population
B: OS since the date of diagnosis in TP and PsP groups
C: TTP since the date of diagnosis in the general population
D: TTP since the date of diagnosis in TP and PsP groups
E: OS since the date of diagnosis in the TP/PD, TP/SD, PsP/PD and PsP/SD groups

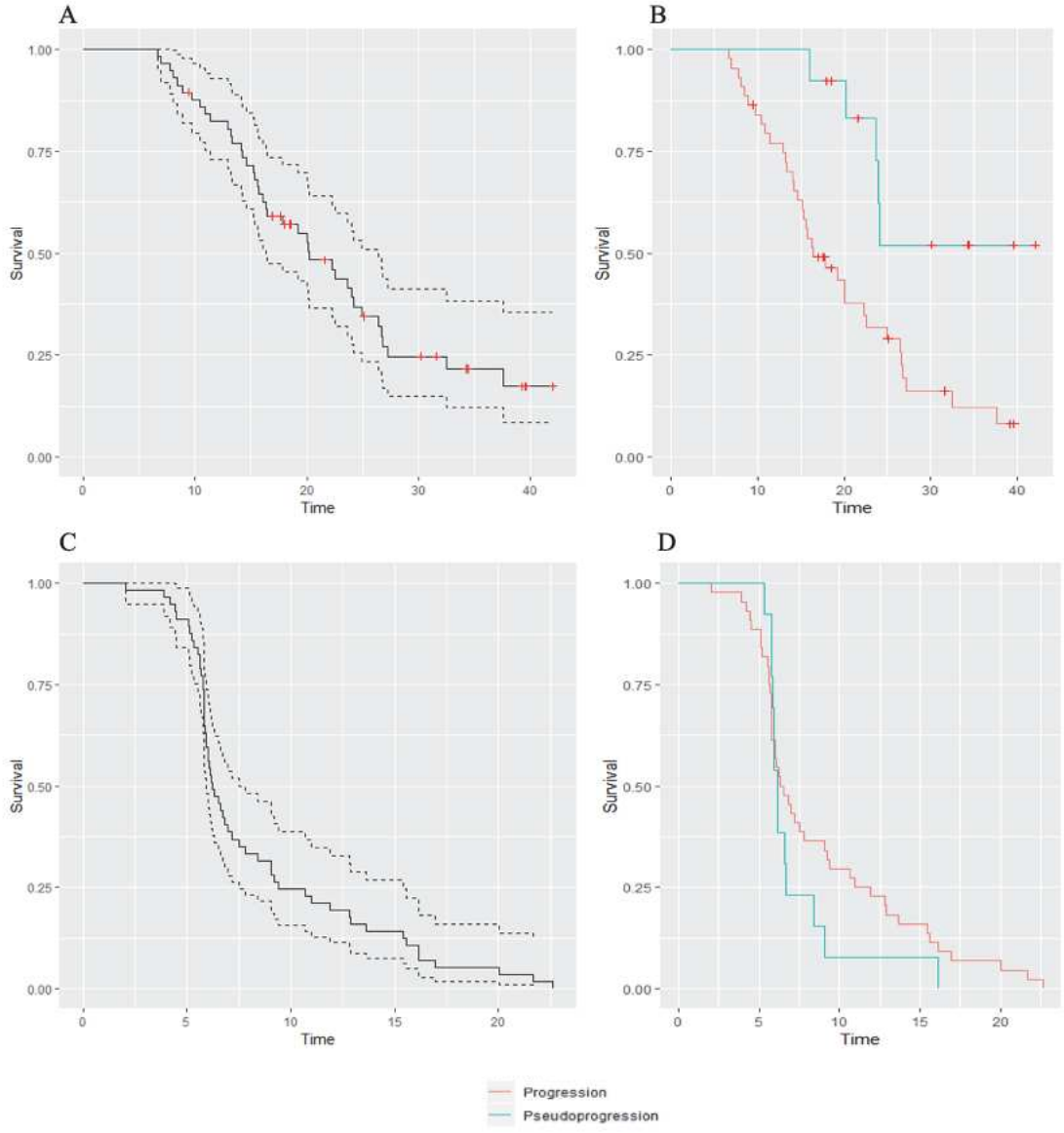

E

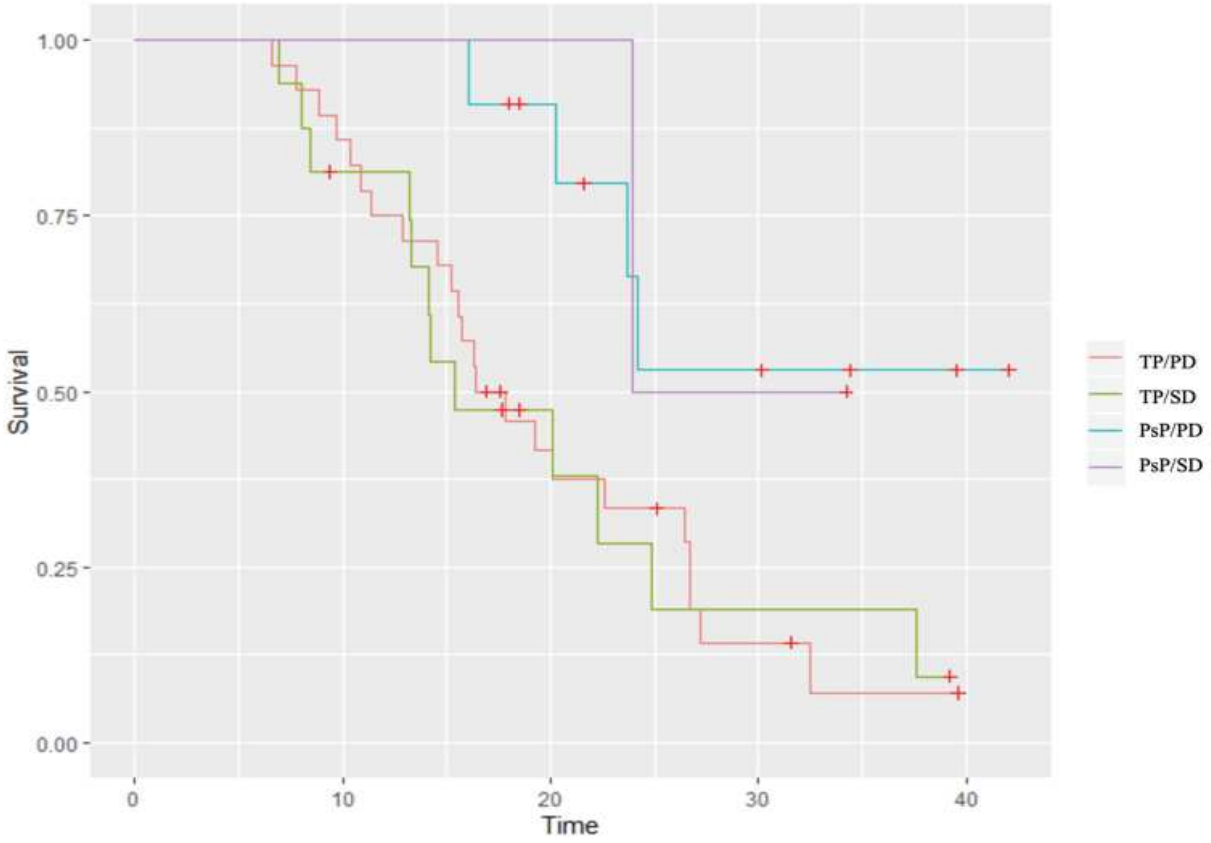

	Total (n=57)	TP (n=44)	PsP (n=13)	p value
Death no. (%)				
Yes	40 (70%)	35 (80%)	5 (38%)	**0.012**
No	17 (30%)	9 (20%)	8 (62%)	
TTP from the date of diagnostic (months)				
Median	6.2	6.4	6.1	0.300
95% CI	5.9-7.5	5.8-9.2	5.9-9.0	
OS from the date of diagnostic (months)				
Median	20.2	16.4	NR	**0.004**
95% CI	16.3-26.4	15.2-24.9	24.0-31.8	

CI: Confidence Interval; NR: not reached; **OS**: Overall Survival; **TTP**: Time to Progression

Appendix 1: Flow chart of patients selection

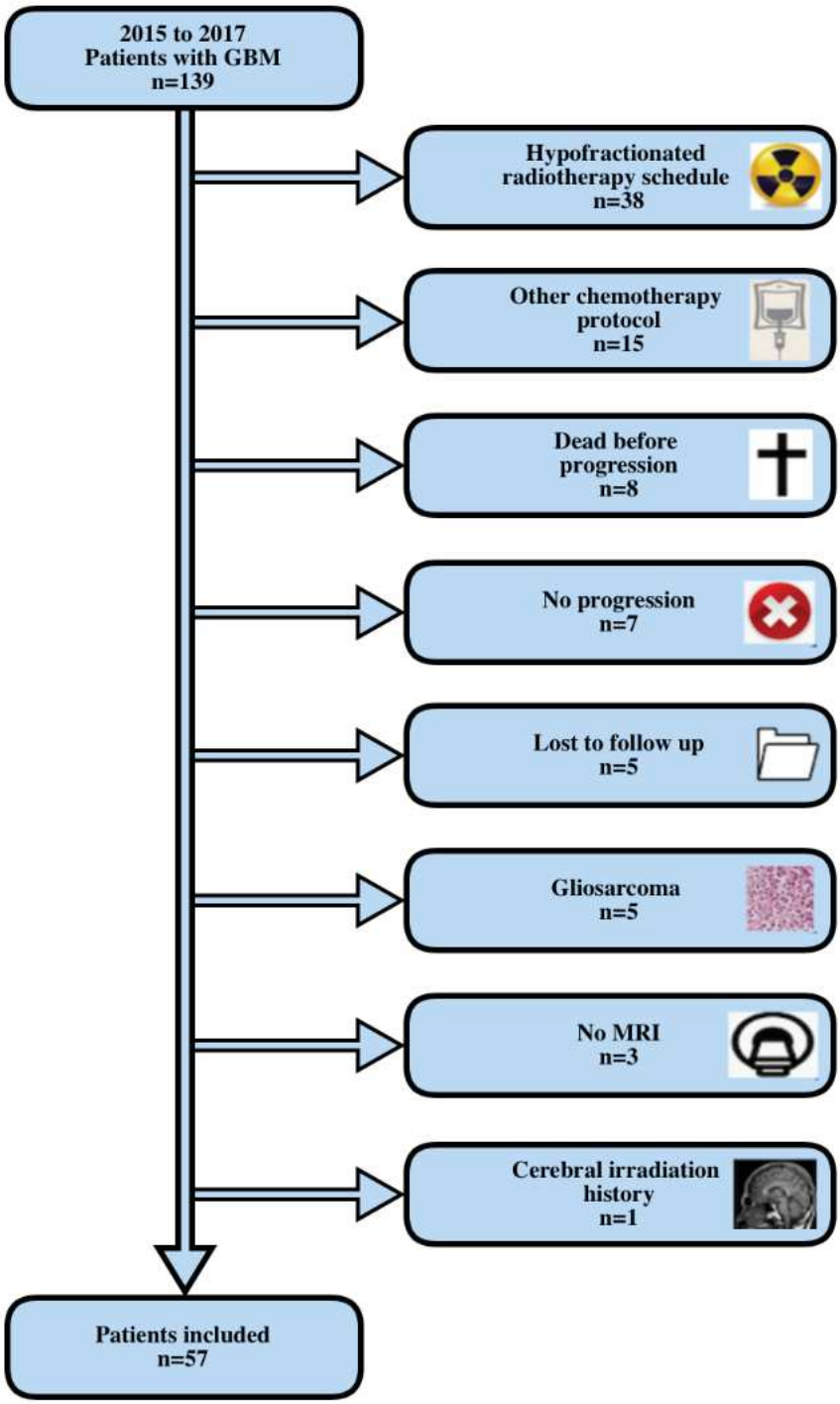

Appendix 2: Description of neurological symptoms

Clinical characteristics	Clinical characteristics before CRT				Clinical characteristics at progression				Clinical evolution: before CRT versus time to progression				
	Total (n=57)	TP (n=44)	PsP (n=13)	p value	Total (n=57)	TP (n=44)	PsP (n=13)	p value		Total (n=57)	TP (n=44)	PsP (n=13)	p value
Asthenia no. (%)									**Asthenia no. (%)**				
0	40 (70%)	31 (70%)	9 (69%)		8 (14%)	7 (16%)	1 (8%)		**Stable**	15 (26%)	11 (25%)	4 (31%)	
1	17 (30%)	13 (30%)	4 (31%)	1.000	35 (61%)	25 (57%)	10 (77%)	0.837	**Worse**	40 (70%)	31 (70%)	9 (69%)	0.843
2	0 (0%)	0 (0%)	0 (0%)		12 (21%)	10 (23%)	2 (15%)		**Better**	2 (4%)	2 (5%)	0 (0%)	
3	0 (0%)	0 (0%)	0 (0%)		2 (4%)	2 (4%)	0 (0%)						
Headaches no. (%)									**Headaches no. (%)**				
0	42 (74%)	33 (75%)	9 (69%)		46 (81%)	37 (84%)	9 (69%)		**Stable**	35 (61%)	28 (63%)	7 (54%)	
1	14 (25%)	10 (23%)	4 (31%)	0.781	10 (17%)	6 (14%)	4 (31%)	0.396	**Worse**	9 (16%)	6 (14%)	3 (23%)	0.675
2	1 (1%)	1 (2%)	0 (0%)		1 (2%)	1 (2%)	0 (0%)		**Better**	13 (23%)	10 (23%)	3 (23%)	
Nausea no. (%)									**Nausea no. (%)**				
0	54 (95%)	42 (95%)	12 (92%)		55 (96%)	43 (98%)	12 (92%)		**Stable**	54 (94%)	41 (93%)	13 (100%)	
1	3 (5%)	2 (5%)	1 (8%)	0.547	2 (4%)	1 (2%)	1 (8%)	0.407	**Worse**	1 (2%)	1 (2%)	0 (0%)	1.000
									Better	2 (4%)	2 (5%)	0 (0%)	
Vertigo									**Vertigo no. (%)**				
0	55 (96%)	42 (95%)	13 (100%)		51 (89%)	39 (89%)	12 (92%)		**Stable**	49 (86%)	37 (84%)	12 (92%)	
1	2 (4%)	2 (5%)	0 (0%)	1.000	6 (11%)	5 (11%)	1 (8%)	1.000	**Worse**	6 (10%)	5 (11%)	1 (8%)	1.000
									Better	2 (4%)	2 (5%)	0 (0%)	
Visual trouble no. (%)									**Visual trouble no. (%)**				
0	45 (79%)	35 (80%)	10 (77%)		45 (79%)	35 (80%)	10 (77%)		**Stable**	47 (82%)	38 (86%)	9 (70%)	
1	11 (19%)	9 (20%)	2 (15%)	0.308	12 (21%)	9 (20%)	3 (23%)	1.000	**Worse**	6 (11%)	4 (9%)	2 (15%)	0.249
2	2 (2%)	0 (0%)	1 (8%)		0 (0%)	0 (0%)	0 (0%)		**Better**	4 (7%)	2 (5%)	2 (15%)	
Language disorder no. (%)									**Language disorder no. (%)**				
0	40 (70%)	31 (70%)	9 (69%)		33 (58%)	25 (57%)	8 (61%)		**Stable**	35 (61%)	24 (55%)	11 (85%)	
1	17 (30%)	13 (30%)	4 (31%)	1.000	15 (26%)	11 (25%)	4 (31%)	0.861	**Worse**	18 (32%)	16 (36%)	2 (15%)	0.158
2	0 (0%)	0 (0%)	0 (0%)		8 (14%)	7 (16%)	1 (8%)		**Better**	4 (7%)	4 (9%)	0 (0%)	
3	0 (0%)	0 (0%)	0 (0%)		1 (2%)	1 (2%)	0 (0%)						
Memory disorder no. (%)									**Memory disorder no. (%)**				
0	45 (79%)	35 (80%)	10 (77%)		28 (49%)	20 (45%)	8 (62%)		**Stable**	39 (68%)	30 (68%)	9 (69%)	
1	12 (21%)	9 (20%)	3 (23%)	1.000	27 (47%)	22 (50%)	5 (38%)	0.720	**Worse**	17 (30%)	13 (29%)	4 (31%)	1.000
2	0 (0%)	0 (0%)	0 (0%)		2 (4%)	2 (5%)	0 (0%)		**Better**	1 (2%)	1 (2%)	0 (0%)	
Confusion no. (%)									**Confusion no. (%)**				
0	51 (89%)	40 (91%)	11 (85%)		40 (70%)	29 (66%)	11 (85%)		**Stable**	42 (74%)	31 (71%)	11 (84%)	
1	6 (11%)	4 (9%)	2 (15%)	0.611	14 (25%)	12 (27%)	2 (15%)	0.451	**Worse**	13 (23%)	12 (27%)	1 (8%)	0.174
2	0 (0%)	0 (0%)	0 (0%)		3 (5%)	3 (7%)	0 (0%)		**Better**	2 (3%)	1 (2%)	1 (8%)	
Epilepsy no. (%)									**Epilepsy no. (%)**				
Yes	19 (33%)	18 (41%)	1 (8%)		11 (19%)	8 (18%)	3 (23%)		**Stable**	43 (76%)	32 (73%)	11 (85%)	
No	38 (67%)	26 (59%)	12 (92%)	**0.042**	46 (81%)	36 (82%)	10 (77%)	0.700	**Worse**	3 (5%)	1 (2%)	2 (15%)	**0.032**
									Better	11 (9%)	11 (25%)	0 (0%)	
Dysesthesia no. (%)									**Dysesthesia no. (%)**				
0	52 (91%)	40 (91%)	12 (92%)		47 (82%)	35 (80%)	12 (92%)		**Stable**	46 (81%)	33 (75%)	13 (100%)	
1	5 (9%)	4 (9%)	1 (8%)	1.000	8 (14%)	7 (16%)	1 (8%)	0.801	**Worse**	8 (14%)	8 (18%)	0 (0%)	0.233
2	0 (0%)	0 (0%)	0 (0%)		1 (2%)	1 (2%)	0 (0%)		**Better**	3 (5%)	3 (7%)	0 (0%)	
3	0 (0%)	0 (0%)	0 (0%)		1 (2%)	1 (2%)	0 (0%)						
Paralysis no. (%)									**Paralysis no. (%)**				
0	42 (74%)	30 (68%)	12 (92%)		36 (63%)	28 (64%)	8 (62%)		**Stable**	34 (60%)	25 (57%)	9 (69%)	
1	14 (24%)	13 (30%)	1 (8%)	0.277	12 (21%)	8 (18%)	4 (31%)	0.782	**Worse**	16 (28%)	12 (27%)	4 (31%)	0.391
2	1 (2%)	1 (2%)	0 (0%)		7 (12%)	6 (14%)	1 (8%)		**Better**	7 (12%)	7 (16%)	0 (0%)	
3	0 (0%)	0 (0%)	0 (0%)		2 (4%)	2 (5%)	0 (0%)						

Appendix 3: RANO criteria

	RANO criteria 2010		Modified RANO criteria 2017 (Ellingson *et al*)
Complete Response (CR)	All Complete disappearance of measurable and non-measurable enhancing lesions at least 4 weeks No new lesion Stable or improved T2/FLAIR lesions No corticosteroids Clinically stable or improved		All Complete disappearance of measurable and non-measurable enhancing lesions at least 4 weeks No corticosteroids Clinically stable or improved
Partial response (PR)	All Measurable enhancing lesions: ≥50% decrease in the sum of the product of perpendicular diameters at least 4 weeks No progression of nonmeasurable lesions No new lesion Stable or improved T2/FLAIR lesions Corticosteroids dose stable or decreased Clinically stable or improved		All Measurable enhancing lesions: ≥50% decrease in the sum of the product of perpendicular diameters or ≥65% decrease in total volume at least 4 weeks Corticosteroids dose stable or decreased Clinically stable or improved
Stable disease (SD)	All No CR nor PR nor PD Stable T2/FLAIR lesions Corticosteroids dose stable or decreased		No CR nor PR nor PD
Progression disease (PD)	<12 weeks after CRT New enhancement outside the radiation field (80% isodose line) Histopathological proof of progression	≥12 weeks after CRT Any Measurable enhancing lesions: ≥25% increase in the sum of the product of perpendicular diameters Increase in T2/FLAIR lesions New lesion Progression of non-measurable lesions that became measurable Clinical deterioration	Any In two sequential MRI separated by ≥ 4 weeks Enhancing lesions: ≥25% increase in the sum of the product of perpendicular diameters or ≥40% increase in the total volume Clinical deterioration

Appendix 4: Progression criteria based on RANO criteria

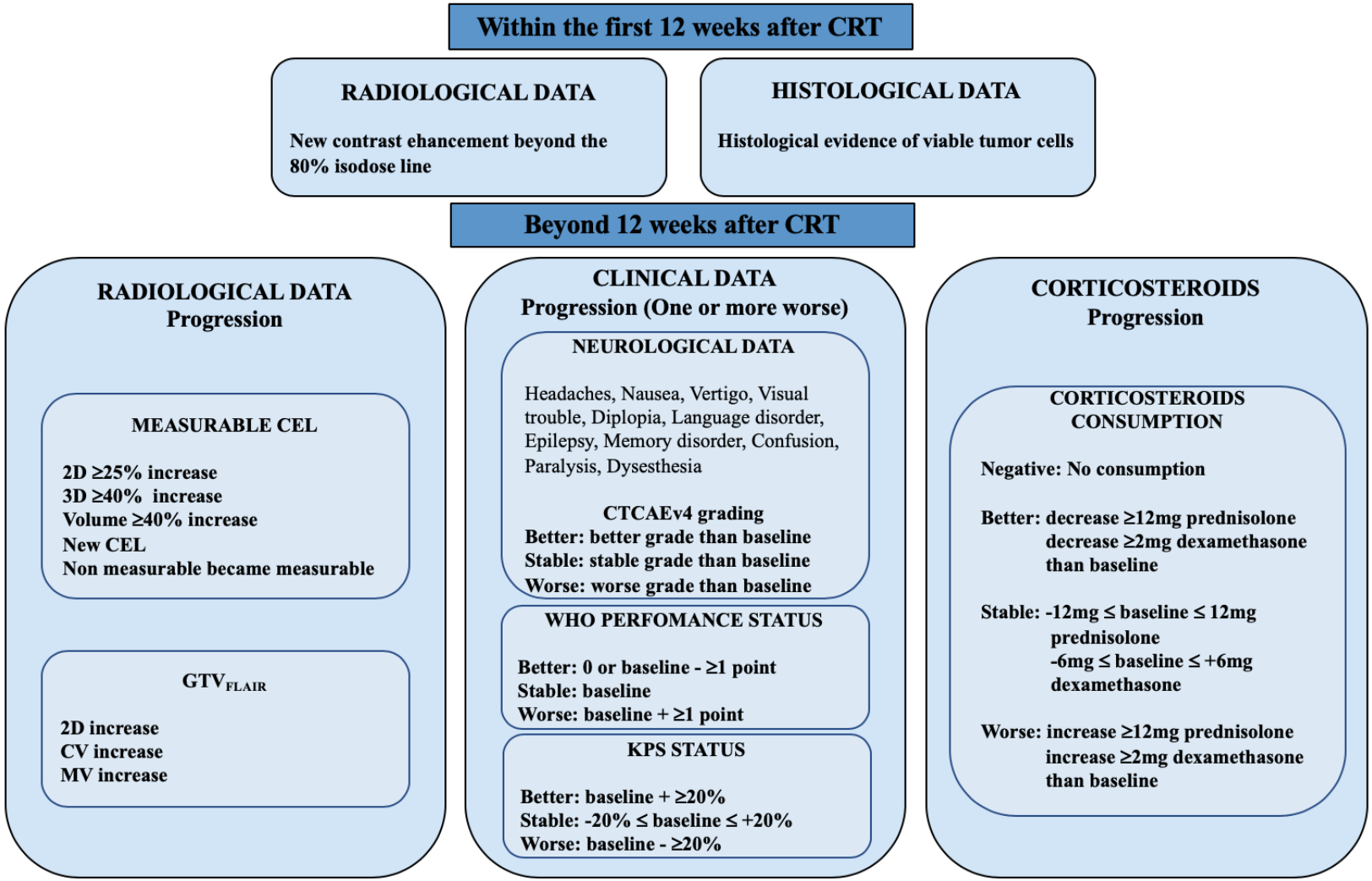

CEL: contrast enhanced lesions**; CRT:** chemoradiotherapy; **CV**: Calculated Volume; **MV**: Measured Volume

CONCLUSION GENERALE

Le doute diagnostique d'une pseudoprogression versus une vraie progression est une situation commune en pratique clinique, et le diagnostic de certitude reste un challenge pour le praticien. Pourtant, il ne devrait pas être si ambigu et complexe afin d'assurer une prise en charge optimale des patients. Hormis la confirmation anatomopathologique, il n'existe, à ce jour, pas de marqueur prédictif spécifique de pseudoprogression, malgré une littérature relativement riche. De plus, les études retrouvées dans la littérature présentent des méthodologies très hétérogènes manquant de reproductibilité et des résultats peu comparables. Des biomarqueurs non invasifs, notamment radiologiques, pourraient résoudre le dilemme, mais des recherches supplémentaires sont nécessaires. En effet, des efforts restent encore à fournir sur la standardisation des protocoles d'acquisition d'imagerie, sur l'interprétation des résultats et sur la publication de recommandations. De plus, la disponibilité et l'accès à certains examens d'imagerie en routine clinque sembleraient judicieux, les imageries multimodales ayant, par exemple, déjà confirmé leur supériorité aux examens conventionnels dans le diagnostic de pseudoprgression. En outre, une définition stricte et consensuelle de la pseudoprogression semble nécessaire à la réalisation d'essais de qualité.

Ce travail a permis d'identifier dix facteurs prédictifs de pseudoprogression en analyse univariée et trois en analyse multivariée. Ces derniers ont conduit à la construction d'un score de probabilité de pseudoprogression, pouvant guider le clinicien en cas de doute diagnostic. Ces résultats restent à confirmer par une étude prospective, et à approfondir par l'ajout de données supplémentaires. Les résultats d'examens d'imageries multimodales ou encore les données génomiques ou protéomiques pourraient non seulement améliorer le diagnostic de pseudoprogression, mais également permettre une adaptation personnalisée de la prise en charge du patient. L'analyse de ces résultats par des algorithmes spécifiques d'intelligence

artificielle pourrait optimiser le diagnostic de pseudoprogression. Ainsi, l'intégration de l'ensemble des données dans un modèle prédictif « big data » d'aide à la décision thérapeutique semble prometteur.

Université de Strasbourg

Faculté de médecine

DECLARATION SUR L'HONNEUR

Document avec signature originale devant être joint :
- à votre mémoire de D.E.S.
- à votre dossier de demande de soutenance de thèse

Nom : LE FEVRE **Prénom :** Clara

Ayant été informé(e) qu'en m'appropriant tout ou partie d'une œuvre pour l'intégrer dans mon propre mémoire de spécialité ou dans mon mémoire de thèse de docteur en médecine, je me rendrais coupable d'un délit de contrefaçon au sens de l'article L335-1 et suivants du code de la propriété intellectuelle et que ce délit était constitutif d'une fraude pouvant donner lieu à des poursuites pénales conformément à la loi du 23 décembre 1901 dite de répression des fraudes dans les examens et concours publics,

Ayant été avisé(e) que le président de l'université sera informé de cette tentative de fraude ou de plagiat, afin qu'il saisisse la juridiction disciplinaire compétente,

Ayant été informé(e) qu'en cas de plagiat, la soutenance du mémoire de spécialité et/ou de la thèse de médecine sera alors automatiquement annulée, dans l'attente de la décision que prendra la juridiction disciplinaire de l'université

J'atteste sur l'honneur
Ne pas avoir reproduit dans mes documents tout ou partie d'œuvre(s) déjà existante(s), à l'exception de quelques brèves citations dans le texte, mises entre guillemets et référencées dans la bibliographie de mon mémoire.

A écrire à la main : « J'atteste sur l'honneur avoir connaissance des suites disciplinaires ou pénales que j'encours en cas de déclaration erronée ou incomplète ».

J'atteste sur l'honneur avoir connaissance des suites disciplinaires ou pénales que j'encours en cas de déclaration erronée ou incomplète.

Signature originale :

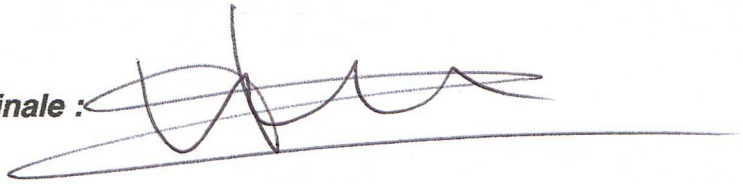

A Strasbourg, le 26/09/2019

Photocopie de cette déclaration devant être annexée en dernière page de votre mémoire de D.E.S. ou de Thèse.

RESUME :

Introduction Le diagnostic de pseudoprogression (PsP) au cours du suivi des patients atteints d'un glioblastome (GBM) est un vrai dilemme. Actuellement, aucun facteur prédictif universel n'a été mis en évidence. Le but de cette étude était d'identifier des facteurs prédictifs de PsP afin d'aider le clinicien à la décision thérapeutique.

Méthodes Les patients suivis pour un GBM prouvé histologiquement, et traités par une chirurgie optimale et une chimioradiothérapie, selon le protocole EORTC/NCIC, ont été inclus. Les données cliniques, histologiques, radiologiques et d'irradiation ont été analysées au moment de l'IRM dosimétrique (baseline) et au moment de l'IRM montrant une progression (IRM progression). Les patients ont été classés dans le groupe PsP ou dans le groupe vraie progression (TP) selon les données de l'IRM qui a suivi l'IRM progression. Une analyse de corrélation a été effectuée avec les variables ayant une p valeur ≤0.200 en analyse univariée. Le modèle multivarié incluait les variables ayant un coefficient de corrélation r compris entre -0.5 et 0.5.

Résultats Cinquante-sept patients ont été inclus dans l'étude, 44 (77%) dans le groupe TP et 13 (23%) dans le groupe PsP. En analyse univariée, les potentiels facteurs prédictifs de PsP étaient : l'absence d'épilepsie au moment de l'IRM dosimétrique (p=0.042), et sa stabilité (p=0.032), la méthylation du promoteur de MGMT (p=0.044), la mutation d'ATRX (p=0.043), la diminution de la taille de la nécrose en deux dimensions (p=0.041) et en trois dimensions (p=0.024), la $V_{80\%}$ et la D_{min} du volume incluant la prise de contraste, la nécrose et la cavité chirurgicale, sur l'IRM progression (p=0.023 and p=0.017), et du volume de la prise de contraste seule (p=0.039 and p=0.029). En analyse multivariée, les facteurs prédictifs de PsP étaient : la $V_{80\%}$ du volume de l'œdème sur l'IRM progression (p=0.027), le nombre de prises de contraste sur l'IRM progression (p=0.035) et la classe de réponse thérapeutique selon RANO (p=0.019).

Conclusion

Actuellement le diagnostic de certitude de PsP nécessite une confirmation histologique. Cependant, en routine clinique, l'analyse des IRM conventionnelles de suivi est le plus souvent utilisée. L'étude a identifié des facteurs prédictifs potentiels de PsP qu'il conviendrait de confirmer par une analyse prospective, complétée de données d'imagerie et de données génétiques.

Rubrique de classement : ONCOLOGIE option Radiothérapie

Mots-clés : Glioblastome, IRM, MGMT, Progression, Pseudoprogression, RANO

Adresse de l'auteur :

1 place de la porte de l'Hôpital

67000 Strasbourg